The Role of Mitochondrial Membrane Potential and Uncoupling Protein 2 in Hypoxic Pulmonary Vasoconstriction and Pulmonary Hypertension.

Inaugural Dissertation
Submitted to the
Faculty of Medicine
in partial fulfillment of the requirements
for the “Doktor der Humanbiologie” (Dr. biol. hom.) Degree
of the Faculty of Medicine
of the Justus-Liebig University Giessen

by
Pak Oleg
of
Bishkek, Kyrgyzstan
Giessen 2014

From the Excellence Cluster Cardiopulmonary System, University of Giessen and Marburg Lung Center (UGMLC), Member of the German Center for Lung Research (DZL),
The Faculty of Medicine of the Justus-Liebig University Giessen

Director: Werner Seeger
Prof. Norbert Weissmann (supervisor)
Prof. Christian Apitz
Prof. Dietmar Schranz

Date of Doctoral Defense: 2nd Dcember 2014

“I declare that I have completed this dissertation single-handedly without the unauthorized help of a second party and only with the assistance acknowledged therein. I have appropriately acknowledged and referenced all text passages that are derived literally from or are based on the content of published or unpublished work of others, and all information that relates to verbal communications. I have abided by the principles of good scientific conduct laid down in the charter of the Justus Liebig University of Giessen in carrying out the investigations described in the dissertation.”

Date, Place_____ Signature _____

I. Table of contents

II. List of figures and tables

III. List of abbreviations

$[Ca^{2+}]_i$	Cytosolic calcium concentration
$[Ca^{2+}]_m$	Mitochondrial calcium concentration
$^1O_2$	Singlet oxygen
4-HNE	4-hydroxynonenal
5-HTT	Hydroxytryptamine transporter protein
ACE	Angiotensin converting enzyme
Acot1/2	Acyl-CoA thioesterase 1 and 2
AMP/ATP	Adenosine monophosphate - adenosine triphosphate ratio
AKT	Protein kinase B
ALK1	Activin receptor-like kinase 1
AMP	Adenosine monophosphate
AMPK	AMP-activated protein kinase
ANT	Adenine nucleotide translocase
Arg2	Arginase 2
ARNT	Aryl hydrocarbon nuclear trans locator
ATP	Adenosine triphosphate
BA	Bongkrek acid
bFGF	Basic fibroblast growth factor
BMPR2	Bone morphogenetic protein receptor 2
BSA	Bovine serum albumin
cADPR	Cyclic adenosine diphosphate ribose
cAMP	Cyclic adenosine monophosphate
Cat	Catalase
Ccnd2	G1/S-specific cyclin-D2
CCCP	Carbonyl cyanide 3-chlorophenylhydrazone
cGMP	Cyclic guanosine monophosphate
CHO-K1	Chinese hamster ovary cells
CMV promoter	Cytomegalovirus promoter
COPD	Chronic obstructive pulmonary disease
COX5b	Cytochrome c oxidase subunit 5B
Cpt1b	Carnitine palmitoyltransferase 1b
Cpt2	Carnitine palmitoyltransferase 2
CREB	cAMP response element
CTEPH	Chronic thromboembolic pulmonary hypertension

Cyt C	Cytochrome c
DAG	Diacylglycerol
DAPI	4'-6-diamidino-2-phenylindole
DCA	Dichloroacetate
DCF	Dichlorofluorescein
DHEA	Dehydroepiandrosterone
DHR123	Dihydrorhodamine 123
DiOC6(3)	3,3´ - dihexyloxacarbocyanine iodide
DNA	Deoxyribonucleic acid
DNP	2,4-Dinitrophenol
EC	Endothelial cells
EGF	Epidermal growth factor
EF-1α promoter	Human elongation factor-1 alpha
Ehhadh	Enoyl-Coenzyme A, hydratase/3-hydroxyacyl Coenzyme A dehydrogenase
ERK	Extracellular-signal-regulated kinases
Erdosteine	2-[(2-oxothiolan-3-yl)carbamoylmethylsulfanyl]acetic acid
ESR	Electron spin resonance (or electron paramagnetic resonance) spectroscopy
EPR	Electron paramagnetic resonance spectroscopy
ER	Endoplasmic reticulum
FADH2	Reduced form of flavin adenine dinucleotide
FCS	Fetal calf serum
FCCP	Carbonyl cyanide 4-(trifluoromethoxy)phenylhydrazone
FOXO1	Forkhead box protein O1
FPAH	Familial pulmonary hypertension
FRET	Fluorescence resonance energy transfer
GDP	Guanosine diphosphate
GFR	Growth Factor Receptor
Glut1	Glucose transporter 1
Gpx	Glutathione peroxidase
H^+	Proton
H_2O_2	Hydrogen peroxide
HeLa cells	Cervical cancer cells taken from Henrietta Lacks
HEt	Hydroethidine
HIF	Hypoxia inducible factor
HIV	Human immunodeficiency virus

HO•	Hydroxyl radical
HO_2	Hydroperoxyl
HO-2	Heme-oxygenase-2
HOCl	Hypochlorous acid
HOX	Hypoxia
HPLC	High-performance liquid chromatography
HPRT	Hypoxanthine phosphoribosyltransferase
HPV	Hypoxic pulmonary vasoconstriction
HREs	HIF-responsive elements
HyPer	Hydrogen peroxide sensor
IGF-1	Insulin-like growth factor
IL	Interleukins
IMM	Inner mitochondrial membrane
IP_3	Inositol-1,4,5-trisphosphate
IPAH	Idiopathic pulmonary arterial hypertension
JC1	5,5’,6,6’-tetrachloro-1,1’,3,3’-tetraethylbenzimidazolylcarbocyanine iodide
JNK	c-Jun N-terminal kinases
K_v channels	Voltage-dependent potassium channels
LDHA	Lactate dehydrogenase A
LO	Lipoxygenases
Max dP/dt	Maximum rate of pressure change in the right ventricle
MCT	Monocrotaline
MCU	Mitochondrial calcium uniporter
MEFs	Mouse embryonic fibroblasts
Min dP/dt	Minimum rate of pressure change in the right ventricle
mitoK_{ATP}	Mitochondrial ATP-sensitive potassium channel
MLC	Myosin light chain
mRNA	Messenger RNA
MWT	Medial wall thickness
N_2	Nitrogen
NAC	N-acetyl-L-cysteine
NAD^+	Nicotinamide adenine dinucleotide
NADH	Reduced form of nicotinamide adenine dinucleotide
NADPH oxidases	Nicotinamide adenine dinucleotide phosphate oxidases
NCX	Sodium calcium exchanger

NFAT	Nuclear factor of activated T
NF-kB	Nuclear factor kappa-light-chain-enhancer of activated B cell
NMR	Nuclear magnet resonance
NO	Nitric oxide
NOX	Normoxia
NOX1-5	NADPH oxidase 1-5
O_2	Oxygen
$O_2^{\bullet-}$	Superoxide anion
O_3	Ozone
$OONO^-$	Peroxynitrite
ORF	Open reading frame
p38	p38 mitogen-activated protein kinases
PAP	Pulmonary arterial pressure
PASMC	Pulmonary artery smooth muscle cells
PBS	Phosphate buffered saline
PC12	Cell line derived from a pheochromocytoma of the rat adrenal medulla
PCH	Pulmonary capillary hemangiomatosis
PDGF	Platelet-derived growth factor
PDGFRs	Platelet-derived growth factor receptors
PDK1	Pyruvate dehydrogenase kinase 1
pERK	Phosphorylated extracellular-signal-regulated kinases
Pfkfb3	6-phosphofructo-2-kinase/fructose-2,6-biphosphatase 3
PH	Pulmonary hypertension
PHD	Pyruvate dehydrogenase
PHD2	Prolyl hydroxylase 2
Pi	Phosphoric acid
PKC	Protein kinase C
Pkm	Pyruvate kinase, muscle form
pO_2	Partial pressure of O_2
PPARγ	Peroxisome proliferator-activated receptor
Prx	Peroxiredoxins
PVDF	Polyvinylidene fluoride
PVOD	Pulmonary veno-occlusive disease
Pyr	Pyruvate
Q	Perfusion

RhoA	Ras homolog gene family, member A
Rhod123	Rhodamine 123
Rhod2	1-[2-Amino-5-(3-dimethylamino-6-dimethylammonio-9-xanthenyl)phenoxy]-2-(2-amino-5-methylphenoxy)ethane-N,N,N',N'-tetraacetic acid, tetraacetoxymethyl ester, chloride
RhoGD	Rho guanine nucleotide dissociation inhibitor
roGFP	Reduction-oxidation sensitive green fluorescent protein
ROS	Reactive oxygen species
rSmad	Receptor-regulated Smads
RV	Right ventricle
RV/LV+S	Ratio of right ventricle to left ventricle and septum
RVEDP	Right ventricular end-diastolic pressure
RVSP	Right ventricular systolic pressure
rxYFP	Yellow fluorescent protein-based redox sensor
RyR	Ryanodine-sensitive receptors
scr siRNA	Scrambled small interfering RNA
SEM	Standard error
SERCA	Sarco/endoplasmic reticulum Ca^{2+}
Slc25a20	Carnitine/acylcarnitine translocase
SMAD	Family of proteins related to *Drosophila* "mothers against decapentaplegic" (Mad) and *Caenorhabditis elegans* Sma
SMC	Smooth muscle cells
SNPs	Single nucleotide polymorphisms
SOCC	Store-operated calcium channels
SOD	Superoxide dismutase
SR	Sarcoplasmic reticulum
Src	v-src sarcoma (Schmidt-Ruppin A-2) viral oncogene homolog (avian)
STAT3	Signal transducer and activator of transcription 3
TBS-T buffer	Tris Buffer Saline + 0.1% Tween20
TCA cycle	Tricarboxylic acid cycle
TEMPO	2,2,6,6-tetramethylpiperidine-N-oxyl
Tempol	4-hydroxy-2,2,6,6-tetramethylpiperidin-1-oxyl
Tg	Transgenic
TGF-β	Transforming growth factor beta
TMRE	Tetramethylrhodamine
TMRM	Tetraethylrhodamine methyl

Tnfaip3	Tumor necrosis factor, alpha-induced protein 3
TRPC	Transient receptor potential cation channels
UCP	Uncoupling protein
$UCP2^{-/-}$	UCP2 knockout mice
V	Ventilation
V/Q	Pulmonary ventilation/perfusion ratio
VDAC	Voltage-dependent anion channels
VEGF	Vascular endothelial growth factor
VHL	von Hippel-Lindau protein
VOCC	Voltage operated calcium channels
XO	Xanthine oxidases
β_2M	Beta2-microglobulin
ΔmH^+	Electrochemical proton gradient
Δp	Proton-motive force
$\Delta\psi_m$	Mitochondrial membrane potential

1. Introduction

1.1. Hypoxic pulmonary vasoconstriction (HPV)

1.1.1. Physiological relevance of HPV

In order to guarantee optimal pulmonary oxygen (O_2) uptake and to supply tissue with sufficient O_2, the degree of local pulmonary blood perfusion (Q) is matched to the respective level of ventilation (V)[1-4]. When lung ventilation is impaired locally, constriction of small precapillary pulmonary arteries in this area serves as a crucial mechanism to maintain the ventilation-perfusion ratio in the normal range (Figure 1). This mechanism is called hypoxic pulmonary vasoconstriction (HPV) and is an essential physiological reaction of the pulmonary vasculature to match pulmonary blood perfusion to alveolar ventilation during acute hypoxia[1] (Figure 1). Thus, local alveolar hypoxia, for example due to local obstruction of the bronchus by a lung tumor or mucus plug, leads to vasoconstriction of precapillary arteries and redistributes perfusion from poorly ventilated areas of the lung to better ventilated areas (Figure 1). However, global acute hypoxia, as occurring *e.g.* in exacerbation of lung diseases can lead to the vasoconstriction of most pulmonary arteries and may result in an acute prominent increase of the pulmonary arterial pressure (PAP).

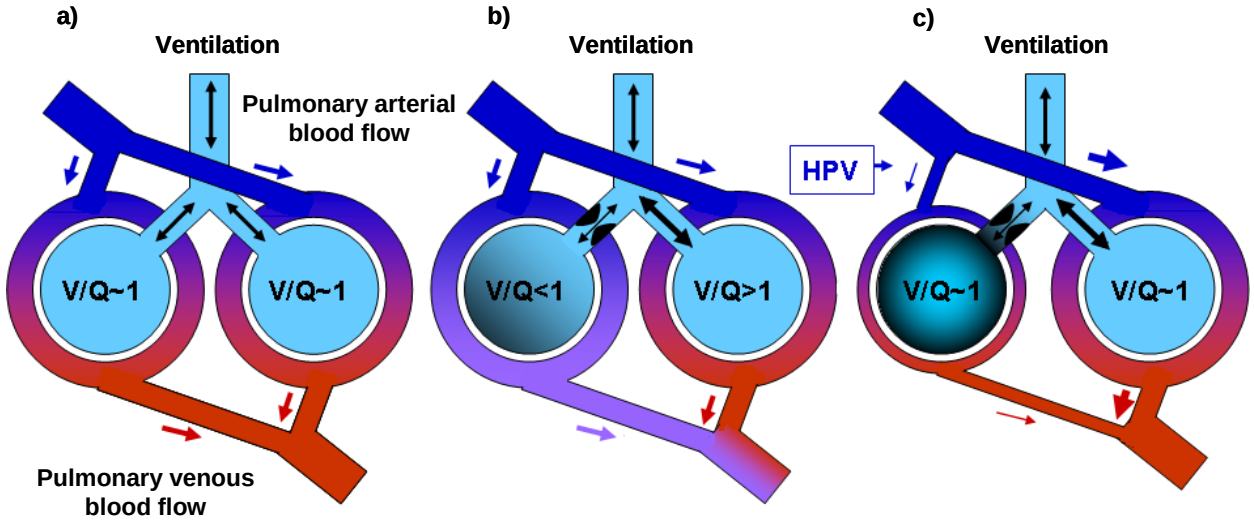

Figure 1. Ventilation-perfusion matching.
a) Under physiological conditions, the alveolar ventilation (V) is equal to the perfusion (Q), V/Q~1. b) Local obstruction of a bronchus decreases the ventilation resulting in reduction of V/Q (V/Q less than 1), and enhancement of the ventilation of neighboring areas of the lung (redirecting airflow) increasing the V/Q ratio (V/Q higher than 1). c) HPV leads to the decrease of the perfusion of poorly ventilated areas in favor of better ventilated areas, thereby improving the ventilation-perfusion matching (V/Q~1) and systemic arterial oxygenation[1, 3].

In contrast to the pulmonary vessels, most systemic arteries dilate in response to local hypoxia in order to provide the hypoxic organ with more O_2 by an increase of blood flow[1]. An exception is the fetal vasculature in the placenta[5]. These vessels, like pulmonary arteries, constrict in response to hypoxia redirecting the fetal flow from insufficiently oxygenated areas of the placenta toward regions with better maternal perfusion[5].

The trigger for a flurry of investigations in the research area of HPV was the publication of one of the most important articles about HPV in 1946 by von Euler and Liljestrand[6]. They found an increase of PAP in cats within few seconds during ventilation with 10.5% O_2[6]. After that initial finding, HPV has been confirmed in different animal species[7-9] and humans[10]. The HPV response differs among animal species with regard to the sensitivity to the hypoxic stimulus, as well as a magnitude of the response[11], *e.g.* the threshold for HPV in isolated lungs of rats is ~60 mmHg[12] and around 75 mmHg in isolated lungs of rabbits[13]. In isolated and perfused rabbit lungs, HPV starts after a few seconds of the acute hypoxic challenge and has a biphasic shape. The first maximal increase of mean PAP (mPAP) occurs at ~5 minutes (first phase), called acute hypoxic response, then a small decline in mPAP is observed, and afterwards mPAP again gradually increases with the second maximum of mPAP at ~90 minutes (second phase), called sustained hypoxic response[9]. The same biphasic response occurs in human where mPAP increases to a first maximum within 15 minutes and to a second maximum at ~2h[3]. The biphasic HPV response is associated with a biphasic rise in cytosolic (intracellular) calcium ($[Ca^{2+}]_i$) in pulmonary artery smooth muscle cells (PASMC)[14]. However, some studies indicate that the second phase is dependent on endothelium and activation of Rho-associated protein kinase (ROCK) and not on a rise of $[Ca^{2+}]_i$[15]. Activation of ROCK plays a key role in the sustained response of the pulmonary vasculature to hypoxia by an increase of the sensitization of myosin light chains (MLC) to $[Ca^{2+}]_i$[15]. Other studies do not demonstrate the second phase of HPV at all[16]. The explanation for this discrepancy is still unknown[3].

The trigger of HPV is alveolar hypoxia, since inhalation of a hypoxic gas mixture evokes HVP even in conditions when the lungs are perfused with normally oxygenated perfusate or blood[9, 17]. Local arterial hypoxia also can be a trigger of HPV in view of the fact that forward perfusion with hypoxic blood stimulates the elevation of mPAP in rats[18]. In contrast, reverse perfusion of the pulmonary circulation with hypoxic blood via the left atrium does not trigger HPV, therefore the venous part of the pulmonary circulation can be excluded as a sensor of HPV[18]. Experiments in the isolated perfused lung[9], in pulmonary arteries isolated from lungs[19] or within lung slices[20], as well as in isolated PASMC[21] have demonstrated that the effector and sensor cell type of HPV is located in precapillary PASMC and that HPV does not depend on neural or humoral influences from outside the lung[1]. Additional confirmation that HPV is a physiological adaptive mechanism attributed to the lung itself is shown by a study presenting that HPV was preserved in patients after the bilateral lung transplantation[22].

The role of the endothelium in acute HPV is not clear. Early studies in isolated pulmonary arteries demonstrated that removal of the endothelium preserved the acute HPV response, however, later studies showed that endothelium-denuded arteries lost the vasoconstrictor response to the acute hypoxic stimulus while maintaining a contractile response to other antagonists[3]. Despite this controversy it is clear that the endothelium can modulate the acute HPV response via alterations of the release of vasoconstrictors and vasodilators[3]. In contrast to acute HPV (first phase), in which the role of endothelium is not clear, most investigations have found that the endothelium plays an essential role during sustained HPV[23, 24]. Removal of the endothelium significantly attenuates sustained HPV, but does not have any effect on $[Ca^{2+}]_i$ concentration within the PASMC. This finding suggests that the endothelium regulates Ca^{2+} sensitization of precapillary PASMC during sustained hypoxia[23].

1.1.2. Mechanisms of HPV

Despite the intensive research of the mechanism of HPV in the past decades, the exact O_2 sensor and the underlying signal transduction pathway have not been fully identified and significant controversy remains[1, 25]. Within the molecular mechanism of HPV, three main parts such as O_2 sensors, mediators and effectors have been distinguished (Figure 2)[3]. As possible O_2 sensors mitochondria[13, 26, 27], nicotinamide adenine dinucleotide phosphate (NADPH)-oxidases[28, 29], cytochrome P450[30] and potassium channels[31] have been proposed. The mitochondria or NADPH-oxidases use O_2 as substrate; therefore they could directly sense the lack of O_2[1, 3]. On the other hand, O_2 can interact with different proteins, *e.g.* heme-containing protein[32] or can directly modify the sulphur-containing residues of proteins (including organelles and proteins described above)[31] leading to reversible alteration of their structure and/or conformation that may initiate the HPV signaling pathway[1]. Many potential O_2 sensors have been tested in experiments during acute hypoxia. Roth *et al.*[33] provided evidence that a deletion of the heme-oxygenase-2 (HO-2) gene, an enzyme that catalyses heme degradation, does not abolish HPV in mice. The studies on the role of NADPH oxidases in genetically modified mice have demonstrated conflicting results. Archer *et al.* published evidence that knockout of gp91phox, the heme-containing protein of the NADPH oxidase, did not have any influence on acute HPV[29]. In contrast, Weissmann *et al.* demonstrated a significant reduction of the hypoxic response in isolated perfused mouse lungs from mice with genetic knockout of the cytosolic p47 subunit of NADPH oxidases, whereas the response to a thromboxane mimetic was preserved in those mice[28].

Reactive oxygen species (ROS)[13], the cellular redox state[34], the adenosine monophosphate (AMP) - adenosine triphosphate (ATP) ratio[35], and Ca^{2+} homeostasis have been suggested as mediators of HPV[21]. The effectors of HPV are ion channels (*e.g.* K_v (potassium) channels), intracellular Ca^{2+} stores and different protein kinases[3]. In particular, increase of $[Ca^{2+}]_i$ concentration is a key event in the HPV

response[3]. $[Ca^{2+}]_i$ can be increased by both influx of extracellular Ca^{2+} via SOCC (store-operated calcium channels) and VOCC (voltage operated calcium channels), or release of Ca^{2+} from intracellular stores such as sarcoplasmic reticulum (SR) via RyR (ryanodine-sensitive receptors)[36] during acute hypoxia. Ultimately, the acute hypoxia-induced increase of cytosolic $[Ca^{2+}]_i$ concentration activates myosin light chain kinase causing actin-myosin interaction and PASMC contraction. Mitochondria can be O_2 sensor organelles and can mediate HPV via the alteration of the ROS production, $[Ca^{2+}]_i$ and ATP homeostasis[1, 2, 13, 36-38]. One obvious and important conclusion that can be made from the available literature about HPV is that PASMC contain all three parts of the HPV mechanism: the initial sensor of hypoxia, its mediator and the effector mechanism[1, 3].

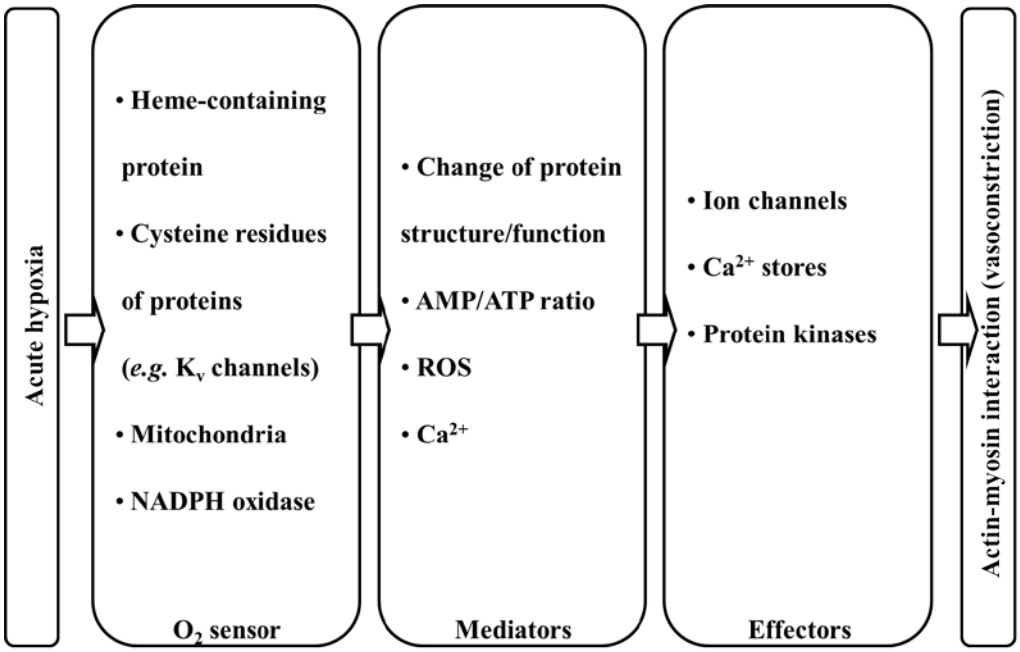

Figure 2. Mechanisms of acute hypoxic pulmonary vasoconstriction (HPV).
The trigger, acute hypoxia, is sensed by various possible O_2 sensors and translated by different mediators to effectors ultimately resulting in actin-myosin interaction within PASMC, and finally leading to the vasoconstriction of the small precapillary pulmonary arteries[1, 3].
Abbreviations: AMP/ATP ratio - adenosine monophosphate/adenosine triphosphate ratio; Ca^{2+} - calcium; K_v channels - potassium channels; NADPH oxidase - nicotinamide adenine dinucleotide phosphate-oxidase; O_2 - oxygen; ROS - reactive oxygen species.

1.2. Pulmonary hypertension (PH)

1.2.1. Definition and characteristics of PH

In contrast to acute hypoxia, chronic hypoxia results in pathological alterations of the pulmonary vasculature and can lead to the development of pulmonary hypertension (PH)[1, 25, 39-41] (Figure 3). Chronic hypoxia may be the result of respiratory diseases such as COPD (Chronic Obstructive Pulmonary Disease), lung fibrosis, or residence in high altitude and *etc*[1]. At an altitude of 3000m, which is often

encountered in ski resorts, the inspired pO_2 (partial pressure of O_2) is only about 70% of that at sea level and at an altitude of 5000m, the highest point at which humans can live, the inspired pO_2 is 50% of that at sea level[42]. By definition, a mean PAP greater than 25 mmHg at rest is considered as PH[43]. Besides chronic hypoxia, a number of different pathological stimuli can lead to the development of PH[44]. Therefore, PH is defined as a severe progressive disorder which is the outcome of different causes and is characterized by the extensive narrowing of the pulmonary vascular bed, leading to an increase in pulmonary vascular resistance, which ultimately produces compensatory right ventricular (RV) hypertrophy and may result in heart failure and premature death[45].

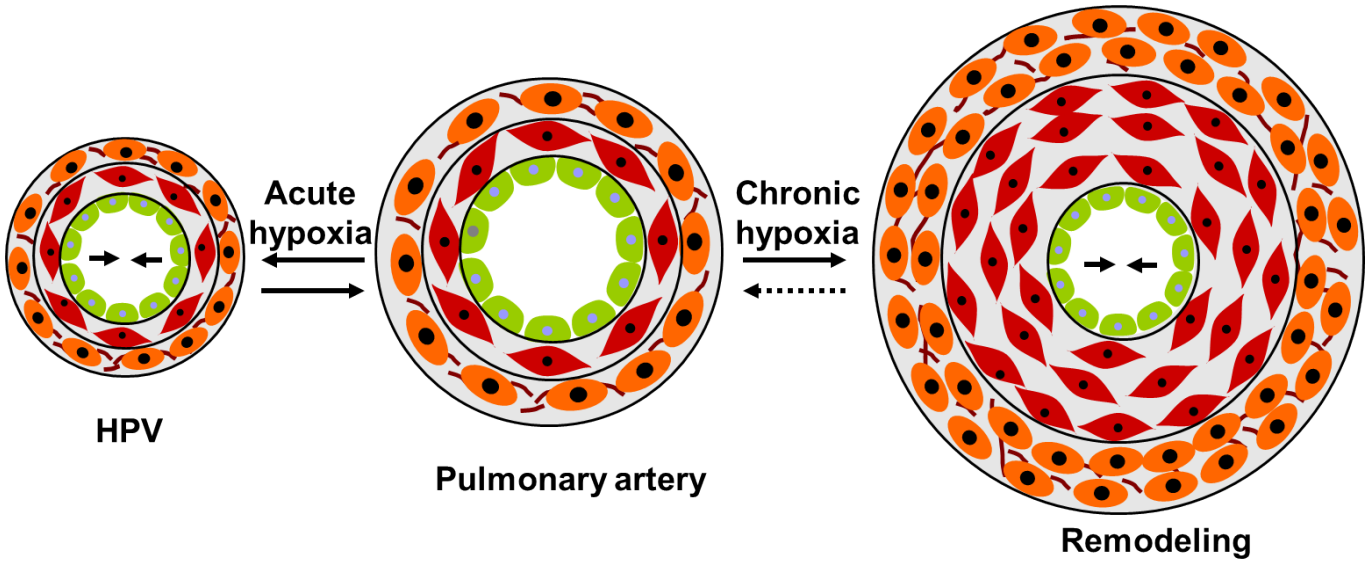

Figure 3. Effect of acute and chronic hypoxia on the pulmonary vasculature.
Acute hypoxia is a trigger of HPV for optimization of the ventilation/perfusion ratio. Chronic hypoxia leads to pathological thickening of the vascular wall resulting in narrowing of the vascular lumen (pulmonary vasculature remodeling), increase of pulmonary pressure and PH[25, 41]. HPV is a completely reversible process, whereas pulmonary vasculature remodeling is only partially reversible[46].
Green - endothelial cells, red - smooth muscle cells and brown - fibroblasts.
Abbreviations: HPV – hypoxic pulmonary vasoconstriction; PH – pulmonary hypertension.

Pulmonary arterial hypertension was first described by Romberg in 1881. The term “primary pulmonary hypertension” was used to define the clinical features and hemodynamics of patients who had an increased PAP without evident etiology of PH[47]. Primary pulmonary hypertension is now referred to as idiopathic pulmonary arterial hypertension (IPAH). IPAH is a very rare disease affecting only a few persons per million and most frequently affecting otherwise normal middle aged women[48]. Prior to the development of treatments for PH, IPAH was a fatal disease with a poor prognosis and average survival of 2.8 years[49]. Other forms of PH occur more frequently than IPAH. For example PH can occur in 50.2%[50, 51] of patients with severe COPD which affects approximately 6% of the total population in

USA[52]. Moreover, PH in COPD is an independent prognostic factor associated with low survival rate[53]. Additionally, 10% of patients with systemic sclerosis which has a rate of approximately about 7-489 cases per million population, will develop PH[54, 55].

The main histopathological finding in PH is pulmonary vascular remodeling (Figure 4). Pulmonary vascular remodeling is an imbalance between proliferation (hyperplasia) and apoptosis, where proliferation of endothelial cells (EC), PASMC and fibroblasts is increased, while apoptosis of those cells is decreased[39, 41]. Recently, it has been suggested that in early stages of PH increased apoptosis can be initial trigger for the selection of apoptosis-resistant EC[56]. The impact of different vascular cells on pulmonary vasculature remodeling is dependent on the form, severity and stage of PH. In addition, pulmonary vascular remodeling is characterized by hypertrophy (increased cell growth) of vascular cells, migration of PASMC, as well as recruitment and differentiation of local fibroblasts, pericytes, mononuclear cells and EC[41]. It has been shown that bone marrow-derived cells can be incorporated into the pulmonary vasculature (neoplasia)[57]. Besides these mechanisms, remodeling is aggravated by the loss of precapillary vessels[58] and *in situ* thrombosis[59].

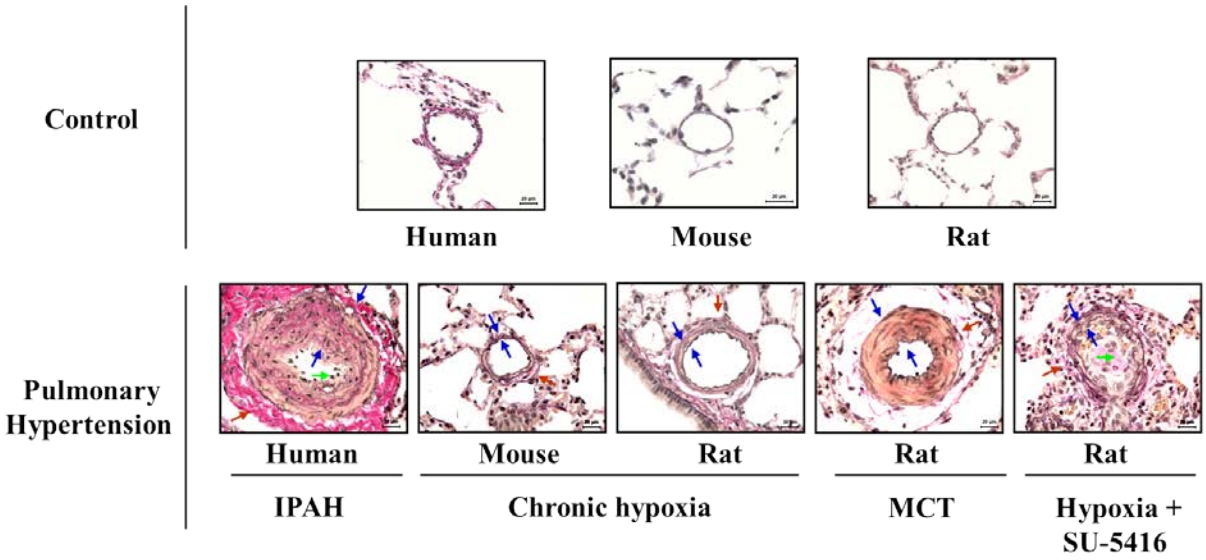

Figure 4. Morphological changes of pulmonary arteries in pulmonary hypertension (PH).
PH is characterized by pulmonary vasculature remodeling which is a result of thickening of the arterial wall. All lung samples are stained by elastic van Gieson where elastic fibres are blue/black/brown; nuclei are black/brown; collagen fibers are red; media, epithelia, nerves, erythrocytes are yellow. Pictures were made by microscopy with 40x magnification. Blue arrows depict medial layer hypertrophy; green arrows depict EC proliferation; red arrows depict adventitial layer remodeling.
Abbreviations: Control - lungs from control (healthy) animals and donor human lung; IPAH - idiopathic pulmonary arterial hypertension; Chronic hypoxia - chronic exposure of rats or mice to 10% O_2 hypoxia; MCT - monocrotaline-induced PH in rats; Hypoxia + SU-5416 - exposure of rats to chronic hypoxia combined with SU-5416 injection (VEGF 2 receptor antagonist).

Patients with IPAH and other specific forms of PH, *e.g.* PH associated with left-to-right shunt or human immunodeficiency virus (HIV) have a very specific vasculopathy with the appearance of plexiform lesions, which consist of a network of vascular channels surfaced by EC that completely obliterate the vascular lumen[39].

1.2.2 Classification of PH

The first classification of PH was proposed in 1973 at the international conference on primary PH sanctioned by the World Health Organization[44, 60], and divided PH only in two categories, primary PH with unknown specific causes or risk factors of PH and secondary PH with the presence of specific causes or risk factors of PH[39]. The updated Dana Point classification for PH (2008, the Fourth World Symposium on PH) is based on the consensus of an international assembly of experts (Table 1).

This new classification scheme stratifies PH into 5 groups by considering similarities into pathophysiological mechanisms, clinical manifestations, and therapeutic approaches. These groups are: 1st - pulmonary arterial hypertension; 2nd - PH associated with left-sided heart diseases; 3rd - PH related with hypoxia/lung diseases, 4th - thromboembolic PH and 5th - PH with unclear multifactorial mechanisms[44] (Table 1). In 2013, at the Fifth World Symposium on PH held in Nice (France), a new classification of PH was proposed with only minor modifications to the Dana Point classification. However, the exact recommendations from this symposium have not yet been published.

Table1 Updated Clinical Classification of Pulmonary Hypertension, Dana Point, 2008[60]

1. Pulmonary arterial hypertension (PAH)
1.1. Idiopathic PAH
1.2. Heritable PAH
1.2.1. BMPR2
1.2.2. ALK1, endoglin (with or without hereditary hemorrhagic telangiectasia)
1.2.3. Unknown
1.3. Drug- and toxin-induced PAH
1.4. PAH associated with
1.4.1. Connective tissue diseases
1.4.2. HIV infection
1.4.3. Portal hypertension
1.4.4. Congenital heart diseases
1.4.5. Schistosomiasis
1.4.6. Chronic hemolytic anemia
1.5 Persistent pulmonary hypertension of the newborn
1'. Pulmonary veno-occlusive disease (PVOD) and/or pulmonary capillaryhemangiomatosis (PCH)
2. Pulmonary hypertension owing to left heart disease
2.1. Systolic dysfunction
2.2. Diastolic dysfunction
2.3. Valvular heart disease
3. Pulmonary hypertension owing to lung diseases and/or hypoxia
3.1. Chronic obstructive pulmonary disease
3.2. Interstitial lung disease
3.3. Other pulmonary diseases with mixed restrictive and obstructive pattern
3.4. Sleep-disordered breathing
3.5. Alveolar hypoventilation disorders
3.6. Chronic exposure to high altitude
3.7. Developmental abnormalities
4. Chronic thromboembolic pulmonary hypertension (CTEPH)
5. Pulmonary hypertension with unclear multifactorial mechanisms
5.1. Hematologic disorders: myeloproliferative disorders, splenectomy
5.2. Systemic disorders: sarcoidosis, pulmonary Langerhans cell histiocytosis: lymphangioleiomyomatosis, neurofibromatosis, vasculitis
5.3. Metabolic disorders: glycogen storage disease, Gaucher disease, thyroid disorders
5.4. Others: tumoral obstruction, fibrosing mediastinitis, chronic renal failure on dialysis

Abbreviations: BMPR2 - Bone morphogenetic protein receptor 2; ALK1 - activin receptor-like kinase 1

1.2.3. Animal models of PH

Currently, various techniques are used in different animals to induce experimental PH, including the application of pharmacologic and toxic agents [*e.g.* bleomycin, monocrotaline (MCT), and smoke exposure], genetic manipulations, and exposure to environmental factors (*e.g.* hypoxia) or surgical interventions (*e.g.* closure of the ductus arteriosus)[39]. All of these approaches are proposed to simulate the different groups of PH (Table 2)[39].

Table 2. Animal models of PH and PH classification*

PH Group	Animal Models
1. Pulmonary arterial hypertension	Monocrotaline injection (MCT)[61]; MCT + pneumonectomy[62]; BMPR2 knockout[63]; IL-6 Tg^+mice[64]; IL-13 Tg mice[65], Fawn-hooded rat[34]; S100A4 overexpressing mice[66]; SHIV-nef-infected macaques[67]; Chronic hypoxia + SU-5416[68]; Schistosomiasis[69]; Left-to-right shunt[70], closure of the ductus arteriosus[71]
2. Pulmonary hypertension owing to left heart disease	Congestive heart failure models[72]
3. Pulmonary hypertension owing to lung diseases and/or hypoxia	Chronic hypoxia[73], chronic hypoxia + SU-5416[68]; Intermittent hypoxia[74]; Cigarette smoke exposure[75]; Bleomycin[76]; 5-HTT overexpression[77]
4. Chronic thromboembolic pulmonary hypertension	Repeated microembolization with microspheres[78]
5. Pulmonary hypertension with unclear multifactorial mechanisms	?

*modified from Pak O. *et al*[39].

Abbreviations: BMPR2 - Bone morphogenetic protein receptor 2; IL-6 Tg^+ - transgenic mice over-expressing Interleukin 6; IL-13 Tg - transgenic mice over-expressing Interleukin 13; S100A4 overexpressing mice - mice over-expressing S100A4, a member of the S100 family of small calcium binding proteins; SHIV-nef-infected macaques - macaques infected with a chimeric viral construct containing the HIV (Human immunodeficiency virus) nef (Negative Regulatory Factor) gene; SU-5416 - VEGF (Vascular Endothelial Growth Factor) 2 receptor antagonist; 5-HTT -5-Hydroxytryptamine transporter protein.

The most universally used animal models of PH, the so-called classical animal models of PH, are the chronic exposure of different animals to normobaric/hypobaric hypoxia and the injection of MCT in rats[39]. Chronic exposure (usually 4-5 weeks) of animals to hypoxia leads to an elevation in PAP, vascular remodeling and RV hypertrophy[33] (Figure 4). The MCT model in rat was first suggested more than 50 years ago by Lalich and Merkow[79]. MCT is a phytotoxin, which is present in the seed and vegetation of the plant *Crotalaria spectabilis* and is activated by mixed function of oxidases (mostly by the cytochrome P450) in the liver to form the reactive compound MCT-pyrrole which affects the pulmonary vasculature and triggers the remodeling process in rats[39] (Figure 4). In contrast to the hypoxic model that mimics group III of the Dana Point classification of PH, the MCT model has some features of group 1 of this classification[39]

All classical models of PH (MCT injection and chronic hypoxic exposure) lack the specific pathological characteristics of IPAH, namely the plexiform lesions and neointima formation[39]. Therefore, it was suggested that the combination of an alteration of VEGF (Vascular Endothelial Growth Factor) signaling and exposure to chronic hypoxia might mimic the neointima formation. It was successfully demonstrated

that pharmacologic inhibition of the VEGF receptor 2 combined with chronic hypoxia results in severe PH, which has, similar to human PH, vasculopathy - neointima formation[68] (Figure 4). Inhibition of the VEGF receptor 2 in this model serves as the initiating factor leading to apoptosis of EC and therefore to selection of apoptosis-resistant EC which can contribute to plexiform lesion formation[56].

Although the animal models described above have been proven to be useful for the investigation of signaling pathways which contribute to pulmonary vascular remodeling in PH, there is no "ideal" animal model of PH[39]. All existing animal model of PH lack some important features displayed in the human disease[39].

1.2.4 Pathogenesis of PH

The past few decades have witnessed a remarkable increase in the knowledge of the cellular and molecular mechanisms that are responsible for pulmonary vascular remodeling in PH, especially after Cournand and Richards pioneered right-heart catheterization[80]. However, the complex picture of PH pathogenesis is still not completely resolved[25]. Despite the diverse etiology of PH and its underlying signaling pathways, morphologically all groups of PH share similarities and are characterized by abnormal pulmonary vasculature remodeling affecting all three layers of the blood vessel wall: the adventitia, the media and the tunica intima, with maximal impact on the medial layer[81, 82] (Figure 4). Genetic mutations[83-85], an imbalance of vasoconstrictors and vasodilators[86-88], growth factors[89], cytokines and chemokines[90, 91] could all be initial triggers of pulmonary vasculature remodeling in PH (Figure 5). These initial triggers of PH determine which of the numerous underlying molecular pathways are at play, including an activation of various transcriptional factors [*e.g.* HIF (hypoxia inducible factor)[34], FOXO1 (forkhead box protein O1)[92], NF-κB (nuclear factor kappa-light-chain-enhancer of activated B cells)[93], PPARγ (peroxisome proliferator-activated receptor)[94]], change of $[Ca^{2+}]_i$ concentration[40], alterations of mitochondrial function[34] , *etc*. For example, various vasoconstrictors increase the concentration of $[Ca^{2+}]_i$ which is a key regulator of PASMC contraction and proliferation in PH[37, 40, 95] (Figure 5). In the molecular pathways of pathogenesis of PH the mitochondria can play an important role via inhibition of respiration, modification of mitochondrial membrane potential ($\Delta\psi_m$), cellular metabolism (control anaerobic glycolysis) alteration of ROS production and Ca^{2+} homeostasis[37, 40, 82, 96] (Figure 5).

It was shown that ~60% of patients with familial pulmonary arterial hypertension (FPAH) and 10-20% of patients with sporadic IPAH were heterozygous for a mutation in bone morphogenetic protein receptor type II (BMPRII)[83, 84]. The presence of BMPRII mutations is much less frequent in patients (up to 6-8%) with PH due to congenital left-to-right shunt[85]. BMPRII is a member of the TGF-β (transforming growth factor-beta) superfamily and can translate a pathological signal through SMAD (a family of proteins related to *Drosophila* "mothers against decapentaplegic" (Mad) and *Caenorhabditis elegans* Sma)[97], p38

(p38 mitogen-activated protein kinases)[98], pERK (phosphorylated extracellular signal-regulated kinase), JNK (c-Jun N-terminal kinases) and AKT (protein kinase B)[99]. Mutations in the activin-receptor-like kinase 1 (ALK1) gene that is also a part of the TGF-β superfamily can also trigger PH development in association with hereditary hemorrhagic teleangiectasia[100]. One downstream effector of the BMPRII pathway is PPARγ which has anti-proliferative, anti-inflammatory, proapoptotic, and direct vasodilatory effects in the vasculature[94]. Recently, it has been demonstrated that altered PPARγ signaling can participate in development of PH[94].

Polymorphisms in genes that differ from normal by a single alternative nucleotide resulting in a change of the function/location of the encoded protein (SNPs, single nucleotide polymorphisms) may also explain the susceptibility to PH among humans. For example, a correlation between I/D (insertion/deletion) polymorphism of ACE (angiotensin converting enzyme) and high altitude PH was shown in the Kyrgyz population[101]. Yu *et al.* published a study demonstrating that 54(C→G) SNP of TRPC6 (Transient receptor potential cation channel, subfamily C, member 6) gene may predispose individuals to an increased risk of IPAH by linking the aberrant TRPC6 transcription polymorphism with abnormalities in NF-kB and inflammatory pathways[93].

An imbalance between pulmonary artery vasoconstrictors and vasodilators has been suggested as a mechanism for PH pathogenesis[40]. In patients with IPAH the level of vasodilators [prostaglandin I2[86] and nitric oxide (NO)[87]] was reduced whereas the level of vasoconstrictors (thromboxane[86] and endothelin-1[88]) was increased. Experimental studies in chronic hypoxia-induced PH documented that endothelin-1 was important for an increase of PASMC proliferation[102].

Several growth factors could play an important role in vascular remodeling in PH such as VEGF[103], PDGF (platelet-derived growth factor)[104], EGF (epidermal growth factor)[105], bFGF (insulin-like growth factor)[106] and IGF-1-(insulin-like growth factor)[107]. For example, expression of PDGF and its receptor (PDGFRs, platelet-derived growth factor receptors) was increased in the pulmonary vasculature of IPAH patients[89] and application of tyrosine kinase inhibitors reversed the experimental remodeling in chronic hypoxia-induced PH and MCT-induced PH in rats[89, 104].

In addition, inflammation appears to play a significant role in the chronic hypoxia-induced remodeling process in human disease[82] and in experimental models of PH[108, 109]. Increased circulating levels of monocyte chemoattractant protein-1, tumor necrosis factor, IL (interleukin)-1β and IL-6 were discovered in IPAH patients[82]. Overexpression of IL-6 induced severe PH[64], while IL-6 deficiency protected mice against chronic hypoxic exposure[109]. Moreover, lung-specific IL-13 over-expressing transgenic (Tg) mice demonstrated a spontaneously developing PH phenotype with increased expression and activity of arginase 2 (Arg2)[65]. Arg2 is an enzyme that utilizes the arginine, and therefore decreases NO synthesis by the NO synthase in precapillary PASMC (L-arginine is a substrate for nitric oxide synthase). Several

chemokines have an impact on PH, *e.g.* chemokine ligand 2 increases a migration and proliferation of PASMC of IPAH patients[110].

Various therapies of PH have become available; however, modern treatments can alleviate the symptoms and even revert the characteristic vascular remodeling process, but cannot cure the disease[39].

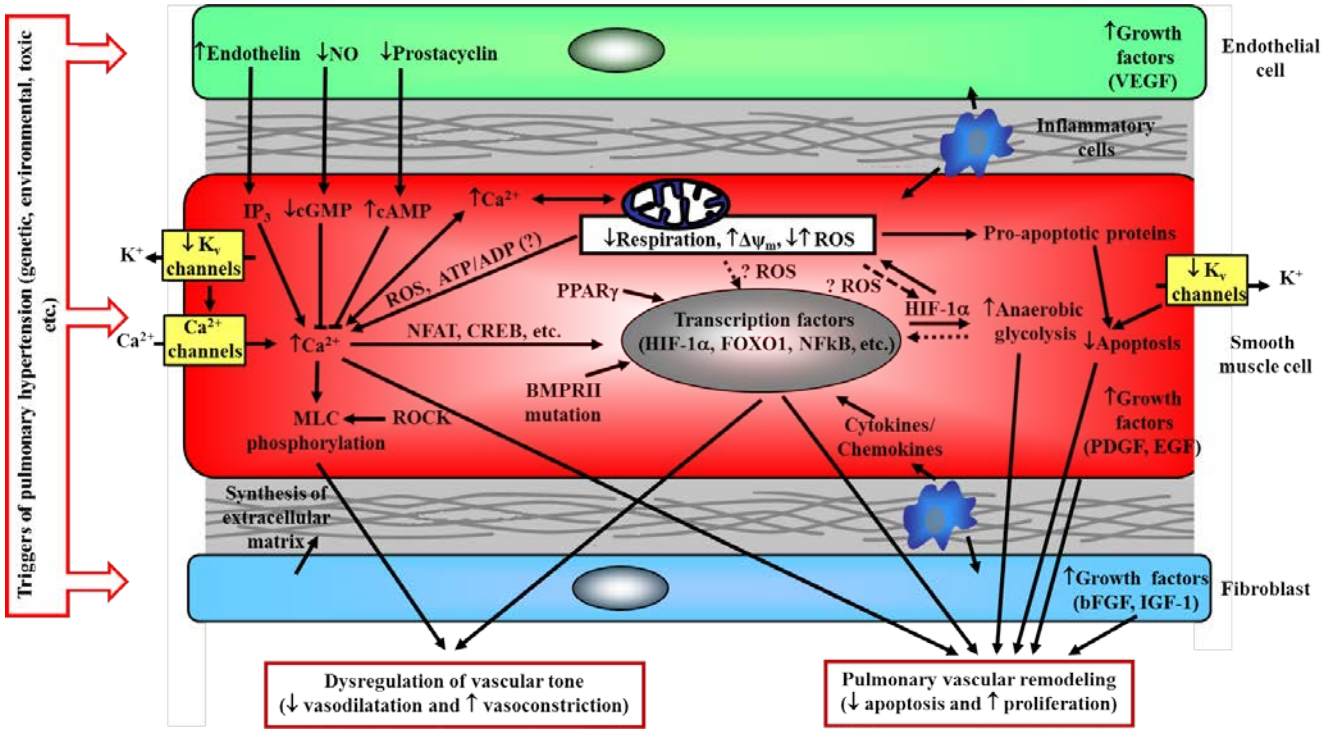

Figure 5. Role of pulmonary arterial smooth muscle cells (PASMC) in the pathogenesis of pulmonary vasculature remodeling in PH. Pulmonary vasculature remodeling is a result of an imbalance between proliferation and apoptosis of all three layers of the pulmonary arterial wall[25, 39, 41]. The most prominent remodeling occurs within the medial layer of pulmonary vessels[40]. Different pathological triggers stimulate the various molecular pathways (inflammation, Ca^{2+} homeostasis, growth factors, disbalance of vasoconstrictors and vasodilatators, mitochondria, transcription factors including HIF and *etc*.) within endothelial cells (EC), PASMC and fibroblasts to promote their proliferation and attenuate apoptosis[25, 39-41, 58, 82]. Dysregulation (vasoconstriction) of the vascular tone can contribute to the severity of PH[82].

Mitochondria play an important role in pulmonary vasculature remodeling. Factors triggering the development of PH may alter the level of mitochondrial ROS and ATP production, oxidative phosphorylation and release of proapoptotic proteins[37, 38, 40, 95]. Ca^{2+} and ROS can be mediators of different molecular pathways linking the alteration of mitochondrial function with the increased proliferation of PASMC. For example, alterations in the redox state may lead to HIF stabilization which may promote metabolic alterations, including the increase of anaerobic glycolysis[38, 40, 95].

Abbreviations: VEGF - vascular endothelial growth factor; PDGF - platelet-derived growth factor; EGF - epidermal growth factor; IGF-1 -insulin-like growth factor; bFGF - basic fibroblast growth factor; BMPRII - bone morphogenetic protein receptor type II; CREB - cAMP response element-binding protein; Ca^{2+} - calcium; cGMP - cyclic guanosine monophosphate, cAMP - cyclic adenosine monophosphate, FOXO1 - Forkhead box protein O1; HIF-1α - alpha subunit of hypoxia inducible factor; NFAT - Nuclear factor of activated T-cells , NF-κB - nuclear factor kappa-light-chain-enhancer of activated B cells; NO – nitric oxide; pERK - phosphorylated extracellular-signal-regulated kinases; MLC - myosin light chain; ROS - reactive oxygen species; $\Delta\psi_m$ - mitochondrial membrane potential; K^+ - potassium; K_v - potassium channels; IP_3 - Inositol trisphosphate; PPARγ - peroxisome proliferator-activated receptor gamma, ROCK - Rho-associated protein kinase.

1.3. Role of mitochondria in HPV and PH

For some time, mitochondria have been suggested to be O_2 sensing organelles in hypoxia-dependent regulatory processes like HPV and chronic hypoxia-induced PH[1, 38]. The idea that mitochondria could act as O_2 sensors arose from the fact that mitochondria consume more than 90% of O_2 within the cell[111, 112]. O_2 limitation can affect different aspects of mitochondrial function such as respiratory rate, concentration of ATP, cytosolic [NADH]/[NAD+] redox state (reduced form of nicotinamide adenine dinucleotide/nicotinamide adenine dinucleotide), mitochondrial Ca^{2+} uptake and alterations in ROS production[1, 38]. An additional argument in favor of the importance of functional mitochondria in O_2 sensing comes from studies of immortalized neonatal adrenomedullary chromatin cells with normal functional or impaired mitochondria. Those cells, which lack functional mitochondria, fail to respond to the hypoxia[113, 114].

Hence, mitochondria have been considered important factors in non-hypoxia dependent pulmonary vascular remodeling because they participate in numerous proliferative and antiapoptotic signaling pathways[1]. Further support for the role of mitochondria comes from the observation of a child with a mitochondrial A3243G point mutation exhibiting severe PH[115] and from patients with mitochondrial respiratory chain abnormalities showing PH[116].

1.3.1. Mitochondrial membrane potential ($\Delta\psi_m$)

Mitochondrial respiration and ATP synthesis are two crucial pathways lying at the heart of cellular metabolism[117]. During respiration, energy derived from electrons passing along multi-subunit enzyme complexes of the electron transport chain (respiratory chain), which are embedded in the inner mitochondrial membrane (IMM), is used to pump the protons (H^+) against their concentration gradient from the matrix to the intermembrane space across the non-permeable IMM[118, 119]. Protons extrusion generates the electrochemical proton gradient ($\Delta\mu H^+$) across the IMM that results in accumulation of net protons within the intramembrane space. Ten protons are extruded for each electron pair passing from NADH to O_2 by complexes, I, III and IV of the electron transport chain[118]. In bioenergetics, $\Delta\mu H^+$ is a thermodynamic measure of the energy that is necessary to remove a proton gradient from equilibrium and is expressed in kilojoule per mole (kj mol^{-1}). The unit of $\Delta\mu H^+$ (kj mol^{-1}) can be transferred into the unit of electric potential (mV) which is referred to as proton-motive force (Mitchell's "proton-motive force") and expressed by the symbol Δp[119]. Δp consists of an electrical, $\Delta\psi_m$ (mitochondrial membrane potential, ~150-180 mV) and a chemical component, ΔpHm (mitochondrial pH gradient, ~30-60 mV) across the IMM. Thus Δp is equal approximately to 180-220 mV[117] (Figure 6). Because it is more easily measured in various cells, $\Delta\psi_m$ is often incorrectly used for expression of Δp. As written above, the $\Delta\psi_m$ is the predominant force (or central intermediate) in the oxidative phosphorylation and contributes

approximately 80-85% of Δp[120, 121]. In addition to being the central intermediate of aerobic energy production, $\Delta\psi_m$ is a driving force of other physiological process within mitochondria, including Ca^{2+} uptake and heat production in brown fat[122].

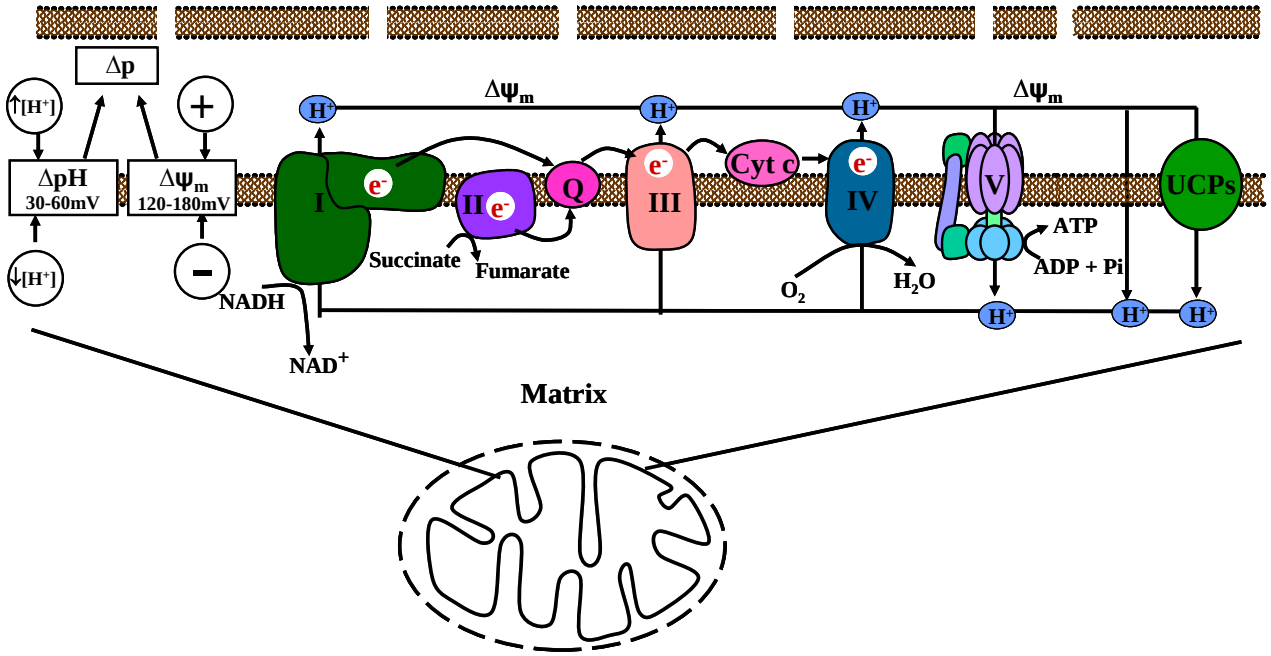

Figure 6. Mitochondrial membrane potential ($\Delta\psi_m$).

$\Delta\psi_m$ is the most important part of Mitchell's "proton motive force" (makes up to 85%) and is produced by extrusion of protons (H^+) from the mitochondrial matrix to the intermembrane space, using an energy gradient from electrons passing along the respiratory chain[119-121]. The proton motive force (Δp) drives the synthesis of ATP by ATP synthase[119]. Some protons can escape the intermembrane space via either uncoupling proteins (UCPs) or passive proton leak back to the matrix that decreases $\Delta\psi_m$[123]. Thus, the proton circuit consist of three modules: 1) Complex I-IV, the "substrate oxidation" module, 2) Complex V, the "ATP turnover" module and 3) the "Proton leak" module[118].

Abbreviations: I, II, III, IV and V - respiratory chain complexes; Q - coenzyme Q; Cyt C - cytochrome c; $\Delta\psi_m$ - mitochondrial membrane potential; ΔpH - proton gradient; Δp is Mitchell's "proton-motive force"; ADP - adenosine diphosphate; ATP - adenosine triphosphate; NAD^+ - nicotinamide adenine dinucleotide; NADH - reduced form of NAD^+; Pi - phosphoric acid; UCPs -uncoupling proteins.

Controlled return of protons along their gradient into the mitochondrial matrix through the F_0F_1 ATP synthase, complex V of the respiratory chain, drives the conversion of adenosine diphosphate (ADP) into ATP[119]. This process is called chemiosmosis and Peter Mitchell who first described this process, was awarded by the 1978 Nobel Prize in Chemistry. Some protons can return back into the mitochondrial matrix via a proton "leak" [either passive proton leak or through uncoupling proteins (UCPs - UnCoupling Protein)] that uncouples mitochondrial respiration from ATP synthesis[123] (Figure 6).

Complexes I, III and IV of the electron transport chain together with complex V and the proton leak create a proton circuit across the IMM that is the center of bioenergetics.

1.3.2. Mitochondria as source of reactive oxygen species (ROS)

The term ROS describes a family of chemical species that are the result of incomplete reduction of O_2[124]. The first description of ROS was made by Gomberg in 1900[125]. ROS includes highly reactive free oxygen radicals such as superoxide anion ($O_2^{\bullet-}$), hydroxyl radical (HO•) and non-radicals that are either oxidizing agents and/or easily converted into radicals, such as hypochlorous acid (HOCl), ozone (O_3), singlet oxygen ($^1O_2$), and "diffusible" hydrogen peroxide (H_2O_2). There are numerous potential sources of ROS within cells such as NADPH oxidases (Nox 1-5 and Duox 1-2)[73], xanthine oxidases[126], cyclooxygenases, cytochrome P450 enzymes[127], lipoxygenases[128], NO synthases[129] and mitochondria[1] (Figure 7).

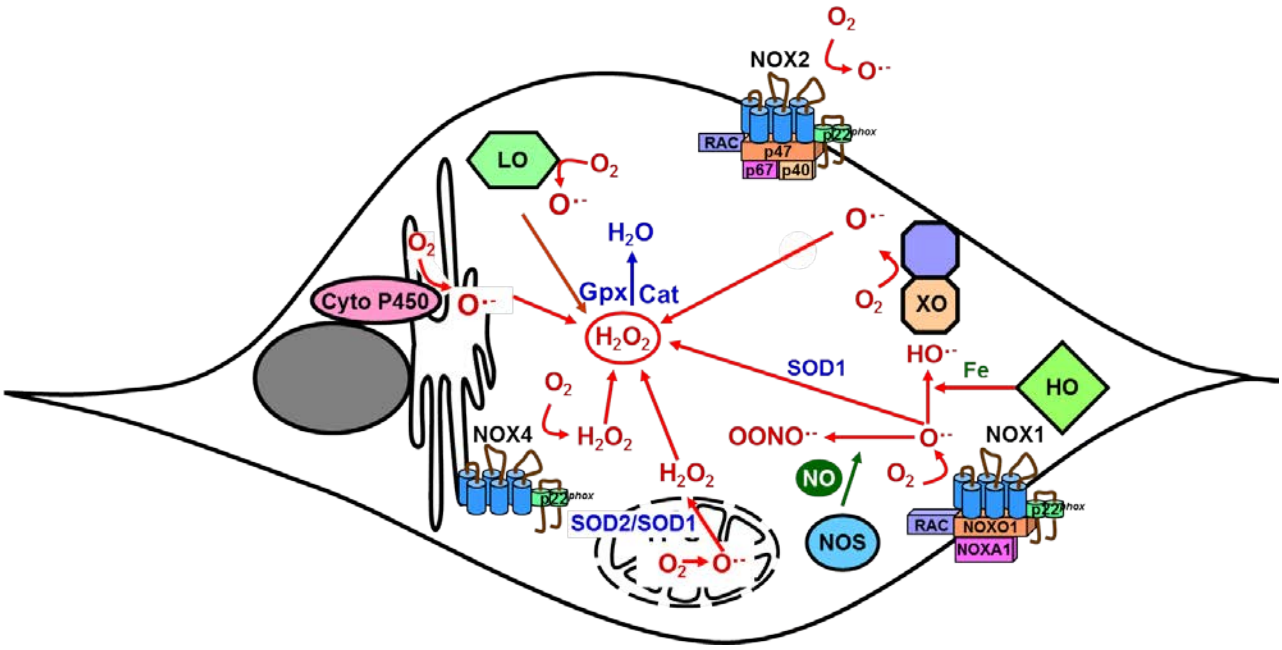

Figure 7. Scheme of possible sources of reactive oxygen species (ROS) within cells.
The cell has variety of potential sources of ROS and some of them are indicated in the scheme: mitochondria, NADPH oxidases (NOX 1, 2 and 4), lipoxygenase (LO), heme oxygenase (HO), xanthine oxidases (XO), nitric oxide synthase (NOS) and cytochrome P450 enzymes (Cyto P450) [1, 73, 124, 126-129]. The ROS-defense systems within cells comprises several enzymes specialized on removal of $O_2^{\bullet-}$ or H_2O_2 including superoxide dismutase 2 (mitochondrial SOD2), superoxide dismutase 1 (cytosolic SOD1), catalase (Cat), and glutathione peroxidases(Gpx)[130, 131].
Abbreviations: H_2O_2 - hydrogen peroxide; HO•·- Hydroxyl radical; Fe - ferrum; $O_2^{\bullet-}$ superoxide anion; $OONO^-$ peroxynitrite; NO - nitric oxide.

Previously, more than 50 years ago, ROS were considered only as toxic substances, but recently, evidence has been published suggesting that ROS can participate in a wide range of different physiological cellular

processes including maintenance of intracellular homeostasis, adaptation to cellular stress, and participation in whole organ function[124, 130, 132, 133]. In these processes an increase or decrease of ROS can ultimately result in enhancement of proliferation or migration of cells instead of their damage[73, 124]. Despite the fact that the research field about ROS as a messenger molecule is rapidly expanding, many aspects of cellular ROS metabolism are not yet well understood. Mitochondria are generally considered to be the most important source of ROS within a cell[1, 38] (Figure 8). In particular, it is a well-known fact that one-electron reduction of O_2 is thermodynamically favorable for most oxidoreductases[132]. The first report showing that mitochondria can produce ROS was published in 1966[134]. During energy transduction, a small number of electrons "leak" to O_2 forming the $O_2^{\bullet-}$ by one-electron reduction of O_2. Reduction of molecular O_2 that has two unpaired electrons with parallel spin in different antibonding orbitals leads to transfer of a lone electron to its antibonding orbital. Approximately 90-95% of the O_2 consumed by mammalians is utilized to supply cellular energy through oxidative phosphorylation[111, 112] and ~0.2% to 1-2% of O_2 consumed by the mitochondrial electron transport system is used to produce ROS[135]. The concentration of $O_2^{\bullet-}$ within the mitochondrial matrix is in the range 10-200 pM[130]. This wide variance in the range reported of what percentage of cellular O_2 consumption ultimately is used for ROS production can be explained by the discrepancy in methodological approaches used to measure these values. The data from *in vitro* experiments based on isolated mitochondria indicate that 1-2% of cellular O_2 is used to produce ROS, while more physiological experiments in whole cells show that only 0.2% of cellular O_2 consumption results in ROS emission within mitochondria[136]. This discrepancy may at least in part be caused by the presence of ROS detoxifying systems in intact cells and concentration of ROS regulatory components like Ca^{2+}, NADH/NAD or the $\Delta\psi_m$. The specific sites of electron leakage are not known with certainty, but most scientific literature suggests that complexes I and III are predominantly responsible for $O_2^{\bullet-}$ production within mitochondria[131]. Complex I (NADH:ubiquinone oxidoreductase, composed of ~45 subunits) produces $O_2^{\bullet-}$ probably only into the matrix of mitochondria and complex III (Ubiquinol:cytochrome c oxidoreductase, composed 11 subunits) can generate $O_2^{\bullet-}$ on both sides of the IMM into the matrix and/or into the intermembrane space of mitochondria[137]. The relative importance of these two sites varies in different tissue and species[138]. In mitochondria isolated from heart and lung, complex III is thought to be responsible for most of ROS production, and in mitochondria isolated from brain, complex I appears to be the primary source of ROS under normal conditions[132]. In addition, there are some publications showing that complex II of the respiratory chain also can generate $O_2^{\bullet-}$ under certain conditions[139]. There are other sites of ROS production in the mitochondria, beyond the electron transport chain including α-ketoglutorate dehydrogenase and dihydroorotate dehydrogenase,[130]. However, their impact on mitochondrial ROS generation is low and their physiological significance unclear. $O_2^{\bullet-}$ produced by mitochondria is too highly charged to readily cross the IMM. However, $O_2^{\bullet-}$ that is produced

by complex III and released into the intermembrane space may be carried to the cytoplasm via voltage-dependent anion channels (VDAC)[140]. The discovery of a specific mitochondrial superoxide dismutase (SOD2) confirmed the biological significance of mitochondria in $O_2^{\bullet-}$ production within cells.

The ROS-defense systems within mitochondria comprise several enzymes specialized in the removal of $O_2^{\bullet-}$ or H_2O_2 and non-enzymatic antioxidants[130] (Figure 8). SOD2, a manganese-dependent enzyme in the mitochondrial matrix, and superoxide dismutase 1 (SOD1), a copper or zinc-dependent enzyme in the cytosol and the intermembrane space convert $O_2^{\bullet-}$ into H_2O_2 that is further deactivated by catalase to water and O_2[130, 131]. Additionally, H_2O_2 can be deactivated by the various glutathione peroxidases to reduced glutathione and water and by the peroxiredoxins to water[131]. Thus, $O_2^{\bullet-}$ is the primordial mitochondrial ROS. H_2O_2 is more stable than $O_2^{\bullet-}$ and capable to move across membranes[121]. Cytochrome c of the respiratory chain has antioxidant property itself and it can scavenge $O_2^{\bullet-}$[141].

With regard to the above described mitochondrial ROS related systems, one should distinguish among the amount of ROS generated by mitochondria under specific conditions (physiological, pathological or artificially induced conditions), the mitochondrial location of ROS release, ROS removal by antioxidant defense systems and finally, ROS emission into different cellular compartments which is the net result of ROS production, ROS removal and ROS diffusion capacity across the mitochondrial membranes[133]. A summarized scheme of possible ROS sources and ROS-defense systems in mitochondria is shown in Figure 8.

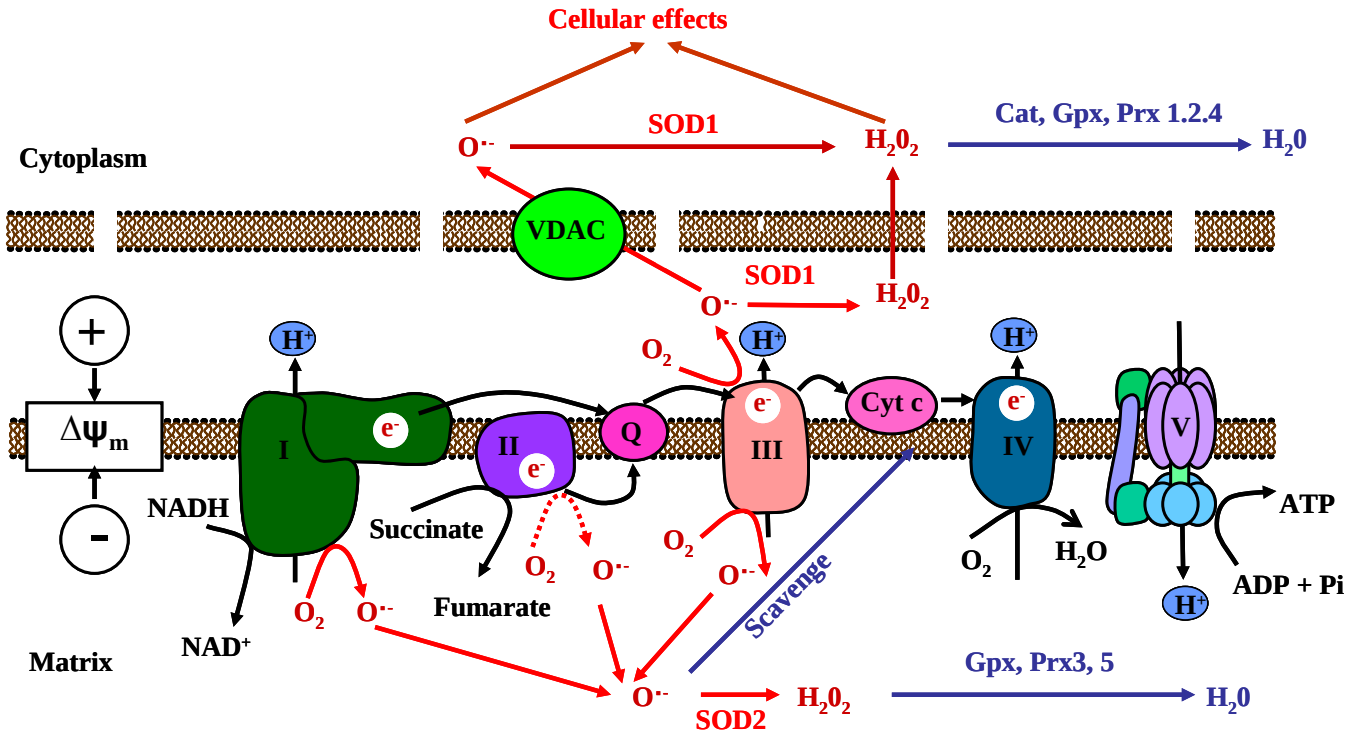

Figure 8. ROS and ROS-defense systems in mitochondria.

Complexes I and III are shown as main source of ROS[131, 132]. Complex I releases $O_2^{\bullet-}$ into the matrix[131, 137]. Complex III can release $O_2^{\bullet-}$ in both directions into the matrix and into the intermembrane space[131, 137]. Complex II likely also produces $O_2^{\bullet-}$ under certain circumstances[139]. $O_2^{\bullet-}$ produced during oxidative phosphorylation can diffuse via VDAC into the cytosol or can be transformed to H_2O_2 by SOD2 within the intermembrane space and the mitochondrial matrix, and by SOD1 within cytosol[140]. H_2O_2 is more stable than $O_2^{\bullet-}$ and is capable of moving across mitochondrial membranes[121]. The ROS-defense systems within mitochondria comprises several enzymes specialized on removal of $O_2^{\bullet-}$ or H_2O_2 and non-enzymatic antioxidants[130]. Cytochrome c of respiratory chain has antioxidant property itself and it can scavenge $O_2^{\bullet-}$[141].

Abbreviations: I, II, III, IV and V - complexes of respiratory chain; $O_2^{\bullet-}$- superoxide; H_2O_2 - hydrogen peroxide; Q - coenzyme Q; Cyt C -- cytochrome c; SOD1, 2 -- superoxide dismutase 1 and 2; Cat - catalase; Gpx glutathione; Prx 1-5 - peroxiredoxins; VDAC - Voltage-dependent anion channels.

1.3.3. $\Delta\psi_m$ and ROS

Most experimental studies demonstrate a direct relationship between the $\Delta\psi_m$ and ROS production, and show that even a slight increase of the $\Delta\psi_m$ enhances ROS emission, while a decrease of $\Delta\psi_m$ attenuates ROS release[142-144]. In 1971, Loschen *et al.* performed a pioneering experiment leading to the widely accepted concept that $\Delta\psi_m$ control ROS production in isolated mitochondria[145]. They observed a total inhibition of the succinate-induced increase of ROS production after application of an uncoupler (pentachlorophenol)[145]. An increase of $\Delta\psi_m$ by each 10mV interval doubles the mitochondrial rate of ATP production, while the rate of mitochondrial ROS emission rises exponentially in isolated

mitochondria [122]. Furthermore, Rottenberg *et al.* showed that the correlation between $\Delta\psi_m$ and the $O_2^{\bullet-}$ generation rate was much stronger than between $O_2^{\bullet-}$ generation and the proton-motive force (Δp)[146]. More recently, Starkov *et al.* verified the relationships between ROS production, NADH/NAD^+ ratio and $\Delta\psi_m$ in rat brain mitochondria [147]. He proposed that the ROS production by mitochondria was regulated both by $\Delta\psi_m$ and by the NADPH redox state[147]. $\Delta\psi_m$ can regulate the rate of ROS production in complex I[147] as well as in complex III of the respiratory chain[146]. For example, ROS production by complex III increases exponentially in yeast mitochondria at a $\Delta\psi_m$ above 140mV[146]. Additionally, ROS production within complex I caused by reverse electron flow is highly dependent on $\Delta\psi_m$ [148]. It disappears as mitochondria are uncoupled, and it cannot occur if $\Delta\psi_m$ is blocked by an inhibitor[148]. The same connection between a rise of $\Delta\psi_m$ and the increase of ROS emission was described in intact cells (for example, the uncoupler, 2,4-dinitrophenol (DNP) attenuated ROS production in rat cardiomyocytes) [149]. In summary, most scientific literature suggests that Δp provides the driving force for ATP production, while the $\Delta\psi_m$ provides the charge gradient for mitochondrial Ca^{2+} sequestration, and regulates ROS, thus controlling cellular functions[117].

There are, however, experiments that question the connection between $\Delta\psi_m$ and ROS[150, 151]. The main problem of this controversial finding is that an increase of $\Delta\psi_m$ induces the increase of ROS only under specific conditions. Under normal physiological conditions, mitochondria are in a state with non-maximum $\Delta\psi_m$ (as is always the case when ATP is being synthesized)[150]. In this scenario, ROS production is minimal, but under special conditions, the increase of $\Delta\psi_m$ can initiate an increase of mitochondrial ROS production, as has been shown *in vitro*[142-144] and *in vivo*[152-154] studies. Therefore, an increase of $\Delta\psi_m$ leads to an increase of ROS production by mitochondria most probably only under special conditions (*e.g.* stress)[142-144].

It is interesting that mitochondrial ROS production is more sensitive to uncoupling-induced changes in $\Delta\psi_m$ than the ATP synthesis[148]. Therefore, the proton leak which uncouples the respiration from ATP synthesis may be a defensive mechanism to attenuate $O_2^{\bullet-}$ generation in conditions when the $\Delta\psi_m$ is high[132, 155]. Skulachev *et al.* proposed that mitochondria possess a special mechanism that prevents a strong increase in electrochemical proton gradient ($\Delta\mu H^+$) when ADP is exhausted[123]. He called this mechanism - “mild” uncoupling. This mechanism is particularly important in state 4 of mitochondrial respiration[123]. State 4 respiration is defined as the amount of O_2 consumption that persists during inhibition of the ATP synthase, *e.g.* in the absence of ADP[119]. During state 4, $\Delta\psi_m$ is high with concomitant high electron pressure which increases the probability of ROS emission. This distinguishes the condition from a situation when respiration (electron flow) and ATP synthase activity are high, *e.g.* in metabolic active cells. Korshunov *et al.* showed that low concentrations of uncouplers abolished the H_2O_2 production in state 4 respiration in heart muscle mitochondria[142]. Teleologically it could be

concluded for that reason that the proton leak is maximal when the mitochondria are hyperpolarized[121]. Therefore, it is important to keep in mind that the proton leak may be particularly high when the cellular ATP level is high or ADP levels are low. The mechanism of the increase of the proton leak is not clear[118]. The total proton leak can be thought of as the sum of two process: basal leak (unregulated proton leak) and inducible proton leak (regulated by specific proteins located within IMM)[121, 156]. Passive proton leak was first described in isolated rat liver mitochondria where there was no ATP turnover (state 4, see explanation above)[157]. In this situation, state 4 respiration (O_2 consumption) increases disproportionally as Δp rises ($\Delta\psi_m$ is the main component of Δp), which can be explained by a passive proton leak across the IMM[158]. This proton leak behaves in a non-ohmic manner, because it is correlated with the driving force ($\Delta\psi_m$) in a nonlinear fashion, therefore disobeying Ohm's Law[156, 159]. Importantly, this non-ohmic proton leak is also apparent in intact cells, demonstrating that this process is not caused by damage to the IMM during isolation of mitochondria[156] and thus is essential for cellular function[158]. The rate of the basal leak accounts for 20-30% of the resting metabolic rate of hepatocytes and up to 50% of the respiration of rat skeletal muscle[156]. The proton leak significantly correlates with the membrane phospholipid content of the polyunsaturated fatty acid, docosahexaenoic acid[160]. Another explanation for the disproportionate increase in respiration at high Δp (state 4) is "electron slip", whereby electrons are transferred through the complexes of the respiratory chain without the pumping of protons across IMM[156]. However, this process (electron slip) has not been persuasively confirmed experimentally to occur under physiological condition[156].

On the other hand, the inducible proton leak can occur through special proteins of IMM, such as UCPs[158]. Nowadays, inducible proton leak is considered to be a major mechanism to adjust the $\Delta\psi_m$ to mitochondrial ROS emission[155]. UCP1, the most studied UCPs, acts as an uncoupler and dissipates $\Delta\psi_m$ in brown fat tissue to generate heat in mammals during non-shivering thermogenesis[158]. Dlaskova *et al* found that mitochondria isolated from brown fat tissue of UCP1 knockout mice were characterized by increased $\Delta\psi_m$ as well as by the increased ROS production[161]. Activity and expression of UCP1 is regulated by fatty acid, noradrenaline stimulation, thyroide hormone receptor activation transcriptional factors and PPARγ[158]. As a regulatory mechanism, increased ROS production may induce a proton leak to reduce the $\Delta\psi_m$ in a feedback manner[121]. ROS-induced oxidative stress has been shown to activate mild uncoupling, resulting in dissipation of $\Delta\psi_m$ without influencing ATP synthesis, but with a significant decrease of ROS formation[123]. The mechanism of ROS-induced mitochondrial depolarization is also not yet clear. Skulachev *et al.* demonstrated that uncoupling proteins can be responsible for this protective mechanism in the acute phase of oxidative stress[123]. Thus, proton leak and ROS generation can correlate with each other via a feedback loop[159]. Additionally, uncoupling of mitochondria prevents dielectric breakdown of the mitochondrial membrane[118].

In conclusion, higher $\Delta\psi_m$ probably initiates higher ROS production. Therefore, proton leaks are analogous to a "pressure valve" in the sense that they decrease $\Delta\psi_m$ to limit ROS production and therefore protect cells against oxidative stress[162]. However, under pathological conditions or upon stress, the alteration of $\Delta\psi_m$ and therefore the modulation of mitochondrial ROS emission may serve as a sensor mechanism to adjust to the new conditions or, if adaptation failed, lead to the development of disease.
Another mechanism, which may regulate the interaction between $\Delta\psi_m$ and ROS, is the allosteric regulation of the cytochrome c oxidase by phosphorylation[163]. Under basic (normal) conditions cytochrome c oxidases are phosphorylated which reduces their activity[163]. This decrease of activity results in a decrease of $\Delta\psi_m$ and ROS production[163]. Different pathological triggers dephosphorylate or phosphorylate complex IV, and therefore modulate the level $\Delta\psi_m$ and ROS production.

1.3.4. Mitochondria and HPV

As mentioned before, mitochondria are one possible candidate for the O_2 sensor that triggers HPV[1]. In our previous study, we showed an increase of $\Delta\psi_m$ and $O_2^{\bullet-}$ release, most probably by complex III of the respiratory chain and inhibition of the mitochondrial electron chain at complex IV (inhibition cytochrome c and aa3) during HPV[13]. These data support the "ROS hypothesis" and contradict the "Redox hypothesis" of HPV. The ROS hypothesis (Figure 9c) suggests that acute hypoxia triggers the increased mitochondrial ROS production which results in Ca^{2+} release from the SR possibly via the oxidation of the cysteine residues of RyR and opening of IP_3 (inositol trisphosphate)-gated calcium store[3, 164]. The hypoxia-induced release of Ca^{2+} from SR can be a trigger of capacitative Ca^{2+} entry via SOCC and/or VOCC that further increases the $[Ca^{2+}]_i$[24]. Alternatively, increased ROS could provoke the influx of extracellular Ca^{2+} through TRPC6 channels[21]. According to this theory, a paradoxical increase of ROS production during acute hypoxia may occur within complex III of the respiratory chain[26]. In contrast, the redox hypothesis proposes an inhibition of the mitochondrial respiratory chain by acute hypoxia which may result in a more reduced cytosolic redox state and a decrease of ROS concentration, causing inhibition of K_v channels, subsequent PASMC cell membrane depolarization, Ca^{2+} influx via the VOCC and finally vasoconstriction[31, 165] (Figure 9a). K_v channels in this model play a key role. In normoxia, cysteine residues of K_v channels are oxidized by ROS maintaining them in open state, while reduction of these residues by acute hypoxia leads to their closure and subsequent depolarization of cell membrane[34, 165]. The discrepancy of these theories remains unclear[1, 3, 36]. We should keep in mind that existing approaches to measure ROS have many pitfalls including lack of specificity and sensitivity that can explain difficulties in evaluation of the ROS level upon acute hypoxia[1]. Application of antioxidants during HPV did not reveal the role ROS in HPV[36]. The lack of antioxidants that specifically act within mitochondria can be a reason for these controversial results. The same controversial results have been

obtained from studies investigating the influence of mitochondrial inhibitors on vascular tone in normoxia and during HPV[1].

Little is known about the role of $\Delta\psi_m$ in HPV and only a few studies have investigated the effect of acute hypoxia on the $\Delta\psi_m$. As mentioned above, Sommer *et al*. descibed a hyperpolarization of mitochondria upon an acute hypoxic stimulus in precapillary PASMC isolated from rabbits[13]. The inhibition of the mitochondrial electron chain at complex IV could be the reason for mitochondrial hyperpolarization via a yet unknown mechanism. Michelakis *et al.* described the same effect of acute hypoxia on $\Delta\psi_m$ in rat PASMC [96]. He found that hypoxia evoked a mitochondrial hyperpolarization in PASMC, while the mitochondria from renal artery smooth muscle cells (SMC) depolarized[96]. However, Kang *et al*. proposed the opposite theory[166, 167]. According their theory, acute hypoxia leads to depolarization of mitochondria that decreases the mitochondria's ability to buffer Ca^{2+} and thereby increases a hypoxic-induced rise of $[Ca^{2+}]_i$. This theory reflects his observation from application of FCCP (carbonyl cyanide 4-(trifluoromethoxy)phenylhydrazone) to rabbit PASMC during an acute hypoxic stimulus, where an administration of FCCP augmented a rise of $[Ca^{2+}]_i$ via SR release and capacitative Ca^{2+} entry. Nevertheless, in this study, PASMC from larger pulmonary arteries were used and $\Delta\psi_m$ was not been measured. Additional an argument against Kang's study is a publication that demonstrated the inhibitory effect of chemical uncouplers, DNP and FCCP, on HPV at high concentrations[168].

Another proposal for the HPV mechanism suggests that mitochondria can sense the lack of O_2 via changes of the intracellular AMP/ATP ratio (Figure 9b) resulting in activation of AMPK (AMP-activated protein kinase)[169] and subsequently increased concentration of cADPR (cyclic ADP ribose), which causes Ca^{2+} release from the SR through the RyR[170]. Additionally, it has been shown that AMPK modulates K_v channel function in a similar manner to hypoxia[171] and the non-selective AMPK antagonist, compound C, blocks sustained HPV[35]. There is a potential link between a hypoxic elevation of ROS and AMPK (Figure 9b), in which ROS and $OONO^-$ (peroxynitrite)[172, 173] can activate the AMPK possibly via a change of the intracellular AMP/ATP ratio[174].

Mitochondria might not only be a trigger of HPV, but also could be a mediator of the HPV transduction pathway[3]. Alterations in $[Ca^{2+}]_i$ concentration act as a main signal for PASMC contraction[3]. Mitochondria have long been known for their role in $[Ca^{2+}]_i$ metabolism[175]. Under normal conditions, the concentration of Ca^{2+} within the mitochondrial matrix $[Ca^{2+}]_m$ is equal to the cytosolic $[Ca^{2+}]_i$. Different pathological or physiological stimuli lead to mitochondrial uptake of Ca^{2+} driven electrophoretically by the $\Delta\psi_m$ from the cytosol through the mitochondrial calcium uniporter (MCU). An increase of $[Ca^{2+}]_m$ can change activity of TCA (tricarboxylic acid cycle) enzymes, respiratory complexes, and opening of the permeability transition pore[176]. Mitochondria release Ca^{2+} into cytosol through several different routes[175]. However, the contribution of the mitochondria to the Ca^{2+} homeostasis in PASMC during acute hypoxia is poorly

understood[177]. It was shown that mitochondrial Ca^{2+} uptake may attenuate the hypoxia-induced rises in $[Ca^{2+}]_i$ in rabbit PASMC during hypoxia. In contrast, Wang *et al.* reported that acute hypoxia caused the Ca^{2+} release from mitochondria of rat PASMC[178].

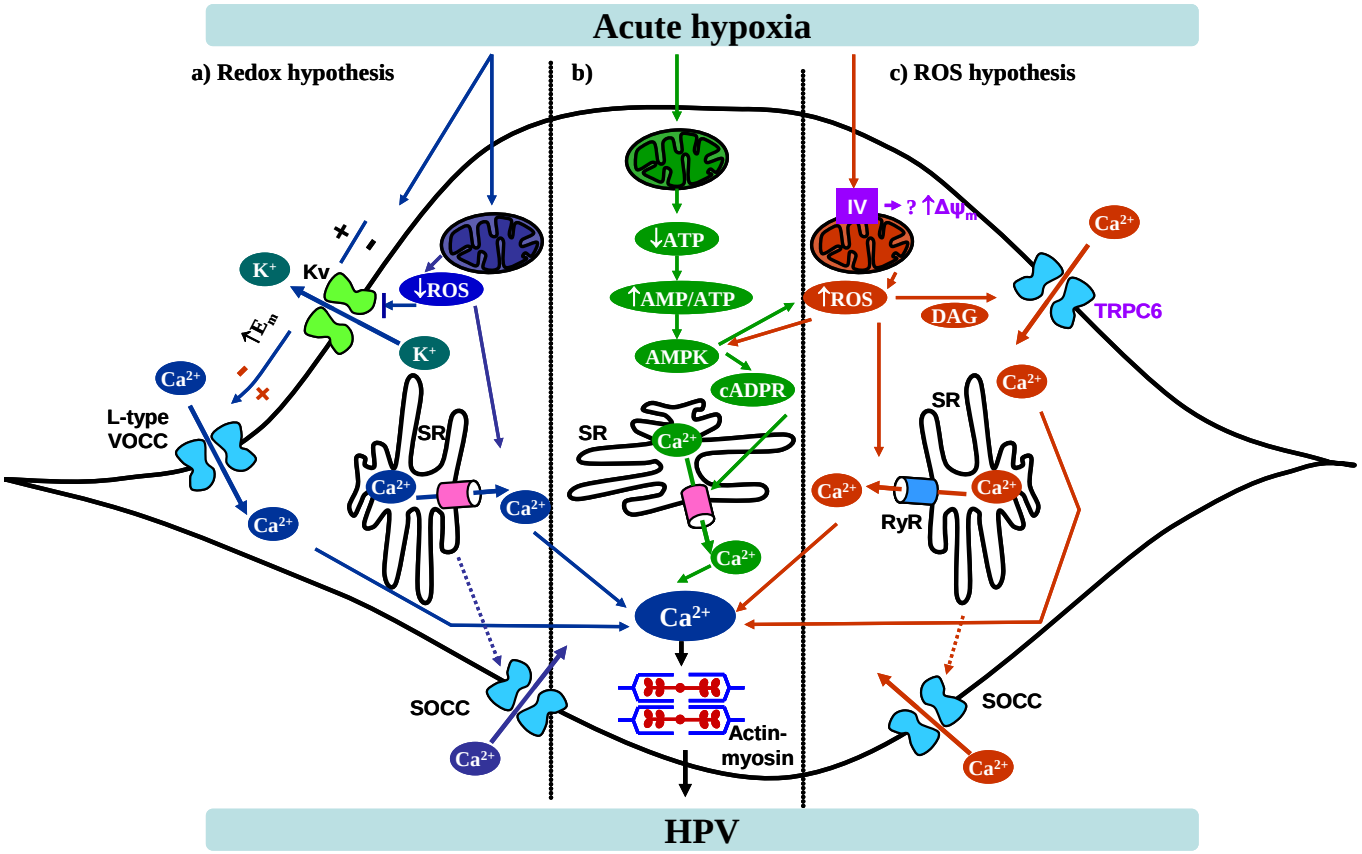

Figure 9. Possible role of mitochondria in HPV.

Mitochondria can act as O_2 sensor or modulate the course of HPV.

a) Redox hypothesis. Acute hypoxia leads to a more reduced cytosolic redox state and decreases ROS concentration because of impaired mitochondrial respiration. Decreased redox state and ROS inhibit K_v channels, causing depolarization of the cellular membrane and the activation of voltage-gated calcium channels, influx of Ca^{2+}, and/or release of Ca^{2+} from the SR.

b) The role of AMP-activated kinase (AMPK) in HPV. Acute hypoxia increases the AMP/ATP ratio that activates the AMPK, which results in an increase of the cADPR concentration and the opening of calcium channels of the SR.

c) ROS hypothesis. Acute hypoxia increases ROS levels resulting in the opening of the Ca^{2+} stores via oxidation of ryanodine-sensitive receptors and/or influx of Ca^{2+} through the TRPC6 channels.

Abbreviations: AMP/ATP ratio - adenosine monophosphate/adenosine triphosphate ratio**;** AMPK - 5' adenosine monophosphate-activated protein kinas; cADPR - cyclic adenosine diphosphate ribose; Ca^{2+} - calcium; L-type VOCC- voltage operated calcium channels; K_v - potassium channels; SOCC - store-operated calcium channels; SR - sarcoplasmic reticulum; TRPC6 - transient receptor potential cation channels; RyR - ryanodine-sensitive receptors; ROS – reactive oxygen species; $\Delta\psi_m$ – mitochondrial membrane potential.

Modified from J. T. Sylvester *et al.*

1.3.5. Mitochondria and PH

Mitochondria can play an important role in the pathogenesis of PH via the regulation of $[Ca^{2+}]_i$ homeostasis, mitochondrial ROS production, release of proapoptotic proteins and alteration of cellular metabolism[37, 38, 40, 82, 96] (Figure 10).

Modulation of mitochondrial ROS may play an essential role in pulmonary vascular remodeling in PH[37, 179, 180] Similar to mitochondrial ROS in HPV; there are two antithetic opinions about the role of ROS in PH development. One group of scientists have found a decrease of ROS emission[95] (Figure 10 pathway "1a"), whereas other groups have found a large body of evidence suggesting an increase of ROS (Figure 10 pathway "1b") is a cause of PH development via the alteration of hypoxia-inducible factor 1 (HIF-1α) stabilization[38], the function of ROS sensitive proteins[172, 173] and cellular Ca^{2+} homeostasis[3, 164]. Severe hypoxia leads to the activation of different transcription factors including (HIF1), which was first described by Semenza *et al.* in 1995[181]. The importance of HIF in PH was proven using mice with partial deficiency of HIF-1α (HIF-$1\alpha^{+/-}$)[182]. These mice were characterized by attenuation of the increase of PAP and RV hypertrophy upon chronic hypoxic exposure[182]. HIF1 is a heterodimer of two proteins: HIF-1α and HIF-1β (or ARNT - aryl hydrocarbon nuclear trans-locator)[181]. In well-oxygenated conditions, HIF-1α is maintained in a hydroxylated state by PHD (prolyl hydroxylase) leading to proteasomal degradation of HIF-1α, which is mediated by the E23 ubiquitin ligase von Hippel-Lindau (VHL). Chronic hypoxia stabilizes HIF-1α through an alteration of PHD2 function and lack of O_2 that is the substrate for PHD2[181]. The exact mechanism of hypoxia-induced stabilization of HIF-1α is under investigation, but it has been suggested that mitochondrial ROS can mediate the stabilization of HIF-1α [38, 183]. Evidence for increased ROS inducing HIF-1α stabilization are the following: overexpression of catalase (which leads to removal of H_2O_2) abolished the HIF-1α protein accumulation in response to hypoxia, and H_2O_2 application in normoxic conditions stabilized HIF-1α[38]. Arguments for decreased ROS inducing HIF-1α stabilization are from a study that demonstrated that downregulation of SOD2 by siRNA, which decreases H_2O_2 concentration, activated the HIF-1α translocation to the nucleus[183]. However, it is possible that an increase of $O_2^{\bullet-}$ as the result of SOD2 downregulation is actually responsible for HIF-1α stabilization and not the decrease in H_2O_2 concentration. After stabilization, the HIF1α is translocated into the nucleus, binds to HIF-responsive elements (HREs) and turns on various genes to stimulate immediate and long-term responses to chronic hypoxia including expression of enzymes of the anaerobic glycolysis such as pyruvate dehydrogenase kinase isozyme 1 (PDK1)[184], lactate dehydrogenase A (LDHA)[185], glucose transporter (Glut1)[186] and *etc*. Therefore, in hypoxia cellular ATP production is shifted from an oxidative (aerobic) to a less efficient glycolytic (anaerobic) metabolism, which is called "metabolic shift" (Figure 10 pathway 3). A metabolic shift has also been observed in non-hypoxic PH[187]. MCT-induced PH leads to

the same metabolic shift as in chronic hypoxia through stabilization of HIF-1α[188]. Additionally, vascular cells isolated from IPAH patients are also characterized by increased anaerobic glycolysis[189]. However, the mechanism of non-hypoxic stabilization of HIF-1α is still unknown. It is possible that ROS also could play a role in this process[38, 190]. The increased anaerobic glycolysis is linked to increased proliferation and attenuated apoptosis by still not completely clear molecular pathways (Figure 10 pathway 3)[181, 191, 192]. The restoration of glucose oxidation by deletion of the gene for malonyl-coenzyme A decarboxylase and subsequent blocking of the fatty acid oxidation, leads to prevention of PH development in mice upon chronic hypoxia[193]. Moreover, dichloroacetate (DCA) treatment also prevented the development of PH[194, 195]. DCA is an inhibitor of the PDK1 and thus increases glucose substrate supply to the mitochondria, which decreases anaerobic glycolysis. The metabolic shift, which was found in PH, shows similarities to the metabolic changes occurring in cancer cells (called the "Warburg effect"). In cancer cells a high rate of anaerobic glycolysis provides several advantages for proliferating cell: 1) it allows cells to use the most abundant extracellular nutrient, glucose, to produce abundant ATP; 2) glucose degradation provides cells with the intermediates needed for biosynthetic pathways, including ribose sugars for nucleotides, glycerol and citrate for lipids, nonessential amino acids[192].

As written before, mitochondria are a reservoir for excess $[Ca^{2+}]_i$[40, 196] and changes in $[Ca^{2+}]_i$ concentration play a significant role in remodeling of the pulmonary vasculature via activation of Ca^{2+} dependent enzymes (*e.g.* PKC[197]), receptors (*e.g.* ryanodine-sensitive receptors)[3, 164] and transcription factors (*e.g.* CREB[198], NFAT[199]) (Figure 10 pathway 2). Little is known about $[Ca^{2+}]_m$ and PH and further investigations are necessary. The interplay of mitochondria with the endoplasmic reticulum (ER) is an important component of mitochondrial Ca^{2+} regulation. Recently, it has been shown that the disruption of the ER-mitochondria contact attenuates apoptosis of PASMC by decreasing the ER-to-mitochondria phospholipid transfer and intermitochondrial Ca^{2+} that leads to an excess of pulmonary vascular remodeling in chronic hypoxia-induced PH in mice[200]. The decrease of $[Ca^{2+}]_m$ leads to inhibition of Ca^{2+}-sensitive mitochondrial enzymes which decreases mitochondria-dependent apoptosis[200]. In addition to ROS-mediated alteration of HIF-1α stabilization, mitochondrial ROS also can modulate $[Ca^{2+}]_i$ homeostasis via the oxidation/reduction of different Ca^{2+} channels and ROS-sensitive enzymes[165, 201] (Figure 10 pathway 2). In this regard downstream targets of ROS may be TRPC3 (transient receptor potential cation channel, member 3) channels that have been shown to be activated by ROS in porcine aortic EC [201].

Mitochondria induce cell death by releasing proapoptotic mediators and thus initiating apoptosis[37]. Release of proapoptotic proteins can be dependent on $\Delta\psi_m$[37]. Mitochondrial depolarization promotes apoptosis while mitochondrial hyperpolarization locks cells into an apoptosis-resistance state[37] (Figure 10 pathway 4). Therefore, preserved $\Delta\psi_m$ can be a sign of higher proliferative and less proapoptotic cells as

in the case of cancer cell lines[202]. The decrease of apoptosis plays an essential role in the vascular remodeling of the medial layer in PH; however, the exact mechanism of triggering of apoptosis in PH is still not fully understood[37, 56, 165]. It has been shown that the metabolic shift in PH can suppress $K_v1.5$ expression, leading to an attenuation of apoptosis of PASMC[165] (Figure 10 pathway 4). Additionally, BMPR2 mutations in mice (BMPR2-mutant mice) lead to an increase of ROS of mitochondrial origin and a decrease of mitochondria-induced apoptosis which is the cause of pulmonary vasculature remodeling[203]. In contrast, in early stages of experimental PH, EC apoptosis could be an initiating trigger, leading either directly to the degeneration of pre-capillary arterioles or to the selection of hyperproliferative, apoptosis-resistant EC that may contribute to "angioproliferative" plexiform lesions[56]. Consequently, apoptosis could play a dual cellular-specific or course-specific role in pathogenesis of PH[165].

As written above, one of the key characteristics of normal function of "happy" mitochondria is the $\Delta\psi_m$. Studies investigating the contribution of $\Delta\psi_m$ to PH development have shown controversial results. Some investigators find an increase[34] (*i.e.* hyperpolarization) and others a decrease (*i.e*. depolarization) of $\Delta\psi_m$[204] in experimental models of PH and IPAH. Chen *et al.* found significant hyperpolarization of human PASMC during chronic hypoxia that was connected with the decrease of mitochondrial permeability and attenuated apoptosis[205]. Conversely, another study that used the same cell line (human PASMC), experimental conditions (5% O_2 and 24h incubation) as well as the same fluorescent approach (Rhodamine-123) for $\Delta\psi_m$ measurement reported a depolarization of the $\Delta\psi_m$ during the chronic hypoxic exposure concomitant with increased H_2O_2 production[204]. These authors found that hypoxia induced an opening of mitoK_{ATP} channels (mitochondrial ATP-dependent potassium channels) leading to depolarization of mitochondria that inhibited the release of cytochrome c into cytosol and the activation of caspase-dependent mechanisms, therefore decreased human PASMC apoptosis[204]. MitoK_{ATP} depolarizes mitochondria via influx of potassium into mitochondria in the opposite direction to proton movement. Increase of mitochondrial H_2O_2 production is also explained by the opening of mitoK_{ATP} channels. However, the exact mechanism by which mitoK_{ATP} channels affects the production of H_2O_2 and cytochrome release has not been elucidated. Additional evidence for the hyperpolarization in PH comes from Bonnet *et al* and Paulin *et al.* [34, 206]. They also demonstrated the increase of $\Delta\psi_m$ in experimental PH that was associated with simultaneous decrease of ROS, the attenuation of apoptosis[34, 206] and the decrease of intermitochondrial Ca^{2+} concentration[200, 206]. The sequence of these events in PH is completely unclear. Even more, it is not certain how an increase of $\Delta\psi_m$ is connected with a decrease of ROS in this model.

In summary, the role of $\Delta\psi_m$ in hypoxia- and non-hypoxia dependent molecular pathways of PH needs to be further elucidated.

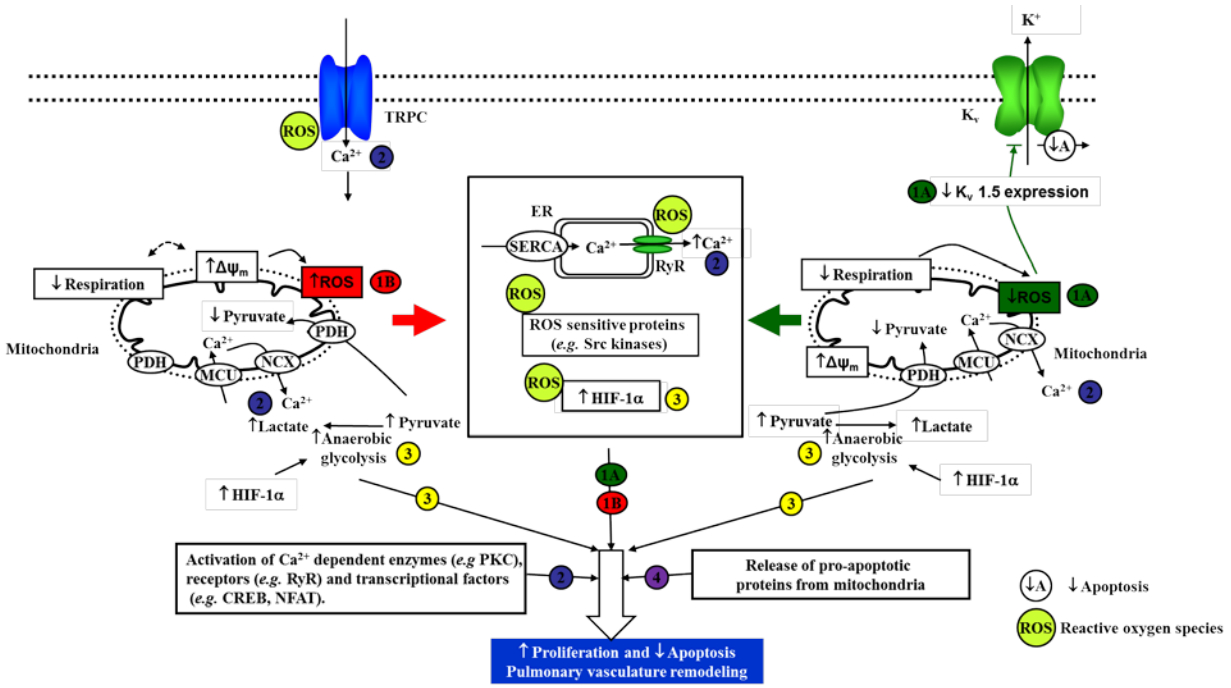

Figure 10. Role of mitochondria in the pathogenesis of PH.

Mitochondria can play an important role in the pathogenesis of PH by participating in different molecular signaling pathways including the regulation of $[Ca^{2+}]_i$ homeostasis, mitochondrial ROS production, release of proapoptotic proteins and alteration of cellular metabolism[38].

Numbers depict the pathways:

1) Mitochondria are the main source of ROS within cells. There are two main theories about the role of ROS in PH: 1A) Triggers of PH decrease mitochondrial respiration and thus ROS production. Decreased ROS triggers HIF-1α stabilization and K_v 1.5 downregulation[95]. K_v 1.5 downregulation leads to decreased apoptosis of PASMC[165]. 1B) Triggers of PH increase mitochondrial ROS production that initiates Ca^{2+} release from SR[201], HIF-1α stabilization[38] and activation of different proteins[38] (*e.g.* Src enzyme[172], pERK[207, 208]). HIF-1α is a transcriptional factor that activates expression of various proteins including growth factors (*e.g.* VEGF) and key enzymes for activation of anaerobic glycolysis[184-186].

2) The change in $[Ca^{2+}]_i$ concentration, probably, plays an important role in remodeling of the pulmonary vasculature via activation of Ca^{2+} dependent enzymes (*e.g.* PKC[197]), receptors (*e.g.* RyR) [3, 164] and transcriptional factors (*e.g.* CREB[198], NFAT[199]). Mitochondria act as key regulator of $[Ca^{2+}]_i$ concentration. They uptake Ca^{2+} via the MCU and release it to cytosol via different exchangers (*e.g.* Na/Ca^{2+} exchanger)[175].

3) Cellular metabolism in PH is characterized by a metabolic shift from aerobic to anaerobic glycolysis[187]. The stabilization of HIF-1α is an essential initiating event in this process[182]. The increased anaerobic glycolysis is linked to an increased proliferation and attenuated apoptosis by still not completely clear molecular pathways[181, 191, 192]. The restoration of glucose oxidation leads to prevention of PH development[193-195].

4). Mitochondria induce cell death by releasing proapoptotic mediators and thus initiating apoptosis[37]. Decrease of apoptosis plays an essential role in pulmonary vasculature remodeling of the medial layer in PH[165].

Abbreviations: ER - endoplasmic reticulum, K_v - potassium channels; HIF-1α - hypoxia inducible factor 1a, PDH - pyruvate dehydrogenase, ROS - reactive oxygen species, MCU - mitochondrial calcium uniporter, NCX sodium-calcium exchanger, TRPC - transient receptor potential cation channels, RyR - ryanodine-sensitive receptors; SERCA - sarco/endoplasmic reticulum Ca^{2+}-ATPase, NFAT - nuclear factor of activated T-cells; CREB - cAMP response

element-binding protein; PKC - protein kinase C; SRC - v-src sarcoma (Schmidt-Ruppin A-2) viral oncogene homolog (avian); pERK - extracellular signal-regulated kinases; HIF-1α - hypoxia-inducible factor 1-α; Ca^{2+} - calcium; ROS – reactive oxygen species; $\Delta\psi_m$ – mitochondrial membrane potential.

1.4. Uncoupling protein 2 (UCP2)

1.4.1. Definition, molecular structure and tissue distribution

As stated before, proton leak through the IMM towards the intermembrane space may occur through different classes of small mitochondrial membrane proteins, called UCPs[209]. Thus, UCPs may regulate the $\Delta\psi_m$ and ROS production[210]. Mammals express five UCPs homologues, UCP1-UCP5[211]. UCP2, a IMM protein, is widely expressed in different organs including the brain, lung, spleen, kidney, liver and heart, and was discovered in 1996 through its sequence homology and 59% amino-acid identity to the brown fat specific UCP1 that was found in 1976[212]. It should be remembered that the pattern of mRNA expression of UCP2 is not identical to its protein expression pattern[211]. UCP1 is responsible for heat generation by increasing the permeability of the IMM to protons in brown adipose tissue[213]. In contrast to UCP1, which is the only UCP for which a function in increasing proton conductance has been proven[211], the role of UCP2 is still not clear[151]. However, UCP1 knockout mice overexpress UCP2 mRNA five-fold in brown adipose tissue which suggests that UCP2 can act in a similar fashion to UCP1[160]. The molecular structure of UCP2 is not known. Recently, Berardi *et al.*, suggested that the structure of UCP2 closely resembles the bovine ADP/ATP carrier, determined by NMR (nuclear magnet resonance) molecular fragment searching[214]. Structurally, UCPs are homodimers and contain three repeats of approximately 100 amino acids that form the alpha helices that are connected with long hydrophilic loops oriented towards the matrix side, whereas the amino and carboxyl termini extend into the intermembrane space[215]. In humans, the UCP2 and UCP3 genes are both located on chromosome 11q13 and transcription initiation of UCP2 is only 7-8 kb downstream from the UCP3 stop codon[216]. There are 8 exons in the UCP2 gene and exon 1 and 2 are untranslated[216]. In various genetic studies, a relationship between UCP2 and obesity, fatty acid metabolism or diabetes mellitus type II[216] has been found, but there are no published investigations about the role of UCP2 polymorphisms in PH.

1.4.2. Mechanism of action

Although the precise physiological/pathological functions of UCP2 are still not fully understood, scientific evidence has described UCP2 as a negative regulator of $\Delta\psi_m$ and mitochondria-derived ROS emission, especially upon different stimuli. Currently, four different mechanisms of UCP2 function are suggested (Figure 11). Historically, UCP2 has been considered to be a pure uncoupling protein that mediates a proton leak toward to the intermembrane space and therefore decrease the $\Delta\psi_m$[217, 218] and ROS production[219-221] (Figure 11, b). Negre-Salvayre *et al.* first described that inhibition of UCP2 with

guanosine diphosphate (GDP) resulted in a sharp increase of mitochondrial ROS[219]. Recently, attenuation of ROS production after overexpression of UCP2 was shown[220, 221], and UCP2 knockout results in an increase of mitochondrial ROS emission[222]. Additionally, it has been described that increased ROS could activate UCP2 through the oxidation of lipids of the IMM[223] or directly increase proton flow through UCP2 pores[224]. In this scenario, UCP2 serves as a counter-regulatory mechanism against the increased ROS production within mitochondria.

However, several publications could not demonstrate the uncoupling effect of UCP2[212, 213], mainly because they could not find increased respiration by activation of UCP2 which would be expected by its uncoupling property. Bouillaud *et al.* suggested an alternative theory, ”the metabolic hypothesis” concerning the physiological function of the UCP2[225] (Figure 11c). In this theory, UCP2 plays a role as a “metabolic switch” which restrains mitochondrial glucose metabolism via inhibition of pyruvate entry into the mitochondrial matrix and compensatory increase of fatty acid metabolism[226]. The term “metabolic switch” should be not confused with the term “metabolic shift” that was described above and corresponds to effect of chronic hypoxia on cellular metabolism. Fatty acids stimulate the expression of UCP2/3[227], and UCP2 promotes the feeding of the TCA cycle with products of fatty acid oxidation[226]. Thereby UCP2 could decrease ROS production by inhibiting the entry of pyruvate into the oxidative pathway resulting in attenuation of the enormous redox pressure of pyruvate[225]. In connection with this theory, it was suggested that UCP2 serves as a pyruvate anionic uniporter that pumps the excess pyruvate from the mitochondrial matrix into the intermembrane space and therefore restricts the pyruvate availability for mitochondrial respiration[213, 225] (Figure 11d). Additionally, Hurtaud *et al.* showed in macrophages that UCP2 is mandatory for efficient mitochondrial oxidation of glutamine, an alternative fuel for the respiratory chain in absence of glucose[228]. These articles support the “metabolic theory” and suggest that in addition to fatty acids, other molecular pathways feed the respiratory chain in conditions of a lack of glucose. In conclusion, the “metabolic theory” suggests that UCP2 activity results in a condition similar to the Warburg effect, decreasing pyruvate oxidation and promoting anaerobic glycolysis in presence of O_2[225].

One group from Graz, Austria, suggested that UCP2/3 is the conductive subunit of a Ca^{2+} selective mitochondrial ion channel at the IMM[229] (Figure 11a). They showed that knockdown of UCP2 by specific siRNA or their overexpression dramatically changes the mitochondrial Ca^{2+} capacity, as well as the velocity of mitochondrial Ca^{2+} sequestration[229]. The increase of the Ca^{2+} influx into mitochondria associates with a decrease of the $\Delta\psi_m$ as a result of accumulation of positively charged Ca^{2+} ions within the mitochondrial matrix[230]. However, these data should be confirmed by other scientific groups[225] especially in light of the fact that the introduction of mammalian UCPs into yeast fails to provide evidence of the MCU presence in these eukaryotic microorganisms[225].

Although the molecular mechanism of UCP2 remains to be resolved, it is widely accepted that UCP2 decreases ROS production and alters proliferation[213].

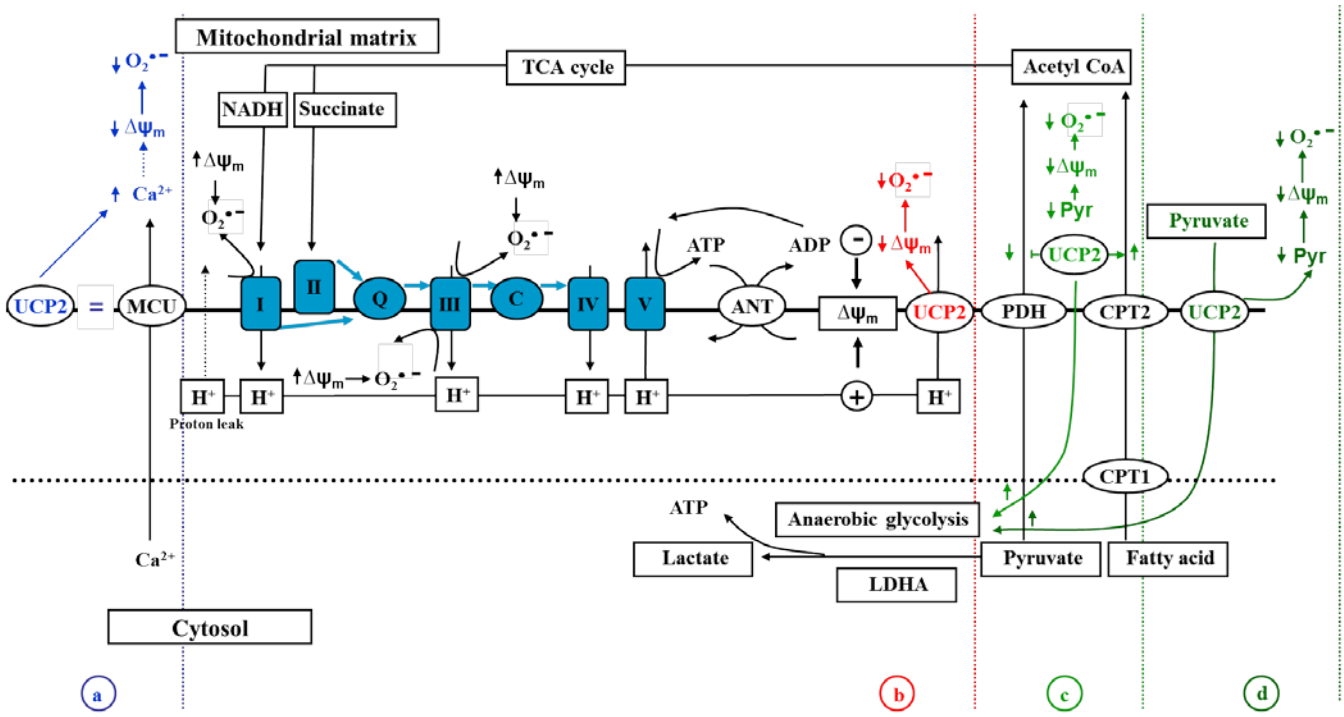

Figure 11. Hypothetical functions of uncoupling protein (UCP2) and its effects on $\Delta\psi_m$ and ROS production.

a) UCP2 is a conductive part of the MCU that increases influx of Ca^{2+} ions into the mitochondrial matrix[229].

b) UCP2 acts as protonophore that uncouples $\Delta\psi_m$ and ATP synthesis resulting in decreased $\Delta\psi_m$ and ROS production[219-221].

c) UCP2 acts as "metabolic switch" between glucose and fatty acid metabolism. The excess of fatty acid or lack of glucose activates entry of fatty acid into the mitochondrial matrix and causes a compensatory decrease of pyruvate uptake by mitochondria[225]. These processes could decrease electrons entry into the respiratory chain and thus decrease $\Delta\psi_m$ and ROS production[225].

d) UCP2 acts as pyruvate anionic uniporter that pumps pyruvate out of the matrix towards the intermembrane space[213, 225] .

Abbreviations: I, II, III; IV and V - complexes of respiratory chain; ADP - adenosine diphosphate; ATP - adenosine triphosphate; ANT - adenine nucleotide translocase; CPT1 and 2 - Carnitine palmitoyltransferase I and II; MCU - mitochondrial calcium uniporter; NADH - reduced form of NAD^+ (nicotinamide adenine dinucleotide); LDHA - lactate dehydrogenase A; Q - coenzyme Q, C - cytochrome c; PDH - Pyruvate dehydrogenase; TCA cycle - tricarboxylic acid cycle; Pyr - pyruvate; UCP2 - uncoupling protein 2; Ca^{2+} - calcium $O_2^{\bullet-}$- superoxide; H^+; $\Delta\psi_m$ – mitochondrial membrane potential.

1.4.3. UCP2 and cellular function

An increasing number of reports point to the relevance of UCP2 in important physiological and pathophysiological pathways, such as insulin secretion, neuronal activity, immune response, obesity, diabetes, and cancer[210, 213]. Therefore, the presence of UCP2 has both favorable and unfavorable effects depending on the disease[225]. For example, the most accepted function of UCP2 in β-cells of the pancreas indicates that UCP2 acts as a negative regulator of insulin secretion[231]. In pancreatic β-cells, fluctuations of nutrients cause alterations in both expression and activation of UCP2[231]. In this context, increase of UCP2 expression and/or UCP2 activity decreases the $\Delta\psi_m$ that reduces the generation of ATP and subsequently decreases ATP/ADP ratio within β-cells. The decrease of the ATP/ADP ratio attenuates the closing of the ATP-sensitive K^+ channel in the plasma membrane, which prevents membrane depolarization, opening of VDCC, and influx of Ca^{2+} into the cytosol of β- cells, which subsequently stops the exocytosis of granules containing insulin[231].

The role of UCP2 in the signaling pathway of HPV and PH to date has not been investigated. UCP2 could influence these processes by interaction with ROS, Ca^{2+} and ATP regulated pathways, as well as by interference with proliferation and apoptosis. In this regard, Derdak *et al.* described that UCP2-deficient mice ($UCP^{-/-}$) exhibit increased oxidative stress along with enhanced NF-kB activation that induces proliferation and decreases apoptosis of intestinal epithelial cells[232]. In line with this article, Nino Fong *et al.* demonstrated that $UCP2^{-/-}$ mice display increased transactivation of NF-kB which may contribute to enhanced expression of antiapoptotic genes such as Tnfaip3 (Tumor necrosis factor, alpha-induced protein 3) and pro-proliferative genes such as Ccnd2 (G1/S-specific cyclin-D2) in pancreatic β-cells[233]. Pecqueur and colleagues also showed that UCP2 knockdown is associated with increased proliferation of mouse embryonic fibroblasts (MEFs) and T cells[226]. Possibly, UCP2 knockout increases proliferation via activation of p38 and ERK[234]. In contrast, overexpression of UCP2 in Chinese hamster ovary (CHO-K1) cells, cells that normally do not express any of the UCPs, in chick embryo fibroblasts and in HeLa cells (cervical cancer cells taken from Henrietta Lacks) decreases their proliferation[235]. Additionally, UCP2 can modulate the production of important pro-proliferative cytokines, *e.g.* mast cells of UCP2 knockout mice exhibited higher histamine release and interleukin-6 (IL-6) production while overexpression of UCP2 demonstrated an opposite effect[236]. Furthermore, UCP2 expression is necessary for full differentiation of human pluripotent stem cells[237]. Chen *et al.* showed that UCP2 downregulation was important for myogenic differentiation[238].

On the other hand, the anti-cancer effects of paclitaxel in the melanoma cell line a375 and BLM are associated with downregulation of UCP2, increase of mitochondrial ROS production and activation of JNK, p38 and ERK[239]. UCP2 deficiency significantly decreases cell proliferation of progenitor cells from

bone marrow at the erythropoietin-dependent phase of erythropoiesis[240]. A discrepancy of the role of UCP in cellular proliferation can be attributed to cell- or trigger-specific effects of UCP2 functions.
In our laboratory it has been shown that UCP2 knockout ($UCP2^{-/-}$) magnifies the HPV response in isolated lung experiments. However, the exact mechanisms have not been elucidated (unpublished thesis of Timm Hoeres, Giessen).

1.5. Aims of this study

Despite a long history of research, the role of mitochondria in the response of the pulmonary vasculature to acute and chronic hypoxia, resulting in HPV and PH, still remains unknown. Alterations in the $\Delta\psi_m$ may be crucial in both processes. UCP2, a mitochondrial uncoupling protein, is known to modulate several mitochondrial functions including the $\Delta\psi_m$, ROS and glucose metabolism, although the exact molecular mechanism of its action has not yet been completely elucidated. It was previously shown that lungs of $UCP2^{-/-}$ mice exhibit increased HPV and increased pulmonary vascular remodeling under baseline conditions.

Against this background, the aims of this study were 1) to identify the role of $\Delta\psi_m$ in HPV and PH, 2) to investigate if increased HPV and pulmonary vascular remodeling in $UCP2^{-/-}$ mice are related to alterations in $\Delta\psi_m$, and 3) to decipher up- and downstream signaling mechanisms of $\Delta\psi_m$ alterations (Figure 12). In order to answer these questions, the following investigations were performed:

- Alterations of $\Delta\psi_m$ were investigated in isolated precapillary PASMC during acute hypoxia and in animal models of PH, as well as in human PAH.
- The physiological relevance of $\Delta\psi_m$ alterations was tested in isolated PASMC of $UCP2^{-/-}$ mice and after knockdown of UCP2 by siRNA during acute hypoxia and in PASMC proliferation.
- Upstream and downstream signaling mechanisms of alterations in $\Delta\psi_m$, including ROS metabolism, were investigated in models of PH and during UCP2 knockdown on cellular level. The effect of a proliferative stimulus (chronic hypoxia) was tested in $UCP2^{-/-}$ cells.

The hypothesis tested is that during acute hypoxia and PH, $\Delta\psi_m$ is increased, resulting in HPV and pulmonary vascular remodeling. Knockout of UCP2 should exhibit augmented $\Delta\psi_m$ hyperpolarization, thus increasing HPV and pulmonary vasculature remodeling. As a downstream mediator for this pathway, increased ROS production is proposed. Under a proliferative stimulus (*e.g.* chronic hypoxia), $UCP2^{-/-}$ may additionally exert anti-proliferative functions and attenuate pulmonary vasculature remodeling, as it may counteract the metabolic switch by increasing pyruvate metabolism of the mitochondria.

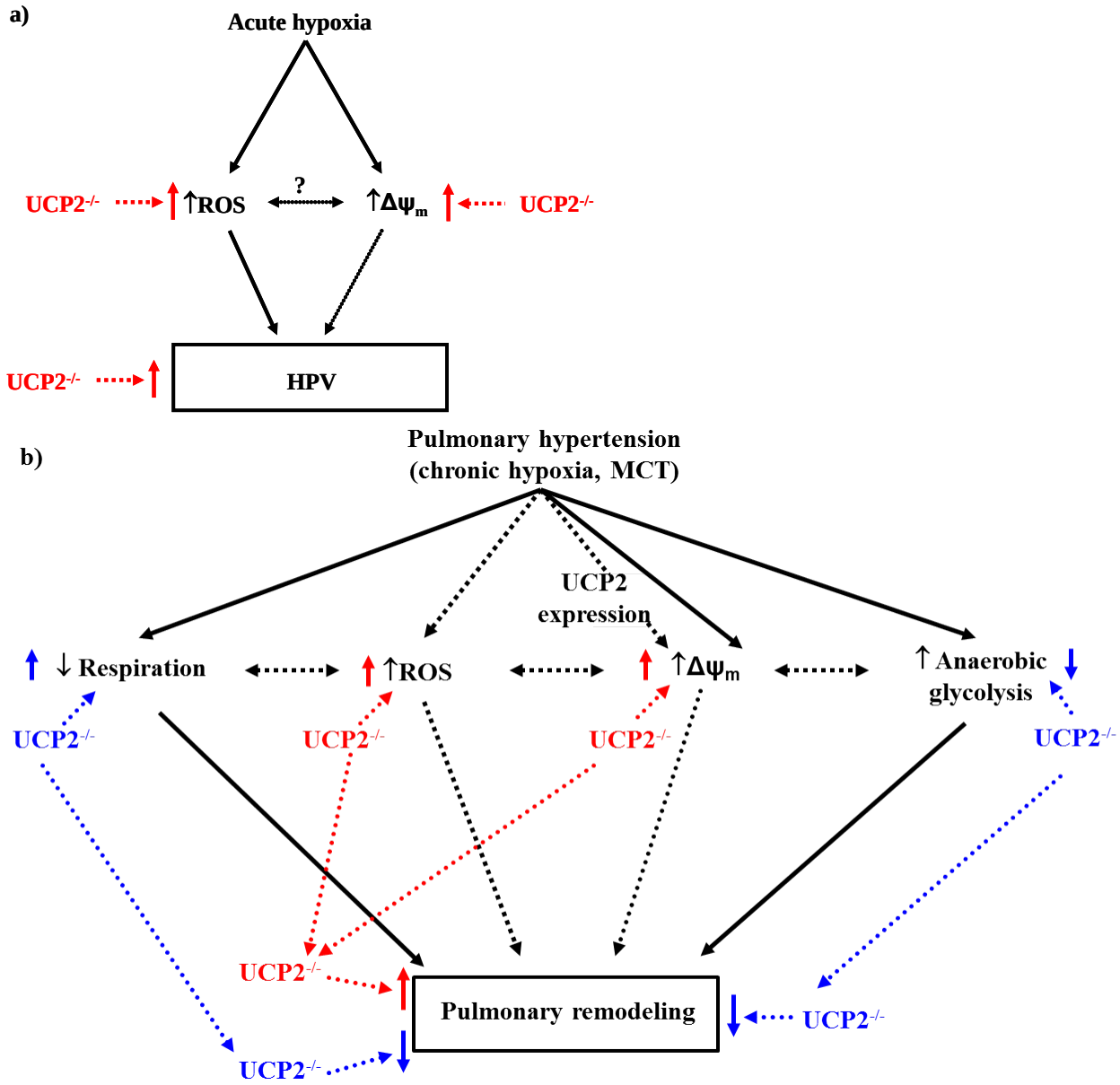

Figure 12. Aims of the study.

A) Is acute hypoxia associated with $\Delta\psi_m$ alterations and are these alterations of physiological significance in these processes? Does the knockout of UCP2 ($UCP2^{-/-}$) magnify the acute hypoxia-induced $\Delta\psi_m$ alterations and ROS production?

B) Is PH associated with $\Delta\psi_m$ alterations and are these alterations of physiological significance in PH? Does $UCP2^{-/-}$ augment $\Delta\psi_m$ /ROS production and therefore increase pulmonary vasculature remodeling under baseline conditions? Does $UCP2^{-/-}$ decrease pulmonary vasculature remodeling via the attenuation of the metabolic switch in hypoxia-induced PH?

Abbreviations: Black arrows depict the hypothetical pathway of HPV and PH, solid lines represent proven and dashed lines unproven interactions. Red arrows depict the possible mechanism of augmentation of HPV and pulmonary vascular remodeling by $UCP2^{-/-}$. Blue lines depict the possible mechanism of attenuation of pulmonary vascular remodeling by $UCP2^{-/-}$.

$\Delta\psi_m$ - mitochondrial membrane potential; $UCP2^{-/-}$ - knockout of uncoupling protein 2; ROS - reactive oxygen species; HPV - hypoxic pulmonary vasoconstriction; MCT - induced PH.

2. Material and methods

2.1. Reagents

[3H]-Thymidine	GE Healthcare, Little Chalfont, UK
2-Mercapto-ethanol	Sigma-Aldrich, St. Louis, USA
Acetic Acid, Glacial 99%	Sigma-Aldrich, St. Louis, USA
Acetone 99,5%	Sigma-Aldrich, St. Louis, USA
ADP	Sigma-Aldrich, St. Louis, USA
Albumin, Bovine serum	Sigma-Aldrich, St. Louis, USA
Alexa fluor 488 labeled antibody against DIG antigen	Roche Applied Science, Penzberg, Germany
Anti-cyclin D1 antibody	Cell Signaling Technology, Danvers, USA
Anti-DDK antibody	OriGene, Rockville, USA
Anti-human von Willebrand factor antibody	Dako, Hamburg, Germany
Anti-LDHA antibody	Cell Signaling Technology, Danvers, USA
Anti-PDK1 antibody	Cell Signaling Technology, Danvers, USA
Anti-α-smooth muscle actin antibody	Sigma-Aldrich, St. Louis, USA
Anti-β-actin antibody	Sigma-Aldrich, St. Louis, USA
Anti-UCP2 antibody	Santa Cruz Biotechnology, Santa Cruz, USA
Atimycin A	Sigma-Aldrich, St. Louis, USA
Bongkrek acid	Sigma-Aldrich, St. Louis, USA
$CaCl_2$	Sigma-Aldrich, St. Louis, USA
CMH (1-Hydroxy-3-methoxycarbonyl-2,2,5,5-tetramethylpyrrolidine)	Alexis Corporation, San Diego, USA
Collagenase type IV	Sigma-Aldrich, St. Louis, USA
Complete	Roche Applied Science, Penzberg, Germany
Crystal violet	Sigma-Aldrich, St. Louis, USA
Cy3-labeled α-smooth muscle actin antibody	Sigma-Aldrich, St. Louis, USA
Denhardt's reagent	Sigma-Aldrich, St. Louis, USA
Dextran sulphate	Sigma-Aldrich, St. Louis, USA
DMSO (Dimethyl Sulfoxide)	Sigma-Aldrich, St. Louis, USA
ECL plus western blot detecting system	GE Healthcare, Little Chalfont, UK
EDTA (Ethylenediamine-tetraacetic acid)	Sigma-Aldrich, St. Louis, USA
EGTA (Ethylene glycol-bis(ß-amino-ethylether)-N,N,N',N'tetraacetic acid)	Sigma-Aldrich, St. Louis, USA
Ethanol (70%, 95%, 99,6%)	SAV LP GmbH, Flintsbach, Germany
FCCP (Carbonyl cyanide 4-(trifluoromethoxy)phenylhydrazone)	Sigma-Aldrich, St. Louis, USA
FCS (Fetal calf serum)	Invitrogen, Carlsbad, USA
Fe_3O_4 (Iron particles)	Sigma-Aldrich, St. Louis, USA
Formaldehyd alcohol free 3.7%	Otto Fischar GmbH&Co, Saarbrücken, Germany
H_2O_2 30%	Merck, Darmstadt, Germany
HCl	Sigma-Aldrich, St. Louis, USA
Heparin	Rathiopharm GmbH, Ulm, Germany
Hepes (2-(-4-2-hydroxyethyl)-piperazinyl-1-ethansulfonate)	Sigma-Aldrich, St. Louis, USA
HyPer	Evrogen Company, Moscow, Russian

	Federation
iScript cDNA Synthesis Kit	Bio-Rad, Hercules, USA
Isoflurane	Forene® Abbott, Wiesbach, Germany
Isopropanol (99,8%)	Fluka Chemie, Buchs, Swithland
iTaq SYBR Green supermix with ROX	Bio-Rad, Hercules , USA
JC1 (5,5',6,6'-tetrachloro-1,1',3,3'-tetraethylbenzimidazolylcarbocyanine iodide)	Sigma-Aldrich, St. Louis, USA
Ketavet (Ketamin hydrochloride)	Pfizer, Karlsruhe, Germany
KH_2PO_4	Sigma-Aldrich, St. Louis, USA
LB Agar	Invitrogen, Carlsbad, USA
LNA™ mRNA Detection Probes	Exiqon, Vedbaek, Denmark
Low melting agarose	Sigma-Aldrich, St. Louis, USA
M199 medium	Invitrogen, Carlsbad, USA
Medetomidin	Pfizer, Karlsruhe, Germany
Medical X-Ray film	Agfa, Mortsel, Belgium
Medium for human SMC (smooth muscle cells)	PromoCell, Heidelberg, Germany
Methanol	Fluka Chemie, Buchs, Swithland
$MgCl_2$	Sigma-Aldrich, St. Louis, USA
Milk powder	Carl ROTH, Karlsruhe, Germany
Mini-PROTEAN vertical electrophoresis system	Bio-Rad, Hercules, USA
MitoSox	Invitrogen, Carlsbad, USA
MnTBAP (Mn(III)tetrakis(4-benzoic acid)porphyrin Chloride)	Sigma-Aldrich, St. Louis, USA
Monocrotaline	Sigma-Aldrich, St. Louis, USA
Myc-DDK-tagged ORF clone of Mus musculus UCP1 plasmide	OriGene, Rockville, USA
Myc-DDK-tagged ORF clone of Mus musculus UCP2 plasmide	OriGene, Rockville, USA
NAC (N-acetyl-L-cysteine)	Sigma-Aldrich, St. Louis, USA
NaCl	Sigma-Aldrich, St. Louis, USA
NaH_2PO_4	Sigma-Aldrich, St. Louis, USA
NaOH	Sigma-Aldrich, St. Louis, USA
Nuclear Fast Red	Sigma-Aldrich, St. Louis, USA
Oligomycin	Sigma-Aldrich, St. Louis, USA
OPTI-MEM medium	Invitrogen, Carlsbad, USA
Paraformaldehyde, 4%	Merck, Darmstadt, Germany
pMD2.G	Addgene, Boston, USA
PMSF	Sigma-Aldrich, St. Louis, USA
Proteinase K	Sigma-Aldrich, St. Louis, USA
pSOD (peg superoxide dismutase)	Sigma-Aldrich, St. Louis, USA
psPAX2	Addgene, Boston, USA
PVDF membrane	Pall Corporation, Dreieich, Germany
pWPXL	Addgene, Boston, USA
Pyruvate	Sigma-Aldrich, St. Louis, USA
Pyruvate assay kit	Cayman, Ann Arbor, USA
Rhod2	Invitrogen, Carlsbad, USA
RNeasy RNA extraction kit	Qiagen, Hilden, Germany
ROCK	Rho-associated protein kinase

Rotenone	Sigma-Aldrich, St. Louis, USA
Rotiphorese Gel 30 Acrylamide	Roth, Karlsruhe, Germany
Scrambled siRNA	Biospring, Frankfurt, Germany
SDS (Sodium dodecyl sulfate)	Sigma-Aldrich, St. Louis, USA
Sodium vanadate	Sigma-Aldrich, St. Louis, USA
Succinate	Sigma-Aldrich, St. Louis, USA
SYBR® Safe DNA gel stain	Invitrogen, Carlsbad, USA
Taurine	Sigma-Aldrich, St. Louis, USA
TEMED (N,N,N',N'-Tetramethyl-1-,2-diaminomethane)	Sigma-Aldrich, St. Louis, USA
TEMPO (2,2,6,6-tetramethylpiperidine-N-oxyl)	Sigma-Aldrich, St. Louis, USA
Thromboxane mimetic, U 46619	Sigma-Aldrich, St. Louis, USA
TMRE (etramethylrhodamine, Ethyl Ester, Perchlorate)	Sigma-Aldrich, St. Louis, USA
Trypsin	PAN, Aidenbach,Germany
Turbofectin 8	OriGene, Rockville, USA
Tween-20	Sigma-Aldrich, St. Louis, USA
UCP2 siRNA (Rat, mouse)	Biospring, Frankfurt, Germany
WT-ovationTM Pico RNA Amplification System	NuGEN, San Carlos, USA
Xtreme transfection reagent	Roche Applied Science, Penzberg, Germany
Xylazine	Bayer Healthcare, Leverkusen, Germany
Yeast tRNA	Sigma-Aldrich, St. Louis, USA

2.2. Equipment

1.4F micromanometer catheter	Millar Instruments, Houston, USA
Autoregulatory control unit (model 4010, O_2 controller)	Labotect; Göttingen, Germany
Biemer microvessel clip	Aesculap, Tuttlingen, Germany
Cell culture incubator, Hera Cell Heraeus	Thermo Fisher Scientific, Waltham, USA
Closed perfusion chamber	PeCon, Erbach, Germany
Confocal microscope, Leica TCS SP5X	Leica Microsystems, Manheim, Germany
Digital camera microscope DC 300F	Leica Microsystems, Wetzlar, Germany
Electrophoresis chambers	Biometra, Göttingen, Germany
Flattening bath for paraffin sections, HI 1210	Leica Microsystems, Wetzlar, Germany
Flattening table, HI 1220	Leica Microsystems, Wetzlar, Germany
Fluid-filled force transducer	B. Braun Melsungen AG, Melsungen, Germany
Homeothermic plate control unit	AD Instruments, Spechbach, Germany
Homogenplus	Schuett-biotec GmbH, Göttingen Germany
Inverted microscope (IX70)	Olympus, Hamburg, Germany
Laser microdissection system, Leica LMD7000	Leica Microsystems, Bernried, Germany
Makro for muscularization degree, wall thickness, septum	Leica Microsystems, Wetzlar, Germany
Medical X-Ray film processor (curix 60)	Agfa, Mortsel, Belgium
Microplate reader Infinite m200	Tecan Group Ltd, Männedorf, Switzerland
Mini-PROTEAN vertical electrophoresis system	Bio-Rad, München, Germany
MiniVent type 845	Hugo Sachs Elektronik, March-Hugstetten, Germany
MS 100 spectrometer	Magnettech, Berlin, Germany
Mx3000P QPCR Systems	Agilent Technologies, Santa Clara, USA
NanoDrop	PeqLab, Erlangen, Germany
Opened heated chamber	PeCon, Erbach, Germany
Oxygraphy-2K	Oroboros Instruments, Innsbruck, Austria
Peristaltic pump, ISM834A V2.10	Ismatec, Glattbrugg, Switzerland
Polychrome II monochromator and IMAGO CCD camera	Till Photonics, Munich, Germany
Precelly®24 homogeniser	PeqLab, Erlangen., Germany
Rectal thermometer	Indus Instruments, Houston, USA
Scintillation counter, TRI-CARB 2000	Canberra-Packard, Meriden, USA
Software Q Win V3 Leica Microsystems Nussloch, Germany	Leica Microsystems, Wetzlar, Germany
Stereo light microscope	Leica Microsystems, Wetzlar, Germany
Surgical instruments	Martin Medizintechnik, Tuttlingen, Germany
Table Top Laboratory Animal Anesthesia System	VetEquip Inc, Pleasanton, USA
Tissue embedding machine, EG 1140H	Leica Microsystems, Wetzlar, Germany
Tissue processing automated machine, TP 1050	Leica Microsystems, Wetzlar, Germany
Top Laboratory Animal Anesthesia System	VetEquip Inc, Pleasanton, USA

2.3 Consumable

48-well cell culture plates	Greiner bio-one, Frickenhausen,Germany
Blotting papers	Bio-Rad, München,Germany
Cover slips 24x36mm	Menzel, Germany
Falcon Tubes 15 and 50 ml	Greiner bio-one, Frickenhausen,Germany
Glass Bottles: 0.1; 0.2; 1L	Schott Duran, Germany
Glass Pipetes	Greiner bio-one, Frickenhausen,Germany
Medical adhesive bands 3M	Durapore® St. Paul, MN, USA
Napkins	Tork, Mannheim, Germany
Needle (20G, 11/2",0.9x40mm	BD Microlance, Becton Dickinson, Germany
Neelde (18G,11/2",1.20x38mm)	Unolok, Horsham,U.K
Pipette filter tips, 10µl	Eppendorf, Hamburg, Germany
Plastic Syringe (1,3,5, 10ml and 20ml)	Braun Melsungen,Germany
Single use gloves Transaflex®	Ansell, Surbiton, UK
Single use syringes Inject Luer®, 1ml, 2ml, 5ml, 10ml	Braun, Melsungen, Germany
Tissue Culture Dish 100mm	Greiner bio-one, Frickenhausen,Germany
Tissue Culture Flask 250mm	Greiner bio-one, Frickenhausen,Germany
Feather disposal scalpel	Pfmmediacl, Köln, Germany
Tissue Culture Flask 750mm	Greiner bio-one, Frickenhausen,Germany
Petri dishes	Greiner bio-one, Frickenhausen,Germany

2.4. Methods:

2.4.1 Experimental animals

All animal experiments were approved by the local authorities and ethics committee. Adult male Sprague-Dawley rats and C57BL/6J mice of either sex were studied. UCP2$^{-/-}$ mice were obtained from the Jackson Laboratory[241]. All animal studies were approved by the local authority for animal research (Regierungspräsidium Giessen, reference number - GI 20/10 Nr. 105/2010 and GI 20/10 A34/2011). All animal manipulations before the death of the animals by circulatory arrest were performed by Karin Quanz, Alexandra Pichl and Prof. Dr. Norbert Weißmann. Afterwards the cell isolation was performed by the author of this thesis. The protocol for human tissue donation was approved by the ethics committee at the faculty of medicine, Justus-Liebig university of Giessen, in accordance with national legislation and the guidelines for good clinical practice / international conference on harmonization under the numbers 31/93 and 10/06.

2.4.2. Anesthesia

Mice were deeply anesthetized intraperitoneally by ketamine (100 mg/kg, Pfizer, Karlsruhe, Germany) and xylazine (8 mg/kg, Bayer Healthcare, Leverkusen, Germany). Rats were anesthetized intraperitoneally by ketamine (50mg/kg) and medetomidin (100µg/kg, Pfizer, Karlsruhe, Germany). In *vivo* cardiac hemodynamic measurement was performed under isoflurane (Forene® Abbott, Wiesbach, Germany) anesthesia with an inhalation system (Table Top Laboratory Animal Anesthesia System, VetEquip Inc, Pleasanton, USA).

2.4.3. MCT (monocrotaline) injection and chronic hypoxia

Adult male Sprague-Dawley rats (300-350g in body weight; Charles River Laboratories) were treated with injection of saline or 60 mg/kg MCT (Sigma-Aldrich, St. Louis, USA) to induce PH[89]. All rats were examined after 21 days of MCT injection.

Chronic hypoxic pulmonary vascular remodeling was induced by exposure of mice (C57BL/6J mice or UCP2$^{-/-}$ mice) to 28 days of normobaric chronic hypoxia (10% O_2) in a ventilated chamber[33] (Figure 13). The level of hypoxia was held constant by the autoregulatory control unit (model 4010, O_2 controller, Labotect; Göttingen, Germany) supplying either nitrogen (N_2) or O_2. Excess humidity in the recirculating system was prevented by condensation in a cooling system. CO_2 was continuously removed by soda lime. Cages were opened for a short time once per day for cleaning as well as for food and water resupply.

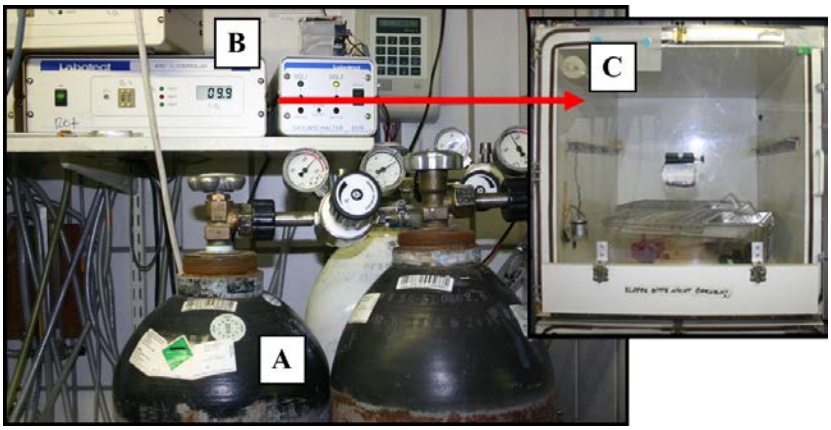

Figure 13. Hypoxic chamber and oxygen (O_2) pressure monitor.
Abbreviations: A - gas balloon with nitrogen (N_2); B - O_2 monitor; C - hypoxic chamber.

2.4.4. Invasive hemodynamic measurements

In *vivo* cardiac hemodynamic studies were preformed under isoflurane (Forene® Abbott, Wiesbach, Germany) anesthesia with an inhalation system (Table Top Laboratory Animal Anesthesia System, VetEquip Inc, Pleasanton, USA)[242]. Maintenance of anesthesia was provided by continuous inhalation of 1.5% isoflurane mixed with O_2 (Air Liquid, Siegen, Germany). After endotracheal intubation, mice were placed supine on a homeothermic plate (AD Instruments, Spechbach, Germany) and connected to a small animal ventilator MiniVent type 845 (Hugo Sachs Elektronik, March-Hugstetten, Germany). Body temperature was controlled by the rectal probe connected to the control unit (AD Instruments, Spechbach, Germany) and was kept at 37°C during the catheterization.

2.4.4.1 Right heart catheterization

The right external jugular vein was carefully exposed and afterwards, careful removal of the connective tissue surrounding the jugular vein was performed[242]. The tip of a high fidelity 1.4F micromanometer catheter (Millar Instruments, Houston, USA), presoaked with physiological saline solution for 30 min, was inserted in the caudal direction into the vein. Afterwards, the catheter was quickly moved into the right atrium and then right ventricle (RV). After stabilization of the signal, the pressure was recorded. All data were collected and analyzed using PowerLab data acquisition systems and LabChart 7 for Windows software (MPVS-Ultra Single Segment Foundation System, AD Instruments, Spechbach, Germany). The parameters measured were heart rate, right ventricular systolic pressure (RVSP), end-diastolic pressure (RVEDP), and the maximal and minimal first derivative of ventricular pressure (dP/dtMax and dP/dtMin, respectively).

2.4.4.2. Left heart catheterization

The right carotid artery was carefully exposed. A Biemer microvessel clip (Aesculap, Tuttlingen, Germany) was placed on the proximal part of the carotid artery. A tiny incision was made near the distal end of the artery. The tip of the 1.4F micromanometer catheter was inserted into the vessel. Simultaneously, the clip was released and the catheter was quickly moved into the left ventricle (LV) until the typical pressure signal was displayed on the monitor. After stabilization of the signal, the pressure was recorded.

At the end of the experiment, the mice were sacrificed and their hearts were harvested for further examination.

2.4.5. Assessment of vascular remodeling and right ventricular hypertrophy

After systolic arterial pressure and RVSP were recorded, the animals were exsanguinated. Afterwards the lungs were flushed with saline solution through the pulmonary artery, and perfused through the pulmonary artery and tracheae with a mixture of 3.5-3.7% formaldehyde (Otto Fischar GmbH&Co, Germany) with a constant pressure of 22 cm H_2O and 11 cm H_2O, respectively. The lungs and the heart were removed as a block. The lung lobes were embedded in paraffin blocks, and 3 µm sections were cut from all lobes.

For estimation of medial wall thickness (MWT) 3 µm lung sections were stained for elastica using common histopathological procedures (Van Gieson's stain) and nuclei were counterstaining by Nuclear Fast Red (Sigma-Aldrich, Saint Louis, USA)[243]. MWT was defined as the distance between the lamina elastica interna and lamina elastica externa. Percentage of MWT was examined by light microscopy using a computerized morphometric system (Qwin, Leica Microsystems, Wetzlar, Germany) and was calculated by the formula:

% MWT = (2 x wall thickness/external diameter) x 100

The muscularization of small peripheral pulmonary vessels was assessed by staining with an Anti-α-smooth muscle actin antibody (dilution 1:900, clone 1A4, Sigma-Aldrich, St. Louis, USA) and counterstaining with methyl green.

The RV was dissected from the LV and septum (LV+S), and these dissected samples were dried for 3 days at 50°C and weighed to obtain the right to LV plus septum ratio (RV/LV+S) or RV and LV mass to body weight.

2.4.6. Isolation of pulmonary artery smooth muscle cells (PASMC)

PASMC (Figure 14) were isolated from pulmonary precapillary arteries and cultured as described previously[13]. Briefly, the pulmonary artery was cannulated by a handmade cannula and M199 (Medium 199, Invitrogen, Carlsbad, USA) growth medium containing 5mg/ml glow melting point agarose, 5mg/ml Fe_3O_4, 1% penicillin, and 1% streptomycin was injected into rats (12 ml) and mice (3 ml). In this mixture, iron particles do not pass through capillaries and therefore only precapillary arteries were filled with the rapidly solidifying agarose and iron. Lung tissue was minced with scissors for 5 min in 1ml PBS (phosphate buffered saline). The tissue mixture was then suspended in 10ml PBS in a falcon tube, which was placed in a magnetic holder. The pulmonary arteries containing the iron particles and agarose accumulate on the tubing walls. The supernatant was aspirated and the arteries, after rinsing 3 times with PBS, were transferred into Petri dishes containing 10ml of M199 with 80U/ml collagenase and were then incubated at 37°C for 60 min. The tissue mixture was disrupted by drawing it through 15 and 18 gauge needles 5-6 times each. The resulting suspension, containing the medial layer of the arteries attached to iron particles, was placed in clear plastic tubes and rinsed three times with M199 containing 10% FCS (fetal calf serum) in the magnetic holder, as described above. The medial layer of the pulmonary artery attached to iron was finally re-suspended in medium, transferred to culture flasks and incubated at 37°C in the cell incubator for 4 to 5 days. Upon reaching 80% confluence, the grown cells were trypsinized and divided into the fresh culture flasks.

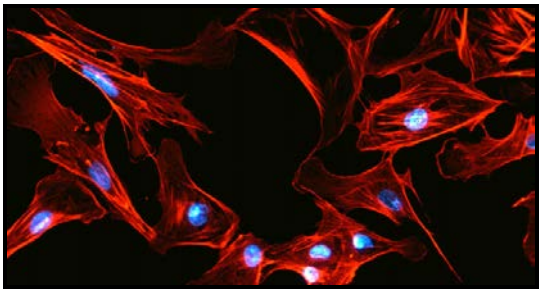

Figure 14. Representative picture of PASMC isolated from small precapillary pulmonary vessels of the mice.
Precapillary PASMC were labeled with an antibody against α-smooth muscle actin conjugated with Cy3 (red fluorescence) and the nuclei were stained by DAPI (4'-6-Diamidino-2-phenylindole, blue fluorescence).

Mouse PASMC (2-1 passage) were cultured in human medium for SMC (PromoCell, Heidelberg, Germany) with 15% FCS (PromoCell, Heidelberg, Germany) and rat PASMC (2-1 passage) were cultured in M199 (Invitrogen, Carlsbad, USA) with 10% FCS. For experimental procedures, the cells were incubated with MnTBAP (Manganese (III) tetrakis (4-benzoic acid)porphyrin chloride) and bongkrek acid (BA) in a dose of 50.0µM, DCA in a dose of 500.0µM, with FCCP doses of 1.0µM, 2,5µM, 5.0µM and with a ROS scavengers mixture consisting of 25.0µM NAC (N-acetyl-L-cysteine) and

1.0µM TEMPO (2,2,6,6-tetramethylpiperidine-N-oxyl). All reagents were purchased from Sigma-Aldrich, St. Louis, USA.

2.4.7. Measurement of $\Delta\psi_m$

$\Delta\psi_m$ was investigated by using JC1 (5,5',6,6'-tetrachloro-1,1',3,3'-tetraethylbenzimidazolylcarbocyanine iodide)[13]. JC-1 is a lipophilic, cationic dye that can selectively enter into mitochondria and reversibly change the emission spectrum from green (530nm) to red (590nm) upon excitation at 490nm as $\Delta\psi_m$ increases (Figure 15a).

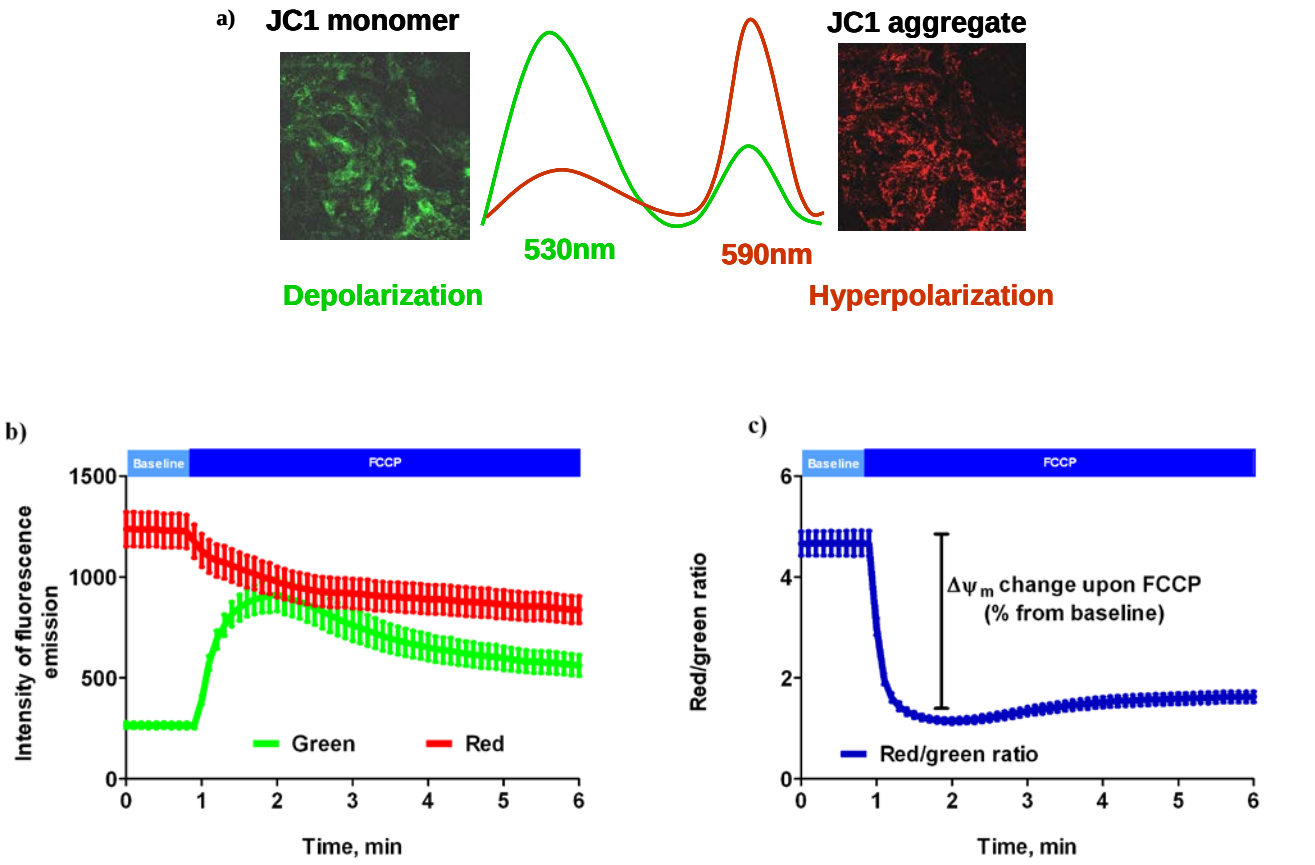

Figure 15. Scheme of the effect of mitochondrial depolarization and hyperpolarization on the characteristics of JC1 fluorescence (a). Example of $\Delta\psi_m$ evaluation by FCCP-stimulated mitochondrial depolarization (b and c).
Depolarization of mitochondria leads to release of JC1 into the cytosol in form of JC1 monomers that emit light at 530nm and hyperpolarization of mitochondria results in accumulation of JC1, which aggregate within mitochondria and emit light at 590nm (a). Application of 0.5µM FCCP induces mitochondrial depolarization, thereby increasing the green fluorescence emission and decreasing the red fluorescence emission (b) and subsequently decreases the red/green ration (c). The difference between the baseline $\Delta\psi_m$ and $\Delta\psi_m$ after FCCP stimulation was calculated in percentage (Figure15 c). Data presented as mean±SEM, n=36 of precapillary PASMC.

Precapillary PASMC seeded on coverslips were incubated in 50nM JC1 diluted in medium for 20min and were then transferred in an opened heated chamber (PeCon, Germany) which was filled with 500µl Hepes-Ringer buffer buffer (HRB; 136.4 mM NaCl, 5.6 mM KCl, 1 mM $MgCl_2$, 2.2 mM $CaCl_2$, 10 mM Hepes [4-(2-hydroxyethyl)-1-piperazineethanesulfonic acid], 5 mM glucose, pH 7.4). FCCP at a dose of 0.5µM was used to induce the collapse of $\Delta\psi_m$ (mitochondrial depolarization) that is characterized by an increase of green fluorescence emission and decrease of red fluorescence emission (Figure 15 b). As the result, the red/green ratio was decreased upon FCCP application (Figure 15c). The difference between the baseline $\Delta\psi_m$ and $\Delta\psi_m$ after FCCP stimulation was calculated as a percentage and used as additional parameter for an evaluation of the $\Delta\psi_m$ (Figure15 c).

Fluorescent signal was analyzed using a Polychrome II monochromator and IMAGO CCD camera (Till Photonics, Germany) coupled to an inverted microscope (IX70; Olympus, Germany). Ratio of red and green fluorescent signals and percent of $\Delta\psi_m$ drop induced by FCCP compared to baseline was analyzed.

To study the effect of acute hypoxia, precapillary PASMC loaded with 1µg/ml JC1 were transferred in a closed perfusion chamber (PeCon, Germany) and acute hypoxia was induced by switching from normoxic perfusion buffer (with a flow of 1 ml/min) to hypoxic buffer, which had been pregassed with N_2 (Figure 16). For control experiments the normoxic perfusion buffer was switched to a second normoxic perfusion buffer. All reagents were purchased from Sigma-Aldrich, St. Louis, USA.

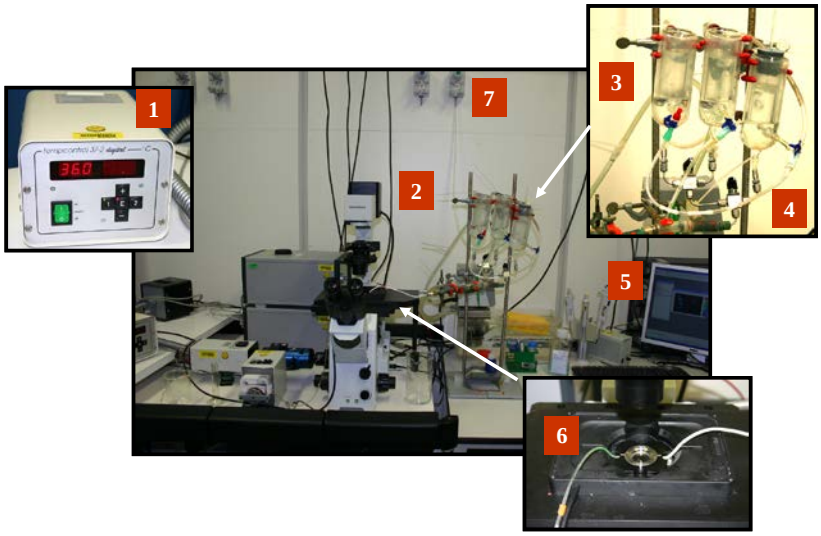

Figure 16. Set-up of acute hypoxic experiments in isolated PASMC.
Acute hypoxia was induced by switching the perfusing buffer of the closed perfusion chamber from normoxic buffer to hypoxic buffer gassed with N_2, resulting in a decrease of pO_2 to ~18 mmHg. 1 -the temperature control of the heating system; 2 - the inverted microscope (Olympus IX70) connected to the fluorescent light source and CCD camera; 3 - heated perfusion reservoirs with buffer; 4 - tube that connects reservoir with N_2 (7); 5 - computer with Till Photonics software; 6 - closed perfusion chamber (PeCon); 7 - source of N_2.

JC1 measurements during acute hypoxia were confirmed by measurements with the fluorescent dye TMRE (tetramethylrhodamine, Ethyl Ester, Perchlorate) using confocal microscopy (TCS SP5X, Leica Microsystems, Manheim, Germany). TMRE is a lipophilic, cationic fluorescent dye that accumulates within mitochondria according to their $\Delta\psi_m$ in a Nernstian fashion[244]. There are two alternative approaches to measure $\Delta\psi_m$ in cells by TMRE. One is to use a high concentration of TMRE (quenching mode), more than 100nM, to induce quenching of the fluorescent signal upon hyperpolarization of mitochondria due to accumulation of TMRE within mitochondria. We used in this study the alternative approach, which is measurement with low dose TMRE (non-quenching mode). Cells were loaded with, 10 nM TMRE for 30 minutes in HRB. Afterwards, buffer was exchanged. $\Delta\psi_m$ hyperpolarization caused an increase of mitochondrial TMRE concentration[245, 246], which resulted in increased emission of light at 580nm, when excited with 550 nm.

2.4.8. Measurement of ROS

2.4.8.1. Measurement of mitochondrial superoxide ($O_2^{\bullet-}$) release by MitoSOX

For acute hypoxic experiments, 5µM MitoSOX (Invitrogen, Carlsbad, USA) was used for detection of mitochondrial ROS in an experimental setting as described for the JC1 measurements of $\Delta\psi_m$[13]. Before the acute hypoxic exposure precapillary PASMC were incubated for 15 min in 5µM MitoSOX diluted in HRB buffer at 37°C. After accumulation in mitochondria, MitoSOX becomes fluorescent upon oxidation by $O_2^{\bullet-}$. Excitation of MitoSOX was 510nm and emission was measured at 580nm.

2.4.8.2. Determination of cytosolic hydrogen peroxide (H_2O_2) concentration by HyPer

For intracellular H_2O_2 detection, the coding information for the H_2O_2-sensitive, enhanced yellow fluorescent protein variant HyPer (Hydrogen Peroxide sensor) from Evrogen Company (Moscow, Russian Federation)[247] was subcloned under the control of the EF-1α (human elongation factor-1 alpha) enhancer/promoter into the pWPXL plasmid (distributed by Addgene, Boston, USA) and packed with a second-generation lentivirus transduction system with pMD2.G, as the envelope and psPAX2, as a packing vector (Addgene, Boston, USA). Lentiviral transduction was carried out with a titer of at least 1×10^7 particles according to established protocols (see http://tronolab.epfl.ch/ for more details). Experiments were carried out as outlined for the $\Delta\psi_m$ imaging in precapillary PASMC seeded on coverslip 3 days after lentiviral transduction. HyPer has two excitation peaks with maxima at 420 nm and 500 nm, and one emission peak with a maximum at 516 nm. H_2O_2 increases the excitation at 500nm and decreases the excitations at 420nm of the HyPer construct, thus ratiometric measurements are possible

2.4.8.3. Measurement of $O_2^{\bullet-}$ release by electron spin resonance (ESR) spectroscopy

Intracellular and extracellular $O_2^{\bullet-}$ levels in precapillary PASMC were measured by ESR spectroscopy (electron spin resonance or electron paramagnetic resonance) using the spin probe 1-Hydroxy-3-methoxycarbonyl-2,2,5,5-tetramethylpyrrolidine (CMH, Alexis Corporation, San Diego, USA) and a MS 100 spectrometer (Magnettech, Berlin, Germany)[248]. Precapillary PASMC in passages 2-1 were counted and divided in two samples (control and sample with pSOD [polyethylen-glycol conjugated SOD, Sigma-Aldrich, St. Louis, USA] 100 000 cells each). One sample was incubated with 0.1M pSOD for 2h. After pSOD incubation 0.5mM CMH was added to both samples. $O_2^{\bullet-}$ portion was determined as the differences of the ESR signal of the samples with and without pSOD.

2.4.9. Laser-assisted microdissection

Cryosections (8 µm) from lung tissue were mounted on glass slides. After hemalaun staining for 45 seconds, the sections were subsequently immersed in 70% and 96% ethanol and stored in 100% ethanol until used. Intrapulmonary arteries with a diameter of less than 100 µm were selected and microdissected under optical control using the Laser Microdissection System (LMD7000, Leica Microsystems, Wetzlar, Germany). Vessels were collected by gravity into a reaction tube containing 300 µl of RNA (ribonucleic acid) lysis buffer. RNA was isolated using the RNeasy Micro Kit (Qiagen N.V., Hilden, Germany). mRNA (messenger RNA) was converted into cDNA (complementary deoxyribonucleic acid) and amplified by WT-ovationTM Pico RNA Amplification System (NuGEN, San Carlos, USA).

2.4.10. RNA isolation and real-time polymerase chain reaction (PCR)

Total RNA (1µg), extracted from isolated PASMC or lung homogenate by RNeasy Micro Kit (Qiagen N.V., Hilden, Germany) was reverse-transcribed using the iScript cDNA Synthesis Kit (Bio-Rad, Hercules, USA). Afterwards, total cDNA including the cDNA obtained from laser microdissected vessels was used to carry out real-time PCR (polymerase chain reaction) using a master mix for RT PCR (iTaq SYBR Green supermix with ROX, Bio-Rad, Hercules, USA) and Mx3000P QPCR Systems (Agilent Technologies, Santa Clara, USA). Housekeeping genes were HPRT (Hypoxanthine phosphoribosyltransferase) for MCT-induced PH and β_2M (β2-microglobulin) for chronic hypoxic experiments. A list of primers is provided below in Table 3.

The cycling protocol was 1×(95°C, 10 min) and 45×(95°C, 5s; 62°C, 5s, 72°C, 10s). The data for the amplification curves were acquired after the extension phase at 72°C. The threshold value was set for each gene in the middle of the overlapping region of the exponential phases. Each gene was measured in duplicate. The formation of the specific products was verified by dissociation curves and by analysis on an agarose gel with SYBR® Safe DNA gel stain (Invitrogen, Carlsbad, USA). The ΔCt values were

calculated by subtracting the Ct values of the target gene from the endogenous control (ΔCt = Ct[endogenous control] - Ct[target]) and the fold change $2^{\Delta\Delta Ct}$ comparing experimental and control conditions was calculated as described previously[249].

Table 3. List of primers for real time PCR.

Species	Primer	Orientation	Sequence	Accessing number
Mice	Acot1/2	Sence	TGAAGAAGCCGTGAACTACCTG	NM_012006.2
		Antisence	CCTTCAGGAAGGAGGCCATA	NM_134188.3
	Slc25a20	Sence	CCCTGGACACGGTCAAGGTCCG	NM_020520.4
		Antisence	GGCGCAGCCATGCCCCGATA	
	Ehhadh	Sence	GGCTAGAGCCCTGCAGTACGCC	NM_023737.3
		Antisence	GCGATGCCTCGGCCCATCGT	
	Cpt2	Sence	CCTGCCCAGGCTGCCTATCCCTAA	NM_009949.2
		Antisence	TGCGCATGCAGCTCCTTCCCAAT	
	Cpt1b	Sence	CCTCCGAAGCAGGAGCCCCCT	NM_009948.2
		Antisence	TCACGGTCCAGTTTGCGGCGA	
	LDHA	Sence	CCATCATCTCGCCCTTGAGT	NM_010699.1
		Antisence	GGCCATCGGCCTGAGCGTGG	
	PDK1	Sence	CGTCACGCTGGGCGAGGAGG	NM_172665.4
		Antisence	GGGGCACAGCACGGGACGTT	
	Pfkfb3	Sence	TTGCATCCTCTGACCTCTCCCGGTG	NM_001177757.1
		Antisence	GATTTTGAGCACCGCATGCCCCG	
	Pkm	Sence	AATGTGGCTCGGCTGAATTT	NM_011099.3
		Antisence	CGCAACAGGACGGTAGAGAA	
	Glut1	Sence	TGTGGAGCAACTGTGCGGCCC	NM_011400.3
		Antisence	CTGCCGGAAGCCGGAAGCGA	
	UCP2	Sence	AAGGGCTCAGAGCATGCAG	NM_011671.4
		Antisence	TGGAAGCGGACCTTTACCAC	
	β2M	Sence	AGCCCAAGACCGTCTACTGG	NM_009735.3
		Antisence	TTCTTTCTGCGTGCATAAATTG	
Rat	LDHA	Sence	GATGTGCACAAGCAGGTGGT	NM_017025.1
		Antisence	TCACGGTCCAGTTTGCGGCGA	
	PDK1	Sence	ATTGCCCATATCACGCCTCT	NM_053826.2
		Antisence	TCGATGGACTCCGTTGACAG	
	HPRT	Sence	CTCAGTCCCAGCGTCGTGAT	NM_012583.2
		Antisence	AGCACACAGAGGGCCACAAT	
	β2M	Sence	CGGTGACCGTGATCTTTCTG	NM_012512.2
		Antisence	AGGAAGTTGGGCTTCCCATT	

Abbreviations: pfkfb3 - 6-phosphofructo-2-kinase/fructose-2,6-biphosphatase 3; Pkm - pyruvate kinase, muscle form; LDHA - lactate dehydrogenase; Glut1 - glucose transporter 1; PDK1 - pyruvate dehydrogenase kinase 1; acot1/2 - acyl-CoA thioesterase 1 and 2; cpt1b - carnitine palmitoyltransferase 1b; cpt2 - carnitine palmitoyltransferase 2; Slc25a20 - carnitine/acylcarnitine translocase; ehhadh - enoyl-Coenzyme A, hydratase/3-hydroxyacyl Coenzyme A dehydrogenase; UCP2 - uncoupling protein 2; β_2M - β_2-microglobulin; HPRT - hypoxanthine phosphoribosyltransferase.

2.4.11. RNA interference by synthetic siRNA

Selective targeting of UCP2 was performed using a pool of specific siRNAs (small interfering RNA) (Table 4). As a control, a siRNA sequence (scrambled) was employed that does not target any gene in the rat and mouse genome. The siRNAs were synthesized commercially (BioSpring GmbH, Frankfurt am Main, Germany). Transfection of UCP2 siRNA was performed in low-serum and antibiotic-free medium (1% FCS in M199). The medium was changed 4h before transfection. 100 nM of UCP2 siRNA was transfected using 1µl X-tremeGENE siRNA Transfection Reagent (Roche Applied Science, Penzberg, Germany) per cm^2 of the well. Both siRNA and transfection reagent were diluted in OPTI-MEM medium (Invitrogen, Carlsbad, USA). After five hours of transfection, the medium was changed to 20% FCS human medium for SMC (PromoCell, Heidelberg, Germany) containing antibiotics (1% penicillin and streptomycin).

Table 4. List of siRNA sequences against UCP2

Species	siRNA	Duplex sense-antisense
Mice	UCP2_1	AA*CA*GU*UC*UA*CA*CC*AA*GG*GC*U- A*GC*CC*UU*GG*UG*UA*GA*AC*UG*U
	UCP2_2	AA*AG*AU*AC*UC*UC*CU*GA*AA*GC*C- G*GC*UU*UC*AG*GA*GA*GU*AU*CU*U
	UCP2_3	AA*CG*UA*GU*GA*UG*UU*UG*UC*AC*C- G*GU*GA*CA*AA*CA*UC*AC*UA*CG*U
Rat	UCP2_1	AA*CU*GU*AC*UG*AG*CU*GG*UG*AC*C- G*GU*CA*CC*AG*CU*CA*GU*AC*AG*U
	UCP2_2	AA*AG*AU*AC*UC*UC*CU*GA*AA*GC*C- G*GC*UU*UC*AG*GA*GA*GU*AU*CU*U
	UCP2_3	AA*CG*UA*GU*AA*UG*UU*UG*UC*AC*C- G*GU*GA*CA*AA*CA*UU*AC*UA*CG*U

* 2'OMe (methylated) nucleotide

2.4.12. UCP1 and UCP2 overexpression in mouse precapillary PASMC

UCP1 and UCP2 overexpression was performed using the TrueORF vector system[250] that over-expressed the open reading frame (ORF) of the UCP1 or UCP2 mouse gene with two epitope tags (C-terminal Myc (sequence is N-EQKLISEEDL-C) and DDK (sequence is DYKDDDDK epitope) under the strong eukaryotic CMV (cytomegalovirus) enhancer/promoter (OriGene, Rockville, USA). Mouse precapillary PASMC from passage 2-1 were seeded in 48-well plates at a density of 6×10^3 cells/well for proliferation and 40×10^3 cells/well in 6-well plates in 20% FCS/human medium for SMC (PromoCell, Heidelberg, Germany) for western blot. Next day cells were transfected with 0.25µg/cm^2 plasmid DNA at a 1:3 ration with transfection reagent turbofectin 8 (OriGene, Rockville, USA) diluted in OPTI-MEM medium (Invitrogen, Carlsbad, USA). After 6h of transfection, the medium was changed to normal cultured

medium. Western blot and proliferation assays were performed as described below 2 days after transfection.

2.4.13. Western blot analysis

Tissue extracted by Precelly®24 Homogeniser (Peqlab, Erlangen., Germany), or cell lysates from precapillary PASMC were separated on a 10 % SDS (sodium dodecyl sulfate) polyacrylamide gel, followed by electrotransfer to a 0.45µm PVDF (polyvinylidene fluoride) membrane (Pall Corporation, Dreieich, Germany). After blocking with 5% non-fat dry milk in TBS-T buffer (Tris Buffer Saline + 0.1% Tween 20) for 1 hour, the membrane was incubated overnight at room temperature with one of the following antibodies: anti-PDK1 (rabbit antibody, dilution 1:1000, Cell Signaling Technology, Inc. Danvers, USA), anti-LDHA (rabbit antibody, dilution 1:1000, Cell Signaling Technology, Inc. Danvers, USA), anti-DDK (mouse monoclonal antibody, dilution 1:1000, OriGene, Rockville, USA), anti-cyclin D1 (rabbit antibody, dilution 1:1000, Cell Signaling Technology, Inc. Danvers, USA), anti-UCP2 (goat antibody, dilution 1:200, Santa Cruz Biotechnology, Santa Cruz, USA) and monoclonal mouse anti-β-actin (dilution 1:50000, Sigma-Aldrich, St. Louis, USA). After washing the membranes in TBS-T buffer, specific immunoreactive signals were detected by enhanced chemiluminescence (GE Healthcare, Little Chalfont, UK) using a proprietary secondary antibody coupled to horseradish-peroxidase diluted 1:5000.

2.4.14. Measurement of precapillary PASMC proliferation

2.4.14.1. [3H]-Thymidine proliferation assay of PASMC

For assessment of proliferation, mouse precapillary PASMC from passage 2 were seeded in 48-well plates at a density of 8×10^3 cells/well in 20% FCS/human medium for SMC (PromoCell, Heidelberg, Germany). Cells were rendered quiescent by incubation in 5% FCS in human medium for SMC for 24 hours. Subsequently, they were stimulated with 20% FCS/human medium to induce cell cycle re-entry. [3H]-Thymidine (GE Healthcare, Little Chalfont, UK) was used at a concentration of 0.5 µCi per well. Subsequently, cells were washed 3x with ice-cold PBS and lysed with 0.5M NaOH (sodium hydroxide) on a shaker for 4 h. The [3H]-Thymidine concentration of the cell lysates was assessed by a scintillation counter (Canberra-Packard, TRI-CARB 2000, Meriden, USA).

2.4.14.2. Evaluation of PASMC growth rate based on crystal violet staining

Mouse precapillary PASMC from passage 2-1 were seeded in 48 well plates at a density of 10 x 10^3 cell/well in 20% FCS/human medium for SMC (PromoCell, Heidelberg, Germany). Cells were rendered quiescent by incubation in 5% FCS in human medium for SMC for 24 hours. Subsequently, they were stimulated with 20% FCS/human medium for SMC to induce cell cycle re-entry for 24h. Seeded cells

were washed with PBS and fixed in 4% paraformaldehyde (Merck, Whitehouse Station, USA) for 15 min, then stained with 0.1% crystal violet (Sigma-Aldrich, St. Louis, USA) for 20 min. After removing the supernatant, plates were dried and 10% acetic acid (Sigma-Aldrich, St. Louis, USA) was added to each well for 20 min incubation with shaking. Absorbance was measured at 590 nm by multimode plate reader Infinite m200 (Tecan Group Ltd, Männedorf, Switzerland).

2.4.15. Non-isotopic in situ hybridization on mouse lung sections

Non-isotopic in situ hybridization was performed on 8μm thick TissueTek®-embedded mouse lung cryostat sections from wild type and UCP2$^{-/-}$ mice as described previously[73]. The sections were incubated with DIG-labeled (digoxigenin-labeled) UCP2 probes (LNA™ mRNA Detection Probes, Exiqon, Vedbaek, Denmark) in 2x hybridization solution [1M NaCl, 0.02M Tris,pH7.5, 2 x Denhardt's reagent, 2mM EDTA (ethylenediamine-tetraacetic acid), 2g dextran sulphate, 0.2mg/ml yeast tRNA (transfer RNA)] at 55°C for overnight. The following day, slides were washed with buffer ranging from low to very highly stringent conditions as follows: on shaking platform 2x SSC (saline-sodium citrate buffer) for 1h at room temperature, 0.1x SSC at 60°C. The sections were treated with blocking buffer (2% Blocking reagent, Roche Applied Science, Penzberg, Germany) for 30 min, followed by incubation with a Alexa fluor 488 labeled antibody against DIG antigen (Roche Applied Science, Penzberg, Germany) in a dilution of 1:20 for 2h at room temperature. After antibody incubation, sections were washed in TBT buffer (50mM, 1M Tris-HCl,pH 7.5, 150mM NaCl and 0.1% Triton X-100) three times for 15min each. Afterwards, slides were incubated with a mouse monoclonal Cy3-labeled α-smooth muscle actin antibody (Sigma, Hamburg, Germany) at a dilution of 1:500 in PBS, for 1h. After washing (3 x 3min) in PBS, sections were mounted in carbonate-buffered glycerol (pH-8.6). In situ hybridization was evaluated with appropriate filter sets for Cy3 and Alexa fluor 488 with Leica microscope (Leica Microsystems, Wetzlar, Germany).

2.4.16. Isolation of pulmonary mitochondria

Lung mitochondria were isolated as described previously with some modifications[251]. Briefly, after deep anesthesia with ketamine/xylazine, as described above, the thorax of the mouse was opened and the lung washed with ice-cold PBS buffer via the pulmonary artery. The lung was removed from the thoracic cavity together with the heart as one bloc and transferred to a dish with medium A (250mM sucrose, 0.5mM Na_2EDTA, 10mM Tris, pH7.4). The lung was separated from the heart and mediastinum and moved into a homogenizer tube (inner diameter 1.9 cm and distance between tube and pestle 0.5-1.0mm). Lung tissue was homogenized using the "schütt homogenplus" homogenizer (Schuett-biotec GmbH, Göttingen Germany) with 200-300rpm. The homogenate was centrifuged at 660g for 10min at 4°C. The

supernatant was centrifuged at 10000g for 10 min at 4°C and the pellet resuspended in medium A with 1g/l BSA (bovine serum albumin). After centrifugation, the pellet was resuspended in medium MiRO5 (0.5mM EGTA, 3mM $MgCl_2$, 60mM K-lactobionate, 20mM Taurine, 10mM KH_2PO_4, 20mM Hepes, 110mM sucrose and 1g/l BSA).

2.4.17. Evaluation of intracellular pyruvate concentration and in lung mitochondria

Pyruvate concentration in precapillary PASMC (48well plates with a density of 10 x 10^{10}) was measured after 24h 20% FCS stimulation. Mitochondria were isolated as described before and stimulated with 5mM pyruvate for 2min. Pyruvate was oxidized by pyruvate oxidase to acetyl phosphate. The product of this reaction, H_2O_2, reacts with 10-acetyl-3,7,-dihydroxyphenoxazine in presence of horseradish peroxidase to produce the fluorescent resorufin. Resorufin fluorescence was measured with excitation 535nm and emission 590nm by Infinite m200 (Tecan Group Ltd, Männedorf, Switzerland) microplate reader.

2.4.18. Evaluation of mitochondrial calcium ($[Ca^{2+}]_m$) concentration

$[Ca^{2+}]_m$ concentration was measured by fluorescent microscopy using 5µM Rhod2 AM (cell-permeant acetoxymethyl (AM) ester form of rhod2 (1-[2-Amino-5-(3-dimethylamino-6-dimethylammonio-9-xanthenyl)phenoxy]-2-(2-amino-5-methylphenoxy)ethane-N,N,N',N'-tetraacetic acid) from Invitrogen, (Carlsbad, USA). Experiments were performed as described for the JC1 measurements of $\Delta\psi_m$. Rhod 2 is a derivative of rhodamine 123 that accumulates into mitochondria electrophoretically. Once inside the matrix, mitochondrial esterases cleave the AM ester to liberate Rhod 2 free acid. Rhod2 is non-fluorescent before Ca^{2+} binding, but becomes fluorescent with increasing Ca^{2+} concentrations exhibiting an emission maximum at 580nm when excited at 590nm[252].

Additionally, $[Ca^{2+}]_m$ was measured with the multimode microplate reader, Infinite m200 (Tecan Group Ltd, Männedorf, Switzerland). Precapillary PASMC from passages 2-1 were seeded in 48well plates at a density of 10 x 10^{10}. After loading precapillary PASMC with 5µM Rhod2 for 20 min, fluorescence was measured by the reader.

2.4.19. High-resolution respirometry

O_2 consumption was determined at 37°C using Oxygraphy-2K (Oroboros Instruments, Innsbruck, Austria)[13]. Rat precapillary PASMC from passage 2 were trypsinized and resuspended in M199 (Invitrogen, Carlsbad, USA). A standard protocol using oligomycin (2.0 µg/ml), FCCP (0.45 µM), rotenone (0.5 µM) and antimycin A (2.5 µM) was used for measurement of cellular respiration. To check the effect of pyruvate on mitochondrial respiration, the following protocol was chosen: 1) for isolated mitochondria – 1.0mM ADP, 5.0mM pyruvate, 1.0µM rotenone, 10.0mM succinate, 0.5µM FCCP and

2.5µM antymicin A; 2) for rat precapillary PASMC after transfection with siRNA against UCP2 – 1.0mM ADP, 5.0mM pyruvate, 1.0µM rotenone, 10.0mM succinate, 2.0µg/ml oligomycin, 0.5µM FCCP, and 2.5µM antimycin A. O_2 consumption was calculated from the recorded data as the time derivative of the O_2 content in the chamber, using DatLab software (Oroboros Instruments, Innsbruck, Austria).

2.4.20. Statistics

Values are given as means ± SEM. Statistical significance of the data was calculated by Student's t test with Welsh's correction or analysis of variance (one way ANOVA) with Bonferroni post hoc test as appropriate. For a multiple comparison of more than four groups, ANOVA with Tukey post hoc test was performed. A p value less than 0.05 was considered to be significant.

3. Results

3.1. $\Delta\psi_m$ and HPV

3.1.1. Effect of acute hypoxia on $\Delta\psi_m$ and ROS release in precapillary PASMC

$\Delta\psi_m$ was increased during perfusion with hypoxic buffer ("acute hypoxia") in precapillary PASMC isolated from wild type (WT) mice (Figure 17). $\Delta\psi_m$ was measured by fluorescence microscopy with JC1 fluorescent dye. Figure 17a depicts a representative measurement of the JC1 fluorescent signal during an acute hypoxic challenge in mouse precapillary PASMC, where the green line depicts the 530nm fluorescence signal, the red line depicts the 590nm fluorescence signal of JC1 fluorescent dye and the blue line depicts the red/green ratio. Figure 17b demonstrates a time course of hypoxia-induced increase of $\Delta\psi_m$ in mouse precapillary PASMC.

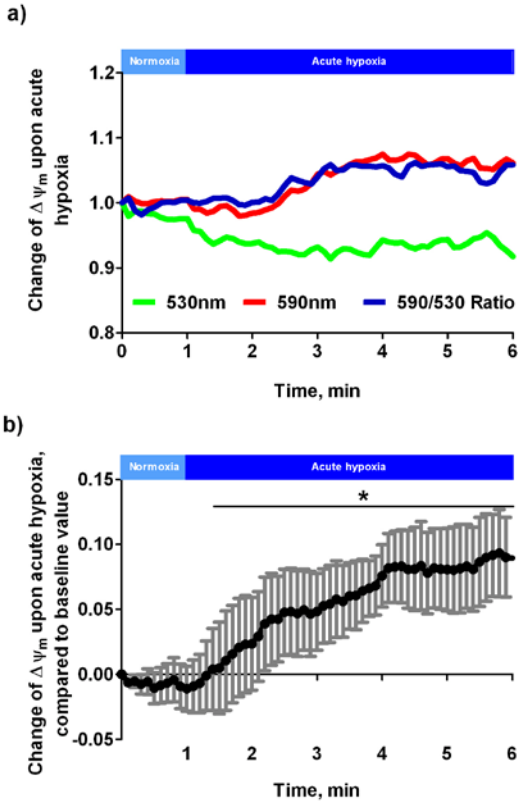

Figure 17. $\Delta\psi_m$ alteration upon acute hypoxia in mouse precapillary PASMC measured by JC1.
Representative picture of the JC1 fluorescent signal. Intensity of light emission of JC1 calculated relative to the baseline value: green line represents light emission at 530nm corresponding to JC1 monomers in depolarized mitochondria, red line represents light emission at 590nm corresponding to JC1 aggregates in hyperpolarized mitochondria and blue line depicts the 590/530 ratio. b) $\Delta\psi_m$ hyperpolarization upon acute hypoxia in wild type precapillary PASMC. Data are presented as the change of 590/530 ratio compared to baseline. Acute hypoxia was applied by switching the normoxic perfusion buffer to the hypoxic (pre-bubbled by N_2) buffer at 1 min. Data were obtained from ≥4 independent precapillary PASMC cell isolations. n=51 PASMC.
* $p<0.05$, compared to baseline with Student's t test.

To confirm that acute hypoxia led to hyperpolarization of mitochondria in precapillary PASMC, data from JC1 experiments were compared to measurements of $\Delta\psi_m$ by TMRE fluorescence staining and confocal microscopy. The acute hypoxic challenge caused an increase of TMRE accumulation within mitochondria measured by a rise of the TMRE fluorescent emission signal at 580 nm corresponding to hyperpolarization of mitochondria (Figure 18).

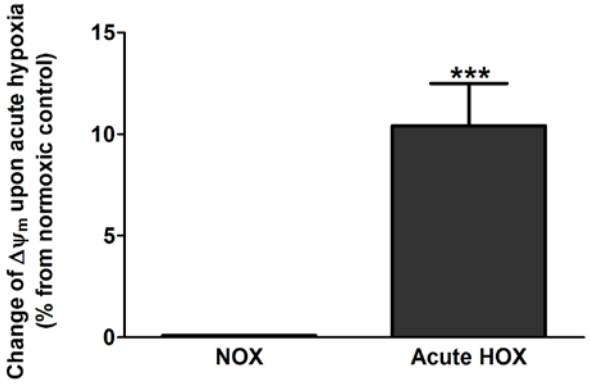

Figure 18. $\Delta\psi_m$ alteration upon acute hypoxia in mouse precapillary PASMC measured by TMRE.

Data are given as percent of $\Delta\psi_m$ change during acute hypoxic perfusion compared to normoxic control. Acute hypoxia was applied by switching the normoxic perfusion buffer to the hypoxic (pre-bubbled by N_2) buffer at 1 min. Data were obtained from ≥4 independent precapillary PASMC cell isolations. n=25 PASMC.
*** p <0.001 with Student's t test.

Mouse precapillary PASMC showed an increase of $O_2^{\bullet-}$ concentration within the mitochondrial matrix after changing the perfusion from normoxic buffer to hypoxic buffer. $O_2^{\bullet-}$ concentration was measured by the fluorescent dye MitoSOX (Figure 19).

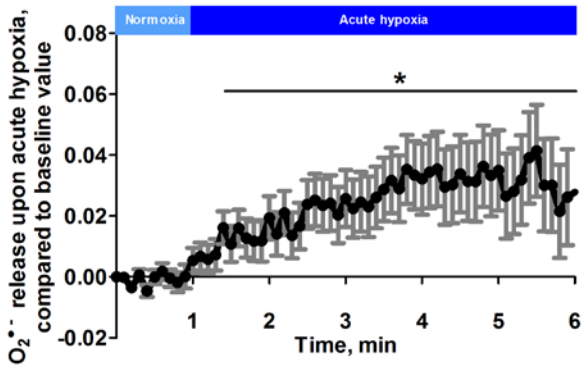

Figure 19. Alteration in mitochondrial superoxide ($O_2^{\bullet-}$) concentration upon acute hypoxia in mouse precapillary PASMC measured by MitoSOX.

The intensity of light emitted by MitoSOX at 580nm corresponds to an increase of fluorescence upon $O_2^{\bullet-}$ induced oxidation of MitoSOX during acute hypoxia. Data are presented as the change of MitoSOX fluorescence compared to baseline. Data were obtained from ≥4 independent precapillary PASMC cell isolations. n=19 PASMC.
* p<0.05 compared to baseline with Student's t test.

Furthermore, acute hypoxia stimulated the increase of H_2O_2 concentration within the cytosol of precapillary PASMC isolated from WT mice (Figure 20) measured by the HyPer construct.

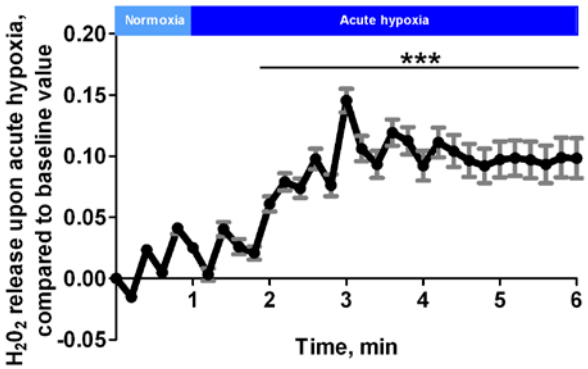

Figure 20. Alteration in intracellular hydrogen peroxide (H_2O_2) concentration upon acute hypoxia in mouse precapillary PASMC measured by HyPer.
H_2O_2 increases excitation at 500nm and decreases excitation at 420nm of the HyPer construct. The level of cellular H_2O_2 is presented as the change in the ratio of excitation intensity at 500nm and 420nm of HyPer compared to baseline. Data were obtained from ≥4 independent precapillary PASMC cell isolations. n=31 PASMC.
*** $p<0.001$ compared to baseline with Student's t test.

The same results were obtained from rat precapillary PASMC (Figure 21). Both rat and mouse precapillary PASMC responded with an increase of $\Delta\psi_m$ and ROS (both mitochondrial $O_2^{\bullet-}$ and intracellular H_2O_2) to the acute hypoxic challenge compared to normoxic control, measured by fluorescence microscopy (Figure 21).

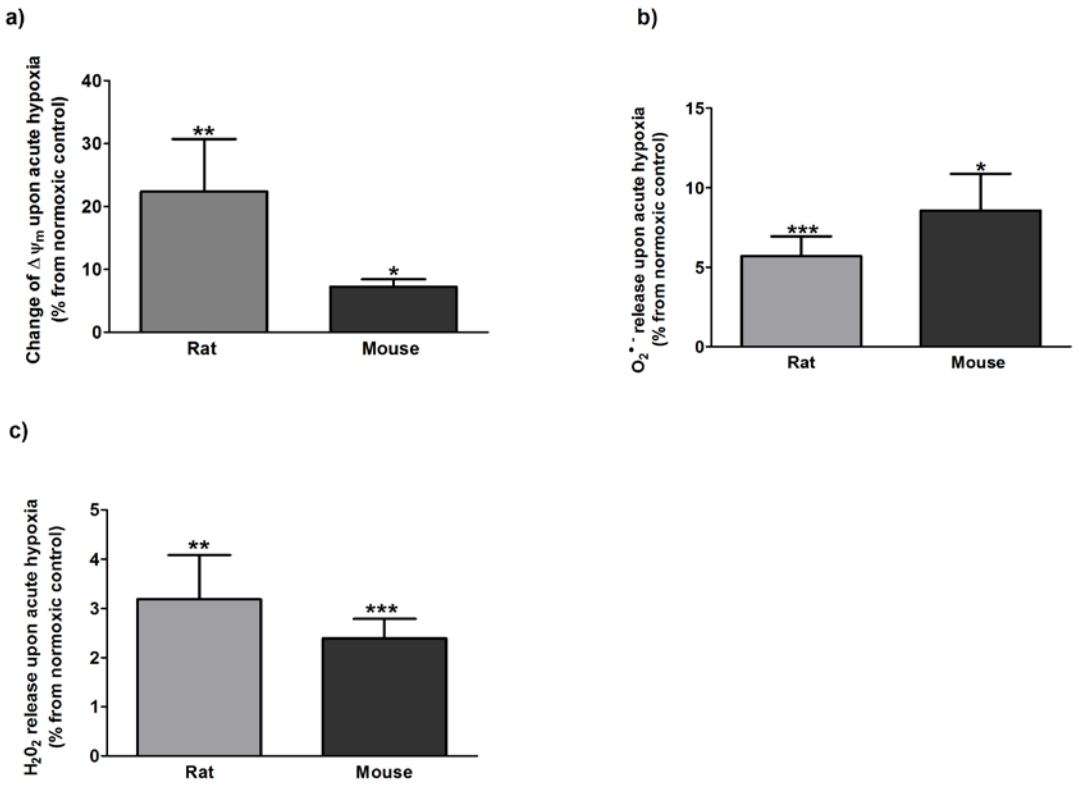

Figure 21. Increase of $\Delta\psi_m$ (a), mitochondrial $O_2^{\bullet-}$ (b), and cytosolic H_2O_2 concentration (c) in precapillary PASMC isolated from different animal species upon acute hypoxia.
Data were obtained from ≥4 independent precapillary PASMC cell isolations and ≥15 individual cells each. Data are presented as percent of change compared to normoxic value.
* $p<0.05$; ** $p<0.01$; *** $p<0.001$ compared to normoxic control with Student's t test.

To elucidate if increased ROS was upstream of $\Delta\psi_m$ alterations and possibly causing $\Delta\psi_m$ alterations during the acute hypoxic challenge, $\Delta\psi_m$ was measured during acute hypoxia in the presence of the unspecific ROS scavengers 25µM NAC (N-acetyl-L-cysteine) and 1µM TEMPO (2,2,6,6-tetramethylpiperidine-N-oxyl) in mouse precapillary PASMC. The ROS scavengers did not alter the acute hypoxia-induced hyperpolarization of mitochondria in precapillary PASMC isolated from WT mice (Figure 22).

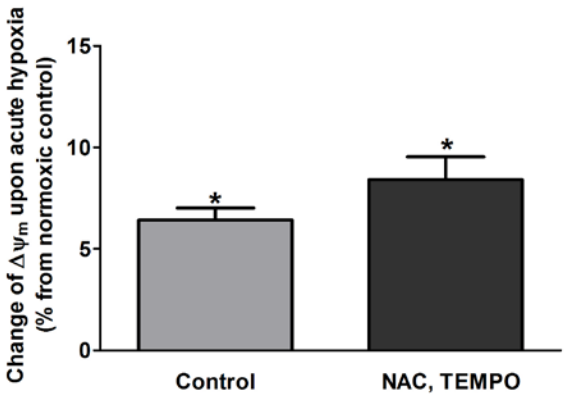

Figure 22. Effect of ROS scavengers on hyperpolarization of $\Delta\psi_m$ during acute hypoxia in mouse precapillary PASMC.

JC1 measurement of $\Delta\psi_m$ during acute hypoxia in the precapillary PASMC isolated from WT mice in the absence (Control) or presence of ROS scavengers (NAC, TEMPO). Data are given as percent of $\Delta\psi_m$ change during acute hypoxic superfusion compared to normoxic control. Data were obtained from ≥4 independent precapillary PASMC cell isolations and ≥50 individual cells each.

* $p<0.05$ compared to normoxic control with Student's t test.

3.1.2. Effect of UCP2 knockout ($UCP2^{-/-}$) on acute hypoxic responses of precapillary PASMC

To investigate the role of $\Delta\psi_m$ and ROS in HPV we studied genetically modified $UCP2^{-/-}$ mice in which full length UCP2 mRNA was not expressed[241]. It has been shown before that acute HPV was significantly higher in isolated perfused lungs of $UCP2^{-/-}$ mice compared to WT mice. In contrast, the vasoconstrictor response to the thromboxane mimetic U46619 did not differ between $UCP2^{-/-}$ and WT mice (unpublished thesis of Timm Hoeres, Giessen). The hypothesis that the increase of acute HPV in $UCP2^{-/-}$ mice was caused by increased $\Delta\psi_m$ during acute hypoxia was tested.

3.1.2.1. Effect of $UCP2^{-/-}$ on $\Delta\psi_m$ and $O_2^{\bullet-}$ emission in precapillary PASMC during acute hypoxia

First, the mRNA expression pattern of UCP2 in mouse lungs was investigated by in-situ hybridization. In figure 23, representative pictures of mRNA UCP2 expression in mouse lungs are shown. PASMC of small pulmonary arteries show the prominent expression of mRNA of UCP2. Lungs of $UCP2^{-/-}$ mice show no sign of expression of mRNA of UCP2.

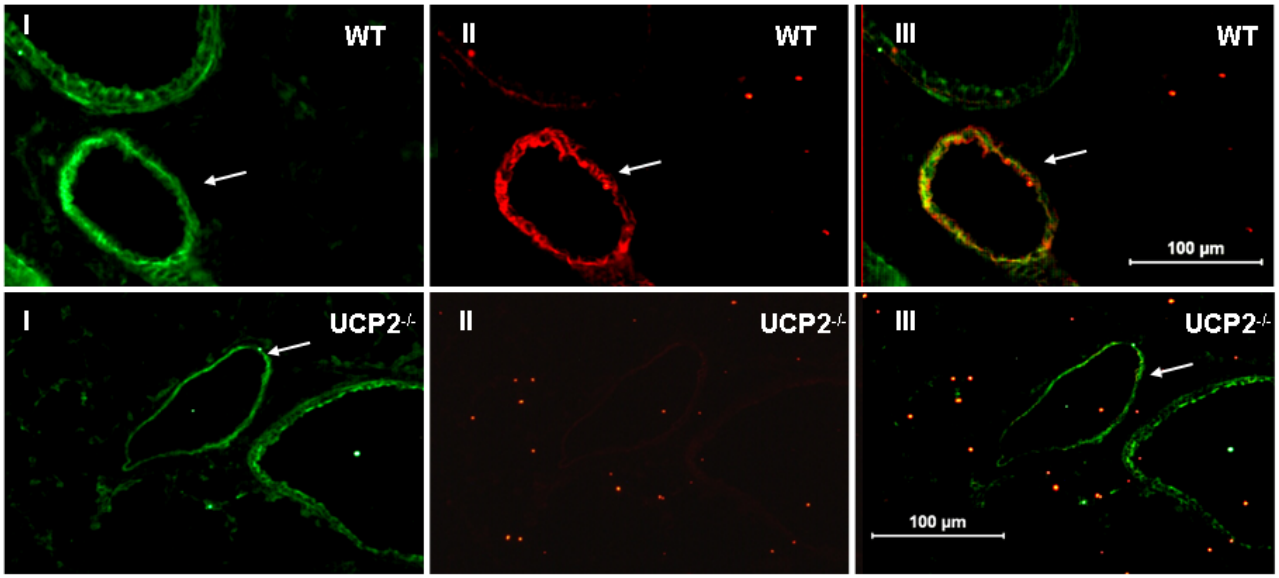

Figure 23. mRNA expression of UCP2 in mouse lung.

Representative pictures of in situ hybridization of mouse lungs of wild type (WT) and UCP2 knockout mice ($UCP2^{-/-}$).

I) Staining of mouse lung cryosections with Cy3-labelled antibody directed against α-smooth muscle actin (green fluorescence).

II) Hybridization of the UCP2 specific probe to the same mouse lung cryosections (red fluorescence).

III) Overlay of the images I) and II) is depicting the predominant co-localization of UCP2 transcripts within the smooth muscle cell layer of the pulmonary artery (yellow fluorescence). The pulmonary artery is depicted by arrow.

Gene deletion of UCP2 amplified the effect of 5 min acute hypoxic superfusion on the acute hypoxia-induced hyperpolarization as measured by JC1 fluorescent dye (Figure 24a), as well as by the increase of mitochondrial $O_2^{\bullet-}$ release measured by MitoSOX fluorescent dye in isolated precapillary PASMC compared to WT PASMC (Figure 24b).

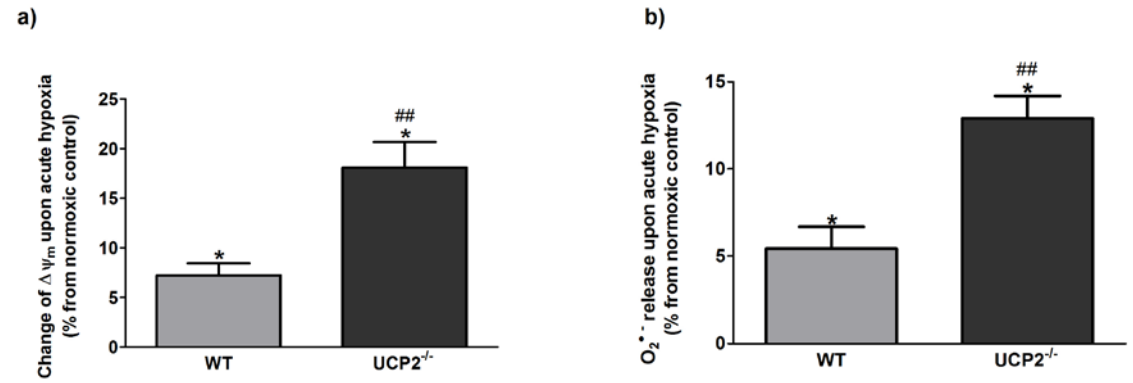

Figure 24. $\Delta\psi_m$ and $O_2^{\bullet-}$ release in precapillary PASMC from wild type (WT) and UCP2 knockout ($UCP2^{-/-}$) mice upon acute hypoxia compared to normoxic control.

a) $\Delta\psi_m$ hyperpolarization in percent in precapillary PASMC from UCP2 knockout ($UCP2^{-/-}$) and wild type (WT) mice during acute hypoxia. Data are given as percent of $\Delta\psi_m$ change during hypoxic superfusion compared to the normoxic control. b) Increase of $O_2^{\bullet-}$ release in % in precapillary PASMC from $UCP2^{-/-}$ and WT mice during acute hypoxia. Data are given as percent MitoSOX fluorescence of normoxic control. Data were obtained from ≥4 independent precapillary PASMC cell isolations and ≥13 individual cells each.

* $p < 0.05$ compared to normoxic control and ## $p < 0.01$ compared to acute hypoxic WT precapillary PASMC with Student's t test.

Alterations of $\Delta\psi_m$ in precapillary WT PASMC during acute hypoxia were not influenced by ROS scavengers (figure 22). In line with result from precapillary WT PASMC, the presence of ROS scavengers (25µM NAC and 1µM TEMPO) in the hypoxic perfusion buffer did not alter the acute hypoxia-induced hyperpolarization of mitochondria in precapillary PASMC isolated from $UCP2^{-/-}$ mice (Figure 25).

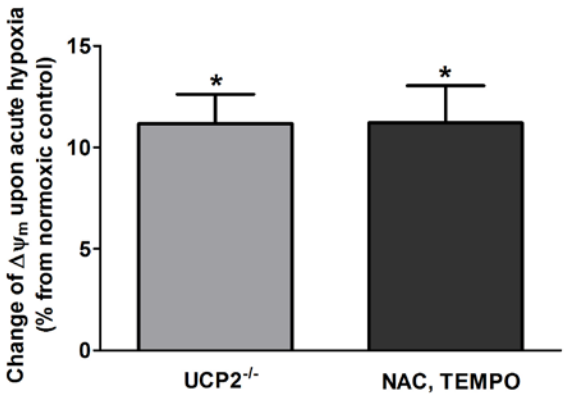

Figure 25. Effect of ROS scavengers on mitochondrial hyperpolarization during acute hypoxia.
JC1 measurement of $\Delta\psi_m$ in precapillary PASMC isolated from UCP2 deficient mice in the absence ($UCP2^{-/-}$) and in the presence of ROS scavengers (NAC, TEMPO). Data are given as percent of $\Delta\psi_m$ change during hypoxic superfusion compared to normoxic control. Data are obtained from ≥4 independent precapillary PASMC cell isolations and ≥31 individual cells each.
* $p < 0.05$ compared to appropriate normoxic control with Student's t test.

3.2. $\Delta\psi_m$ and PH

3.2.1. Evaluation of $\Delta\psi_m$ in IPAH and in animal models of PH

In order to investigate the role of $\Delta\psi_m$ in PH, $\Delta\psi_m$ was measured in PASMC isolated from animals with different forms of experimental PH and from patients with IPAH. Mitochondria were found to be hyperpolarized in PASMC isolated from IPAH patients compared to PASMC isolated from healthy (donor lungs) controls (Figure 26a). PH induced either by MCT injection in rats or by chronic hypoxia in mice (10% O_2, 28 days) resulted in an increase of $\Delta\psi_m$ in precapillary PASMC isolated from such animals (Figure 26a). In addition, in vitro exposure of rat precapillary PASMC to an atmosphere of 1% O_2 for 48h (chronic hypoxia) increased $\Delta\psi_m$ (Figure 26a). To prove that mitochondria were hyperpolarized, 0.5µM of the uncoupling agent FCCP was applied to stimulate a $\Delta\psi_m$ collapse. The FCCP-stimulated decrease of $\Delta\psi_m$ (maximal uncoupling) in PASMC was significantly higher in IPAH patients and experimental PH models than in respective controls, which corresponded to a higher $\Delta\psi_m$ (Figure 26b).

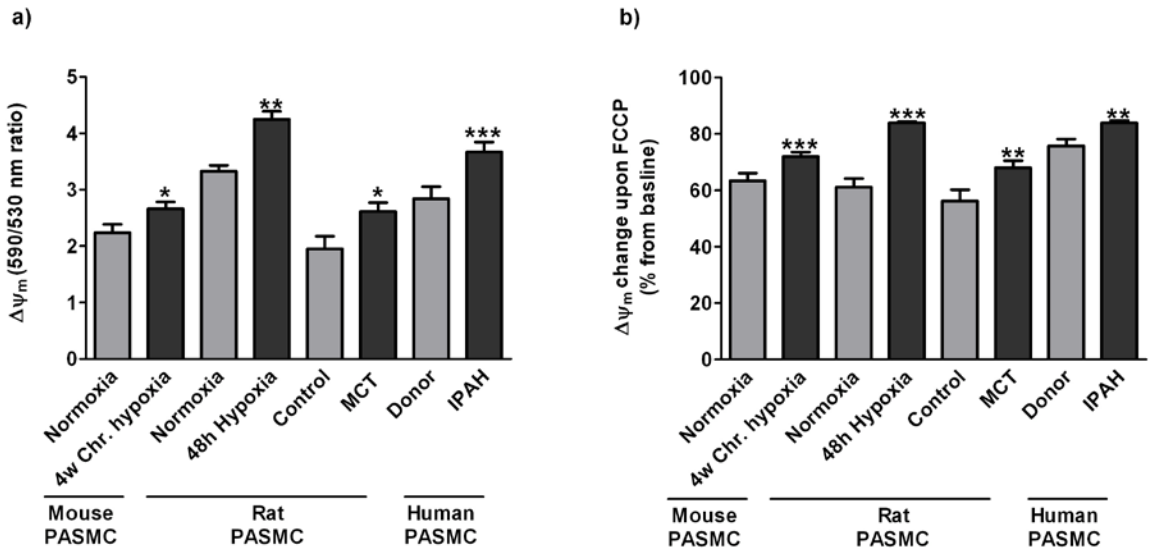

Figure 26. $\Delta\psi_m$ of precapillary PASMC in PH.

a) 590/530 nm ratio of JC1 during measurement of basal $\Delta\psi_m$ in PASMC isolated from patients with idiopathic pulmonary arterial hypertension (IPAH) or healthy donor controls (Donor), from rats with MCT-induced PH (MCT) or untreated rats (Control), from mice with chronic hypoxia-induced PH (4w Chr. Hypoxia) or normoxic mice (Normoxia), and from untreated rats after exposure of the precapillary PASMC to 1% O_2 chronic hypoxia (48h Hypoxia) or normoxia (Normoxia). b) $\Delta\psi_m$ presented as percent of maximal FCCP-induced drop of $\Delta\psi_m$ in those cells. Data were obtained from ≥4 independent precapillary PASMC cell isolations and 4 human samples, respectively. n ≥23 individual cells in each group.* $p<0.05$, **$p<0.01$, ***$p<0.001$, compared to respective controls with Student's t test.

3.2.2. Mechanism of mitochondrial hyperpolarization in PH

3.2.2.1. Correlation of respiration and glucose metabolism with mitochondrial hyperpolarization in PH

To evaluate, if changes in $\Delta\psi_m$ could be related to the alteration of cellular metabolism, mitochondrial respiration was measured using high-resolution respirometry, and the level of key metabolic enzymes was studied by the determination of mRNA and protein quantities in animal models of PH. Furthermore, the $\Delta\psi_m$ and the cellular metabolism was tested in rat precapillary PASMC after exposure to 48 h 1% O_2 hypoxia and MCT-induced PH after treatments that can reverse PH in animal models (re-exposure to normoxia and DCA, respectively). Following *in vitro* exposure to 1% O_2 hypoxia for 48h, rat PASMC were used in these experiments for the following reasons: 1) exposure to 48h 1% O_2 is an accepted model of chronic hypoxia-induced PH and leads to similar alterations of $\Delta\psi_m$ in rat precapillary PASMC and in precapillary PASMC isolated from mice exposed to 4 weeks of chronic hypoxia (Figure 26a-b); 2) for measurement of mitochondrial respiration a critical amount of cells is needed that can be more easily obtained from rats than from mice. Unstimulated mitochondrial respiration, oligomycin-inhibited respiration and maximal respiratory capacity after FCCP stimulation (given as pmol of O_2 consumed per

minute per million cells) were significantly reduced in rat precapillary PASMC after 48h exposure to 1% O_2 hypoxia (Figure 27a). Comparable results were found in precapillary PASMC isolated from rats with MCT-induced PH (Figure 27b).

In parallel, mRNA and protein levels of LDHA, the key enzyme for anaerobic glycolysis, and PDK1, the key enzyme to inhibit mitochondrial pyruvate metabolism, were increased in precapillary PASMC from both models of PH, chronic hypoxia-induced PH in mice and MCT-induced PH in rats (Figure 27 c-g).

Re-exposure of hypoxic precapillary PASMC (48h, 1%O_2) to normoxia (Figure 27a), or treatment of precapillary PASMC isolated from MCT injected rats with 500.0 µM DCA restored endogenous mitochondrial respiration (Figure 27b). DCA is an inhibitor of the pyruvate dehydrogenase kinase[194]. Additionally, protein levels of PDK1 and LDHA returned to normal after re-exposure to normoxia for 24 hours in precapillary PASMC (Figure 27 d-g).

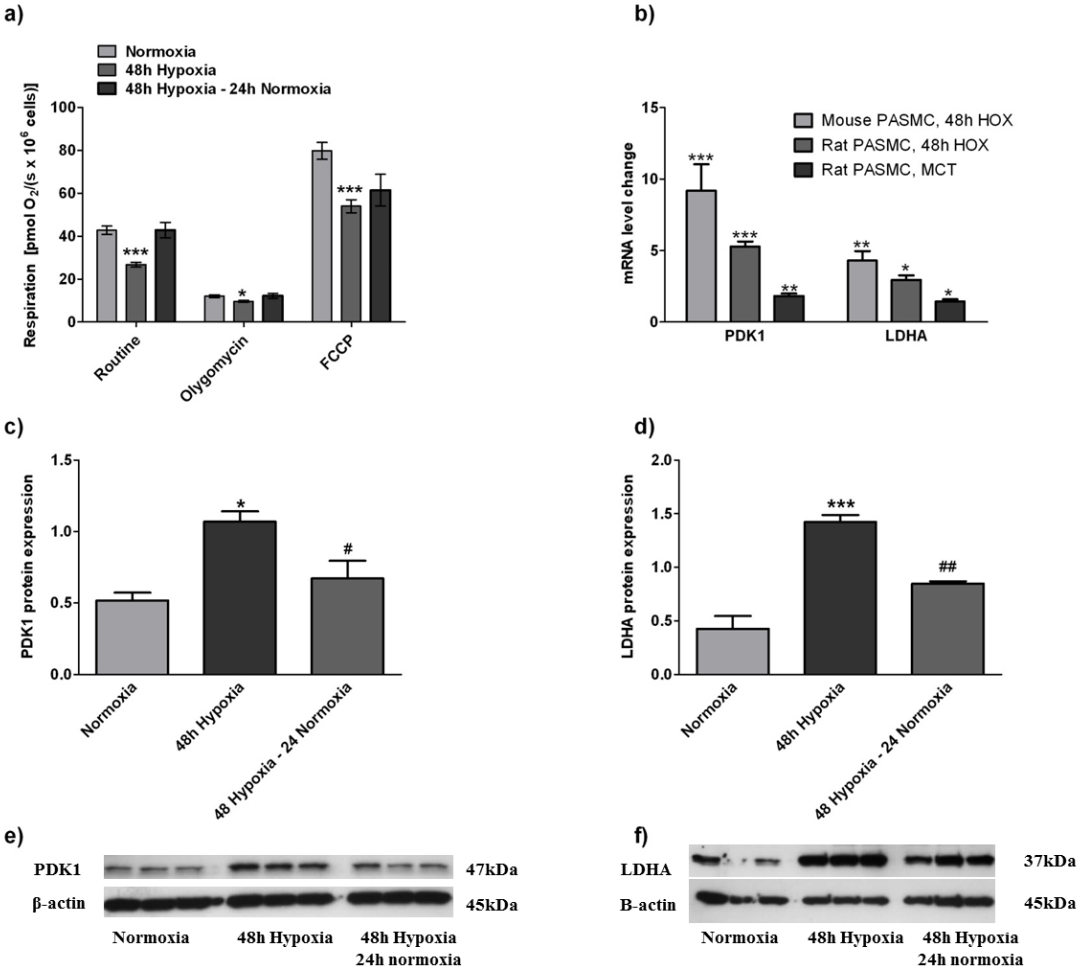

Figure 27. Mitochondrial respiration and markers of anaerobic glycolysis in precapillary PASMC.

a) Mitochondrial respiration after exposure of rat precapillary PASMC to 48h 1% O_2 (48h Hypoxia) and after re-exposure of PASMC to 24h 21% O_2 (48h Hypoxia-24h Normoxia) compared to normoxic controls (Normoxia). Data are given as respiration in pmol of O_2 consumed per minute per million cells where Routine is endogenous, unstimulated respiration; Oligomycin is oligomycin-inhibited respiration; FCCP represents respiration in the presence of FCCP. b) mRNA expression of key metabolic enzymes in precapillary PASMC isolated from mice (Mouse PASMC, 48h Hypoxia) and rat (Rat PASMC, 48h Hypoxia) after exposure to 48h 1% O_2 and in precapillary PASMC isolated from rats with MCT-induced PH (Rat PASMC, MCT). Data are presented as fold change compared to appropriate controls. c and d) Protein expression of PDK1 (Pyruvate dehydrogenase, isoforme 1) and LDHA (Lactate dehydrogenase A) in rat precapillary PASMC after exposure to 48h 1% O_2 (48h Hypoxia) and after re-exposure of PASMC to 24h normoxia (48h Hypoxia-24h Normoxia) compared to normoxic controls (Normoxia). e and f) Representative pictures of PDK1 and LDHA western blots from rat precapillary PASMC after exposure to 48h 1% O_2 (48h Hypoxia) and re-exposure to normoxia (48h Hypoxia-24h Normoxia). Data were obtained from ≥4 independent precapillary PASMC cell isolations. Mitochondrial respiration measurements were performed with 2.5-5.0 million cells per measurement.

* $p<0.05$, ** $p<0.01$, ***$p<0.001$ compared to respective controls (Normoxia and Control) and # $p<0.05$, ## $p<0.01$ compared to 48h Hypoxia or MCT-induced PH, one-way ANOVA with Bonferroni post hoc test.

Re-exposure to 24h normoxia (21% O_2) and treatment with 500µM DCA also reversed mitochondrial hyperpolarization found in precapillary PASMC isolated from rats with MCT-induced PH and after exposure of precapillary rat PASMC to 1% O_2 for 48h, respectively (Figure 28a-b).

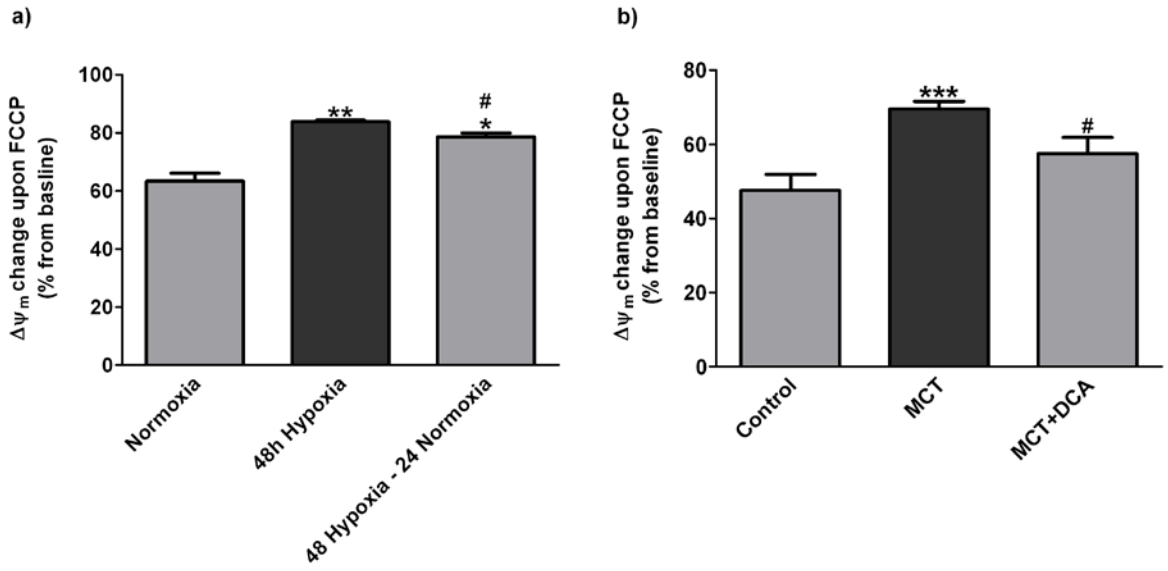

Figure 28. Effect of re-exposure to normoxia on mitochondrial hyperpolarization in precapillary PASMC exposed to 48h 1% O_2 and in precapillary PASMC isolated from rats with MCT-induced PH after DCA treatment.

a) $\Delta\psi_m$ presented as percent of maximal FCCP-induced drop of $\Delta\psi_m$ in precapillary PASMC after 48h exposure to 1% O_2 a (48h Hypoxia) and re-exposure to 24h normoxia (48h Hypoxia-24h Normoxia) compared to the FCCP-induced drop of $\Delta\psi_m$ in precapillary PASMC exposed to normoxia (Normoxia). b) $\Delta\psi_m$ presented as percent of maximal FCCP-induced drop of $\Delta\psi_m$ in precapillary PASMC isolated from rats with MCT-induced PH in the absence (MCT) or in the presence of DCA (MCT+DCA) compared to the FCCP-induced drop of $\Delta\psi_m$ in precapillary PASMC isolated from healthy rats (Control). Data were obtained from ≥4 independent precapillary PASMC cell isolations and ≥24 individual cells each.

** $p<0.01$, *** $p<0.001$ compared to respective control (Normoxia and Control) and # $p<0.05$ compared untreated cells (48h Hypoxia and MCT), one-way ANOVA with Bonferroni post hoc test.

To test if the increase in $\Delta\psi_m$ in precapillary PASMC of the experimental models of PH was related to glycolytically produced ATP, an inhibitor of the ATP/ADP translocase, 50.0 µM BA, was applied. BA inhibited the increase of $\Delta\psi_m$ in precapillary PASMC induced by exposure to hypoxia (48h, 1% O_2), as well as the increase of $\Delta\psi_m$ in PASMC isolated from rats with MCT-induced PH (Figure 29 a-b).

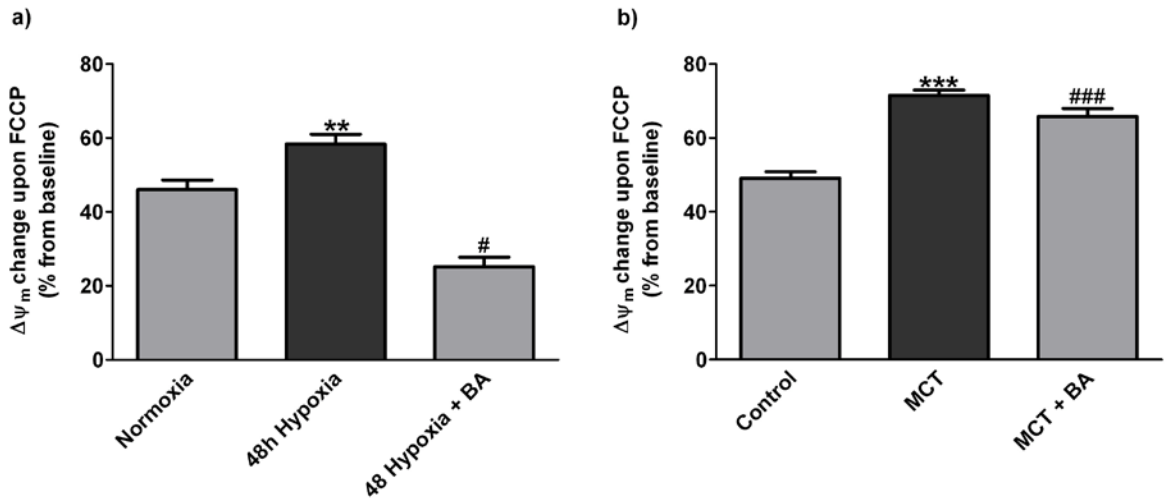

Figure 29. Effect of bongkrek acid, an inhibitor of the ADT/ATP translocase, on mitochondrial hyperpolarization in precapillary PASMC from experimental models of PH.
a) $\Delta\psi_m$ presented as percent of maximal FCCP-induced drop of $\Delta\psi_m$ in precapillary PASMC in normoxia (Normoxia) or after exposure to 48h 1% O_2 in the absence (48h Hypoxia) or in the presence of bongkrek acid (48h Hypoxia+BA). b) $\Delta\psi_m$ presented as percent of maximal FCCP-induced drop of $\Delta\psi_m$ in precapillary PASMC isolated from healthy control rats (Control) and from rats with MCT-induced PH in the absence (MCT) or in the presence of BA (MCT+BA). Data were obtained from ≥4 independent precapillary PASMC cell isolations and ≥15 individual cells each.
** $p<0.01$, *** $p<0.001$ compared to appropriate controls (Normoxia and Control) and # $p<0.05$, ### $p<0.001$ compared untreated groups (48h Hypoxia and MCT), one-way ANOVA with Bonferroni post hoc test.

3.2.2.2. Application of ROS scavengers and mitochondrial hyperpolarization in PH

To elucidate the effect of ROS scavengers on mitochondrial hyperpolarization of precapillary PASMC in experimental PH, ROS scavengers (25µM NAC and 1µM TEMPO) were applied in precapillary PASMC exposed for 48 h to 1% O_2 or precapillary PASMC isolated from rats with MCT-induced PH. In contrast to the effect of the ROS scavengers on acute hypoxia-induced mitochondrial hyperpolarization, where mitochondrial hyperpolarization was preserved in the presence of ROS scavengers, in experimental models of PH such as chronic hypoxic PH, as well as MCT-induced PH, treatment of PASMC with the ROS scavengers reversed the hyperpolarization of mitochondria (Figure 30 a-b).

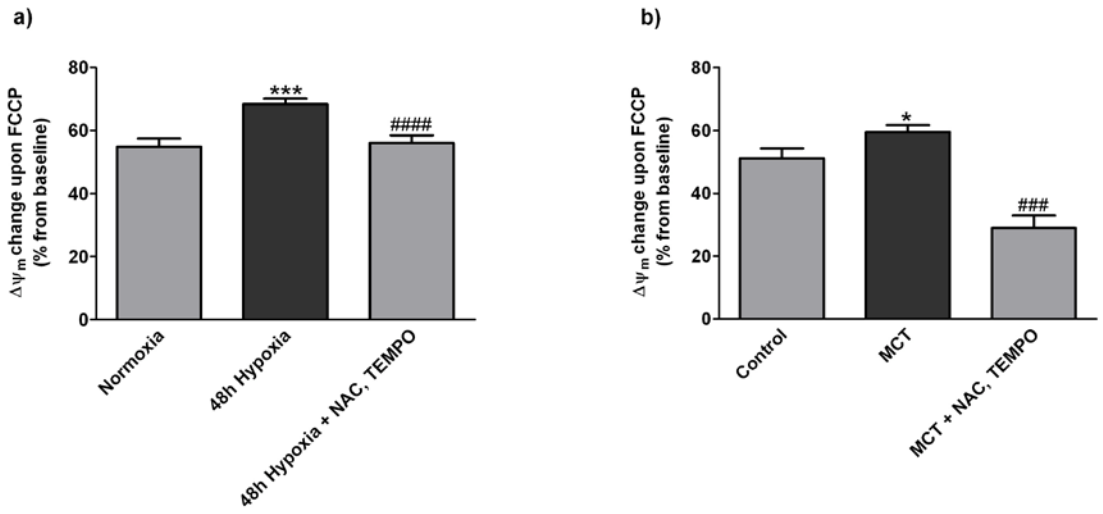

Figure 30. Effect of ROS scavengers on mitochondrial hyperpolarization in precapillary PASMC from experimental models of PH.

a) $\Delta\psi_m$ presented as percent of maximal FCCP-induced drop of $\Delta\psi_m$ in precapillary PASMC exposed to normoxia (Normoxia) or to 48h 1% O_2 in the absence (48h Hypoxia) or in the presence of ROS scavengers (48h Hypoxia + NAC, TEMPO). b) $\Delta\psi_m$ presented as percent of maximal FCCP-induced drop of $\Delta\psi_m$ in precapillary PASMC isolated from healthy control rats (Control) and rats with MCT-induced PH in the absence (MCT) or in the presence of ROS scavengers (MCT + NAC, TEMPO). Data were obtained from ≥4 independent precapillary PASMC cell isolations and ≥30 individual cells each.

* $p<0.05$, *** $p<0.001$ compared to appropriate controls (Normoxia and Control) and ### $p<0.001$ compared to untreated groups (48h Hypoxia and MCT), one-way ANOVA with Bonferroni post hoc test.

3.2.2.3. mRNA and protein expression of UCP2 in PH

To investigate the role of UCP2 in mitochondrial hyperpolarization in PH, the level of expression of mRNA of UCP2 was studied in chronic hypoxia-induced PH. Exposure of WT mice to four weeks of chronic hypoxia (10% O_2) decreased mRNA expression of UCP2 determined in lung tissue homogenate and microdissected precapillary pulmonary arteries (Figure 31).

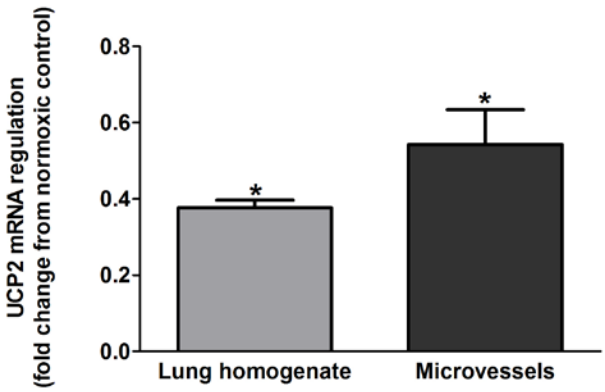

Figure 31. Effect of exposure of WT mice to 4 weeks of 10% O_2 (chronic hypoxia) on UCP2 mRNA expression.

UCP2 mRNA expression in mouse lung tissue (homogenate) and in laser microdissected small pulmonary vessels upon 4 weeks of 10% O_2 (chronic hypoxia). Data are given as fold change compared to normoxic controls (n=4).
* $p<0.05$ compared to normoxic controls with Student's t test.

Additionally, the level of UCP2 protein expression in lung homogenate in chronic hypoxia-induced PH, MCT-induced PH and human IPAH was investigated. The exposure of WT mice to four weeks of chronic hypoxia (10% O_2) and MCT injection in rats decreased the protein level of UCP2 determined in lung tissue homogenate (Figure 32 a-d). UCP2 protein expression was also decreased in lung homogenate of IPAH patients compared to donor (healthy) lung (Figure 32 e-f).

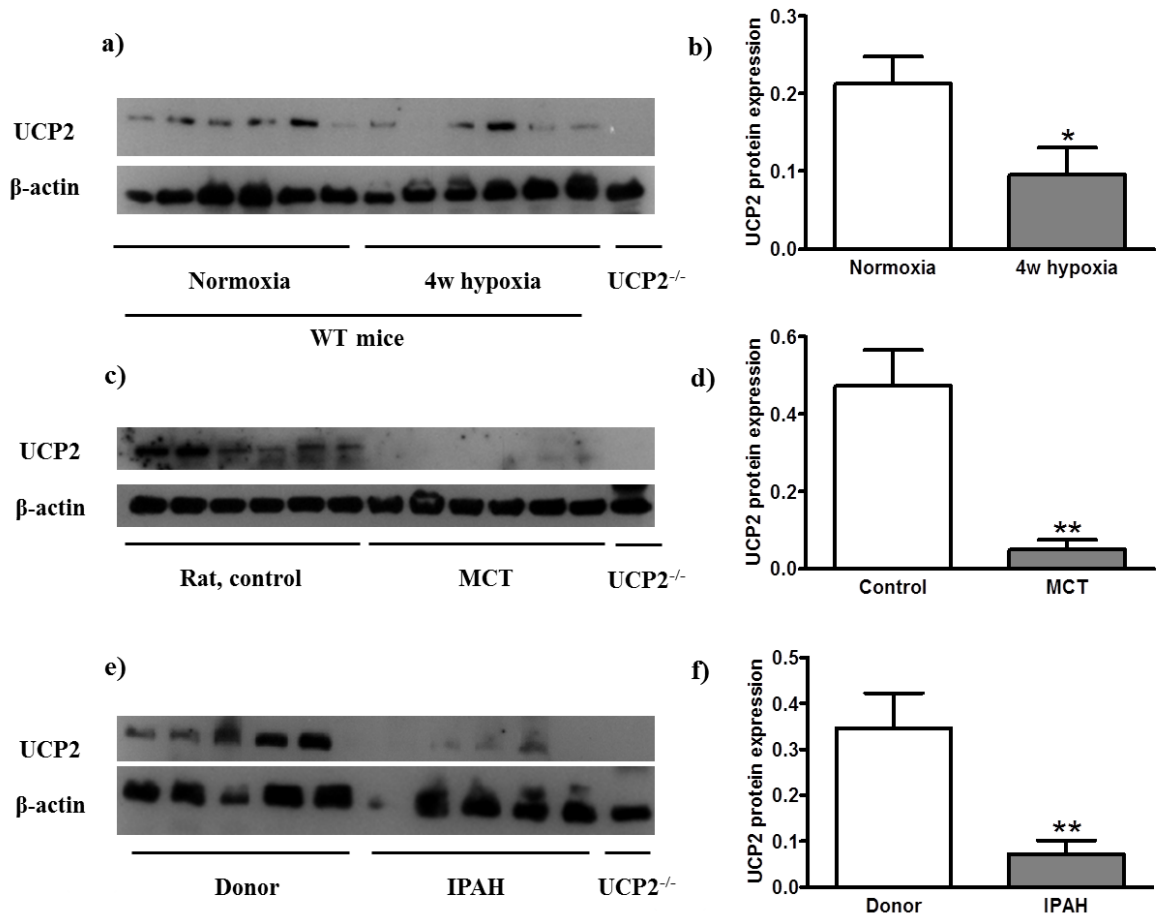

Figure 32. UCP2 protein expression in lungs of experimental models of PH and idiopathic pulmonary arterial hypertension (IPAH) patients.

UCP2 protein expression in lung tissue (homogenate) of WT (wild type) mice exposed to 4 weeks of 10% O_2 (4w hypoxia, a-b, n=6 in each group), from rats with MCT-induced PH (c-d, n=6 in each group) and from IPAH patients (e and f, n=5 in each group). Data presented as ratio of UCP2 to β-actin expression. Lung homogenate from $UCP2^{-/-}$ (knockout) mice served as negative control.

* $p<0.05$ and ** $p<0.001$ compared to respective controls (lung tissue from control mice, control rats and human donor) with Student's t test.

3.3. UCP2 and pulmonary vascular remodeling

3.3.1. Effect of $UCP2^{-/-}$ on the pulmonary vasculature and right ventricle

The increase of $\Delta\psi_m$ in animal models of PH and IPAH was associated with UCP2 downregulation; therefore, the effect of $UCP2^{-/-}$ on the pulmonary vasculature was determined. Under normoxic conditions $UCP2^{-/-}$ mice exhibited mild PH characterized by a slightly increased RVSP (Table 5) and higher ratio of RV mass to LV mass plus septum and RV mass to body weight compared to WT animals (Figure 33a-b). In contrast, systemic systolic pressure (Table 5) and ratio of LV mass to body weight was similar in both groups (Figure 33c). The heart rate was also similar in both animal groups (Table 5).

Table 5. Hemodynamics of the right ventricle.

	WT	UCP2$^{-/-}$
n	6	6
Heart rate, BPM	592.5±11.7	570.4±11.3
Systemic systolic pressure, mmHg	102.5±8.7	99.6±2.1
RVSP, mmHg	29.5±0.4	35.5±0.9***
RVEDP, mmHg	1.4±0.4	2.1±0.4
Max dP/dt, mmHg/s	3297.0±58.1	3309.0±200.5
Min dP/dt, mmHg/s	-3347.0±160.7	-2727.0±159.4*

Abbreviations: WT - wild type mice; UCP2$^{-/-}$ - UCP2 deficiency mice; PAP - pulmonary arterial pressure; RVSP - right ventricular systolic pressure, RVEDP - right ventricular end-diastolic pressure; Max dP/dt and Min dP/dt - minimum and maximum rate of pressure change in the RV.
* p<0.05, *** p<0.001 compared to WT control with Student's t test.

Furthermore, UCP2$^{-/-}$ mice were characterized by an increase of the minimum rate of pressure change in the RV (Min dp/dt WT: -3347.0±160.7; UCP2$^{-/-}$: -2727.0±159.4).

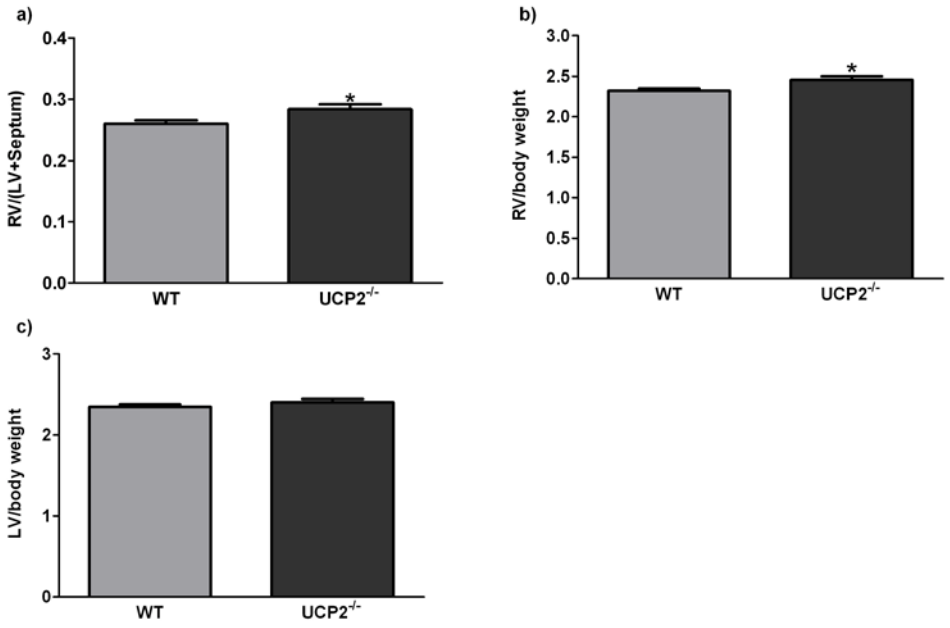

Figure 33. Effect of UCP2$^{-/-}$ on the right ventricle.
Ratio of right ventricle (RV) to left ventricle (LV) + septum (a), RV mass to body weight (b) and LV mass to body weight (c) in wild type (WT) and UCP2 knockout (UCP2$^{-/-}$) mice.
* p<0.05 compared to WT with Student's t test. n=9 each

It was shown before, that lungs of UCP2$^{-/-}$ mice have an increased ratio of muscularized to non-muscularized vessel (unpublished thesis of Timm Hoeres, Giessen). Morphometric analysis of the MWT of pulmonary vessels now also showed that gene deletion of UCP2 resulted in a prominent remodeling of

the pulmonary vasculature, mainly medial layer as indicated by the increase of MWT of small pulmonary arteries with a diameter of less that 100µm (Figure 34 a-b) compared to these arteries in WT mice.

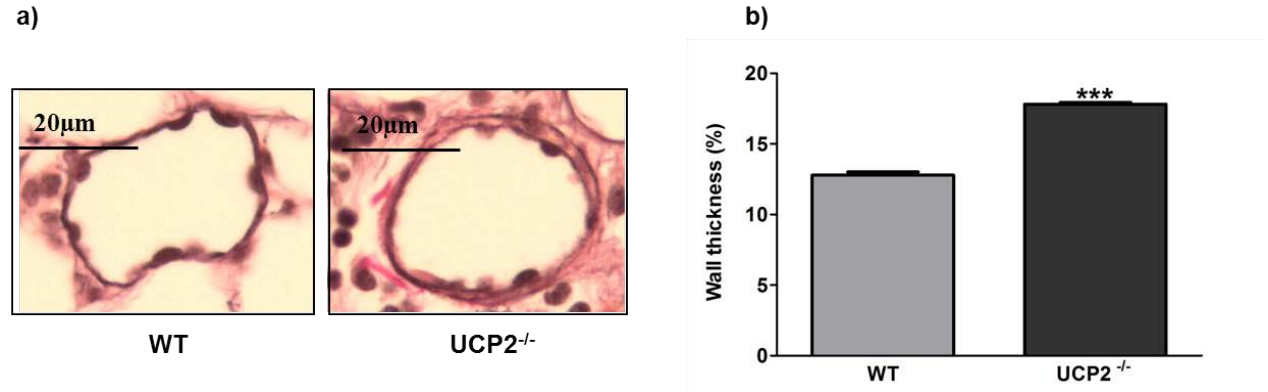

Figure 34. Effect of UCP2$^{-/-}$ on pulmonary vasculature remodeling.
Representative pictures of pulmonary arteries of wild type (WT) and UCP2 knockout (UCP2$^{-/-}$) mice lungs stained for elastica according to common histopathological procedures (Van Gieson's stain). Nuclei were counterstaining by Nuclear Fast Red. MWT (medial wall thickness) was defined as the distance between the lamina elastica interna and lamina elastica externa. b) Increased MWT given as percentage of MWT that was examined by light microscopy using a computerized morphometric system calculated by the formula MWT = (2 x wall thickness/external diameter) x 100. n=4 in each group.
***p<0.001 compared to WT with Student's t test.

α-smooth muscle actin staining of lung slides demonstrated that excessive pulmonary vascular remodeling in UCP2$^{-/-}$ mice was caused by the increase of the SMC layer (Figure35).

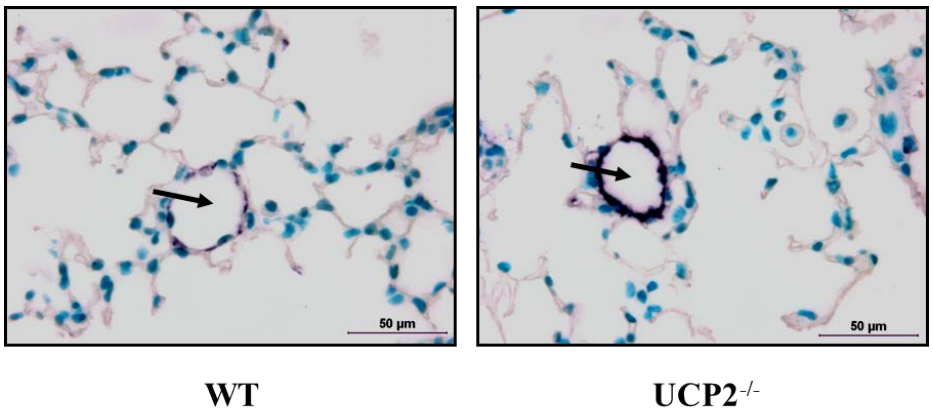

Figure 35. Representative pictures of pulmonary arteries of WT and UCP2$^{-/-}$ mice.
Mouse lung sections from wild type (WT) and UCP2 knockout (UCP2$^{-/-}$) mice were stained with an anti-α-smooth muscle actin antibody (Purple color) and counterstained with methyl green (Greenishcolor). Arrow depicts the small pulmonary arteries

3.3.2. Proliferation of precapillary PASMC isolated from UCP2$^{-/-}$ mice

3.3.2.1. Effect of UCP2$^{-/-}$ on $\Delta\psi_m$ and $O_2^{\bullet-}$ release in precapillary PASMC

Under normoxic conditions precapillary PASMC isolated from UCP2$^{-/-}$ mice showed a significantly higher $\Delta\psi_m$ than those from WT mice (Figure 36a). FCCP stimulation induced a significantly higher drop

of $\Delta\psi_m$ in precapillary PASMC isolated from UCP2$^{-/-}$ mice than in precapillary PASMC isolated from WT mice, which corresponded to a higher $\Delta\psi_m$ in UCP2$^{-/-}$ mice compared to WT mice (Figure 36b). Increased $\Delta\psi_m$ in precapillary PASMC was accompanied by enhanced $O_2^{\bullet-}$ levels in precapillary PASMC of UCP2$^{-/-}$ mice as measured by ESR spectroscopy (Figure 36c).

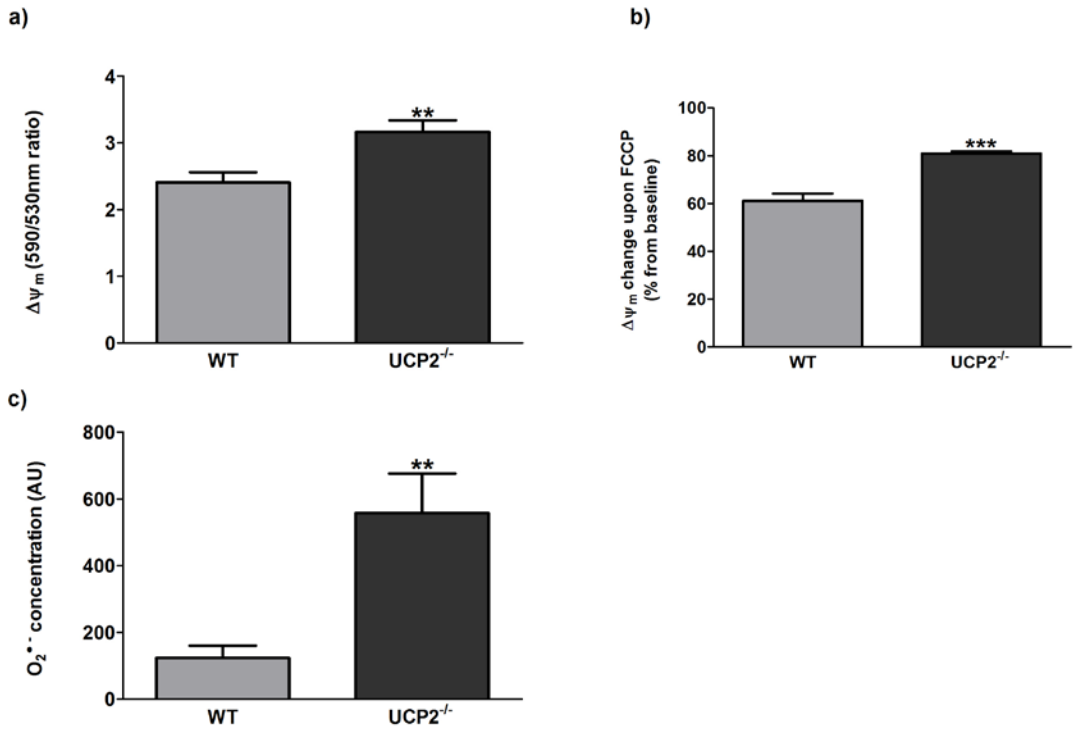

Figure 36. $\Delta\psi_m$ and $O_2^{\bullet-}$ release in precapillary PASMC isolated from WT and UCP2$^{-/-}$ mice.
a) 590/530 nm ratio of JC1 during measurement of $\Delta\psi_m$ in precapillary PASMC from wild type (WT) and UCP2 knockout (UCP2$^{-/-}$) mice. b) $\Delta\psi_m$ presented as percent of maximal FCCP-induced drop of $\Delta\psi_m$ in precapillary PASMC from mice WT and UCP2$^{-/-}$ mice. c) $O_2^{\bullet-}$ production in precapillary PASMC from WT and UCP2$^{-/-}$ mice. Data were assessed by ESR spectroscopy. Data were obtained from ≥4 independent precapillary PASMC cell isolations. $\Delta\psi_m$ was measured ≥18 individual cells each. $O_2^{\bullet-}$ concentration is given in arbitrary units (AU) for 100 000 cells.
** $p<0.01$, *** $p<0.001$ compared to WT with Student's t test.

To verify the impact of precapillary PASMC in pulmonary vascular remodeling in UCP2$^{-/-}$ mice, the proliferation rate of precapillary PASMC isolated from UCP2$^{-/-}$ mice was studied. Precapillary PASMC isolated from UCP2$^{-/-}$ mice were characterized by a more prominent proliferation after FCS stimulation compared to precapillary PASMC isolated from WT mice (Figure 37). The proliferation rate was investigated by two different approaches: [3H]-Thymidine incorporation (Figure 37a) and colorimetric growth assay with 0.1% crystal violet staining (Figure 37b).

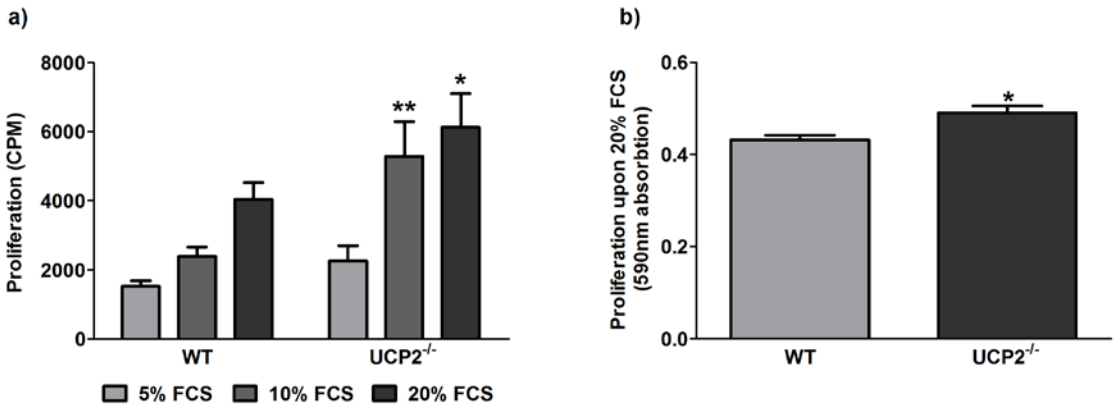

Figure 37. Proliferation of precapillary PASMC isolated from WT and UCP2$^{-/-}$ mice.

Proliferation of precapillary PASMC isolated from wild type (WT) and UCP2 knockout (UCP2$^{-/-}$) mice measured by [3H]-Thymidine incorporation (a) and by the colorimetric growth assay with 0.1% crystal violet staining of 4% paraformaldehyde fixed cells (b) upon FCS (fetal calf serum) stimulation. Data were obtained from ≥4 independent precapillary PASMC cell isolations. [3H]-Thymidine incorporation is displayed in counts per minute (CPM) per 8000 cells. Crystal violet staining was evaluated in 10000 cells.
*p<0.05, ** p<0.01 compared to corresponded WT. For Figure a one-way ANOVA with Tukey post hoc test was performed, for figure b, the Student's t test.

3.3.2.2. Role of $\Delta\psi_m$ in proliferation of precapillary PASMC isolated from UCP2$^{-/-}$ mice

Incubation with different doses of FCCP, 1.0 µM, 2.5 µM and 5.0 µM for 3 days resulted in a significant decrease of $\Delta\psi_m$ in precapillary PASMC isolated from UCP2$^{-/-}$ mice (38a). FCCP doses of 2.5 and 5.0 µM decreased $\Delta\psi_m$ in precapillary PASMC isolated from UCP2$^{-/-}$ mice to the level of $\Delta\psi_m$ in precapillary PASMC isolated from WT mice (Figure 38a). Incubation with the same concentrations of FCCP decreased the proliferation of precapillary PASMC isolated from UCP2$^{-/-}$ mice upon 20% FCS stimulation to the similar level as those measured in precapillary PASMC isolated from WT mice (Figure 38b).

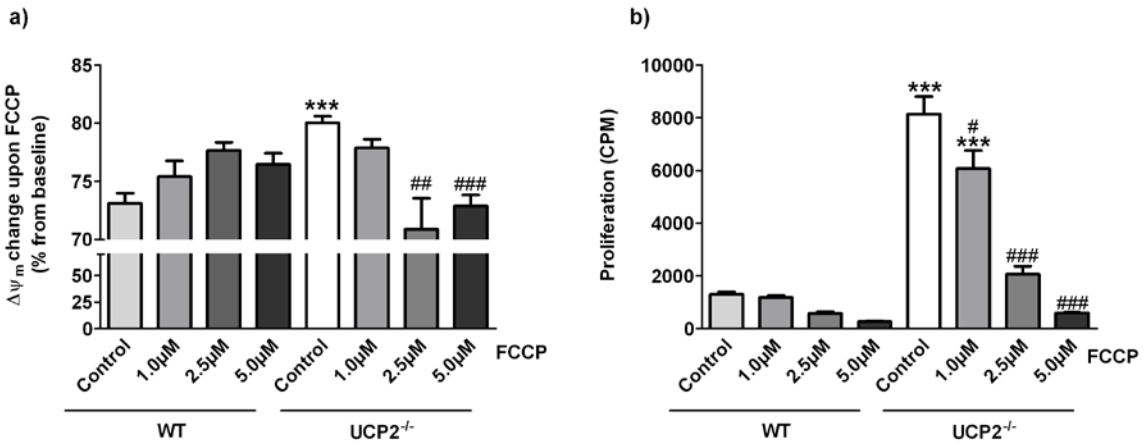

Figure 38. Effect of FCCP on $\Delta\psi_m$ and proliferation of precapillary PASMC isolated from UCP2$^{-/-}$ mice.

a) $\Delta\psi_m$ in percent of maximal FCCP-induced uncoupling compared to the baseline values in the absence of FCCP (Control) and after 72h treatment with 1.0µM, 2.5µM and 5.0µM FCCP in precapillary PASMC isolated from wild type (WT) and UCP2 knockout (UCP2$^{-/-}$) mice. b) Proliferation of precapillary PASMC from WT and UCP2$^{-/-}$ mice in the absence of FCCP (Control) and after 72h treatment with 1.0µM, 2.5µM and 5.0µM FCCP. Data were obtained from ≥4 independent precapillary PASMC cell isolations. $\Delta\psi_m$ was measured ≥19 individual cells each. Proliferation is displayed in counts per minute (CPM) per 8000 cells.

*** $p<0.001$ compared to precapillary PASMC from WT mice without treatment and # $p<0.05$, ## $p<0.01$, ### $p<0.001$ compared to UCP2$^{-/-}$ untreated group with one-way ANOVA with Tukey post hoc test.

3.3.2.3. Effect of UCP1 and UCP2 overexpression on proliferation of precapillary PASMC isolated from UCP2$^{-/-}$ mice

Proliferation of precapillary PASMC after overexpression of UCP2 and UCP1, which is known to act solely via uncoupling, was determined. Overexpression of UCP1 and UCP2 decreased the proliferation of precapillary PASMC isolated from UCP2$^{-/-}$ mice upon 20% FCS stimulation (Figure 39). Overexpression of UCP1 and UCP2 were confirmed by a western blot (Figure 39b).

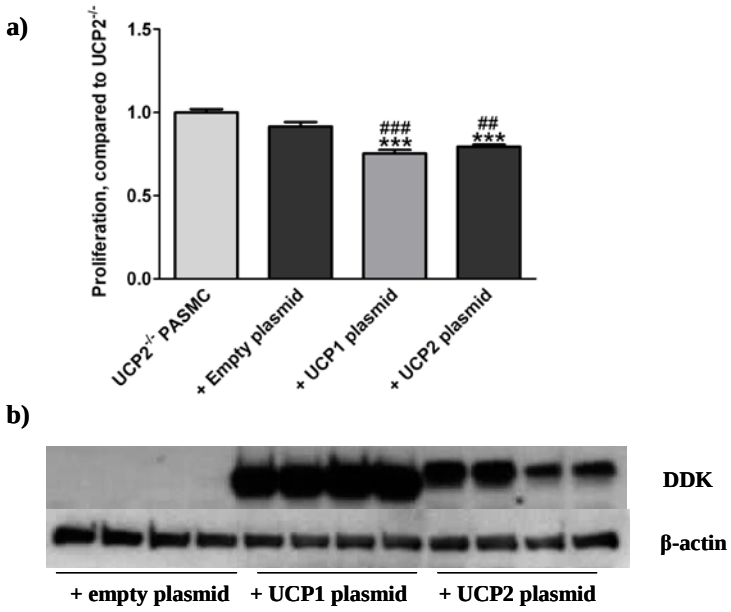

Figure 39. Effect of UCP1 and UCP2 overexpression on the proliferation of precapillary PASMC isolated from UCP2$^{-/-}$ mice.

a) Proliferation of precapillary PASMC from UCP2 knockout (UCP2$^{-/-}$) mice after 72h transfection with UCP1 or UCP2 over-expressing plasmids. b) Western blot with anti-DDK (plasmids contain UCP1 and UCP2 protein with c-terminal DDK tag) and anti β-actin (loading control) antibody. Data were obtained from ≥4 independent precapillary PASMC cell isolations. Proliferation is displayed in counts per minute (CPM) per 8000 cells.

*** $p<0.001$ compared to UCP2$^{-/-}$ PASMC, ## $p<0.05$, ### $p<0.001$ compare empty plasmid group with one-way ANOVA with Tukey post hoc test.

3.3.2.4. Role of ROS in proliferation of precapillary PASMC isolated from UCP2$^{-/-}$ mice.

ROS scavenging by 25µM NAC and 1µM TEMPO inhibited the increased $O_2^{\bullet-}$ production (Figure 40a) and the enhanced proliferation (Figure 40b) in precapillary PASMC isolated from UCP2$^{-/-}$ mice compared to precapillary PASMC isolated from WT mice. Additionally, MnTBAP inhibited the increased proliferation of precapillary PASMC isolated from UCP2$^{-/-}$ mice (Figure 40c).

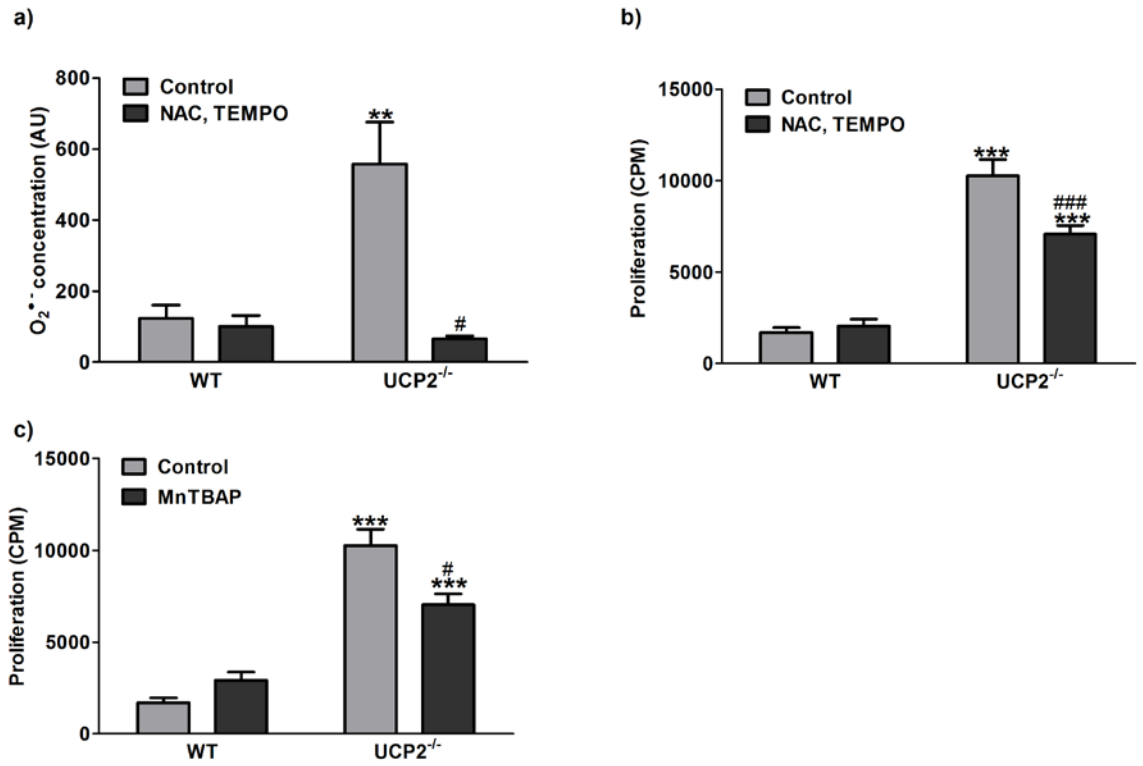

Figure 40. Effect of ROS scavengers on $O_2^{\bullet-}$ generation and proliferation of precapillary PASMC isolated from UCP2$^{-/-}$ mice.

a) $O_2^{\bullet-}$ production in precapillary PASMC from wild type (WT) and UCP2 knockout (UCP2$^{-/-}$) mice in the absence (Control) or in presence of the unspecific radical scavengers NAC and TEMPO. Data were assessed by ESR spectroscopy. b) Proliferation of precapillary PASMC from UCP2$^{-/-}$ mice and WT mice in the absence (Control) or in presence of the unspecific radical scavengers NAC and TEMPO. c) Proliferation of precapillary PASMC isolated from UCP2$^{-/-}$ mice and WT mice in the absence (Control) or presence of MnTBAP. Data were obtained from ≥4 independent precapillary PASMC cell isolations. Proliferation is displayed as counts per minute (CPM) per 8000 cells. $O_2^{\bullet-}$ concentration is given in arbitrary units (AU) for 100 000 cells.

**p<0.01, ***p<0.001, ***p<0.001 compared to WT and †p<0.05, ††p<0.01, †††p<0.001 compared to untreated UCP2$^{-/-}$ PASMC, one-way ANOVA with Tukey post hoc test.

To support the hypothesis that increased $\Delta\psi_m$ in precapillary PASMC isolated from UCP2$^{-/-}$ mice was not a secondary effect of increased ROS in those cells, $\Delta\psi_m$ was measured after the application of ROS scavengers. No alterations in $\Delta\psi_m$ could be detected under these conditions (Figure 41).

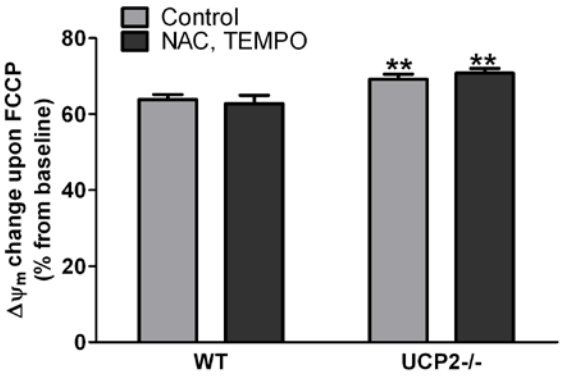

Figure 41. Effect of ROS scavengers on $\Delta\psi_m$ in precapillary PASMC isolated from WT and UCP2$^{-/-}$ mice.

$\Delta\psi_m$ presented as percent of maximal FCCP-induced drop of $\Delta\psi_m$ after 48h treatment of precapillary PASMC with ROS scavengers (NAC and TEMPO) or untreated precapillary PASMC of wild type (WT) and UCP2 knockout (UCP2$^{-/-}$) mice (Control).

Data were obtained from ≥4 independent precapillary PASMC cell isolations and ≥31 individual cells each.

**p<0.01 compared to WT without ROS scavengers with one-way ANOVA with Tukey post hoc test.

3.3.2.5. $\Delta\psi_m$, ROS release and proliferation of precapillary PASMC after UCP2 knockdown by siRNA

Knockdown of UCP2 by specific siRNA in precapillary PASMC isolated from WT mice had the same effect as UCP2$^{-/-}$ and led to an increase of $\Delta\psi_m$ (Figure 42a-b), $O_2^{\bullet-}$ production (Figure 42c), and enhanced proliferation (Figure 42b). Success of siRNA transfection was confirmed by real-time PCR (Figure 42d).

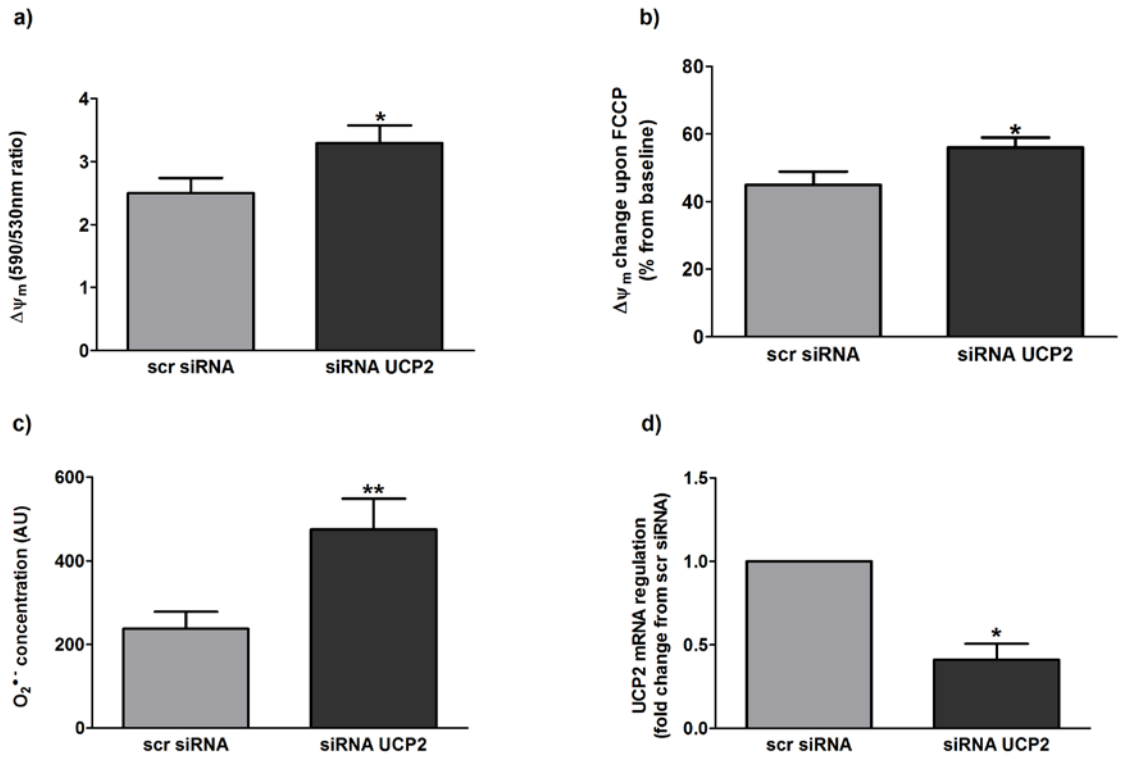

Figure 42. Effect of UCP2 downregulation on $\Delta\psi_m$ and $O_2^{\bullet-}$ release in precapillary PASMC.

590/530 nm ratio of JC1 during measurement of $\Delta\psi_m$ in precapillary PASMC transfected with scr (scr siRNA) or siRNA against UCP2 (siRNA UCP2). b) $\Delta\psi_m$ presented as percent of maximal FCCP-induced drop of $\Delta\psi_m$ in precapillary PASMC after transfection with scr (scr siRNA) or siRNA against UCP2 (siRNA UCP2). c) $O_2^{\bullet-}$ production of precapillary PASMC transfected by scr (scr siRNA) or siRNA against UCP2 (siRNA UCP2). Data were assessed by ESR spectroscopy. d) Real time PCR control of efficiency of UCP2 knockdown by specific siRNA. Data were obtained from ≥4 independent precapillary PASMC cell isolations. $\Delta\psi_m$ was measured ≥21 individual cells each. $O_2^{\bullet-}$ concentration is given in arbitrary units (AU) for 100 000 cells.

**p<0.01, ***p<0.001, ***p<0.001 compared to scr siRNA with Student's t test.

FCCP at a dose of 1.0 µM reversed the hyperpolarization of mitochondria in precapillary PASMC transfected with siRNA against UCP2 (Figure 43a) to the level of $\Delta\psi_m$ in precapillary PASMC transfected with scr siRNA. Incubation with the same dose, 1.0µM FCCP, decreased the enhanced proliferation of precapillary PASMC transfected with UCP2 siRNA (Figure 43b) to a similar level as in precapillary PASMC transfected with scr siRNA. FCCP in doses of 2.5 µM and 5.0 µM demonstrated an unspecific effect of FCCP on the proliferation of precapillary PASMC transfected with scr siRNA (Figure 43b).

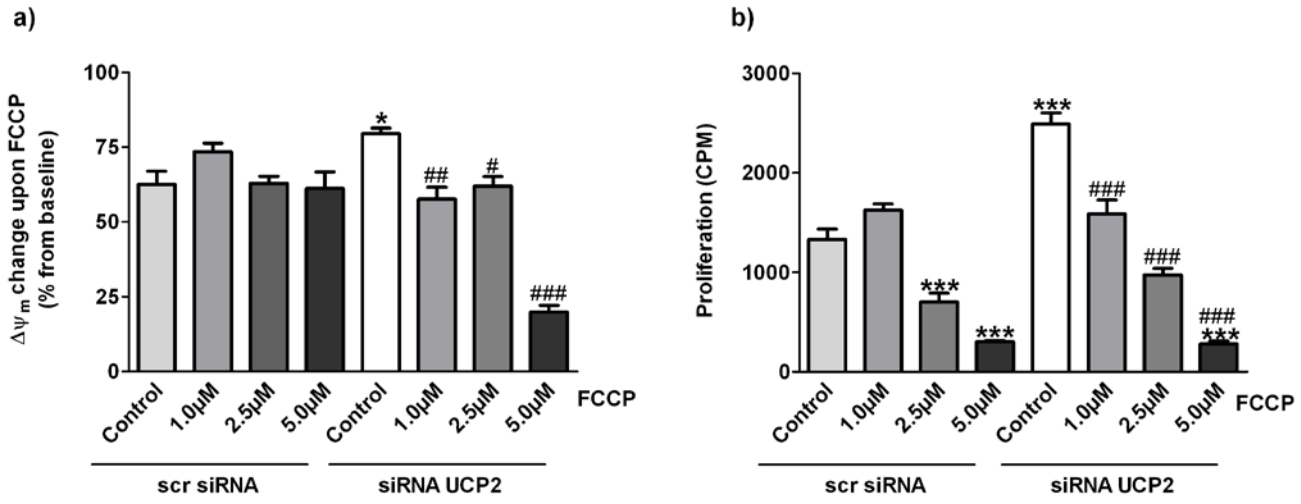

Figure 43. Effect of FCCP on $\Delta\psi_m$ and proliferation of precapillary PASMC after UCP2 knockdown by siRNA.

a) $\Delta\psi_m$ in percent of maximal FCCP-induced uncoupling compared to the baseline values in the absence of FCCP (Control) and after 72h treatment with 1.0μM, 2.5μM and 5.0μM FCCP in precapillary PASMC transfected with scr siRNA or siRNA UCP2. b) Proliferation of precapillary PASMC after 72h transfection with siRNA against UCP2 (siRNA UCP2) or scr siRNA in the absence (Control) of FCCP and after 72h treatment with 1.0μM, 2.5μM and 5.0μM FCCP. Data were obtained from ≥4 independent precapillary PASMC cell isolations. $\Delta\psi_m$ was measured ≥12 individual cells each. Proliferation is displayed as counts per minute (CPM) per 8000 cells.

*p<0.05, *** p<0.001 compared to PASMC after scr siRNA transfection without treatment and # p<0.05, ## p<0.01, ### p<0.001 compared siRNA UCP2 untreated group with one-way ANOVA with Tukey post hoc test.

In line with the data obtained from precapillary $UCP2^{-/-}$ PASMC, ROS scavenging by 25μM NAC and 1μM TEMPO inhibited the increased $O_2^{\bullet-}$ production (Figure 44a) and the enhanced proliferation (Figure 44d) of precapillary PASMC after knockdown of UCP2 with siRNA. MnTBAP also inhibited the increased proliferation of precapillary PASMC after transfection with siRNA against UCP2 (Figure 44c).

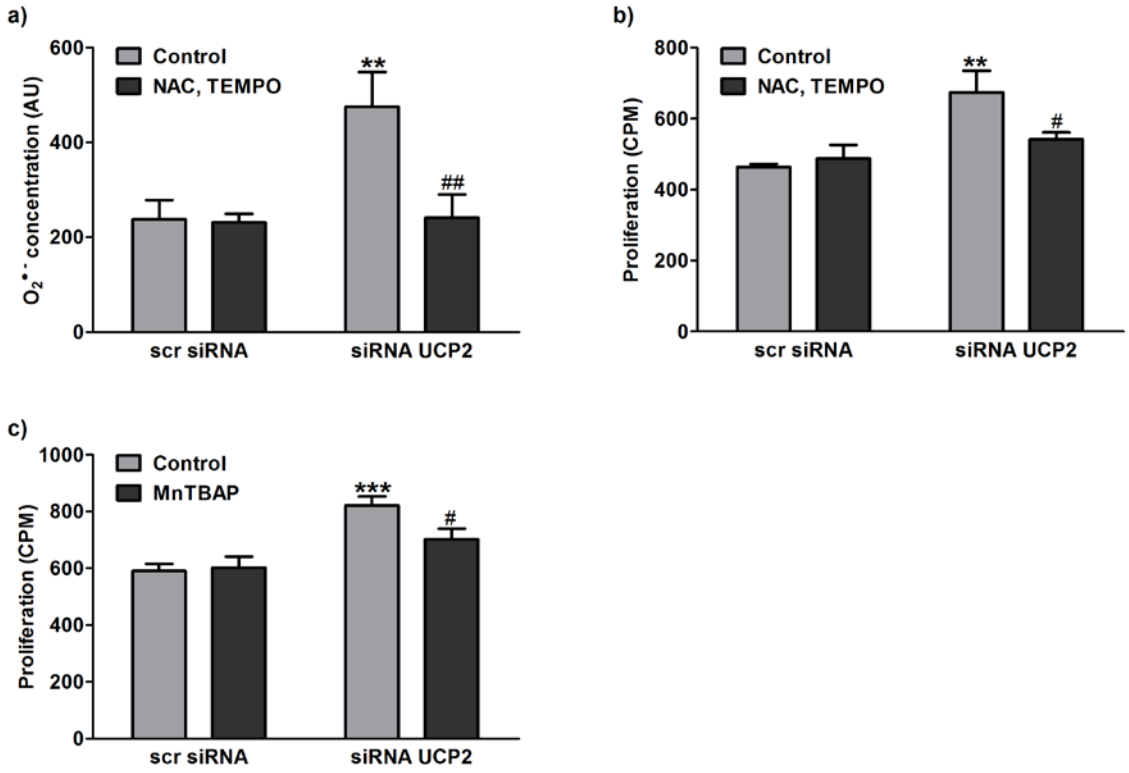

Figure 44. Effect of ROS scavengers on $O_2^{\bullet-}$ release and proliferation of precapillary PASMC after UCP2 knockdown by siRNA.

a) $O_2^{\bullet-}$ production in precapillary PASMC treated with scr siRNA or siRNA against UCP2 in the absence (Control) or in the presence of the unspecific radical scavengers NAC and TEMPO. Data were assessed by ESR spectroscopy. b) Proliferation of precapillary PASMC after transfection with scr siRNA or siRNA against UCP2 in the absence (Control) or in the presence of the unspecific radical scavengers NAC and TEMPO. c) Proliferation of precapillary PASMC after transfection with scr siRNA or siRNA4 against UCP2 in the absence (Control) or presence of MnTBAP. Data were obtained from ≥4 independent precapillary PASMC cell isolations. Proliferation is displayed in counts per minute (CPM) per 8000 cells. $O_2^{\bullet-}$ concentration is given in arbitrary units (AU) for 100 000 cells.

**$p<0.01$ compared to scr siRNA and # $p<0.05$, ## $p<0.01$ compared to siRNA UCP2 transfected precapillary PASMC without treatment, one-way ANOVA with Tukey post hoc test.

3.3.2.6. Effect of UCP2 knockout or knockdown on cyclin D1 expression in precapillary PASMC

Cyclin D1, a well-known proliferative marker, builds a complex with the cyclin-dependent kinase (CDK) that activates DNA replication and cell division[253]. Knockdown of UCP2 by siRNA or knockout of UCP2 in precapillary PASMC resulted in the increase of cyclin D1 expression (Figure 45).

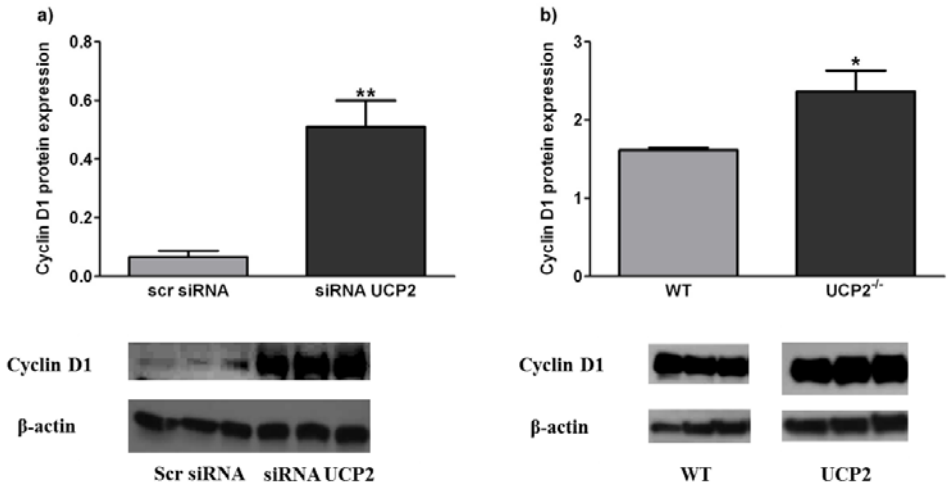

Figure 45. Effect of UCP2 on cyclin D1 expression in precapillary PASMC.

a) Cyclin D1 expression in precapillary PASMC after 72 h transfection with scr (scr siRNA) or siRNA against UCP2 (siRNA UCP2). b) Cyclin D1 expression in precapillary PASMC isolated from wild type (WT) and UCP2 knockout ($UCP2^{-/-}$) mice. Data are obtained from at least four independent precapillary PASMC cell isolations and presented as ratio of cyclin D1 to β-actin expression. n=3 each.
*p<0.05, ** p<0.01 compared control with Student's t test.

3.3.2.7. Effect of UCP2 on mitochondrial respiration, $[Ca^{2+}]_m$, glucose and fatty acid metabolism in precapillary PASMC

To investigate the role of UCP2 in pyruvate metabolism of precapillary PASMC, the effect of application of pyruvate on cellular respiration after transfection of precapillary PASMC with scr siRNA or siRNA against UCP2 and in isolated lung mitochondria from WT and $UCP2^{-/-}$ mice was studied. Both basal (routine) cellular respiration after transfection of siRNA against UCP2 (Figure 46b) and routine respiration of isolated mitochondria from $UCP2^{-/-}$ mice (Figure 46a) were similar to the level of cellular respiration after transfection with scr siRNA and in precapillary PASMC isolated from WT mice, respectively. Application of pyruvate did not result in any changes of mitochondrial respiration in precapillary PASMC after transfection of siRNA against UCP2 or in isolated mitochondria from $UCP2^{-/-}$ mice. Additionally, intracellular baseline levels of pyruvate in precapillary PASMC (Figure 46d) and after pyruvate stimulation in mitochondria (Figure 46e) were similar in both animal groups.

The mRNA expression level of key components of the cellular fatty acid metabolism such as acyl-CoA thioesterase 1 (acot1), carnitine palmitoyltransferase 1a (cpt1b), carnitine palmitoyltransferase 2 (cpt2), carnitine/acylcarnitine translocase (Slc25a20), and hydratase/3-hydroxyacyl Coenzyme A dehydrogenase (ehhadh) was studied, to investigate the role of UCP2 in fatty acid metabolism. Their expression in precapillary PASMC isolated from $UCP2^{-/-}$ was similar to the level of their expression in WT mice (Figure 46c).

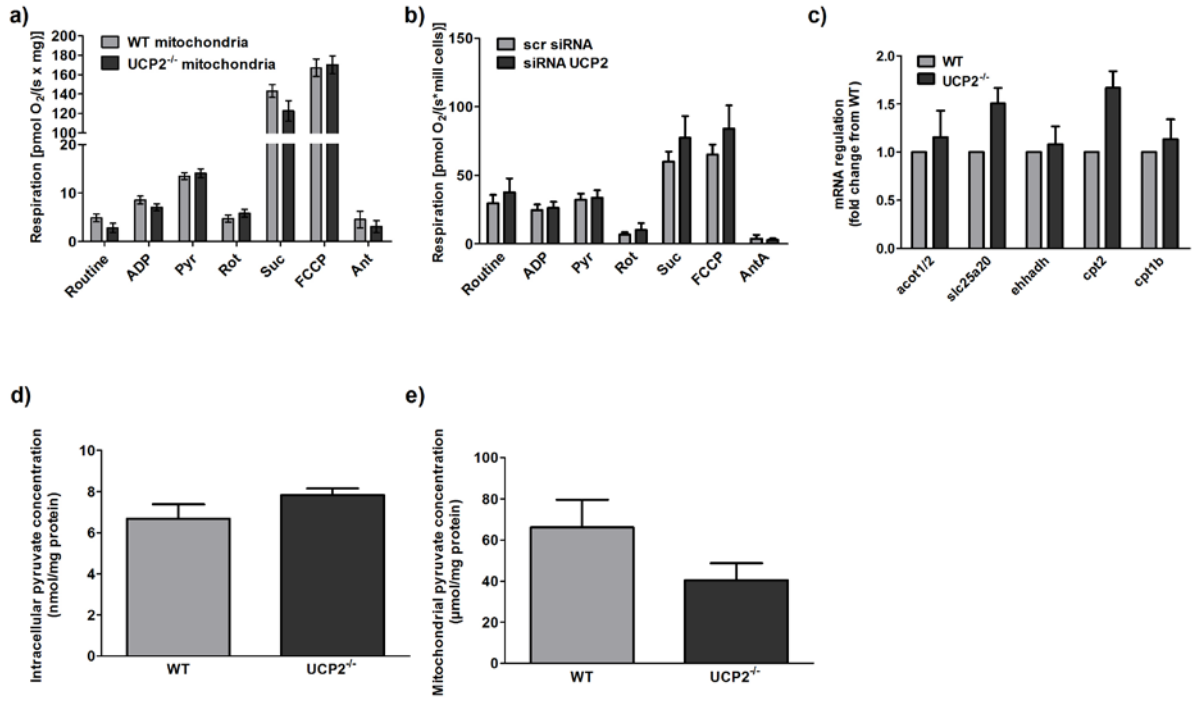

Figure 46. Effect of UCP2 on mitochondrial respiration, mitochondrial pyruvate and fatty acid metabolism.

a) Respiration of isolated lung mitochondria from wild type (WT) and UCP2 knockout ($UCP2^{-/-}$) mice (n=8 each group). Data are shown as the respiration in pmol of O_2 consumed per minute per mg of mitochondria where Routine is endogenous, unstimulated respiration, and ADP (adenosine diphosphate,), Pyr (pyruvate), Rot (rotenone), suc (succinate), FCCP and Ant (antimycin A) are respiration after addition of those respective substances. b) Cellular respiration of precapillary PASMC after transfection with scr siRNA or siRNA UCP2 (n=7 each group). Data are given as respiration in pmol of O_2 consumed per minute per million of cells. Cellular respiration measurements were performed with 2.5-5.0 million cells per measurement. c) mRNA expression of key components of fatty acid metabolism in precapillary PASMC isolated from WT and $UCP2^{-/-}$ mice where acot1/2 is acyl-CoA thioesterase 1 and 2, cpt1b is carnitine palmitoyltransferase 1b, cpt2 is carnitine palmitoyltransferase 2, Slc25a20 is carnitine/acylcarnitine translocase, ehhadh is enoyl-Coenzyme A, hydratase/3-hydroxyacyl Coenzyme A dehydrogenase. Pyruvate concentration in precapillary PASMC (d) and in mitochondria after pyruvate stimulation (e) from WT and $UCP2^{-/-}$ mice (n=3, mitochondrial isolation). Cellular pyruvate concentration was measured in 10000 per measement. Data were obtained from ≥4 four independent precapillary precapillary PASMC cell isolations. No significant changes with Student's t test.

To investigate the possibility that UCP2 acts as MCU, $[Ca^{2+}]_m$ concentration in precapillary PASMC isolated from WT and $UCP2^{-/-}$ mice was studied by Rhod2 fluorescent dye. $[Ca^{2+}]_m$ were in similar range in both animal groups measured by fluorescent microscopy, as well as by the microplate reader (Figure 47a-b).

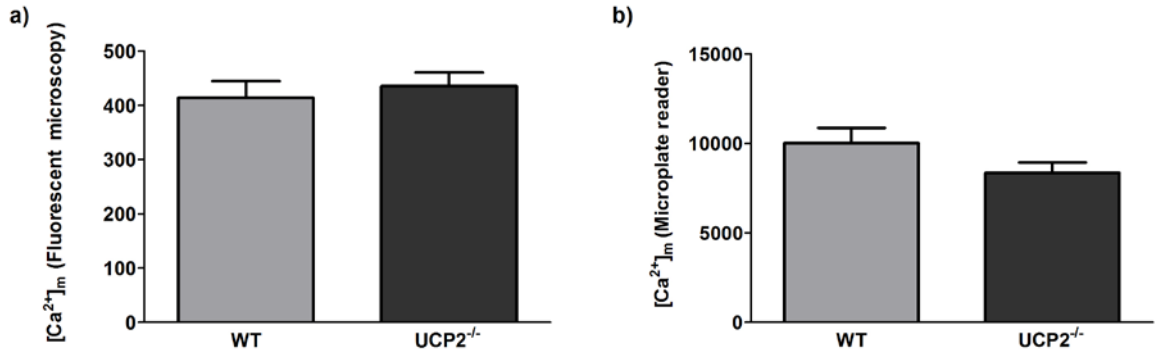

Figure 47. Effect of UCP2 on mitochondrial calcium concentration ($[Ca^{2+}]_m$).

$[Ca^{2+}]_m$ measured by fluorescence microscopy (a, n≥49 cells each) and multimode microplate reader (b, 10000 cells per measement measement) in precapillary PASMC isolated from wild type (WT) and UCP2 knockout ($UCP2^{-/-}$) mice. Data were obtained from ≥4 four independent precapillary precapillary PASMC cell isolations.
No significant changes with Student's t test.

3.3.3. Effect of UCP2 on $\Delta\psi_m$, respiration and glucose metabolism in PASMC during chronic hypoxia

The level of $\Delta\psi_m$ of precapillary PASMC isolated from $UCP2^{-/-}$ mice with hypoxia-induced PH was similar to the level of $\Delta\psi_m$ in WT mice with chronic hypoxia-induced PH (Figure 48a). The decrease of mitochondrial respiration because of chronic hypoxic exposure was similar in precapillary PASMC transfected with scr siRNA or siRNA against UCP2 (Figure 48b). Additionally, hypoxic (48h, 1% O_2) exposure of precapillary PASMC transfected with siRNA against UCP2 increased the mRNA expression of LDHA and PDK1 to the same levels as in precapillary PASMC transfected with scr siRNA (Figure 48c). The same was true for precapillary PASMC isolated from $UCP2^{-/-}$ mice, where hypoxia (48h 1% O_2) induced the same degree of anaerobic glucose pathway activation as in hypoxic WT precapillary PASMC (Figure 48 d-f) represented by higher levels of mRNA and protein expression of key components of anaerobic glycolysis metabolism within cells.

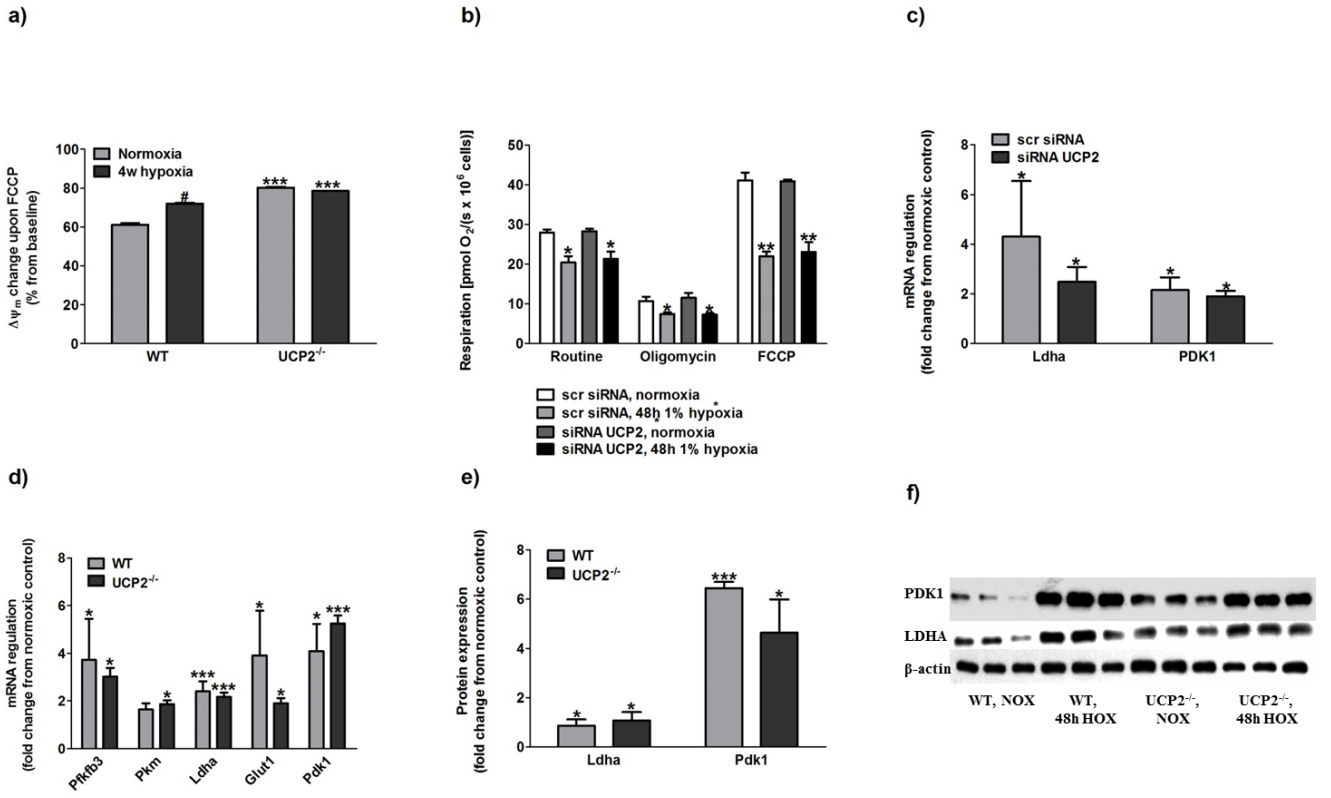

Figure 48. Effect of chronic hypoxic exposure on $\Delta\psi_m$, mitochondrial respiration, and glucose metabolism in WT and UCP2$^{-/-}$ mice.

a) $\Delta\psi_m$ presented as percent of maximal FCCP-induced drop of $\Delta\psi_m$ in precapillary PASMC isolated from wild type (WT) and UCP2 knockout (UCP2$^{-/-}$) mice exposed to 4 weeks of 10% O_2 (4w hypoxia) compared to maximal FCCP-induced drop of $\Delta\psi_m$ in precapillary PASMC isolated from normoxic animals (Normoxia). $\Delta\psi_m$ was measured ≥18 individual cells each. b) Cellular respiration of precapillary PASMC transfected with scr siRNA or siRNA UCP2 after exposure to 48h, 1% O_2 (48h, 1% hypoxia) compared to normoxic control. Data are given as respiration in pmol of O_2 consumed per minute per million cells where Routine is endogenous, unstimulated respiration; Oligomycin is oligomycin-inhibited respiration; FCCP represents respiration in the presence of FCCP. Cellular respiration measurements were performed with 2.5-5.0 million cells per measurement, n=3. c) mRNA expression of PDK1 and LDHA in precapillary PASMC transfected with scr siRNA or siRNA against UCP2 after exposure to 48h, 1% O_2. Data are presented as fold change compared to normoxic value. n=4. d) mRNA expression of enzymes of the anaerobic glycolysis in precapillary PASMC isolated from WT and UCP2$^{-/-}$ mice after exposure to 48h, 1% O_2. Data are presented as a fold change compared to normoxic value where pfkfb3 is 6-phosphofructo-2-kinase/fructose-2,6-biphosphatase 3, Pkm is pyruvate kinase, muscle form, LDHA - lactate dehydrogenase, Glut1 is glucose transporter 1 and PDK1 is pyruvate dehydrogenase kinase 1. n=4 e) Protein expression of LDHA and PDK1 in WT and UCP2$^{-/-}$ precapillary PASMC after exposure to 48h, 1% O_2. Data are presented as a fold change compared to normoxic value. n=3 f) Representative pictures of protein expression of LDHA and PDK1 in WT and UCP2$^{-/-}$ precapillary PASMC after exposure to 48h, 1% O_2 (48h HOX) compared to normoxia (NOX). Data were obtained from ≥4 independent precapillary precapillary PASMC cell isolations.

*p<0.05, **p<0.01, *** p<0.001 compared to normoxic value; # p<0.05 compared to WT with one-way ANOVA with Tukey post hoc test.

4. Discussion

Mitochondria have long been considered to be O_2 sensing organelles taking part in the signaling cascade underlying HPV, as well as important factors in hypoxia and non-hypoxia dependent pulmonary vascular remodeling processes by participating in numerous proliferative and antiapoptotic/ proapoptotic signaling pathways[1, 38]. Nevertheless, the exact impact of mitochondria in these processes is still not clear[1, 82]. In particular, the role of $\Delta\psi_m$, the most important portion of the proton-motive force that drives ATP synthesis and is coupled with the degree of mitochondrial ROS release, is still controversial in HPV and PH development. Evidences exist for and against a role of $\Delta\psi_m$ and ROS in these processes, as well as for an increase or a decrease of these factors in HPV and PH. UCP2 is thought to be a negative regulator of $\Delta\psi_m$ and mitochondria-derived ROS[219-221]. UCP deficient mice have been shown to exhibit increased acute HPV and pulmonary vascular remodeling in baseline conditions[179]. Against this background, this studied aimed to investigate the role of $\Delta\psi_m$ in HPV and PH development and the effect of UCP2 knockout on these processes.

The following results were demonstrated by this study:

- Acute hypoxia increased $\Delta\psi_m$ and ROS emission in isolated mouse and rat precapillary PASMC.
- Potentiated HPV in UCP2 knockout mice was associated with augmented mitochondrial hyperpolarization and ROS emission in isolated precapillary PASMC during acute hypoxic exposure.
- In animal models of PH, as well as human IPAH, $\Delta\psi_m$ was increased when compared to controls.
- Factors that may promote mitochondrial hyperpolarization in PH are glycolytically produced ATP and UCP2 downregulation.
- UCP2 knockout resulted in pulmonary vasculature remodeling and RV hypertrophy under normoxic baseline conditions. Pulmonary vascular remodeling was at least in part caused by increased proliferation of precapillary PASMC induced by increased $\Delta\psi_m$ and partially by increased ROS release of these cells. $UCP2^{-/-}$ mice may be used as an experimental model of moderate PH.
- Increase of pulmonary vascular remodeling in $UCP2^{-/-}$ mice after chronic hypoxic exposure may be induced by additional metabolic alterations in PASMC of these mice.

Our findings suggest that increases of $\Delta\psi_m$ and mitochondrial ROS regulate HPV and pulmonary vascular remodeling leading to PH. Additionally, metabolic alterations play a role in animal models of PH.

4.1. Role of $\Delta\psi_m$ in HPV

4.1.1. Increase of $\Delta\psi_m$ and HPV

Previously, it was shown by the Weissmann group that acute hypoxia induced a hyperpolarization of mitochondria, an increase of mitochondrial ROS emission and a rise of $[Ca^{2+}]_i$ concentration in small precapillary PASMC isolated from pulmonary arteries of rabbits[13]. These effects were specific for precapillary PASMC and did not occur in renal or aortic SMC during acute hypoxia[13]. As a potential mechanism for the increased ROS, it was proposed that the complex IV sensed the lack of O_2, initiating the increase of ROS emission by complex III of the respiratory chain[13]. The current study confirms the reaction of precapillary PASMC to acute hypoxia in other rodents. Acute hypoxic exposure of precapillary PASMC isolated from mice and rats induced the increase of $\Delta\psi_m$ and ROS emission. In line with our findings, previously published results demonstrated the inhibitory effect of chemical uncouplers, DNP and FCCP on HPV at high concentrations[168]. The effect of DNP was specific for HPV, as 100µM DNP did not inhibit the thromboxan mimetic U46619 induced vasoconstriction.

Mitochondrial hyperpolarization as a response to acute hypoxia in precapillary PASMC was proven by measurement with two different fluorescent dyes, JC1 and TMRE (Figures 17 and 18). Several fluorescent membrane-permanent cationic dyes such as Rhod123 (rhodamine 123), Rhod123 derivatives (TMRE and TMRM [tetraethylrhodamine methyl]), $DiOC_6(3)$ (3,3´ - dihexyloxacarbocyanine iodide) and JC1 have been suggested for directly measuring the $\Delta\psi_m$ by fluorescent microscopy[117]. These positively charged dyes accumulate within negatively charged mitochondria in an inverse proportion to $\Delta\psi_m$ according to the Nernst equation[117]. Hyperpolarization of mitochondria evokes the increase of accumulation of cationic dyes within the mitochondrial matrix, and depolarized mitochondria accumulate less dye. There are merits and pitfalls of each of these dyes[254]. The main disadvantage of Rhod123 is its ability to form putative adducts with some components of the IMM that can lead to misleading results[255]. $DiOC_6(3)$, in addition to measurement of $\Delta\psi_m$, is used to study the plasma membrane potential. Therefore, changes in the plasma membrane potential can mask the change of $\Delta\psi_m$. The most commonly used dyes are TMRE or TMRM and JC1. TMRE and TMRM can be used in quenching or non-quenching modes[118]. In the quenching mode, an increased concentration of the dye leads to quenching of the fluorescent signal upon mitochondrial hyperpolarization. In the non-quenching mode a low concentration of these dyes accumulates in the mitochondria during hyperpolarization and their fluorescent signal increases[118]. Laser illumination of TMRM loaded in mitochondria at high concentrations (quenching mode) generates ROS[256]. Moreover, high concentrations of TMRE exhibit mitochondrial toxicity[244]. Therefore, the non-quenching mode for TMRE with lower concentrations of the dye (10 nM TMRE) was used to study $\Delta\psi_m$ in precapillary PASMC during acute hypoxia. Although the quenching mode is very sensitive to changes in $\Delta\psi_m$, it cannot be used to compare changes in baseline $\Delta\psi_m$[118]. Additionally, TMRE distribution within

cells is dependent on plasma membrane potential. Changes in plasma membrane potential can lead to release of TMRE into extracellular buffer, even though $\Delta\psi_m$ remains unchanged[257]. Therefore, JC1 fluorescence was used as an additional method to determine $\Delta\psi_m$. It was shown that JC1 can measure $\Delta\psi_m$ with greater accuracy in intact cells compared to other cationic dyes[255, 258]. The advantage of JC1 is a ratiometric measurement of $\Delta\psi_m$ by monitoring the ratio of green/red (530/590nm) emission fluorescence[257]. Hyperpolarization of mitochondria increases the red fluorescence (590nm emission) and depolarization raises the green fluorescence (530nm emission). Both reactions are reversible. As a result, JC1 measurement is less sensitive to loss of staining, organelle swelling and dye bleaching[259]. However, JC1 used in doses greater than 1µM can be toxic for mitochondria[257], and some publications demonstrated that JC1 can be a cause of artifacts in $\Delta\psi_m$ studies[118].

The mechanism for the increase of $\Delta\psi_m$ in acute hypoxia remains unclear, but the mitochondrial hyperpolarization may be induced by different factors. In principle at least, four mechanisms are possible: 1) inhibition of ATP synthase, 2) modulation of mitochondrial membrane channels (*e.g.* UCPs, Ca^{2+} channels, ion exchangers), 3) improvement of H^+/e^- stoichiometry and 4) increase of mitochondrial respiration. In possibilities 1-3, additionally, the increased $\Delta\psi_m$ must not be compensated completely by a decreased electron flow through the respiratory chain. These possibilities are described in detail below. 1) As mitochondrial hyperpolarization was associated with slight inhibition of mitochondrial respiration[13], a mechanism similar to the effect of NO on $\Delta\psi_m$[260] was suggested. In this scenario, inhibition of NO at complex IV would be mirrored by the lack of O_2 inhibiting complex IV, resulting in increased glycolytic ATP production, which inhibits ATP synthase and increases $\Delta\psi_m$. In this regard, it is a well known effect of inhibitors of ATP synthase to increase $\Delta\psi_m$ and consecutively decrease respiration according to the classical Mitchell theory, where there is a feedback mechanism of $\Delta\psi_m$ on electron flow[119, 225, 261]. Consequently, acute hypoxia could not only act via complex IV inhibition, but also have a direct effect on $\Delta\psi_m$, and decreased respiration could be a result of mitochondrial hyperpolarization. Both hypotheses could explain why the decreased respiration in acute hypoxia was not associated with decreased $\Delta\psi_m$, as could be expected. Additionally, mitochondrial respiration in acute hypoxia was only reduced by up to ~10% in the range where $\Delta\psi_m$ was increased[13]. This is in line with many publications showing preserved cellular ATP levels during HPV, which argues against a substantial mitochondrial inhibition[1]. Thus, the slight decrease of respiration (and proton pumping across the membrane) may easily be counteracted by other mechanisms increasing $\Delta\psi_m$ such as inhibition of ATP synthase by glycolytic ATP as discussed above. 2) Keeping in mind that the reaction of acute O_2 sensing must be very fast, another potential mechanism can account for mitochondrial hyperpolarization - the fine tuning of the proton leak by acute hypoxia, *e.g.* via modulation of UCP function. Changes of $\Delta\psi_m$ in the measurements of the current study were small (about 7-10% of basal $\Delta\psi_m$). Therefore, the functional alterations of the proton leak may be

small, considering a high basal proton leak in resting cellular metabolic conditions, which is responsible for ~20-30% of respiration (up to 50% in skeletal muscle[156]). The proton leak shuttles protons from the intermembrane space to the mitochondrial matrix, reducing the number of protons passing through ATP synthase. In fact, Gnaiger *et al.* described a decrease of the proton leak and uncoupled respiration in isolated mitochondria by unknown mechanisms during hypoxia[262]. Other possibilities for increasing $\Delta\psi_m$ are the modulation of mitochondrial channels including Ca^{2+} channels and VDAC[230]. Mitochondrial channels could change the $\Delta\psi_m$ by modulation of the activity of the respiratory chain or by use of a proton gradient to transfer ions across IMM[230]. Little is known about their function in acute hypoxia. 3) Another mechanism to increase $\Delta\psi_m$ despite decreased electron flow is to enhance the number of protons that are pumped per electron (called H^+/e^- stoichiometry)[263]. In this regard, Kwast *et al.* showed that in yeast cytochrome c oxidase subunit 5B (COX5b), the hypoxic isoform of COX5, is capable of pumping more protons across the IMM despite utilizing fewer O_2 molecules, thereby producing a stable $\Delta\psi_m$ in hypoxia[264]. 4) An increase of mitochondrial respiration as the underlying mechanism for mitochondrial hyperpolarization seems unlikely, as a decrease of mitochondrial respiration in acute hypoxia was measured in Sommer's study[13].

4.1.2. Increase of ROS and HPV

In addition to the increase of $\Delta\psi_m$, acute hypoxia also induced the increase of mitochondrial ROS production (Figures 19 and 21). The increase of ROS measured in this study supports the hypothesis of increased ROS as the underlying mechanism of HPV ("ROS hypothesis") and questions the hypothesis that a decrease in the redox state ("redox hypothesis") causes HPV[3]. The latter suggests that a reduced level of ROS elicits PASMC contraction through decreased K_v channel currents with subsequent plasma membrane depolarization and influx of Ca^{2+} into the cytosol[37]. Conversely, the concept of increased ROS proposes that an increase in ROS originating from mitochondria or other cellular sources orchestrates the $[Ca^{2+}]_i$ increase in acute hypoxia[1]. In favor of this hypothesis, Weissmann *et al.* found an increase of $O_2^{\bullet-}$ release during acute hypoxia[13, 248] and an inhibition of HPV by the $O_2^{\bullet-}$ scavenger, nitro blue tetrazolium in isolated perfused rabbit lungs[265]. In addition there are numerous reports of increased ROS concentrations in acute hypoxic signaling[26, 77, 248, 266-269]. Limitations of techniques for ROS measurements in *vivo* may be one of the reasons for the discrepancy in the models of ROS in HPV. To overcome this problem, ROS measurements were conducted by two different approaches: 1) MitoSOX for real-time measurements of $O_2^{\bullet-}$ in precapillary PASMC during acute hypoxia (Figure 21b), and 2) measurements with the HyPer plasmid for real-time investigation of H_2O_2 (Figure 21c). All of these measurements consistently provided evidence for an increase in ROS emission during acute hypoxia.

Numerous methods have been used for ROS detection such as cytochrome c reduction, chemiluminescence-based techniques, electron spin resonance [ESR or electron paramagnetic resonance (EPR)] spectroscopy], detection of products of the interaction of intracellular $O_2^{\bullet-}$ with dihydroethidium by high-performance liquid chromatography (HPLC), and fluorescent microscopy with ROS-sensitive fluorescent dyes[270]. Each of these approaches has potential pitfalls and benefits and there is no "ideal" approach or "gold standard" to measure intracellular ROS[1, 270]. Therefore, the choice of method for ROS detection depends on experimental conditions. Cytochrome c reduction and chemiluminescence-based techniques are not sensitive enough to detect small changes and are not capable of verifying a source of ROS. Additionally, measurement of ROS by cytochrome c reduction and HPLC-based detection of products of the interaction of intracellular $O_2^{\bullet-}$ with dihydroethidium cannot detect real-time changes of ROS in live precapillary PASMC[270]. Fluorescence microscopy with ROS-sensitive fluorescent dyes allows real-time monitoring of changes in intracellular ROS level and ESR spectroscopy is an elegant approach for quantitative detection of ROS in baseline conditions that overcomes the limitations of fluorescence based dyes[265]. Thus, fluorescence microscopy with ROS-sensitive fluorescent dyes was used in acute hypoxic experiments and ESR spectroscopy was used to detect the baseline level of ROS in precapillary PASMC. A variety of ROS fluorescent indicators are used nowadays including dihydroethidium (hydroethidine, HEt), dichlorofluorescein (DCF) with its derivatives, dihydrorhodamine 123 (DHR123) and redox-sensitive recombinant proteins such as reduction-oxidation sensitive green fluorescent protein (roGFP), yellow fluorescent protein-based redox sensor (rxYFP), redox-sensitive FRET (Fluorescence resonance energy transfer) protein sensor and HyPer. They can detect different ROS species. For example, HEt and MitoSOX sense $O_2^{\bullet-}$ while DCF, DHR123, HyPer, and roGFP detect H_2O_2. However, their sensitivity for specific ROS species is very questionable[259]. As in the case of fluorescent dyes for $\Delta\psi_m$ measurement, ROS sensitive dyes have their benefits and limitations. For example, limitations of one of the most popular ROS fluorescent sensors, DCF includes the production of ROS upon exposure to light, detection of multiple types of ROS and irreversible nature of the reaction[257]. The aim of this study was to identify the real-time change of mitochondrial ROS production during acute hypoxia in precapillary PASMC. Due to this fact, MitoSOX was chosen to detect the $O_2^{\bullet-}$ in mitochondria[271]. MitoSOX is a mitochondrial targeted HEt, where the positively charged triphenylphosphonium moiety is conjugated to HEt to increase accumulation within mitochondrial matrix[271]. MitoSOX is oxidized by $O_2^{\bullet-}$ to form the hydroxylated product that becomes fluorescent[257]. MitoSOX has numerous pitfalls including mitochondrial toxicity, binding to DNA, reaction with $ONOO^-$ and HOCl[271]. Additionally, MitoSOX loading is dependent on $\Delta\psi_m$[272]. Thus, change in $\Delta\psi_m$ can confound the MitoSOX data. $O_2^{\bullet-}$ produced by mitochondria can be dismutated by mitochondrial SOD2 to H_2O_2 that can be released into the cytosol[130]. Therefore, a second fluorescent approach was used in this study to

confirm the MitoSOX data. The cellular level of H_2O_2 was measured by HyPer. HyPer consist of the circularly permuted yellow fluorescent protein and OxyR that is the H_2O_2 sensitive regulatory domain of *Escherichia coli*[273]. The cellular level of H_2O_2 was increased upon the acute hypoxic stimulus in precapillary PASMC isolated from different rodents (Figures 20 and 21). However, it is possible that the increased level of cytosolic H_2O_2 during the acute hypoxic challenge is a result of higher activity of other sources of H_2O_2 within cells such as NADPH oxidases[1].

The mechanism for the increase of mitochondrial ROS upon the acute hypoxic stimulus is not clear. $\Delta\psi_m$ hyperpolarization that was discussed above can be the reason for increased ROS production during acute hypoxia in precapillary PASMC. The mitochondrial electron transport chain is an inherent source of ROS and most experimental studies demonstrate that ROS production is directly coupled to $\Delta\psi_m$[142, 143]. Application of an uncoupler decreased ROS production[145] while a chemical that augments $\Delta\psi_m$, also increased the rate of $O_2^{\bullet-}$ production[146]. Consequently, at higher $\Delta\psi_m$ the probability of increased ROS generation is also high,[144, 274] and it is known that mitochondrial production of $O_2^{\bullet-}$ is disproportionately enhanced by the increase of $\Delta\psi_m$[275, 276]. In addition, ROS production is more sensitive to uncoupling-induced changes in $\Delta\psi_m$ than ATP synthesis[148]; Even a slight decrease of $\Delta\psi_m$ may lead to a marked decrease of ROS production in isolated mitochondria after succinate application[123]. The same is true for whole organ. Okuda *et al.* showed that infusion of an uncoupler decreased the H_2O_2 level in the perfused liver[277]. Therefore, an inducible proton leak (mild uncoupling) which could be reduced during acute hypoxia could be one possible mechanism of mitochondrial ROS production[155]. Another possibility for a hypoxia induced ROS increase may be that low O_2 concentration leads to cytochrome c reduction and so limits its capability to scavenge $O_2^{\bullet-}$[121]. In agreement with the concept that ROS increase is a trigger for HPV, exogenous $O_2^{\bullet-}$ and H_2O_2 initiate HPV in isolated pulmonary arteries[278-281] and induce an increase in $[Ca^{2+}]_i$ in cultured rat PASMC[164] as well as in pulmonary rat arteries[282]. Additional evidence supporting our findings comes from a publication which demonstrated that overexpression of glutathione peroxidase (Gpx1)[283] or mitochondrial catalase[27, 283] augmented ROS removal and simultaneously attenuated the acute hypoxia induced ROS increase, whereas Gpx1 deletion had the opposite effect[283]. Gpx1 and catalase are essential parts of the ROS removal system within mitochondria and whole cells. Additionally, overexpression of Gpx1 and catalase attenuated the acute hypoxic increase of $[Ca^{2+}]_i$ and contraction of freshly isolated mouse PASMC[283]. Furthermore, this study showed that the increase of $\Delta\psi_m$ is upstream of hypoxia-induced ROS release, based on the finding that application of ROS scavengers did not reverse mitochondrial hyperpolarization during acute hypoxia (Figure 22).

4.1.3. UCP2$^{-/-}$ and HPV

The functional relevance of increased $\Delta\psi_m$ and ROS for HPV was supported by experiments in mice deficient for UCP2. Gene deficiency of UCP2 resulted in a higher increase of ROS and $\Delta\psi_m$ during acute hypoxia in PASMC isolated from UCP2$^{-/-}$ animals compared to WT animals (Figure 24). It was shown in a different study that UCP2$^{-/-}$ animals exhibited an increased HPV starting from similar normoxic pressures in the isolated ventilated and perfused lung (unpublished thesis of Timm Hoeres, Giessen). This effect of UCP2$^{-/-}$ on the pulmonary vasculature was specific for HPV as the thromboxan mimetic, U46619 induced the same level of vasoconstriction in WT and UCP2$^{-/-}$ mice.

Despite the controversy about the possible molecular mechanisms underlying the function of UCP2, there is a broad consensus that UCP2 negatively regulates $\Delta\psi_m$ and ROS production, at least when activated by certain stimuli[210]. Negre-Salvayre *et al.* first described a steep increase of mitochondrial ROS as a result of inhibition of UCP2 with guanosine diphosphate (GDP)[219]. Recently, it was shown that overexpression of UCP2 attenuated ROS production[220, 221], and in conversely, UCP2 knockout resulted in an increase of mitochondrial ROS emission[222]. UCP2 gene transfer in the right tibialis anterior muscles of rats led to a significant reduction of $\Delta\psi_m$[284]. It has been suggested that UCP2 alters $\Delta\psi_m$ and ROS emission via uncoupling (increase of the proton leak), due to the fact that its amino acid sequence is 59% identical to UCP1, which is a pure uncoupling protein[285]. However, there are some experiments that could not show an increase of $\Delta\psi_m$ in UCP2$^{-/-}$ mice[210]. Other possible mechanisms for UCP2 function have been suggested such as acting as a metabolic switch[225] and regulating mitochondrial Ca^{2+} handling (see introduction for more details)[229]. Under these scenarios, UCP2 could decrease ROS production by inhibiting the entry of pyruvate into the oxidative pathway resulting in attenuation of the enormous redox pressure of pyruvate[225]. The increase of Ca^{2+} influx into mitochondria via UCP2 (if UCP2 is indeed a MCU) is also associated with a decrease of $\Delta\psi_m$ via the alteration of mitochondrial function[286]; however in that study the effects of acute hypoxia on pyruvate and fatty acid metabolism and $[Ca^{2+}]_m$ were not tested. The discrepancy of the theories regarding UCP2 function can be explained by the fact that UCP2 functions may change in tissue-specific or stimulus-dependent manners.

Along these lines, it is possible that in UCP2$^{-/-}$ mice the essential mechanism to regulate excess ROS production during acute hypoxia by tuning of $\Delta\psi_m$ was absent. The enhanced ROS emission in these mice induced by acute hypoxia may be responsible for the higher response of the pulmonary vasculature to the hypoxic stimulus compared to WT mice. The mechanism by which acute hypoxia alters UCP2 functions and thus magnifies the increase of mitochondrial hyperpolarization in UCP2$^{-/-}$ mice remains unclear. It may be either a direct activation of UCP2 in WT cells during acute hypoxia which is inhibited in UCP2$^{-/-}$ precapillary PASMC, or a passive effect of $\Delta\psi_m$ properties. The first could be achieved via $O_2^{\bullet-}$ or its by-products, especially 4-HNE (4-hydroxynonenal), which seems improbable, as ROS scavengers did not

affect the acute hypoxia-induced hyperpolarization in PASMC. However, Echtay *et al.* demonstrated that only matrix-targeted antioxidants, such as mitoQ (mitoquinone mesylate: [10-(4,5-dimethoxy-2-methyl-3,6-dioxo-1,4-cycloheexadienl-yl) and mitoE [2-(2-(triphenylphosphonio)ethyl)-3,4-dihydro-2,5,7,8-tetramethyl-2H-1-benzopyran-6-ol bromide] could prevent the UCP2 activation by $O_2^{\bullet-}$ released into the mitochondrial matrix, while non-mitochondrial antioxidants were unable to prevent the UCP2-induced proton leak[287]. The authors concluded that $O_2^{\bullet-}$ released into the mitochondrial matrix is responsible for UCP2 activation[287]. Therefore, further investigation should be conducted to explore the effect of $O_2^{\bullet-}$ released into the mitochondrial matrix on UCP2 activity and mitochondrial hyperpolarization during acute hypoxia. Recently Mailloux *et al*. have suggested another mechanism of UCP2 activation[288]. They showed that glutathionylation of UCP2 by H_2O_2 can play a key role in controlling the ROS-induced proton leak through UCP2. H_2O_2-induced glutathionylation of UCP2 in this model serves as trigger of an increase of the proton leak that decreases $\Delta\psi_m$ and ROS production.

On the other hand the enhanced increase of $\Delta\psi_m$ can be the result of the non-ohmic behavior of the mitochondrial proton conductance, which states that the mitochondrial proton leak rises exponentially with increasing $\Delta\psi_m$ [156]. In conditions of decreased proton conductance, *e.g.* in UCP2$^{-/-}$ mice, the same increase of the $\Delta\psi_m$ can result in a lower increase of the proton leak and thus higher final $\Delta\psi_m$ than under conditions of a relatively high proton conductance. In case of the UCP2$^{-/-}$ mice the lower proton leak would attenuate the increased $\Delta\psi_m$ in acute hypoxia less than in WT cells. In conclusion, acute hypoxia evokes an increase of $\Delta\psi_m$ and ROS emission in precapillary PASMC, probably via alteration of the proton leak. Therefore, UCP2$^{-/-}$ mice, which have higher $\Delta\psi_m$ hyperpolarization and ROS emission during acute hypoxia in PASMC, have higher HPV response in the isolated lung experiment.

4.2. Role of $\Delta\psi_m$ in PH

This study provided evidence that mitochondrial hyperpolarization in precapillary PASMC may act as a novel mechanism for development of PH. Furthermore, possible up- and downstream signaling mechanisms were identified. This finding was supported by the fact that 1) PASMC from two different animal models of PH (experimental PH) and PASMC from IPAH patients showed hyperpolarized mitochondria (Figure 26), 2) reversal of mitochondrial hyperpolarization by re-exposure to normoxia in precapillary PASMC exposed to chronic hypoxia and by application of 500µM DCA in PASMC isolated from rats with MCT-induced PH was associated with reversal of PH[194] (Figure 28), and 3) UCP2$^{-/-}$ mice, that had hyperpolarized mitochondria in their PASMC, showed increased PASMC proliferation and pulmonary vascular remodeling (Figures 37-44). As a possible mechanism for the increase of $\Delta\psi_m$ in PH our own study identified ATP produced by enhanced anaerobic glycolysis (Figure 29), and downregulation of UCP2 (Figures 31 and 32).

$\Delta\psi_m$ was increased in PASMC isolated from patients with IPAH, in precapillary PASMC of rats with MCT-induced PH and mice with chronic hypoxia-induced PH. Additionally, isolated precapillary PASMC that were incubated in hypoxia for 48 hours showed hyperpolarized mitochondria. This model can be used to simulate effects occurring under chronic hypoxia in pulmonary vascular cells[25]. $\Delta\psi_m$ was measured in the presence and absence of a mitochondrial uncoupler, FCCP, to attain maximum depolarization of mitochondria (Figure 15). The change of $\Delta\psi_m$ upon FCCP stimulation can be used as a measure of $\Delta\psi_m$ to avoid artifacts, *e.g.* from loading of the cells with the fluorescent dye[289]. These data are in accordance with a previous study showing mitochondrial hyperpolarization in animal models of PH[13, 34]. Recently, Chen *et al.* published data that exposure to 24h of 5% O_2 leads to a significant hyperpolarization of human PASMC and the authors linked this finding to the decrease of mitochondrial permeability and attenuated apoptosis[205]. Conversely, another study conducted by Hu *et al*. that used the same cell lines purchased from PromoCell GmbH (Heidelberg, Germany) and the same approach for $\Delta\psi_m$ measurement, rhodamine-123 fluorescence, reported a depolarization of the $\Delta\psi_m$ during chronic hypoxic exposure of isolated human PASMC concomitant with increased H_2O_2 production[204]. Hu *et al*. found the opening mitoK_{ATP} was responsible for the depolarization of $\Delta\psi_m$ and the inhibition of human PASMC apoptosis through the attenuation of the release of cytochrome c from mitochondria and the activation of caspase-dependent mechanisms[204]. The reason for this discrepancy remains to be elucidated, however, in our own study, PASMC isolated from small precapillary arteries were used (that is main site of pulmonary vascular remodeling[290]), while both Chen *et al.* [205] and Hu *et al*. [204] used PASMC from bigger vessels. Despite the fact that Hu *et al*. demonstrated the opposite result concerning the chronic hypoxia-induced change in $\Delta\psi_m$, they also found an increase of ROS, as in this study[204].

The increase of $\Delta\psi_m$ in chronic hypoxia could be a characteristic of metabolic adaptation (metabolic shift) due to the lack of O_2. Therefore, one possible mechanism of $\Delta\psi_m$ increase could be the inhibition of ATP synthase induced by an increased production of anaerobic ATP as discussed for acute hypoxia. Moncada *et al.* showed that NO could inhibit mitochondrial respiration and simultaneously increase $\Delta\psi_m$ by reversal of the function of the ATP synthase that was associated with the increased glycolytic ATP production[291]. Furthermore, glycolytically produced ATP was necessary for $\Delta\psi_m$ hyperpolarization during application of NO in astrocytes[260]. Along these lines, it has been shown that chronic hypoxia[292] as well as MCT-induced PH[293] and IPAH[190] led to a metabolic shift in favor of anaerobic glycolysis. Furthermore, normalization of mitochondrial metabolism can reverse PH[195, 293]. In addition, chronic hypoxia caused a metabolic shift characterized by decreased mitochondrial respiration and increased glycolytic activity in pulmonary EC[294]. It seems that HIF-1α stabilization plays a key role in metabolic shift induced either by chronic hypoxia[26] or MCT[188] and IPAH[190]. However, the impact of the metabolic shift in precapillary PASMC that occurs during the pathological changes in PH is not yet fully resolved. The current study

also showed that precapillary PASMC incubated for 48h of hypoxia as well as precapillary PASMC isolated from rats with MCT-induced PH showed signs of a metabolic shift (Figure 27). Such precapillary PASMC exhibited decreased mitochondrial respiration and increased expression of glycolytic enzymes, including increased expression of PDK1, which negatively regulates the conversion of pyruvate to acetyl-CoA by inhibiting the enzyme pyruvate dehydrogenase, and increased expression of LDHA that metabolizes pyruvate anaerobically. Thus, glycolytically produced ATP, might also promote mitochondrial hyperpolarization under conditions of chronic hypoxia or other stimuli of PH. In line with this hypothesis, inhibition of the ATP/ADP translocase in precapillary PASMC by BA inhibited the increase of $\Delta\psi_m$ induced by chronic hypoxic incubation and in MCT-induced PH (Figure 29). ATP/ADP translocase can exchange mitochondrial matrix ADP for cytosolic ATP which is necessary for inhibition of ATP synthase[260, 291]. It was shown that Adenine nucleotide translocator (ANT2) imported glycolytically produced ATP into the mitochondrial matrix in cancer cells, when oxidative phosphorylation was impaired[295]. Additionally, it was shown that human pluripotent cells hydrolyzed glycolytic ATP to maintain $\Delta\psi_m$ that was required for their proliferation and survival[237]. Nevertheless, it remains to be elucidated, if glycolytically produced ATP is responsible for $\Delta\psi_m$ hyperpolarization by interaction with the ATP synthase or other mitochondrial membrane channels. The data here presented suggest that alterations in mitochondrial respiration and metabolism are directly linked to increased $\Delta\psi_m$, as restoration of mitochondrial metabolism by re-exposure to normoxia of precapillary PASMC exposed to chronic hypoxia, and DCA treatment of precapillary PASMC isolated from rats with MCT-induced PH, reversed mitochondrial respiration as well as the $\Delta\psi_m$ to control values. The data further suggest that the increase of $\Delta\psi_m$ is downstream of repressed mitochondrial respiration, because mitochondrial respiration was not altered during chronic hypoxia in rat precapillary PASMC treated with siRNA for UCP2, which showed increased $\Delta\psi_m$ (Figure 46).

As another factor promoting mitochondrial hyperpolarization during chronic hypoxia, namely, downregulation of UCP2 mRNA in lung homogenate and laser microdissected small precapillary vessel with a diameter less than 100µm from WT mice exposed to 4 weeks of normobaric hypoxia (10% O_2), was found (Figure 31). Western blot confirmed results from real-time PCR (Figure 32a-b). Downregulation of UCP2 may be a second mechanism to increase $\Delta\psi_m$ in WT mice in chronic hypoxic conditions, as UCP2 was suggested to decrease $\Delta\psi_m$, as discussed above. This finding is in line with the effect of hypoxia in adipose cells where hypoxia is a cause of UCP2 downregulation[296]. Furthermore, UCP2 is highly expressed in the lung compared to other tissue[212], and its expression in lungs increases after birth[297] which may be evidence of O_2 dependent expression of UCP2. In our own study proton leak was lower in precapillary PASMC after 48h 1% hypoxia (oligomycin-stimulated respiration, Figure 27) which suggests that decrease of a proton leak may occur via UCP2 downregulation. Additionally, UCP2

protein expression was decreased in lung homogenate of rats with MCT-induced PH as well as in lung homogenate of IPAH patients compared to control rats and donor lungs, respectively (Figure 32 c-f). This finding can be explained by the fact that despite discrepancies in the pathogenesis of different forms of PH, they shared similar molecular pathways. As discussed above, in chronic hypoxia-induced PH in mice, in MCT-induced PH in rats, and in IPAH the HIF-1α dependent metabolic shift in favor of the anaerobic glycolysis has been found[26, 190, 292, 293].

Although the experiments described in this thesis with isolated precapillary PASMC support the conclusion that increased $\Delta\psi_m$ in experimental models of PH is maintained by ATP produced via anaerobic glycolysis and UCP2 downregulation, it cannot be excluded that other mechanisms participate in mitochondrial hyperpolarization. In this regard, it has been shown that chronic hypoxia causes an alteration in expression of proteins located in the mitochondrial membrane including VDAC[298-300]. There is a large body of evidence that alterations in VDAC function can cause depolarization and swelling of mitochondria, and lead to apoptosis/cell death[301]. Furthermore, hypoxia-induced alteration in expression of F_1F_O-ATP synthase may also contribute to hypoxic $\Delta\psi_m$ hyperpolarization[302].

In contrast to mitochondrial hyperpolarization induced by acute hypoxia where the ROS scavengers did not have any influence on hyperpolarization, the increase of $\Delta\psi_m$ during chronic hypoxia was negatively regulated by application of ROS scavengers. $\Delta\psi_m$ hyperpolarization of precapillary PASMC due to MCT-induced PH was also reversed by the application of ROS scavengers (Figure 30). These findings suggest that ROS modulates $\Delta\psi_m$ in chronic hypoxic PH and MCT-induced PH in a different manner than during acute hypoxia. It is possible that ROS produced during chronic hypoxia can interfere with diverse pathways that may regulate $\Delta\psi_m$ in this condition. Numerous experiments showed the interaction between the induction of ROS emission and the Warburg effect[26, 38, 181] or HIF-1α expression and stability[38], both pathways which may regulate the metabolic shift and thus hyperpolarization of $\Delta\psi_m$ caused by glycolytically produced ATP. In line with these findings, Bell *et al*. demonstrated that ROS regulates HIF-1α protein stabilization in cancer cell lines and the antioxidant, NAC, abolishes the effect of ROS-induced HIF-1α protein stabilization on increased tumorgenesis[303]. In summary, our own findings suggest that ROS regulates the metabolic shift, which in turn regulates mitochondrial hyperpolarization. However, the exact mechanism needs to be elucidated in further studies.

In contrast to acute hypoxia where increased $\Delta\psi_m$ was specifically found in precapillary PASMC but not in SMC from systemic vessels[13], chronic hypoxia caused mitochondrial hyperpolarization also in other cell types such as rat skeletal muscle cells[298]. Interestingly, in cell cancer lines chronic hypoxia can evoke either hyperpolarization[299, 300] or depolarization[304] of mitochondria.

4.2.1 Effect of UCP2 downregulation on the pulmonary vasculature and PASMC proliferation.

In our own study, MCT injection as well as chronic hypoxic exposure resulted in the downregulation of UCP2. Therefore, we investigated the effect of UCP2 knockout on the pulmonary vasculature. Gene deficiency of UCP2, in addition to increased HPV, resulted in development of mild PH and moderate pulmonary vascular remodeling[179]. Both phenomena are connected by the fact that they can be induced by chronic exposure to hypoxia. In this study both, increased HPV and PH in UCP2$^{-/-}$ mice were associated with increased $\Delta\psi_m$ and ROS production. Thus, UCP2$^{-/-}$ mice may serve as a new experimental model of PH.

UCP2$^{-/-}$ mice demonstrated signs of PH under normoxic baseline conditions[179]. UCP2$^{-/-}$ mice had a slight increase of RVSP, hypertrophy of the RV and prominent vasculature remodeling compared to WT mice (Table 5, Figures 33-35). Echocardiography confirmed the findings of this study on the right heart, showing an increase of RV wall thickness[179]. The discrepancy between prominent pulmonary vascular remodeling and only a slight increase of RVSP may be resolved by RV dysfunction in UCP2$^{-/-}$ mice[179]. As pulmonary vascular resistance is determined by the quotient of PAP and cardiac output, an increase of RVSP or unchanged or reduced RVSP concomitant with a decrease of cardiac output can result in increased vascular resistance[179]. Indeed, RV dysfunction represented by increased Tei index and decreased cardiac output was found in UCP2$^{-/-}$ mice, both parameters measured by echocardiography[179]. Additionally, Min dP/dt was increased in UCP2$^{-/-}$ mice indicating the impairment of diastolic function of the RV (Table 5)[305]. However, it cannot be excluded that the manifestations of RV dysfunction was the result of a direct effect of UCP2 knockout on the heart. It was shown, for example, that alterations in UCP2 function have a direct effect on rat cardiomyocyte function[306].

In view of the fact that the most prominent remodeling in UCP2 knockout mice was found in the medial layer (Figures 34-35), the current study focused on the proliferation of precapillary PASMC isolated from these mice. UCP2 knockout or knockdown increased $\Delta\psi_m$, mitochondrial $O_2^{\bullet-}$ generation and subsequently precapillary PASMC proliferation (Figures 37, 38, 40, 43, 44). Additionally, UCP2 knockout or knockdown increased the expression of the pro-proliferative marker, cyclin D1[253] in precapillary PASMC. In line with the findings of the current study, modulation of UCP2 expression affected the proliferation of different cells types[226, 232, 233, 307, 308]. Derdak *et al.*[232] and Nino Fong *et al.*[233] described that UCP2-deficient mice had increased oxidative stress along with enhanced NF-kB activation that induced proliferation and decreased apoptosis in intestinal epithelial cells and pancreatic β-cells, respectively. Additionally, Chen *et al.* showed that UCP2 downregulation was important for myogenic differentiation[238]. In contrast, overexpression of UCP2-GFP in chick embryo fibroblasts and HeLa cells decreased their proliferation[235].

Increased ROS in UCP2-deficient precapillary PASMC were responsible for enhanced proliferation of these cells, as application of unspecific ROS scavengers consisting of NAC and TEMPO or MnTBAP that act as a SOD mimetic, catalase mimetic[309] and $OONO^-$ scavenger[310] partially inhibited the increased proliferation of precapillary PASMC isolated from $UCP2^{-/-}$ mice or precapillary PASMC isolated from WT mice after siRNA UCP2 knockdown. To estimate the influence of ROS on precapillary PASMC proliferation, ESR spectroscopy with the spin probe CMH (that stabilizes unstable ROS) was used (Figures 40 and 44). ESR is based on absorption of microwave radiation by unpaired electrons in an electromagnetic field [121]. Absorption of microwave energy occurs by transition of unpaired electrons (ROS molecules have unpaired electrons) to a higher energetic state in an applied magnetic field and the number of unpaired electrons presented in the sample is proportional to the amplitude of the ESR signal[270]. The ESR signal was measured in precapillary PASMC with or without cell-permeable pSOD that revealed the ESR signal that comes from $O_2^{\bullet-}$.

As in case of HPV there are two contrary opinions about the role ROS in PH development. The redox hypothesis suggests that a similar sequence of events to that which is responsible for HPV, is involved in pulmonary vasculature remodeling in PH[164]. According to this theory, the trigger of pulmonary vasculature remodeling is the decrease of ROS that is the consequence of a hypoxia-induced decline of mitochondrial respiration and evokes downregulation of K_v 1.5 channels and HIF-1α stabilization[34, 95, 165]. The opposite theory has more supportive evidences[311] that demonstrate: 1) increased oxidative status in patients with PH including enhanced lipid[312], DNA[313] and protein[311] oxidations in PH patients; 2) decreased expression of lung antioxidants including SOD and GPx[314]; 3) beneficial effect of antioxidant treatment such as NAC[315], Tempol (4-hydroxy-2,2,6,6-tetramethylpiperidin-1-oxyl)[316], erdosteine [2- ((2-oxothiolan-3-yl)carbamoylmethyl-sulfanyl)acetic acid][317] and EUK-134[318] in experimental PH. However, it is still not completely verified which downstream signaling pathways in PH are depended on increased ROS. The importance of ROS was shown in HIF-1α stabilization[38], regulation of cytosolic Ca^{2+} concentration[201], mitochondrial function and protein modifications[311]. In line with the results of this study, publications demonstrated: 1) that mild elevation of $O_2^{\bullet-}$ and H_2O_2 stimulates growth responses in a variety of cell types via an activation of early growth-related genes, an alteration in the activity of protein kinases, and an oxidative inactivation of phosphatases, 2) the ability of $O_2^{\bullet-}$ and other O_2 radicals to promote a cellular transformation to a cancer cell type, and 3) the direct or indirect inhibitory effect of a mild increase in intracellular ROS on apoptosis in tumor cells[319, 320]. Additionally, the data of this study are in accordance with studies showing a decrease of proliferation after SOD2 overexpression in cancer cells, including breast cancer, prostate cancer, pancreatic carcinoma cell lines, myeloma[321-323] and cardiac fibroblasts[324]. These studies prove the importance of $O_2^{\bullet-}$ in proliferative cellular processes. The discrepancy of the studies investigating the role of ROS in PH can be attributed to the methodological

problem of ROS measurement (there is no "ideal" method for intracellular ROS detection) and to the probability of different PH-induced alterations in ROS expression depending on the cellular compartment[38, 165].

To support the hypothesis that UCP2 acted via the increased $\Delta\psi_m$ and that the increased $\Delta\psi_m$ was not a secondary effect of increased ROS in these mice, $\Delta\psi_m$ was measured after application of ROS scavengers. In the experiments of this study, no alterations in $\Delta\psi_m$ could be detected under these conditions (Figure 41). However, as discussed above, Echtay *et al.* demonstrated that only matrix-targeted antioxidants could prevent the UCP2 activation by the $O_2^{\bullet-}$ released into the mitochondrial matrix, while the non-mitochondrial antioxidants were unable to prevent the UCP2-induced proton leak[287]. Therefore, further investigations are necessary.

To prove that mitochondrial hyperpolarization was the trigger of increased proliferation of precapillary PASMC after UCP2 knockout or knockdown, precapillary PASMC were incubated with different doses of FCCP for 3 days. Application of FCCP resulted in a significant decrease of $\Delta\psi_m$ and proliferation in those cells (Figures 38 and 43). Interestly, in contrast to ROS scavengers that only partially reversed the enhanced proliferation of precapillary PASMC isolated from $UCP2^{-/-}$ mice, FCCP application completely reversed the abnormal proliferation in those cells suggesting the probability of yet to be discovered signaling mechanisms activated by mitochondrial hyperpolarization. However, the interpretation of these results may be limited, as FCCP application has some unspecific effects such as modulation of mitochondrial respiration and alteration of ROS production[325]. Stockl *et al*. demonstrated that FCCP decreased the proliferation of human fibroblasts in a dose dependent manner and simultaneously increased ROS levels[325]. In contrast, Guimaraes *et al.* found that FCCP decreased ROS production and at the same time decreased the proliferation of hepatic stellate cells[326]. Carriere *et al.* established that other chemical uncoupler, CCCP (Carbonyl cyanide 3-chlorophenylhydrazone) induced an attenuation of preadipocytes proliferation and simultaneously decreased ROS generation[327]. This discrepancy can be attributed to cell-type-specific effects of uncouplers on regulation of ROS. However, further investigations remain to be conducted to finally resolve these discrepancies. Additionally, FCCP application leads to quantitative modifications of mitochondrial protein content[328]. All of these factors could influence the effects of FCCP application on proliferation that were observed in precapillary PASMC isolated from WT mice. To overcome the limitations of FCCP application, overexpression of UCP1 and UCP2 proteins in precapillary PASMC isolated from $UCP2^{-/-}$ mice was performed (Figure 39). UCP2 overexpression decreased the enhanced proliferation of $UCP2^{-/-}$ precapillary PASMC to the same degree as UCP1 overexpression, which is known to act solely via uncoupling[225]. Thus, UCP2 may act by a similar mechanism to UCP1 on proliferation of precapillary PASMC, i.e., via $\Delta\psi_m$.

Although the experiments with isolated precapillary PASMC support the conclusion that increased vascular remodeling of UCP2 deficient mice was caused by alterations of precapillary PASMC, it cannot be excluded that other cell types contributed to the development of pulmonary vascular remodeling in these animals. In this regard, it has been shown that UCP2 located in pulmonary vascular cells as well as in immune cells, contributes to the pulmonary UCP2 expression[329]. Furthermore, recently a study was published that showed a decrease of the bioavailability of NO in endothelium probably via an increase of ROS production in $UCP2^{-/-}$ mice[330]. Therefore, decrease of NO release can contribute to increased PAP in $UCP2^{-/-}$ mice.

In summary the data of our own study suggests that increased pulmonary vascular remodeling in UCP2 deficient mice is due to increased PASMC proliferation , which is caused by increased $\Delta\psi_m$ and partially byROS production, which is in accordance with UCP2 acting as a regulator of $\Delta\psi_m$, *e.g.* via uncoupling as suggest by the literature.

4.2.2. Effect of UCP2 downregulation on $[Ca^{2+}]_m$, glucose and fatty acid metabolism.

As discussed above, the molecular mechanism by which UCP2 regulates $\Delta\psi_m$ and ROS is still under debate (see introduction, Figure 11), and functions of UCP2 in addition to its role as an uncoupler were also investigated in this study.

Trenker *et al.* showed that UCP2 can act as a MCU and it increased the mitochondrial sequestration of Ca^{2+}, thus serving as carrier for Ca^{2+} from the cytosol into the mitochondrial matrix in response to a histamine stimulus[229]. However, in contrast, Mattiasson *et al.* demonstrated that UCP2 overexpression in brain protected against ischemic stress probably via a decrease of $[Ca^{2+}]_m$ overload. This challenges the theory suggesting that UCP2 acts as a Ca^{2+} uniporter[331]. In order to investigate the effect of UCP2 downregulation on mitochondrial calcium, $[Ca^{2+}]_m$ was measured by Rhod2 fluorescent dye in precapillary PASMC isolated from WT and $UCP2^{-/-}$ mice (Figure 47). Rhod2 is a high affinity fluorescent Ca^{2+} probe that selectively targets mitochondria[332]. Similar levels of $[Ca^{2+}]_m$ in both animal groups were found which makes changes in mitochondrial Ca^{2+} metabolism as reason for increased proliferation in UCP2 deficient precapillary PASMC unlikely. However, Rhod2 has many pitfalls including direct effects on mitochondrial structure[333]. Therefore, the result of the Rhod2 experiments should be evaluated with care, and additional experiments should be performed in future studies. An additional argument that UCP2 is not a MCU has been recently revealed: two independent groups of scientists have discovered the molecular bases of MCU[334, 335]. Thus, the data from Trenker *et al.* have been ascribed to an indirect effect on ATP production and hence ER Ca^{2+} loading[336].

Another possible mechanism of UCP2 may be that UCP2 is a key regulator of substrate supply for mitochondrial ATP production[337]. According to this theory, UCP2 increases fatty acid based and

decreases pyruvate based mitochondrial respiration[225] upon different stimuli. A decrease of consumption of pyruvate by mitochondria leads to its accumulation within the cytosol and activation of anaerobic glycolysis[225, 226, 288]. In terms of PH development, decreased mitochondrial pyruvate consumption may either result in a) a "metabolic switch" similar to that which has been shown in PH, and thus promote pulmonary vascular remodeling or b) reduced substrate pressure on the respiratory chain and thus decreased ROS production and PH development. In this study, downregulation of UCP2 was found in experimental models of PH, as well as in IPAH patients, which according to the metabolic hypothesis of UCP2 function could either act as positive or negative factor in PH. However, in this study, no evidence for UCP2 acting as a metabolic regulator in PASMC in normoxia could be found (Figure 46). Basal (routine respiration) and the pyruvate-stimulated mitochondrial respiration was similar in mitochondria isolated from $UCP2^{-/-}$ mice, as well as in precapillary PASMC after transfection with siRNA against UCP2 compared to WT mitochondria and precapillary PASMC transfected with scr siRNA, respectively (Figure 46a-b). Also, the intracellular pyruvate concentration was not different in precapillary PASMC isolated from WT and $UCP^{-/-}$ mice (Figure 46 d). Furthermore, pyruvate concentration was similar in isolated mitochondria from those mice after pyruvate stimulation for 2 min (Figure 46e). In addition, key components of the fatty acid metabolism were studied. Real time PCR of gene expression of key components of fatty acid metabolism did not show any significant differences in their expression in precapillary PASMC isolated from $UCP2^{-/-}$ compared to WT mice (Figure 46c). Crucial components of anaerobic glycolysis such as Ldha and Pdk1 also were not upregulated in precapillary PASMC from $UCP2^{-/-}$ compared to WT (Figure 48f). Thus, in precapillary PASMC and isolated pulmonary mitochondria, UCP2 could not be shown to be the “metabolic switch” or pyruvate uniporter, at least not under baseline conditions. In addition, Herzig S. *et al*. recently identified the DNA/protein sequence of a mitochondrial pyruvate carrier that differs from the UCP2 DNA/protein sequence[338]. Therefore, it seems unlikely that UCP2 acts as a pyruvate carrier.

Despite these findings, it cannot be excluded that UCP2 indeed acts as “metabolic switch” or MCU upon different pathological stimuli or in different cell types. Additionally, UCP2 may play a dual role as an uncoupling protein and a “metabolic switch”, depending on the circumstances[213]. In this regard, it has to be pointed out, that the respiration experiments were performed either in isolated mitochondria or permeabilized PASMC, in order to be able to apply pyruvate as a mitochondrial substrate. These experimental conditions may have resulted in loss of cellular factors activating UCP2, such as $O_2^{\bullet-}$ or fatty acids. However, even in intact cells, respiration without stimulation by any substrate was not different in PASMC isolated from $UCP2^{-/-}$ and WT or in PASMC transfected with siRNA against UCP2. Thus, it is highly unlikely that differences in respiration contributed to increased PASMC proliferation in $UCP2^{-/-}$ PASMC. This finding is in accordance with studies that did not show a decrease of mitochondrial

respiration in UCP2$^{-/-}$ mice[339]. Even an opposite effect was observed in murine embryonic fibroblasts where UCP2 knockout lead to an increase of mitochondrial respiration[226].

4.3. UCP2$^{-/-}$ and chronic hypoxia

UCP2$^{-/-}$ mice exposed to 4 weeks of 10% O_2 did not display any differences in mitochondrial hyperpolarization (Figure 48), degree of right heart hypertrophy or severity of pulmonary vascular remodeling compared to WT controls (unpublished thesis of Timm Hoeres, Giessen). These findings can be explained by downregulation of UCP2 in precapillary PASMC during chronic hypoxia in WT mice resulting in an increased $\Delta\psi_m$ as in UCP2$^{-/-}$ mice. Precapillary PASMC isolated from UCP2$^{-/-}$ mice already had hyperpolarized mitochondria, therefore they could not be further hyperpolarized by downregulation of UCP2 during chronic hypoxia (Figure 48a). This explanation was supported by the finding that chronic hypoxia decreases UCP2 mRNA in precapillary arteries of mice as well as UCP2 protein expression. As UCP2$^{-/-}$ mice still developed hypoxia-induced PH, a mechanism in addition to mitochondrial hyperpolarization had to be active in these mice. Indeed, in precapillary PASMC from UCP2$^{-/-}$ mice the metabolic shift was observed to the same level as in precapillary PASMC isolated from WT mice. This observation could explain chronic hypoxia-induced remodeling in UCP2$^{-/-}$, despite unchanged $\Delta\psi_m$ and be additional evidence against the "metabolic theory" of UCP2 action (Figure 48c-f). If UCP2 is responsible for the metabolic switch from pyruvate to fatty acid metabolism, hypoxia-stimulated expression of key enzymes of anaerobic glycolysis should be less in UCP2$^{-/-}$ mice exposed to chronic hypoxia compared to WT mice.

4.4. Conclusion

This study provides evidence for mitochondrial hyperpolarization as a novel mechanism for regulation of HPV and development of vascular remodeling in PH, and deciphered possible up- and downstream signaling mechanisms. A short summary is presented in Figure 49. Acute hypoxia increased $\Delta\psi_m$ and ROS emission ($O_2^{\bullet-}$ and H_2O_2) in precapillary PASMC (Figure 49a). UCP2 knockout potentiated this process by further increase of $\Delta\psi_m$ and ROS, probably through a lack of fine tuning of $\Delta\psi_m$ (Figure 49a). Different triggers of PH increased $\Delta\psi_m$ in precapillary PASMC (Figure 49b). This increase was probably promoted by glycolytically produced ATP as a result of increased anaerobic glycolysis and decreased mitochondrial respiration. Additionally, experimental PH (4 weeks chronic hypoxic exposure of mice and MCT injection in rats) as well as IPAH increased $\Delta\psi_m$ hyperpolarization at least partially via UCP2 downregulation (Figure 49b). Increased ROS may be a link between the activation of anaerobic glycolysis and the increase of $\Delta\psi_m$, as ROS scavengers inhibited mitochondrial hyperpolarization. However, in acute hypoxia $\Delta\psi_m$ was not influenced by not mitochondrially targeted ROS scavengers. Gene deficiency of UCP2 mimicked the development of PH under normoxic conditions by an increase of proliferation of

precapillary PASMC caused by enhanced $\Delta\psi_m$ and partially caused by increased ROS in those cells. Alteration of the pulmonary vasculature in UCP2$^{-/-}$ mice, thus can be suggested as a new model of moderate PH. The increase of PH in UCP2$^{-/-}$ mice in chronic hypoxia was probably due to the preserved change of cellular metabolism characterized by decreased mitochondrial respiration and increased anaerobic glycolysis.

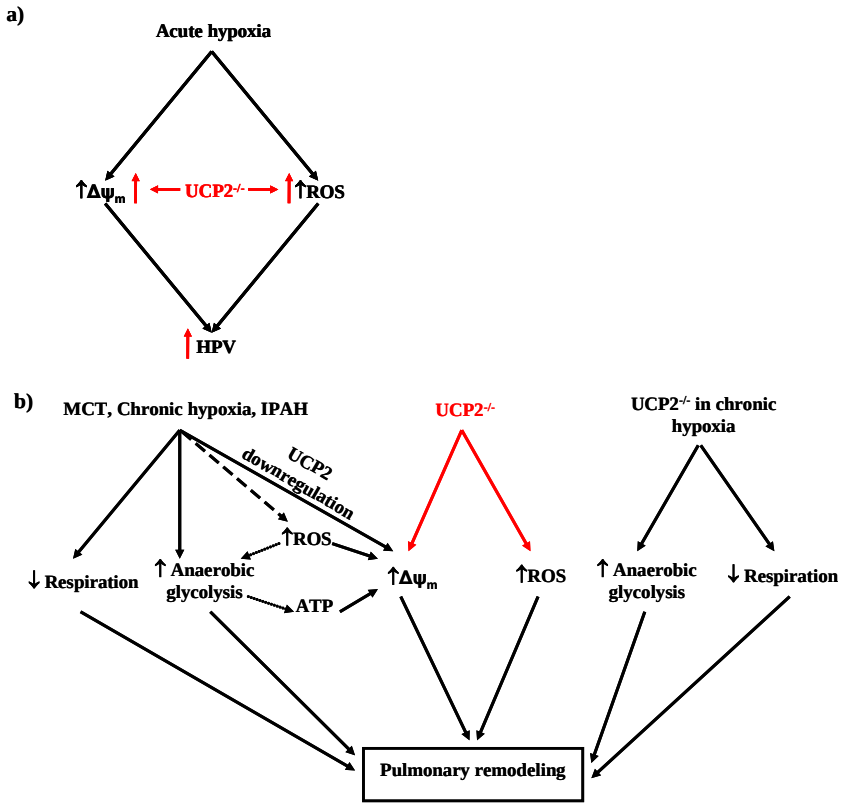

Figure 49. Proposed role of $\Delta\psi_m$ and UCP2 in HPV and in pulmonary vasculature remodeling during PH.

a) Acute hypoxia sensed by mitochondria causes an increase of $\Delta\psi_m$ and mitochondrial ROS emission which may trigger or regulate HPV. UCP2$^{-/-}$ potentiates HPV by enhancement of the increase of $\Delta\psi_m$ and mitochondrial ROS emission probably due to the lack of regulation of $\Delta\psi_m$ by UCP2.

b) Triggers of PH including chronic hypoxia in mice and MCT injection in rats, cause an metabolic switch that is characterized by a decrease of mitochondrial respiration and increase of glycolytic enzymes. $\Delta\psi_m$ hyperpolarization in PH can be a result of increased glycolytically produced ATP and increased ROS production. Additionally, experimental PH (4 weeks chronic hypoxic exposure of mice and MCT injection in rats) as well as IPAH were associated with downregulation of UCP2.

UCP2$^{-/-}$ mice exhibited PH under normoxic conditions promoted by proliferation of precapillary PASMC due to the $\Delta\psi_m$ hyperpolarization and partially to the increased mitochondrial ROS emission. In chronic hypoxia UCP2$^{-/-}$ developed PH to a similar degree as WT mice, probably via sustained metabolic alterations.

Abbreviations: ATP - Adenosine-5'-triphosphate; $\Delta\psi_m$ - mitochondrial membrane potential; UCP2$^{-/-}$ - knockout of uncoupling protein 2; MCT - monocrotaline-induced pulmonary hypertension; ROS - reactive oxygen species.

5. Summary

The pulmonary vasculature constricts in response to acute alveolar hypoxia to redirect blood from poorly to better ventilated areas of the lung, which is an essential self-regulatory physiological response of the pulmonary vessels termed hypoxic pulmonary vasoconstriction (HPV). In contrast, different triggers of pulmonary hypertension (PH), including chronic hypoxia, lead to pathological reactions of the pulmonary vasculature, resulting in pulmonary vasculature remodeling that is characterized by excessive proliferation and attenuated apoptosis of vascular cells concomitant with reduction in the vascular lumen area. Despite intensive research in the last decades, the underlying mechanisms of HPV and vascular proliferation in PH have not yet been fully elucidated. It has been suggested that mitochondria play a key role in HPV, as well as in hypoxia and non-hypoxia dependent pathways that underlie pulmonary vascular remodeling. In both processes the mitochondrial membrane potential ($\Delta\psi_m$), which is an important characteristic of mitochondrial function and the main factor regulating the release of mitochondrial reactive oxygen species (ROS), could play a crucial role. It was hypothesized that knockout of the mitochondrial uncoupling protein 2 (UCP2) results in an increase of $\Delta\psi_m$ and ROS emission that can regulate HPV and vascular remodeling in PH.

Acute hypoxia induced an increase of $\Delta\psi_m$ and ROS emission ($O_2^{\bullet-}$, as well as H_2O_2) in pulmonary artery smooth muscle cells (PASMC) isolated from small precapillary arteries of rats and mice. $\Delta\psi_m$ was also increased in precapillary PASMC isolated from experimental models of PH (chronic hypoxia-induced PH and monocrotaline [MCT]-induced PH) and from patients with idiopathic pulmonary arterial hypertension (IPAH) compared to respective controls. The increase of $\Delta\psi_m$ in PH could have been the result of the utilization of increased glycolytically produced ATP, while concomitantly mitochondrial respiration was decreased in precapillary PASMC. Additionally, mitochondrial hyperpolarization could have also been mediated by UCP2 downregulation. UCP2 deficiency ($UCP2^{-/-}$) caused an increase of $\Delta\psi_m$ and ROS in small precapillary PASMC during normoxic baseline conditions and potentiated the increase of $\Delta\psi_m$ and ROS in acute hypoxia. In parallel, UCP2 deficiency potentiated HPV and showed an increase of right ventricular systolic pressure (RVSP), right ventricle (RV) hypertrophy and vascular remodeling, thus mimicking PH in normoxic baseline conditions. The latter effect can at least partially be attributed to enhanced precapillary PASMC proliferation in UCP2 deficient mice that could be completely reversed by the application of the mitochondrial uncoupler, FCCP and partially by the treatment with ROS scavengers. These findings indicate a crucial role for mitochondrial hyperpolarization and increase of mitochondrial ROS emission in the development of PH. $UCP2^{-/-}$ mice exposed to 4 weeks of hypoxia did not display any differences in $\Delta\psi_m$ compared to wild type (WT) controls. This finding can be explained by downregulation of UCP2 during chronic hypoxia as possible mechanisms to increase $\Delta\psi_m$ in WT mice, which could not be activated in $UCP2^{-/-}$ mice during chronic hypoxia.

The data of the current study thus suggest that an increase of $\Delta\psi_m$ and ROS release could regulate HPV and vascular remodeling in PH. The mechanism for mitochondrial hyperpolarization in PH may be metabolic alterations and downregulation of UCP2 and was regulated by ROS. $UCP2^{-/-}$ deficiency lead to the development of the PH phenotype in mice via increase of $\Delta\psi_m$ and partially via enhance of ROS emission in precapillary PASMC.

6. Zusammenfassung

Die pulmonalvaskuläre Vasokonstriktion als Reaktion auf akute alveoläre Hypoxie dient der Umverteilung der pulmonalen Durchblutung von schlecht zu besser ventilierten Arealen der Lunge und ist ein essentieller selbstregulatorischer Prozess der Lungengefäße, der „hypoxische pulmonale Vasokonstriktion (HPV)“ genannt wird. Im Gegensatz dazu führen verschiedene Auslöser, inklusive akuter Hypoxie, zu pulmonaler Hypertonie (PH), einer pathologischen Reaktion der Lungengefäße, die durch exzessive Proliferation und verminderte Apoptose von Gefäßzellen charakterisiert ist. Trotz intensiver Forschung in den letzten Jahrzehnten konnte der zugrundeliegende Mechanismus der HPV und der vaskulären Proliferation bei der PH noch nicht vollständig geklärt werden. Mitochondrien wurden als Schlüsselfaktor sowohl bei der Entstehung der HPV, als auch in Hypoxie-abhängigen und -unabhängigen Signalwegen des pulmonalvaskulären Gefäßumbauprozesses vorgeschlagen. Bei beiden Vorgängen könnte das mitochondriale Membranpotential ($\Delta\psi_m$), das eine wichtige Charakteristik der mitochondrialen Funktion und ein Hauptfaktor bei der Regulation der Freisetzung von mitochondrialen reactive Sauerstoffspesies (ROS) ist, eine wichtige Rolle spielen. Es wurde daher die Hypothese aufgestellt, dass die Ausschaltung des mitochondrialen Entkopplungsproteins „uncoupling protein 2 (UCP2)“ zu einem Anstieg des $\Delta\psi_m$ und der ROS Freisetzung führt, die die HPV und den vaskulären Gefäßumbau in der PH regulieren kann.

Akute Hypoxie induzierte einen Anstieg des $\Delta\psi_m$ und der ROS Freisetzung [Superoxid ($O_2^{\bullet-}$), sowie Wasserstoffperoxid (H_2O_2)] in pulmonalen glatten Gefäßmuskelzellen (PASMC), die von kleinen präkapillären Arterien aus Ratten und Mäusen isoliert worden waren. Das $\Delta\psi_m$ war auch in präkapillären PASMC isoliert aus experimentellen Modellen der PH [chronisch Hypoxie-induzierte PH und Monocrotalin (MCT)-induzierte PH] und von Patienten mit idiopathischer pulmonal-arterieller Hypertonie im Vergleich zu den entsprechenden Kontrollen erhöht. Der Anstieg des $\Delta\psi_m$ in der PH könnte das Ergebnis einer Nutzung von vermehrt glykolytisch produziertem ATP gewesen sein, bei gleichzeitig verminderter mitochondrialer Respiration in präkapillären PASMC. Zusätzlich war die mitochondriale Hyperpolarisation möglicherweise auch durch eine UCP2 Herunterregulierung verursacht. UCP2 Gendefizienz bewirkte einen Anstieg des $\Delta\psi_m$ und der ROS Konzentration in kleinen präkapillären PASMC während basaler, normoxischer Bedingungen und verstärkte den Anstieg des $\Delta\psi_m$ und der mitochondrialen ROS Konzentration während akuter Hypoxie. Parallel dazu erhöhte die UCP2 Gendefizienz die HPV und UCP2-gendefiziente Tiere zeigten einen erhöhten rechtsventrikulären systolischen Druck, rechtsventrikuläre Hypertrophie und pulmonalvaskulären Gefäßumbau. Somit wurde durch die UCP2 Gendefizienz eine PH unter basalen, normoxischen Bedingungen imitiert. Dieses konnte wenigstens teilweise auf eine erhöhte präkapilläre PASMC Proliferation bei UCP2 defizienten Mäusen

zurückgeführt werden, die komplett durch die Applikation des mitochondrialen Entkopplers, FCCP, und teilweise durch die Behandlung mit ROS Fängern rückgängig gemacht werden konnte. Dies spricht für eine entscheidene Rolle der mitochondrialen Hyperpolarisation und des Anstiegs der ROS Freisetzung bei der Entstehung der PH. Nach 4 Wochen Hypoxieexposition zeigten $UCP2^{-/-}$ Mäuse keinen Unterschied im $\Delta\psi_m$ verglichen mit den Wildtyp (WT) Kontrollen. Dies kann durch die Herunterregulierung von UCP2 während chronischer Hypoxie als möglichem Mechanismus für die $\Delta\psi_m$ Erhöhung in WT Mäusen erklärt werden, so daß dieser Mechanismus nicht bei den $UCP2^{-/-}$ Mäusen während chronischer Hypoxie aktiviert werden konnte.

Die Daten dieser Studie legen daher nahe, dass ein Anstieg des $\Delta\psi_m$ und der ROS Freisetzung die HPV und den vaskuläre Gefäßumbau bei der PH regulieren können. Der Mechanismus, der die mitochondriale Hyperpolarisation im Falle des vaskulären Gefäßumbaus verursacht, ist möglicherweise in metabolischen Veränderungen und einer Herunterregulierung von UCP2 begründet und wird durch ROS reguliert. Der Phänotyp der PH in $UCP2^{-/-}$ defizienten Mäusen wird durch ein erhöhtes $\Delta\psi_m$ und teilweise durch eine erhöhte ROS Freisetzung in präkapillären PASMC unabhängig von metabolischen Veränderungen begünstigt.

7. References:

1. Sommer N, Dietrich A, Schermuly RT, Ghofrani HA, Gudermann T, Schulz R, Seeger W, Grimminger F, Weissmann N. Regulation of hypoxic pulmonary vasoconstriction: Basic mechanisms. *Eur Respir J*. 2008;32:1639-1651
2. Weissmann N, Sommer N, Schermuly RT, Ghofrani HA, Seeger W, Grimminger F. Oxygen sensors in hypoxic pulmonary vasoconstriction. *Cardiovasc Res*. 2006;71:620-629
3. Sylvester JT, Shimoda LA, Aaronson PI, Ward JP. Hypoxic pulmonary vasoconstriction. *Physiol Rev*. 2012;92:367-520
4. Gupte SA, Wolin MS. Relationships between vascular oxygen sensing mechanisms and hypertensive disease processes. *Hypertension*. 2012;60:269-275
5. Myatt L. Control of vascular resistance in the human placenta. *Placenta*. 1992;13:329-341
6. Von Euler US, Liljestrand G. Observations on the pulmonary arterial blood pressure in the cat. *Acta Physiol. Scand*. 1946;12 301–332
7. Peake MD, Harabin AL, Brennan NJ, Sylvester JT. Steady-state vascular responses to graded hypoxia in isolated lungs of five species. *J Appl Physiol*. 1981;51:1214-1219
8. Weissmann N, Akkayagil E, Quanz K, Schermuly RT, Ghofrani HA, Fink L, Hanze J, Rose F, Seeger W, Grimminger F. Basic features of hypoxic pulmonary vasoconstriction in mice. *Respir Physiol Neurobiol*. 2004;139:191-202
9. Weissmann N, Grimminger F, Walmrath D, Seeger W. Hypoxic vasoconstriction in buffer-perfused rabbit lungs. *Respir Physiol*. 1995;100:159-169
10. Westcott RN, Fowler NO, Scott RC, Hauenstein VD, Mc GJ. Anoxia and human pulmonary vascular resistance. *J Clin Invest*. 1951;30:957-970
11. Barer GR, Howard P, Shaw JW. Stimulus-response curves for the pulmonary vascular bed to hypoxia and hypercapnia. *J Physiol*. 1970;211:139-155
12. Dipp M, Evans AM. Cyclic adp-ribose is the primary trigger for hypoxic pulmonary vasoconstriction in the rat lung in situ. *Circ Res*. 2001;89:77-83
13. Sommer N, Pak O, Schorner S, Derfuss T, Krug A, Gnaiger E, Ghofrani HA, Schermuly RT, Huckstorf C, Seeger W, Grimminger F, Weissmann N. Mitochondrial cytochrome redox states and respiration in acute pulmonary oxygen sensing. *Eur Respir J*. 2010;36:1056-1066
14. Robertson TP, Aaronson PI, Ward JP. Hypoxic vasoconstriction and intracellular ca2+ in pulmonary arteries: Evidence for pkc-independent Ca^{2+} sensitization. *Am J Physiol*. 1995;268:H301-307
15. Robertson TP, Dipp M, Ward JP, Aaronson PI, Evans AM. Inhibition of sustained hypoxic vasoconstriction by y-27632 in isolated intrapulmonary arteries and perfused lung of the rat. *Br J Pharmacol*. 2000;131:5-9
16. Kovitz KL, Aleskowitch TD, Sylvester JT, Flavahan NA. Endothelium-derived contracting and relaxing factors contribute to hypoxic responses of pulmonary arteries. *Am J Physiol*. 1993;265:H1139-1148
17. Duke HN. The site of action of anoxia on the pulmonary blood vessels of the cat. *J Physiol*. 1954;125:373-382
18. Marshall C, Marshall BE. Influence of perfusate pO_2 on hypoxic pulmonary vasoconstriction in rats. *Circ Res*. 1983;52:691-696
19. Savineau JP, Gonzalez de la Fuente P, Marthan R. Cellular mechanisms of hypoxia-induced contraction in human and rat pulmonary arteries. *Respir Physiol*. 1995;99:191-198
20. Paddenberg R, Tiefenbach M, Faulhammer P, Goldenberg A, Gries B, Pfeil U, Lips KS, Piruat JI, Lopez-Barneo J, Schermuly RT, Weissmann N, Kummer W. Mitochondrial complex ii is essential for hypoxia-induced pulmonary vasoconstriction of intra- but not of pre-acinar arteries. *Cardiovasc Res*. 2012;93:702-710
21. Weissmann N, Dietrich A, Fuchs B, Kalwa H, Ay M, Dumitrascu R, Olschewski A, Storch U, Mederos y Schnitzler M, Ghofrani HA, Schermuly RT, Pinkenburg O, Seeger W, Grimminger F, Gudermann T. Classical transient receptor potential channel 6 (trpc6) is essential for hypoxic pulmonary vasoconstriction and alveolar gas exchange. *Proc Natl Acad Sci U S A*. 2006;103:19093-19098
22. Robin ED, Theodore J, Burke CM, Oesterle SN, Fowler MB, Jamieson SW, Baldwin JC, Morris AJ, Hunt SA, Vankessel A, et al. Hypoxic pulmonary vasoconstriction persists in the human transplanted lung. *Clin Sci (Lond)*. 1987;72:283-287
23. Robertson TP, Aaronson PI, Ward JP. Ca^{2+} sensitization during sustained hypoxic pulmonary vasoconstriction is endothelium dependent. *Am J Physiol Lung Cell Mol Physiol*. 2003;284:L1121-1126
24. Waypa GB, Schumacker PT. Hypoxic pulmonary vasoconstriction: Redox events in oxygen sensing. *J Appl Physiol*. 2005;98:404-414
25. Pak O, Aldashev A, Welsh D, Peacock A. The effects of hypoxia on the cells of the pulmonary vasculature. *Eur Respir J*. 2007;30:364-372
26. Chandel NS, McClintock DS, Feliciano CE, Wood TM, Melendez JA, Rodriguez AM, Schumacker PT. Reactive oxygen species generated at mitochondrial complex iii stabilize hypoxia-inducible factor-1alpha during hypoxia: A mechanism of O_2 sensing. *J Biol Chem*. 2000;275:25130-25138

27. Waypa GB, Guzy R, Mungai PT, Mack MM, Marks JD, Roe MW, Schumacker PT. Increases in mitochondrial reactive oxygen species trigger hypoxia-induced calcium responses in pulmonary artery smooth muscle cells. *Circ Res*. 2006;99:970-978
28. Weissmann N, Zeller S, Schafer RU, Turowski C, Ay M, Quanz K, Ghofrani HA, Schermuly RT, Fink L, Seeger W, Grimminger F. Impact of mitochondria and nadph oxidases on acute and sustained hypoxic pulmonary vasoconstriction. *Am J Respir Cell Mol Biol*. 2006;34:505-513
29. Archer SL, Reeve HL, Michelakis E, Puttagunta L, Waite R, Nelson DP, Dinauer MC, Weir EK. O_2 sensing is preserved in mice lacking the gp91 phox subunit of nadph oxidase. *Proc Natl Acad Sci U S A*. 1999;96:7944-7949
30. Harder DR, Narayanan J, Birks EK, Liard JF, Imig JD, Lombard JH, Lange AR, Roman RJ. Identification of a putative microvascular oxygen sensor. *Circ Res*. 1996;79:54-61
31. Osipenko ON, Tate RJ, Gurney AM. Potential role for kv3.1b channels as oxygen sensors. *Circ Res*. 2000;86:534-540
32. Gunsalus IC, Sligar SG, Nordlund T, Frauenfelder H. Oxygen sensing heme proteins: Monoxygenases, myoglobin and hemoglobin. *Adv Exp Med Biol*. 1977;78:37-50
33. Roth M, Rupp M, Hofmann S, Mittal M, Fuchs B, Sommer N, Parajuli N, Quanz K, Schubert D, Dony E, Schermuly RT, Ghofrani HA, Sausbier U, Rutschmann K, Wilhelm S, Seeger W, Ruth P, Grimminger F, Sausbier M, Weissmann N. Heme oxygenase-2 and large-conductance Ca^{2+}-activated K^+ channels: Lung vascular effects of hypoxia. *Am J Respir Crit Care Med*. 2009;180:353-364
34. Bonnet S, Michelakis ED, Porter CJ, Andrade-Navarro MA, Thebaud B, Bonnet S, Haromy A, Harry G, Moudgil R, McMurtry MS, Weir EK, Archer SL. An abnormal mitochondrial-hypoxia inducible factor-1alpha-kv channel pathway disrupts oxygen sensing and triggers pulmonary arterial hypertension in fawn hooded rats: Similarities to human pulmonary arterial hypertension. *Circulation*. 2006;113:2630-2641
35. Robertson TP, Mustard KJ, Lewis TH, Clark JH, Wyatt CN, Blanco EA, Peers C, Hardie DG, Evans AM. Amp-activated protein kinase and hypoxic pulmonary vasoconstriction. *Eur J Pharmacol*. 2008;595:39-43
36. Fuchs B, Sommer N, Dietrich A, Schermuly RT, Ghofrani HA, Grimminger F, Seeger W, Gudermann T, Weissmann N. Redox signaling and reactive oxygen species in hypoxic pulmonary vasoconstriction. *Respir Physiol Neurobiol*. 2010;174:282-291
37. Dromparis P, Michelakis ED. Mitochondria in vascular health and disease. *Annu Rev Physiol*. 2013;75:95-126
38. Chandel NS. Mitochondrial regulation of oxygen sensing. *Adv Exp Med Biol*. 2010;661:339-354
39. Pak O, Janssen W, Ghofrani HA, Seeger W, Grimminger F, Schermuly RT, Weissmann N. Animal models of pulmonary hypertension: Role in translational research. *Drug Discovery Today: Disease Models*. 2010;7:89-97
40. Morrell NW, Adnot S, Archer SL, Dupuis J, Jones PL, MacLean MR, McMurtry IF, Stenmark KR, Thistlethwaite PA, Weissmann N, Yuan JX, Weir EK. Cellular and molecular basis of pulmonary arterial hypertension. *J Am Coll Cardiol*. 2009;54:S20-31
41. Stenmark KR, Meyrick B, Galie N, Mooi WJ, McMurtry IF. Animal models of pulmonary arterial hypertension: The hope for etiological discovery and pharmacological cure. *Am J Physiol Lung Cell Mol Physiol*. 2009;297:L1013-1032
42. West JB, American College of P, American Physiological S. The physiologic basis of high-altitude diseases. *Ann Intern Med*. 2004;141:789-800
43. Ghofrani HA, Barst RJ, Benza RL, Champion HC, Fagan KA, Grimminger F, Humbert M, Simonneau G, Stewart DJ, Ventura C, Rubin LJ. Future perspectives for the treatment of pulmonary arterial hypertension. *J Am Coll Cardiol*. 2009;54:S108-117
44. McLaughlin VV, Archer SL, Badesch DB, Barst RJ, Farber HW, Lindner JR, Mathier MA, McGoon MD, Park MH, Rosenson RS, Rubin LJ, Tapson VF, Varga J, American College of Cardiology Foundation Task Force on Expert Consensus D, American Heart A, American College of Chest P, American Thoracic Society I, Pulmonary Hypertension A. Accf/aha 2009 expert consensus document on pulmonary hypertension a report of the american college of cardiology foundation task force on expert consensus documents and the american heart association developed in collaboration with the american college of chest physicians; american thoracic society, inc.; and the pulmonary hypertension association. *J Am Coll Cardiol*. 2009;53:1573-1619
45. Nef HM, Mollmann H, Hamm C, Grimminger F, Ghofrani HA. Pulmonary hypertension: Updated classification and management of pulmonary hypertension. *Heart*. 2010;96:552-559
46. Wagenvoort CA. Morphological substrate for the reversibility and irreversibility of pulmonary hypertension. *Eur Heart J*. 1988;9 Suppl J:7-12
47. Dresdale DT, Schultz M, Michtom RJ. Primary pulmonary hypertension. I. Clinical and hemodynamic study. *Am J Med*. 1951;11:686-705
48. Rich S, Dantzker DR, Ayres SM, Bergofsky EH, Brundage BH, Detre KM, Fishman AP, Goldring RM, Groves BM, Koerner SK, et al. Primary pulmonary hypertension. A national prospective study. *Ann Intern Med*. 1987;107:216-223
49. D'Alonzo GE, Barst RJ, Ayres SM, Bergofsky EH, Brundage BH, Detre KM, Fishman AP, Goldring RM, Groves BM, Kernis JT, et al. Survival in patients with primary pulmonary hypertension. Results from a national prospective registry. *Ann Intern Med*. 1991;115:343-349
50. Thabut G, Dauriat G, Stern JB, Logeart D, Levy A, Marrash-Chahla R, Mal H. Pulmonary hemodynamics in advanced copd candidates for lung volume reduction surgery or lung transplantation. *Chest*. 2005;127:1531-1536
51. Elwing J, Panos RJ. Pulmonary hypertension associated with copd. *Int J Chron Obstruct Pulmon Dis*. 2008;3:55-70

52. Mannino DM. Copd: Epidemiology, prevalence, morbidity and mortality, and disease heterogeneity. *Chest*. 2002;121:121S-126S
53. Chaouat A, Naeije R, Weitzenblum E. Pulmonary hypertension in copd. *Eur Respir J*. 2008;32:1371-1385
54. Chifflot H, Fautrel B, Sordet C, Chatelus E, Sibilia J. Incidence and prevalence of systemic sclerosis: A systematic literature review. *Semin Arthritis Rheum*. 2008;37:223-235
55. Hachulla E, Gressin V, Guillevin L, Carpentier P, Diot E, Sibilia J, Kahan A, Cabane J, Frances C, Launay D, Mouthon L, Allanore Y, Tiev KP, Clerson P, de Groote P, Humbert M. Early detection of pulmonary arterial hypertension in systemic sclerosis: A french nationwide prospective multicenter study. *Arthritis Rheum*. 2005;52:3792-3800
56. Jurasz P, Courtman D, Babaie S, Stewart DJ. Role of apoptosis in pulmonary hypertension: From experimental models to clinical trials. *Pharmacol Ther*. 2010;126:1-8
57. Stevens T, Phan S, Frid MG, Alvarez D, Herzog E, Stenmark KR. Lung vascular cell heterogeneity: Endothelium, smooth muscle, and fibroblasts. *Proc Am Thorac Soc*. 2008;5:783-791
58. Rabinovitch M. Molecular pathogenesis of pulmonary arterial hypertension. *J Clin Invest*. 2008;118:2372-2379
59. Firth AL, Mandel J, Yuan JX. Idiopathic pulmonary arterial hypertension. *Dis Model Mech*. 2010;3:268-273
60. Simonneau G, Robbins IM, Beghetti M, Channick RN, Delcroix M, Denton CP, Elliott CG, Gaine SP, Gladwin MT, Jing ZC, Krowka MJ, Langleben D, Nakanishi N, Souza R. Updated clinical classification of pulmonary hypertension. *J Am Coll Cardiol*. 2009;54:S43-54
61. Schermuly RT, Pullamsetti SS, Kwapiszewska G, Dumitrascu R, Tian X, Weissmann N, Ghofrani HA, Kaulen C, Dunkern T, Schudt C, Voswinckel R, Zhou J, Samidurai A, Klepetko W, Paddenberg R, Kummer W, Seeger W, Grimminger F. Phosphodiesterase 1 upregulation in pulmonary arterial hypertension: Target for reverse-remodeling therapy. *Circulation*. 2007;115:2331-2339
62. Okada K, Tanaka Y, Bernstein M, Zhang W, Patterson GA, Botney MD. Pulmonary hemodynamics modify the rat pulmonary artery response to injury. A neointimal model of pulmonary hypertension. *Am J Pathol*. 1997;151:1019-1025
63. Beppu H, Ichinose F, Kawai N, Jones RC, Yu PB, Zapol WM, Miyazono K, Li E, Bloch KD. Bmpr-ii heterozygous mice have mild pulmonary hypertension and an impaired pulmonary vascular remodeling response to prolonged hypoxia. *Am J Physiol Lung Cell Mol Physiol*. 2004;287:L1241-1247
64. Steiner MK, Syrkina OL, Kolliputi N, Mark EJ, Hales CA, Waxman AB. Interleukin-6 overexpression induces pulmonary hypertension. *Circ Res*. 2009;104:236-244, 228p following 244
65. Cho WK, Lee CM, Kang MJ, Huang Y, Giordano FJ, Lee PJ, Trow TK, Homer RJ, Sessa WC, Elias JA, Lee CG. Il-13 receptor alpha2-arginase 2 pathway mediates il-13-induced pulmonary hypertension. *Am J Physiol Lung Cell Mol Physiol*. 2013;304:L112-124
66. Greenway S, van Suylen RJ, Du Marchie Sarvaas G, Kwan E, Ambartsumian N, Lukanidin E, Rabinovitch M. S100a4/mts1 produces murine pulmonary artery changes resembling plexogenic arteriopathy and is increased in human plexogenic arteriopathy. *Am J Pathol*. 2004;164:253-262
67. Sehgal PB, Mukhopadhyay S, Patel K, Xu F, Almodovar S, Tuder RM, Flores SC. Golgi dysfunction is a common feature in idiopathic human pulmonary hypertension and vascular lesions in shiv-nef-infected macaques. *Am J Physiol Lung Cell Mol Physiol*. 2009;297:L729-737
68. Taraseviciene-Stewart L, Kasahara Y, Alger L, Hirth P, Mc Mahon G, Waltenberger J, Voelkel NF, Tuder RM. Inhibition of the vegf receptor 2 combined with chronic hypoxia causes cell death-dependent pulmonary endothelial cell proliferation and severe pulmonary hypertension. *FASEB J*. 2001;15:427-438
69. Crosby A, Jones FM, Southwood M, Stewart S, Schermuly R, Butrous G, Dunne DW, Morrell NW. Pulmonary vascular remodeling correlates with lung eggs and cytokines in murine schistosomiasis. *Am J Respir Crit Care Med*. 2010;181:279-288
70. Rondelet B, Kerbaul F, Motte S, van Beneden R, Remmelink M, Brimioulle S, McEntee K, Wauthy P, Salmon I, Ketelslegers JM, Naeije R. Bosentan for the prevention of overcirculation-induced experimental pulmonary arterial hypertension. *Circulation*. 2003;107:1329-1335
71. Steinhorn RH, Morin FC, 3rd, Fineman JR. Models of persistent pulmonary hypertension of the newborn (pphn) and the role of cyclic guanosine monophosphate (gmp) in pulmonary vasorelaxation. *Semin Perinatol*. 1997;21:393-408
72. Jasmin JF, Calderone A, Leung TK, Villeneuve L, Dupuis J. Lung structural remodeling and pulmonary hypertension after myocardial infarction: Complete reversal with irbesartan. *Cardiovasc Res*. 2003;58:621-631
73. Mittal M, Roth M, Konig P, Hofmann S, Dony E, Goyal P, Selbitz AC, Schermuly RT, Ghofrani HA, Kwapiszewska G, Kummer W, Klepetko W, Hoda MA, Fink L, Hanze J, Seeger W, Grimminger F, Schmidt HH, Weissmann N. Hypoxia-dependent regulation of nonphagocytic nadph oxidase subunit nox4 in the pulmonary vasculature. *Circ Res*. 2007;101:258-267
74. McGuire M, Bradford A. Chronic intermittent hypercapnic hypoxia increases pulmonary arterial pressure and haematocrit in rats. *Eur Respir J*. 2001;18:279-285
75. Wright JL, Tai H, Churg A. Vasoactive mediators and pulmonary hypertension after cigarette smoke exposure in the guinea pig. *J Appl Physiol*. 2006;100:672-678

76. Schroll S, Arzt M, Sebah D, Nuchterlein M, Blumberg F, Pfeifer M. Improvement of bleomycin-induced pulmonary hypertension and pulmonary fibrosis by the endothelin receptor antagonist bosentan. *Respir Physiol Neurobiol*. 2010;170:32-36
77. Guignabert C, Izikki M, Tu LI, Li Z, Zadigue P, Barlier-Mur AM, Hanoun N, Rodman D, Hamon M, Adnot S, Eddahibi S. Transgenic mice overexpressing the 5-hydroxytryptamine transporter gene in smooth muscle develop pulmonary hypertension. *Circ Res*. 2006;98:1323-1330
78. Zagorski J, Debelak J, Gellar M, Watts JA, Kline JA. Chemokines accumulate in the lungs of rats with severe pulmonary embolism induced by polystyrene microspheres. *J Immunol*. 2003;171:5529-5536
79. Lalich JJ, Merkow L. Pulmonary arteritis produced in rat by feeding crotalaria spectabilis. *Lab Invest*. 1961;10:744-750
80. Motley HL, Cournand A, et al. The influence of short periods of induced acute anoxia upon pulmonary artery pressures in man. *Am J Physiol*. 1947;150:315-320
81. Weissmann N, Grimminger F, Seeger W. Hypoxia in lung vascular biology and disease. *Cardiovasc Res*. 2006;71:618-619
82. Schermuly RT, Ghofrani HA, Wilkins MR, Grimminger F. Mechanisms of disease: Pulmonary arterial hypertension. *Nat Rev Cardiol*. 2011;8:443-455
83. Machado RD, Pauciulo MW, Thomson JR, Lane KB, Morgan NV, Wheeler L, Phillips JA, 3rd, Newman J, Williams D, Galie N, Manes A, McNeil K, Yacoub M, Mikhail G, Rogers P, Corris P, Humbert M, Donnai D, Martensson G, Tranebjaerg L, Loyd JE, Trembath RC, Nichols WC. Bmpr2 haploinsufficiency as the inherited molecular mechanism for primary pulmonary hypertension. *Am J Hum Genet*. 2001;68:92-102
84. Deng Z, Morse JH, Slager SL, Cuervo N, Moore KJ, Venetos G, Kalachikov S, Cayanis E, Fischer SG, Barst RJ, Hodge SE, Knowles JA. Familial primary pulmonary hypertension (gene pph1) is caused by mutations in the bone morphogenetic protein receptor-ii gene. *Am J Hum Genet*. 2000;67:737-744
85. Roberts KE, McElroy JJ, Wong WP, Yen E, Widlitz A, Barst RJ, Knowles JA, Morse JH. Bmpr2 mutations in pulmonary arterial hypertension with congenital heart disease. *Eur Respir J*. 2004;24:371-374
86. Christman BW, McPherson CD, Newman JH, King GA, Bernard GR, Groves BM, Loyd JE. An imbalance between the excretion of thromboxane and prostacyclin metabolites in pulmonary hypertension. *N Engl J Med*. 1992;327:70-75
87. Giaid A, Saleh D. Reduced expression of endothelial nitric oxide synthase in the lungs of patients with pulmonary hypertension. *N Engl J Med*. 1995;333:214-221
88. Stewart DJ, Levy RD, Cernacek P, Langleben D. Increased plasma endothelin-1 in pulmonary hypertension: Marker or mediator of disease? *Ann Intern Med*. 1991;114:464-469
89. Schermuly RT, Dony E, Ghofrani HA, Pullamsetti S, Savai R, Roth M, Sydykov A, Lai YJ, Weissmann N, Seeger W, Grimminger F. Reversal of experimental pulmonary hypertension by pdgf inhibition. *J Clin Invest*. 2005;115:2811-2821
90. Hecker M, Zaslona Z, Kwapiszewska G, Niess G, Zakrzewicz A, Hergenreider E, Wilhelm J, Marsh LM, Sedding D, Klepetko W, Lohmeyer J, Dimmeler S, Seeger W, Weissmann N, Schermuly RT, Kneidinger N, Eickelberg O, Morty RE. Dysregulation of the il-13 receptor system: A novel pathomechanism in pulmonary arterial hypertension. *Am J Respir Crit Care Med*. 2010;182:805-818
91. Humbert M, Monti G, Brenot F, Sitbon O, Portier A, Grangeot-Keros L, Duroux P, Galanaud P, Simonneau G, Emilie D. Increased interleukin-1 and interleukin-6 serum concentrations in severe primary pulmonary hypertension. *Am J Respir Crit Care Med*. 1995;151:1628-1631
92. Piao L, Sidhu VK, Fang YH, Ryan JJ, Parikh KS, Hong Z, Toth PT, Morrow E, Kutty S, Lopaschuk GD, Archer SL. Foxo1-mediated upregulation of pyruvate dehydrogenase kinase-4 (pdk4) decreases glucose oxidation and impairs right ventricular function in pulmonary hypertension: Therapeutic benefits of dichloroacetate. *J Mol Med (Berl)*. 2013;91:333-346
93. Yu Y, Keller SH, Remillard CV, Safrina O, Nicholson A, Zhang SL, Jiang W, Vangala N, Landsberg JW, Wang JY, Thistlethwaite PA, Channick RN, Robbins IM, Loyd JE, Ghofrani HA, Grimminger F, Schermuly RT, Cahalan MD, Rubin LJ, Yuan JX. A functional single-nucleotide polymorphism in the trpc6 gene promoter associated with idiopathic pulmonary arterial hypertension. *Circulation*. 2009;119:2313-2322
94. Hansmann G, Zamanian RT. Ppargamma activation: A potential treatment for pulmonary hypertension. *Sci Transl Med*. 2009;1:12ps14
95. Archer SL, Gomberg-Maitland M, Maitland ML, Rich S, Garcia JG, Weir EK. Mitochondrial metabolism, redox signaling, and fusion: A mitochondria-ros-hif-1alpha-K_v1.5 O_2-sensing pathway at the intersection of pulmonary hypertension and cancer. *Am J Physiol Heart Circ Physiol*. 2008;294:H570-578
96. Michelakis ED, Hampl V, Nsair A, Wu X, Harry G, Haromy A, Gurtu R, Archer SL. Diversity in mitochondrial function explains differences in vascular oxygen sensing. *Circ Res*. 2002;90:1307-1315
97. Nohe A, Keating E, Knaus P, Petersen NO. Signal transduction of bone morphogenetic protein receptors. *Cell Signal*. 2004;16:291-299
98. Rudarakanchana N, Flanagan JA, Chen H, Upton PD, Machado R, Patel D, Trembath RC, Morrell NW. Functional analysis of bone morphogenetic protein type ii receptor mutations underlying primary pulmonary hypertension. *Hum Mol Genet*. 2002;11:1517-1525

99. Grijelmo C, Rodrigue C, Svrcek M, Bruyneel E, Hendrix A, de Wever O, Gespach C. Proinvasive activity of bmp-7 through smad4/src-independent and erk/rac/jnk-dependent signaling pathways in colon cancer cells. *Cell Signal*. 2007;19:1722-1732
100. Trembath RC, Thomson JR, Machado RD, Morgan NV, Atkinson C, Winship I, Simonneau G, Galie N, Loyd JE, Humbert M, Nichols WC, Morrell NW, Berg J, Manes A, McGaughran J, Pauciulo M, Wheeler L. Clinical and molecular genetic features of pulmonary hypertension in patients with hereditary hemorrhagic telangiectasia. *N Engl J Med*. 2001;345:325-334
101. Aldashev AA, Sarybaev AS, Sydykov AS, Kalmyrzaev BB, Kim EV, Mamanova LB, Maripov R, Kojonazarov BK, Mirrakhimov MM, Wilkins MR, Morrell NW. Characterization of high-altitude pulmonary hypertension in the kyrgyz: Association with angiotensin-converting enzyme genotype. *Am J Respir Crit Care Med*. 2002;166:1396-1402
102. Eddahibi S, Guignabert C, Barlier-Mur AM, Dewachter L, Fadel E, Dartevelle P, Humbert M, Simonneau G, Hanoun N, Saurini F, Hamon M, Adnot S. Cross talk between endothelial and smooth muscle cells in pulmonary hypertension: Critical role for serotonin-induced smooth muscle hyperplasia. *Circulation*. 2006;113:1857-1864
103. Tuder RM, Chacon M, Alger L, Wang J, Taraseviciene-Stewart L, Kasahara Y, Cool CD, Bishop AE, Geraci M, Semenza GL, Yacoub M, Polak JM, Voelkel NF. Expression of angiogenesis-related molecules in plexiform lesions in severe pulmonary hypertension: Evidence for a process of disordered angiogenesis. *J Pathol*. 2001;195:367-374
104. Grimminger F, Schermuly RT. Pdgf receptor and its antagonists: Role in treatment of pah. *Adv Exp Med Biol*. 2010;661:435-446
105. Le Cras TD, Hardie WD, Fagan K, Whitsett JA, Korfhagen TR. Disrupted pulmonary vascular development and pulmonary hypertension in transgenic mice overexpressing transforming growth factor-alpha. *Am J Physiol Lung Cell Mol Physiol*. 2003;285:L1046-1054
106. Benisty JI, McLaughlin VV, Landzberg MJ, Rich JD, Newburger JW, Rich S, Folkman J. Elevated basic fibroblast growth factor levels in patients with pulmonary arterial hypertension. *Chest*. 2004;126:1255-1261
107. Iioka Y, Tatsumi K, Sugito K, Moriya T, Kuriyama T. Effects of insulin-like growth factor on nitrogen balance during hypoxic exposure. *Eur Respir J*. 2002;20:293-299
108. Dahal BK, Kosanovic D, Kaulen C, Cornitescu T, Savai R, Hoffmann J, Reiss I, Ghofrani HA, Weissmann N, Kuebler WM, Seeger W, Grimminger F, Schermuly RT. Involvement of mast cells in monocrotaline-induced pulmonary hypertension in rats. *Respir Res*. 2011;12:60
109. Savale L, Tu L, Rideau D, Izziki M, Maitre B, Adnot S, Eddahibi S. Impact of interleukin-6 on hypoxia-induced pulmonary hypertension and lung inflammation in mice. *Respir Res*. 2009;10:6
110. Sanchez O, Marcos E, Perros F, Fadel E, Tu L, Humbert M, Dartevelle P, Simonneau G, Adnot S, Eddahibi S. Role of endothelium-derived cc chemokine ligand 2 in idiopathic pulmonary arterial hypertension. *Am J Respir Crit Care Med*. 2007;176:1041-1047
111. Rolfe DF, Brown GC. Cellular energy utilization and molecular origin of standard metabolic rate in mammals. *Physiol Rev*. 1997;77:731-758
112. Babcock GT. How oxygen is activated and reduced in respiration. *Proc Natl Acad Sci U S A*. 1999;96:12971-12973
113. Thompson RJ, Farragher SM, Cutz E, Nurse CA. Developmental regulation of O_2 sensing in neonatal adrenal chromaffin cells from wild-type and nadph-oxidase-deficient mice. *Pflugers Arch*. 2002;444:539-548
114. Buttigieg J, Brown ST, Lowe M, Zhang M, Nurse CA. Functional mitochondria are required for O_2 but not CO_2 sensing in immortalized adrenomedullary chromaffin cells. *Am J Physiol Cell Physiol*. 2008;294:C945-956
115. Hung PC, Wang HS, Chung HT, Hwang MS, Ro LS. Pulmonary hypertension in a child with mitochondrial a3243g point mutation. *Brain Dev*. 2012;34:866-868
116. Barclay AR, Sholler G, Christodolou J, Shun A, Arbuckle S, Dorney S, Stormon MO. Pulmonary hypertension--a new manifestation of mitochondrial disease. *J Inherit Metab Dis*. 2005;28:1081-1089
117. Perry SW, Norman JP, Barbieri J, Brown EB, Gelbard HA. Mitochondrial membrane potential probes and the proton gradient: A practical usage guide. *Biotechniques*. 2011;50:98-115
118. Brand MD, Nicholls DG. Assessing mitochondrial dysfunction in cells. *Biochem J*. 2011;435:297-312
119. Nicholls DG, Ferguson SJ. *Bioenergetics 3*. San Diego, Calif.: Academic Press; 2002.
120. Kadenbach B, Ramzan R, Moosdorf R, Vogt S. The role of mitochondrial membrane potential in ischemic heart failure. *Mitochondrion*. 2011;11:700-706
121. Stowe DF, Camara AK. Mitochondrial reactive oxygen species production in excitable cells: Modulators of mitochondrial and cell function. *Antioxid Redox Signal*. 2009;11:1373-1414
122. Gerencser AA, Chinopoulos C, Birket MJ, Jastroch M, Vitelli C, Nicholls DG, Brand MD. Quantitative measurement of mitochondrial membrane potential in cultured cells: Calcium-induced de- and hyperpolarization of neuronal mitochondria. *J Physiol*. 2012;590:2845-2871
123. Skulachev VP. Uncoupling: New approaches to an old problem of bioenergetics. *Biochim Biophys Acta*. 1998;1363:100-124
124. D'Autreaux B, Toledano MB. Ros as signalling molecules: Mechanisms that generate specificity in ros homeostasis. *Nat Rev Mol Cell Biol*. 2007;8:813-824
125. Chen AF, Chen DD, Daiber A, Faraci FM, Li H, Rembold CM, Laher I. Free radical biology of the cardiovascular system. *Clin Sci (Lond)*. 2012;123:73-91

126. Hartney T, Birari R, Venkataraman S, Villegas L, Martinez M, Black SM, Stenmark KR, Nozik-Grayck E. Xanthine oxidase-derived ros upregulate egr-1 via erk1/2 in pa smooth muscle cells; model to test impact of extracellular ros in chronic hypoxia. *PLoS One*. 2011;6:e27531
127. Zangar RC, Davydov DR, Verma S. Mechanisms that regulate production of reactive oxygen species by cytochrome p450. *Toxicol Appl Pharmacol*. 2004;199:316-331
128. Cho KJ, Seo JM, Kim JH. Bioactive lipoxygenase metabolites stimulation of nadph oxidases and reactive oxygen species. *Mol Cells*. 2011;32:1-5
129. Satoh M, Fujimoto S, Haruna Y, Arakawa S, Horike H, Komai N, Sasaki T, Tsujioka K, Makino H, Kashihara N. Nad(p)h oxidase and uncoupled nitric oxide synthase are major sources of glomerular superoxide in rats with experimental diabetic nephropathy. *Am J Physiol Renal Physiol*. 2005;288:F1144-1152
130. Murphy MP. How mitochondria produce reactive oxygen species. *Biochem J*. 2009;417:1-13
131. Balaban RS, Nemoto S, Finkel T. Mitochondria, oxidants, and aging. *Cell*. 2005;120:483-495
132. Turrens JF. Mitochondrial formation of reactive oxygen species. *J Physiol*. 2003;552:335-344
133. Starkov AA. The role of mitochondria in reactive oxygen species metabolism and signaling. *Ann N Y Acad Sci*. 2008;1147:37-52
134. Jensen PK. Antimycin-insensitive oxidation of succinate and reduced nicotinamide-adenine dinucleotide in electron-transport particles. I. Ph dependency and hydrogen peroxide formation. *Biochim Biophys Acta*. 1966;122:157-166
135. Bartz RR, Piantadosi CA. Clinical review: Oxygen as a signaling molecule. *Crit Care*. 2010;14:234
136. St-Pierre J, Buckingham JA, Roebuck SJ, Brand MD. Topology of superoxide production from different sites in the mitochondrial electron transport chain. *J Biol Chem*. 2002;277:44784-44790
137. Muller FL, Liu Y, Van Remmen H. Complex iii releases superoxide to both sides of the inner mitochondrial membrane. *J Biol Chem*. 2004;279:49064-49073
138. Barja G. Mitochondrial free radical production and aging in mammals and birds. *Ann N Y Acad Sci*. 1998;854:224-238
139. Lemarie A, Huc L, Pazarentzos E, Mahul-Mellier AL, Grimm S. Specific disintegration of complex ii succinate:Ubiquinone oxidoreductase links ph changes to oxidative stress for apoptosis induction. *Cell Death Differ*. 2011;18:338-349
140. Han D, Antunes F, Canali R, Rettori D, Cadenas E. Voltage-dependent anion channels control the release of the superoxide anion from mitochondria to cytosol. *J Biol Chem*. 2003;278:5557-5563
141. Korshunov SS, Krasnikov BF, Pereverzev MO, Skulachev VP. The antioxidant functions of cytochrome c. *FEBS Lett*. 1999;462:192-198
142. Korshunov SS, Skulachev VP, Starkov AA. High protonic potential actuates a mechanism of production of reactive oxygen species in mitochondria. *FEBS Lett*. 1997;416:15-18
143. Lambert AJ, Brand MD. Superoxide production by nadh:Ubiquinone oxidoreductase (complex i) depends on the ph gradient across the mitochondrial inner membrane. *Biochem J*. 2004;382:511-517
144. Seifert EL, Estey C, Xuan JY, Harper ME. Electron transport chain-dependent and -independent mechanisms of mitochondrial h2o2 emission during long-chain fatty acid oxidation. *J Biol Chem*. 2010;285:5748-5758
145. Loschen G, Flohe L, Chance B. Respiratory chain linked H_2O_2 production in pigeon heart mitochondria. *FEBS Lett*. 1971;18:261-264
146. Rottenberg H, Covian R, Trumpower BL. Membrane potential greatly enhances superoxide generation by the cytochrome bc1 complex reconstituted into phospholipid vesicles. *J Biol Chem*. 2009;284:19203-19210
147. Starkov AA, Fiskum G. Regulation of brain mitochondrial H_2O_2 production by membrane potential and nad(p)h redox state. *J Neurochem*. 2003;86:1101-1107
148. Miwa S, Brand MD. Mitochondrial matrix reactive oxygen species production is very sensitive to mild uncoupling. *Biochem Soc Trans*. 2003;31:1300-1301
149. Sedlic F, Sepac A, Pravdic D, Camara AK, Bienengraeber M, Brzezinska AK, Wakatsuki T, Bosnjak ZJ. Mitochondrial depolarization underlies delay in permeability transition by preconditioning with isoflurane: Roles of ros and Ca^{2+}. *Am J Physiol Cell Physiol*. 2010;299:C506-515
150. Cannon B, Shabalina IG, Kramarova TV, Petrovic N, Nedergaard J. Uncoupling proteins: A role in protection against reactive oxygen species--or not? *Biochim Biophys Acta*. 2006;1757:449-458
151. Shabalina IG, Nedergaard J. Mitochondrial ('mild') uncoupling and ros production: Physiologically relevant or not? *Biochem Soc Trans*. 2011;39:1305-1309
152. Brennan JP, Southworth R, Medina RA, Davidson SM, Duchen MR, Shattock MJ. Mitochondrial uncoupling, with low concentration fccp, induces ros-dependent cardioprotection independent of katp channel activation. *Cardiovasc Res*. 2006;72:313-321
153. Park J, Lee J, Choi C. Mitochondrial network determines intracellular ros dynamics and sensitivity to oxidative stress through switching inter-mitochondrial messengers. *PLoS One*. 2011;6:e23211
154. Mashimo K, Ohno Y. Ethanol hyperpolarizes mitochondrial membrane potential and increases mitochondrial fraction in cultured mouse myocardial cells. *Arch Toxicol*. 2006;80:421-428
155. Mailloux RJ, Harper ME. Uncoupling proteins and the control of mitochondrial reactive oxygen species production. *Free Radic Biol Med*. 2011;51:1106-1115

156. Jastroch M, Divakaruni AS, Mookerjee S, Treberg JR, Brand MD. Mitochondrial proton and electron leaks. *Essays Biochem*. 2010;47:53-67
157. Nicholls DG. The non-ohmic proton leak--25 years on. *Biosci Rep*. 1997;17:251-257
158. Divakaruni AS, Brand MD. The regulation and physiology of mitochondrial proton leak. *Physiology (Bethesda)*. 2011;26:192-205
159. Brookes PS. Mitochondrial h(+) leak and ros generation: An odd couple. *Free Radic Biol Med*. 2005;38:12-23
160. Brand MD, Brindle KM, Buckingham JA, Harper JA, Rolfe DF, Stuart JA. The significance and mechanism of mitochondrial proton conductance. *Int J Obes Relat Metab Disord*. 1999;23 Suppl 6:S4-11
161. Dlaskova A, Clarke KJ, Porter RK. The role of ucp 1 in production of reactive oxygen species by mitochondria isolated from brown adipose tissue. *Biochim Biophys Acta*. 2010;1797:1470-1476
162. Mailloux RJ, Harper ME. Mitochondrial proticity and ros signaling: Lessons from the uncoupling proteins. *Trends Endocrinol Metab*. 2012;23:451-458
163. Huttemann M, Helling S, Sanderson TH, Sinkler C, Samavati L, Mahapatra G, Varughese A, Lu G, Liu J, Ramzan R, Vogt S, Grossman LI, Doan JW, Marcus K, Lee I. Regulation of mitochondrial respiration and apoptosis through cell signaling: Cytochrome c oxidase and cytochrome c in ischemia/reperfusion injury and inflammation. *Biochim Biophys Acta*. 2012;1817:598-609
164. Lin MJ, Yang XR, Cao YN, Sham JS. Hydrogen peroxide-induced ca2+ mobilization in pulmonary arterial smooth muscle cells. *Am J Physiol Lung Cell Mol Physiol*. 2007;292:L1598-1608
165. Archer SL, Weir EK, Wilkins MR. Basic science of pulmonary arterial hypertension for clinicians: New concepts and experimental therapies. *Circulation*. 2010;121:2045-2066
166. Kang TM, Park MK, Uhm DY. Effects of hypoxia and mitochondrial inhibition on the capacitative calcium entry in rabbit pulmonary arterial smooth muscle cells. *Life Sci*. 2003;72:1467-1479
167. Kang TM, Park MK, Uhm DY. Characterization of hypoxia-induced [Ca^{2+}]i rise in rabbit pulmonary arterial smooth muscle cells. *Life Sci*. 2002;70:2321-2333
168. Weissmann N, Ebert N, Ahrens M, Ghofrani HA, Schermuly RT, Hanze J, Fink L, Rose F, Conzen J, Seeger W, Grimminger F. Effects of mitochondrial inhibitors and uncouplers on hypoxic vasoconstriction in rabbit lungs. *Am J Respir Cell Mol Biol*. 2003;29:721-732
169. Evans AM, Hardie DG, Peers C, Mahmoud A. Hypoxic pulmonary vasoconstriction: Mechanisms of oxygen-sensing. *Curr Opin Anaesthesiol*. 2011;24:13-20
170. Aley PK, Murray HJ, Boyle JP, Pearson HA, Peers C. Hypoxia stimulates Ca^{2+} release from intracellular stores in astrocytes via cyclic adp ribose-mediated activation of ryanodine receptors. *Cell Calcium*. 2006;39:95-100
171. Ikematsu N, Dallas ML, Ross FA, Lewis RW, Rafferty JN, David JA, Suman R, Peers C, Hardie DG, Evans AM. Phosphorylation of the voltage-gated potassium channel kv2.1 by amp-activated protein kinase regulates membrane excitability. *Proc Natl Acad Sci U S A*. 2011;108:18132-18137
172. Zou MH, Hou XY, Shi CM, Kirkpatick S, Liu F, Goldman MH, Cohen RA. Activation of 5'-amp-activated kinase is mediated through c-src and phosphoinositide 3-kinase activity during hypoxia-reoxygenation of bovine aortic endothelial cells. Role of peroxynitrite. *J Biol Chem*. 2003;278:34003-34010
173. Toyoda T, Hayashi T, Miyamoto L, Yonemitsu S, Nakano M, Tanaka S, Ebihara K, Masuzaki H, Hosoda K, Inoue G, Otaka A, Sato K, Fushiki T, Nakao K. Possible involvement of the alpha1 isoform of 5'amp-activated protein kinase in oxidative stress-stimulated glucose transport in skeletal muscle. *Am J Physiol Endocrinol Metab*. 2004;287:E166-173
174. Hawley SA, Ross FA, Chevtzoff C, Green KA, Evans A, Fogarty S, Towler MC, Brown LJ, Ogunbayo OA, Evans AM, Hardie DG. Use of cells expressing gamma subunit variants to identify diverse mechanisms of ampk activation. *Cell Metab*. 2010;11:554-565
175. Carafoli E. Calcium signaling: A tale for all seasons. *Proc Natl Acad Sci U S A*. 2002;99:1115-1122
176. Camello-Almaraz C, Gomez-Pinilla PJ, Pozo MJ, Camello PJ. Mitochondrial reactive oxygen species and ca2+ signaling. *Am J Physiol Cell Physiol*. 2006;291:C1082-1088
177. Ward JP, Snetkov VA, Aaronson PI. Calcium, mitochondria and oxygen sensing in the pulmonary circulation. *Cell Calcium*. 2004;36:209-220
178. Wang YX, Zheng YM, Abdullaev I, Kotlikoff MI. Metabolic inhibition with cyanide induces calcium release in pulmonary artery myocytes and xenopus oocytes. *Am J Physiol Cell Physiol*. 2003;284:C378-388
179. Pak O, Sommer N, Hoeres T, Bakr A, Waisbrod S, Sydykov A, Haag D, Esfandiary A, Kojonazarov B, Veit F, Fuchs B, Weisel FC, Hecker M, Schermuly RT, Grimminger F, Ghofrani HA, Seeger W, Weissmann N. Mitochondrial hyperpolarization in pulmonary vascular remodeling - ucp2 deficiency as disease model. *Am J Respir Cell Mol Biol*. 2013
180. Schumacker PT. Lung cell hypoxia: Role of mitochondrial reactive oxygen species signaling in triggering responses. *Proc Am Thorac Soc*. 2011;8:477-484
181. Semenza GL. Hypoxia-inducible factors in physiology and medicine. *Cell*. 2012;148:399-408
182. Yu AY, Shimoda LA, Iyer NV, Huso DL, Sun X, McWilliams R, Beaty T, Sham JS, Wiener CM, Sylvester JT, Semenza GL. Impaired physiological responses to chronic hypoxia in mice partially deficient for hypoxia-inducible factor 1alpha. *J Clin Invest*. 1999;103:691-696

183. Archer SL, Marsboom G, Kim GH, Zhang HJ, Toth PT, Svensson EC, Dyck JR, Gomberg-Maitland M, Thebaud B, Husain AN, Cipriani N, Rehman J. Epigenetic attenuation of mitochondrial superoxide dismutase 2 in pulmonary arterial hypertension: A basis for excessive cell proliferation and a new therapeutic target. *Circulation*. 2010;121:2661-2671
184. Kim JW, Tchernyshyov I, Semenza GL, Dang CV. Hif-1-mediated expression of pyruvate dehydrogenase kinase: A metabolic switch required for cellular adaptation to hypoxia. *Cell Metab*. 2006;3:177-185
185. Semenza GL, Jiang BH, Leung SW, Passantino R, Concordet JP, Maire P, Giallongo A. Hypoxia response elements in the aldolase a, enolase 1, and lactate dehydrogenase a gene promoters contain essential binding sites for hypoxia-inducible factor 1. *J Biol Chem*. 1996;271:32529-32537
186. Ebert BL, Firth JD, Ratcliffe PJ. Hypoxia and mitochondrial inhibitors regulate expression of glucose transporter-1 via distinct cis-acting sequences. *J Biol Chem*. 1995;270:29083-29089
187. Patten DA, Lafleur VN, Robitaille GA, Chan DA, Giaccia AJ, Richard DE. Hypoxia-inducible factor-1 activation in nonhypoxic conditions: The essential role of mitochondrial-derived reactive oxygen species. *Mol Biol Cell*. 2010;21:3247-3257
188. Lai YL, Law TC. Chronic hypoxia- and monocrotaline-induced elevation of hypoxia-inducible factor-1 alpha levels and pulmonary hypertension. *J Biomed Sci*. 2004;11:315-321
189. McMurtry MS, Archer SL, Altieri DC, Bonnet S, Haromy A, Harry G, Bonnet S, Puttagunta L, Michelakis ED. Gene therapy targeting survivin selectively induces pulmonary vascular apoptosis and reverses pulmonary arterial hypertension. *J Clin Invest*. 2005;115:1479-1491
190. Fijalkowska I, Xu W, Comhair SA, Janocha AJ, Mavrakis LA, Krishnamachary B, Zhen L, Mao T, Richter A, Erzurum SC, Tuder RM. Hypoxia inducible-factor1alpha regulates the metabolic shift of pulmonary hypertensive endothelial cells. *Am J Pathol*. 2010;176:1130-1138
191. Porporato PE, Dhup S, Dadhich RK, Copetti T, Sonveaux P. Anticancer targets in the glycolytic metabolism of tumors: A comprehensive review. *Front Pharmacol*. 2011;2:49
192. DeBerardinis RJ, Lum JJ, Hatzivassiliou G, Thompson CB. The biology of cancer: Metabolic reprogramming fuels cell growth and proliferation. *Cell Metab*. 2008;7:11-20
193. Sutendra G, Bonnet S, Rochefort G, Haromy A, Folmes KD, Lopaschuk GD, Dyck JR, Michelakis ED. Fatty acid oxidation and malonyl-coa decarboxylase in the vascular remodeling of pulmonary hypertension. *Sci Transl Med*. 2010;2:44ra58
194. McMurtry MS, Bonnet S, Wu X, Dyck JR, Haromy A, Hashimoto K, Michelakis ED. Dichloroacetate prevents and reverses pulmonary hypertension by inducing pulmonary artery smooth muscle cell apoptosis. *Circ Res*. 2004;95:830-840
195. Michelakis ED, McMurtry MS, Wu XC, Dyck JR, Moudgil R, Hopkins TA, Lopaschuk GD, Puttagunta L, Waite R, Archer SL. Dichloroacetate, a metabolic modulator, prevents and reverses chronic hypoxic pulmonary hypertension in rats: Role of increased expression and activity of voltage-gated potassium channels. *Circulation*. 2002;105:244-250
196. Mattson MP, Chan SL. Calcium orchestrates apoptosis. *Nat Cell Biol*. 2003;5:1041-1043
197. Paffett ML, Riddle MA, Kanagy NL, Resta TC, Walker BR. Altered protein kinase c regulation of pulmonary endothelial store- and receptor-operated ca2+ entry after chronic hypoxia. *J Pharmacol Exp Ther*. 2010;334:753-760
198. Leonard MO, Howell K, Madden SF, Costello CM, Higgins DG, Taylor CT, McLoughlin P. Hypoxia selectively activates the creb family of transcription factors in the in vivo lung. *Am J Respir Crit Care Med*. 2008;178:977-983
199. Ramiro-Diaz JM, Nitta CH, Maston LD, Codianni S, Giermakowska W, Resta TC, Bosc LV. Nfat is required for spontaneous pulmonary hypertension in superoxide dismutase 1 knockout mice. *Am J Physiol Lung Cell Mol Physiol*. 2013;304:L613-625
200. Sutendra G, Dromparis P, Wright P, Bonnet S, Haromy A, Hao Z, McMurtry MS, Michalak M, Vance JE, Sessa WC, Michelakis ED. The role of nogo and the mitochondria-endoplasmic reticulum unit in pulmonary hypertension. *Sci Transl Med*. 2011;3:88ra55
201. Song MY, Makino A, Yuan JX. Role of reactive oxygen species and redox in regulating the function of transient receptor potential channels. *Antioxid Redox Signal*. 2011;15:1549-1565
202. Kroemer G, Pouyssegur J. Tumor cell metabolism: Cancer's achilles' heel. *Cancer Cell*. 2008;13:472-482
203. Lane KL, Talati M, Austin E, Hemnes AR, Johnson JA, Fessel JP, Blackwell T, Mernaugh RL, Robinson L, Fike C, Roberts LJ, 2nd, West J. Oxidative injury is a common consequence of bmpr2 mutations. *Pulm Circ*. 2011;1:72-83
204. Hu HL, Zhang ZX, Chen CS, Cai C, Zhao JP, Wang X. Effects of mitochondrial potassium channel and membrane potential on hypoxic human pulmonary artery smooth muscle cells. *Am J Respir Cell Mol Biol*. 2010;42:661-666
205. Chen C, Chen C, Wang Z, Wang L, Yang L, Ding M, Ding C, Sun Y, Lin Q, Huang X, Du X, Zhao X, Wang C. Puerarin induces mitochondria-dependent apoptosis in hypoxic human pulmonary arterial smooth muscle cells. *PLoS One*. 2012;7:e34181
206. Paulin R, Meloche J, Jacob MH, Bisserier M, Courboulin A, Bonnet S. Dehydroepiandrosterone inhibits the src/stat3 constitutive activation in pulmonary arterial hypertension. *Am J Physiol Heart Circ Physiol*. 2011;301:H1798-1809
207. Lee SL, Simon AR, Wang WW, Fanburg BL. H_2O_2 signals 5-ht-induced erk map kinase activation and mitogenesis of smooth muscle cells. *Am J Physiol Lung Cell Mol Physiol*. 2001;281:L646-652
208. Thannickal VJ, Fanburg BL. Reactive oxygen species in cell signaling. *Am J Physiol Lung Cell Mol Physiol*. 2000;279:L1005-1028

209. Brand MD, Chien LF, Ainscow EK, Rolfe DF, Porter RK. The causes and functions of mitochondrial proton leak. *Biochim Biophys Acta*. 1994;1187:132-139
210. Emre Y, Nubel T. Uncoupling protein ucp2: When mitochondrial activity meets immunity. *FEBS Lett*. 2010;584:1437-1442
211. Nedergaard J, Cannon B. The 'novel' 'uncoupling' proteins ucp2 and ucp3: What do they really do? Pros and cons for suggested functions. *Exp Physiol*. 2003;88:65-84
212. Pecqueur C, Alves-Guerra MC, Gelly C, Levi-Meyrueis C, Couplan E, Collins S, Ricquier D, Bouillaud F, Miroux B. Uncoupling protein 2, in vivo distribution, induction upon oxidative stress, and evidence for translational regulation. *J Biol Chem*. 2001;276:8705-8712
213. Baffy G. Uncoupling protein-2 and cancer. *Mitochondrion*. 2010;10:243-252
214. Berardi MJ, Shih WM, Harrison SC, Chou JJ. Mitochondrial uncoupling protein 2 structure determined by nmr molecular fragment searching. *Nature*. 2011;476:109-113
215. Miroux B, Frossard V, Raimbault S, Ricquier D, Bouillaud F. The topology of the brown adipose tissue mitochondrial uncoupling protein determined with antibodies against its antigenic sites revealed by a library of fusion proteins. *EMBO J*. 1993;12:3739-3745
216. Jia JJ, Zhang X, Ge CR, Jois M. The polymorphisms of ucp2 and ucp3 genes associated with fat metabolism, obesity and diabetes. *Obes Rev*. 2009;10:519-526
217. Fink BD, Hong YS, Mathahs MM, Scholz TD, Dillon JS, Sivitz WI. Ucp2-dependent proton leak in isolated mammalian mitochondria. *J Biol Chem*. 2002;277:3918-3925
218. Krauss S, Zhang CY, Lowell BB. The mitochondrial uncoupling-protein homologues. *Nat Rev Mol Cell Biol*. 2005;6:248-261
219. Negre-Salvayre A, Hirtz C, Carrera G, Cazenave R, Troly M, Salvayre R, Penicaud L, Casteilla L. A role for uncoupling protein-2 as a regulator of mitochondrial hydrogen peroxide generation. *FASEB J*. 1997;11:809-815
220. Lee KU, Lee IK, Han J, Song DK, Kim YM, Song HS, Kim HS, Lee WJ, Koh EH, Song KH, Han SM, Kim MS, Park IS, Park JY. Effects of recombinant adenovirus-mediated uncoupling protein 2 overexpression on endothelial function and apoptosis. *Circ Res*. 2005;96:1200-1207
221. Teshima Y, Akao M, Jones SP, Marban E. Uncoupling protein-2 overexpression inhibits mitochondrial death pathway in cardiomyocytes. *Circ Res*. 2003;93:192-200
222. Lee SC, Robson-Doucette CA, Wheeler MB. Uncoupling protein 2 regulates reactive oxygen species formation in islets and influences susceptibility to diabetogenic action of streptozotocin. *J Endocrinol*. 2009;203:33-43
223. Echtay KS, Esteves TC, Pakay JL, Jekabsons MB, Lambert AJ, Portero-Otin M, Pamplona R, Vidal-Puig AJ, Wang S, Roebuck SJ, Brand MD. A signalling role for 4-hydroxy-2-nonenal in regulation of mitochondrial uncoupling. *EMBO J*. 2003;22:4103-4110
224. Diano S, Horvath TL. Mitochondrial uncoupling protein 2 (ucp2) in glucose and lipid metabolism. *Trends Mol Med*. 2012;18:52-58
225. Bouillaud F. Ucp2, not a physiologically relevant uncoupler but a glucose sparing switch impacting ros production and glucose sensing. *Biochim Biophys Acta*. 2009;1787:377-383
226. Pecqueur C, Bui T, Gelly C, Hauchard J, Barbot C, Bouillaud F, Ricquier D, Miroux B, Thompson CB. Uncoupling protein-2 controls proliferation by promoting fatty acid oxidation and limiting glycolysis-derived pyruvate utilization. *FASEB J*. 2008;22:9-18
227. Millet L, Vidal H, Andreelli F, Larrouy D, Riou JP, Ricquier D, Laville M, Langin D. Increased uncoupling protein-2 and -3 mrna expression during fasting in obese and lean humans. *J Clin Invest*. 1997;100:2665-2670
228. Hurtaud C, Gelly C, Chen Z, Levi-Meyrueis C, Bouillaud F. Glutamine stimulates translation of uncoupling protein 2mrna. *Cell Mol Life Sci*. 2007;64:1853-1860
229. Trenker M, Malli R, Fertschai I, Levak-Frank S, Graier WF. Uncoupling proteins 2 and 3 are fundamental for mitochondrial ca2+ uniport. *Nat Cell Biol*. 2007;9:445-452
230. O'Rourke B, Cortassa S, Aon MA. Mitochondrial ion channels: Gatekeepers of life and death. *Physiology (Bethesda)*. 2005;20:303-315
231. Ma ZA, Zhao Z, Turk J. Mitochondrial dysfunction and beta-cell failure in type 2 diabetes mellitus. *Exp Diabetes Res*. 2012;2012:703538
232. Derdak Z, Fulop P, Sabo E, Tavares R, Berthiaume EP, Resnick MB, Paragh G, Wands JR, Baffy G. Enhanced colon tumor induction in uncoupling protein-2 deficient mice is associated with nf-kappab activation and oxidative stress. *Carcinogenesis*. 2006;27:956-961
233. Nino Fong R, Fatehi-Hassanabad Z, Lee SC, Lu H, Wheeler MB, Chan CB. Uncoupling protein-2 increases nitric oxide production and tnfaip3 pathway activation in pancreatic islets. *J Mol Endocrinol*. 2011;46:193-204
234. Emre Y, Hurtaud C, Nubel T, Criscuolo F, Ricquier D, Cassard-Doulcier AM. Mitochondria contribute to lps-induced mapk activation via uncoupling protein ucp2 in macrophages. *Biochem J*. 2007;402:271-278
235. Dikov D, Aulbach A, Muster B, Drose S, Jendrach M, Bereiter-Hahn J. Do ucp2 and mild uncoupling improve longevity? *Exp Gerontol*. 2010;45:586-595
236. Horvath TL, Diano S, Miyamoto S, Barry S, Gatti S, Alberati D, Livak F, Lombardi A, Moreno M, Goglia F, Mor G, Hamilton J, Kachinskas D, Horwitz B, Warden CH. Uncoupling proteins-2 and 3 influence obesity and inflammation in transgenic mice. *Int J Obes Relat Metab Disord*. 2003;27:433-442

237. Zhang J, Khvorostov I, Hong JS, Oktay Y, Vergnes L, Nuebel E, Wahjudi PN, Setoguchi K, Wang G, Do A, Jung HJ, McCaffery JM, Kurland IJ, Reue K, Lee WN, Koehler CM, Teitell MA. Ucp2 regulates energy metabolism and differentiation potential of human pluripotent stem cells. *EMBO J*. 2011;30:4860-4873
238. Chen X, Wang K, Chen J, Guo J, Yin Y, Cai X, Guo X, Wang G, Yang R, Zhu L, Zhang Y, Wang J, Xiang Y, Weng C, Zen K, Zhang J, Zhang CY. In vitro evidence suggests that mir-133a-mediated regulation of uncoupling protein 2 (ucp2) is an indispensable step in myogenic differentiation. *J Biol Chem*. 2009;284:5362-5369
239. Selimovic D, Hassan M, Haikel Y, Hengge UR. Taxol-induced mitochondrial stress in melanoma cells is mediated by activation of c-jun n-terminal kinase (jnk) and p38 pathways via uncoupling protein 2. *Cell Signal*. 2008;20:311-322
240. Elorza A, Hyde B, Mikkola HK, Collins S, Shirihai OS. Ucp2 modulates cell proliferation through the mapk/erk pathway during erythropoiesis and has no effect on heme biosynthesis. *J Biol Chem*. 2008;283:30461-30470
241. Dietrich MO, Antunes C, Geliang G, Liu ZW, Borok E, Nie Y, Xu AW, Souza DO, Gao Q, Diano S, Gao XB, Horvath TL. Agrp neurons mediate sirt1's action on the melanocortin system and energy balance: Roles for sirt1 in neuronal firing and synaptic plasticity. *J Neurosci*. 2010;30:11815-11825
242. Kojonazarov B, Sydykov A, Pullamsetti SS, Luitel H, Dahal BK, Kosanovic D, Tian X, Majewski M, Baumann C, Evans S, Phillips P, Fairman D, Davie N, Wayman C, Kilty I, Weissmann N, Grimminger F, Seeger W, Ghofrani HA, Schermuly RT. Effects of multikinase inhibitors on pressure overload-induced right ventricular remodeling. *Int J Cardiol*. 2012
243. Dahal BK, Kosanovic D, Pamarthi PK, Sydykov A, Lai YJ, Kast R, Schirok H, Stasch JP, Ghofrani HA, Weissmann N, Grimminger F, Seeger W, Schermuly RT. Therapeutic efficacy of azaindole-1 in experimental pulmonary hypertension. *Eur Respir J*. 2010;36:808-818
244. Scaduto RC, Jr., Grotyohann LW. Measurement of mitochondrial membrane potential using fluorescent rhodamine derivatives. *Biophys J*. 1999;76:469-477
245. Ward MW, Rego AC, Frenguelli BG, Nicholls DG. Mitochondrial membrane potential and glutamate excitotoxicity in cultured cerebellar granule cells. *J Neurosci*. 2000;20:7208-7219
246. Chalmers S, McCarron JG. The mitochondrial membrane potential and ca2+ oscillations in smooth muscle. *J Cell Sci*. 2008;121:75-85
247. Weissmann N, Sydykov A, Kalwa H, Storch U, Fuchs B, Mederos y Schnitzler M, Brandes RP, Grimminger F, Meissner M, Freichel M, Offermanns S, Veit F, Pak O, Krause KH, Schermuly RT, Brewer AC, Schmidt HH, Seeger W, Shah AM, Gudermann T, Ghofrani HA, Dietrich A. Activation of trpc6 channels is essential for lung ischaemia-reperfusion induced oedema in mice. *Nat Commun*. 2012;3:649
248. Weissmann N, Kuzkaya N, Fuchs B, Tiyerili V, Schafer RU, Schutte H, Ghofrani HA, Schermuly RT, Schudt C, Sydykov A, Egemnazarow B, Seeger W, Grimminger F. Detection of reactive oxygen species in isolated, perfused lungs by electron spin resonance spectroscopy. *Respir Res*. 2005;6:86
249. Fink L, Kohlhoff S, Stein MM, Hanze J, Weissmann N, Rose F, Akkayagil E, Manz D, Grimminger F, Seeger W, Bohle RM. Cdna array hybridization after laser-assisted microdissection from nonneoplastic tissue. *Am J Pathol*. 2002;160:81-90
250. Carlson SM, Chouinard CR, Labadorf A, Lam CJ, Schmelzle K, Fraenkel E, White FM. Large-scale discovery of erk2 substrates identifies erk-mediated transcriptional regulation by etv3. *Sci Signal*. 2011;4:rs11
251. Gnaiger E, Lassnig B, Kuznetsov AV, Margreiter R. Mitochondrial respiration in the low oxygen environment of the cell. Effect of adp on oxygen kinetics. *Biochim Biophys Acta*. 1998;1365:249-254
252. Trollinger DR, Cascio WE, Lemasters JJ. Selective loading of rhod 2 into mitochondria shows mitochondrial ca2+ transients during the contractile cycle in adult rabbit cardiac myocytes. *Biochem Biophys Res Commun*. 1997;236:738-742
253. Sherr CJ, Roberts JM. Living with or without cyclins and cyclin-dependent kinases. *Genes Dev*. 2004;18:2699-2711
254. Marchetti C, Jouy N, Leroy-Martin B, Defossez A, Formstecher P, Marchetti P. Comparison of four fluorochromes for the detection of the inner mitochondrial membrane potential in human spermatozoa and their correlation with sperm motility. *Hum Reprod*. 2004;19:2267-2276
255. Salvioli S, Ardizzoni A, Franceschi C, Cossarizza A. Jc-1, but not dioc6(3) or rhodamine 123, is a reliable fluorescent probe to assess delta psi changes in intact cells: Implications for studies on mitochondrial functionality during apoptosis. *FEBS Lett*. 1997;411:77-82
256. Hausenloy DJ, Yellon DM, Mani-Babu S, Duchen MR. Preconditioning protects by inhibiting the mitochondrial permeability transition. *Am J Physiol Heart Circ Physiol*. 2004;287:H841-849
257. Dedkova EN, Blatter LA. Measuring mitochondrial function in intact cardiac myocytes. *J Mol Cell Cardiol*. 2012;52:48-61
258. Mathur A, Hong Y, Kemp BK, Barrientos AA, Erusalimsky JD. Evaluation of fluorescent dyes for the detection of mitochondrial membrane potential changes in cultured cardiomyocytes. *Cardiovasc Res*. 2000;46:126-138
259. Foster KA, Galeffi F, Gerich FJ, Turner DA, Muller M. Optical and pharmacological tools to investigate the role of mitochondria during oxidative stress and neurodegeneration. *Prog Neurobiol*. 2006;79:136-171
260. Almeida A, Almeida J, Bolanos JP, Moncada S. Different responses of astrocytes and neurons to nitric oxide: The role of glycolytically generated atp in astrocyte protection. *Proc Natl Acad Sci U S A*. 2001;98:15294-15299

261. Kalbacova M, Vrbacky M, Drahota Z, Melkova Z. Comparison of the effect of mitochondrial inhibitors on mitochondrial membrane potential in two different cell lines using flow cytometry and spectrofluorometry. *Cytometry A*. 2003;52:110-116
262. Gnaiger E, Mendez G, Hand SC. High phosphorylation efficiency and depression of uncoupled respiration in mitochondria under hypoxia. *Proc Natl Acad Sci U S A*. 2000;97:11080-11085
263. Kadenbach B. Intrinsic and extrinsic uncoupling of oxidative phosphorylation. *Biochim Biophys Acta*. 2003;1604:77-94
264. Kwast KE, Burke PV, Staahl BT, Poyton RO. Oxygen sensing in yeast: Evidence for the involvement of the respiratory chain in regulating the transcription of a subset of hypoxic genes. *Proc Natl Acad Sci U S A*. 1999;96:5446-5451
265. Weissmann N, Grimminger F, Voswinckel R, Conzen J, Seeger W. Nitro blue tetrazolium inhibits but does not mimic hypoxic vasoconstriction in isolated rabbit lungs. *Am J Physiol*. 1998;274:L721-727
266. Desireddi JR, Farrow KN, Marks JD, Waypa GB, Schumacker PT. Hypoxia increases ros signaling and cytosolic ca(2+) in pulmonary artery smooth muscle cells of mouse lungs slices. *Antioxid Redox Signal*. 2010;12:595-602
267. de Frutos S, Nitta CH, Caldwell E, Friedman J, Gonzalez Bosc LV. Regulation of soluble guanylyl cyclase-alpha1 expression in chronic hypoxia-induced pulmonary hypertension: Role of nfatc3 and hur. *Am J Physiol Lung Cell Mol Physiol*. 2009;297:L475-486
268. Paddenberg R, Ishaq B, Goldenberg A, Faulhammer P, Rose F, Weissmann N, Braun-Dullaeus RC, Kummer W. Essential role of complex ii of the respiratory chain in hypoxia-induced ros generation in the pulmonary vasculature. *Am J Physiol Lung Cell Mol Physiol*. 2003;284:L710-719
269. Weerackody RP, Welsh DJ, Wadsworth RM, Peacock AJ. Inhibition of p38 mapk reverses hypoxia-induced pulmonary artery endothelial dysfunction. *Am J Physiol Heart Circ Physiol*. 2009;296:H1312-1320
270. Dikalov S, Griendling KK, Harrison DG. Measurement of reactive oxygen species in cardiovascular studies. *Hypertension*. 2007;49:717-727
271. Zielonka J, Kalyanaraman B. Hydroethidine- and mitosox-derived red fluorescence is not a reliable indicator of intracellular superoxide formation: Another inconvenient truth. *Free Radic Biol Med*. 2010;48:983-1001
272. Mukhopadhyay P, Rajesh M, Hasko G, Hawkins BJ, Madesh M, Pacher P. Simultaneous detection of apoptosis and mitochondrial superoxide production in live cells by flow cytometry and confocal microscopy. *Nat Protoc*. 2007;2:2295-2301
273. Belousov VV, Fradkov AF, Lukyanov KA, Staroverov DB, Shakhbazov KS, Terskikh AV, Lukyanov S. Genetically encoded fluorescent indicator for intracellular hydrogen peroxide. *Nat Methods*. 2006;3:281-286
274. Mailloux RJ, Beriault R, Lemire J, Singh R, Chenier DR, Hamel RD, Appanna VD. The tricarboxylic acid cycle, an ancient metabolic network with a novel twist. *PLoS One*. 2007;2:e690
275. Solaini G, Sgarbi G, Lenaz G, Baracca A. Evaluating mitochondrial membrane potential in cells. *Biosci Rep*. 2007;27:11-21
276. Solaini G, Sgarbi G, Baracca A. Oxidative phosphorylation in cancer cells. *Biochim Biophys Acta*. 2011;1807:534-542
277. Okuda M, Lee HC, Kumar C, Chance B. Comparison of the effect of a mitochondrial uncoupler, 2,4-dinitrophenol and adrenaline on oxygen radical production in the isolated perfused rat liver. *Acta Physiol Scand*. 1992;145:159-168
278. Burghuber OC, Strife R, Zirolli J, Mathias MM, Murphy RC, Reeves JT, Voelkel NF. Hydrogen peroxide induced pulmonary vasoconstriction in isolated rat lungs is attenuated by u60,257, a leucotriene synthesis blocker. *Wien Klin Wochenschr*. 1986;98:117-119
279. Jones RD, Thompson JS, Morice AH. The effect of hydrogen peroxide on hypoxia, prostaglandin f2 alpha and potassium chloride induced contractions in isolated rat pulmonary arteries. *Pulm Pharmacol Ther*. 1997;10:37-42
280. Rhoades RA, Packer CS, Roepke DA, Jin N, Meiss RA. Reactive oxygen species alter contractile properties of pulmonary arterial smooth muscle. *Can J Physiol Pharmacol*. 1990;68:1581-1589
281. Wilhelm J, Herget J. Role of ion fluxes in hydrogen peroxide pulmonary vasoconstriction. *Physiol Res*. 1995;44:31-37
282. Pourmahram GE, Snetkov VA, Shaifta Y, Drndarski S, Knock GA, Aaronson PI, Ward JP. Constriction of pulmonary artery by peroxide: Role of ca2+ release and pkc. *Free Radic Biol Med*. 2008;45:1468-1476
283. Wang QS, Zheng YM, Dong L, Ho YS, Guo Z, Wang YX. Role of mitochondrial reactive oxygen species in hypoxia-dependent increase in intracellular calcium in pulmonary artery myocytes. *Free Radic Biol Med*. 2007;42:642-653
284. Marti A, Larrarte E, Novo FJ, Garcia M, Martinez JA. Ucp2 muscle gene transfer modifies mitochondrial membrane potential. *Int J Obes Relat Metab Disord*. 2001;25:68-74
285. Andrews ZB, Horvath TL. Uncoupling protein-2 regulates lifespan in mice. *Am J Physiol Endocrinol Metab*. 2009;296:E621-627
286. Duchen MR. Mitochondria and calcium: From cell signalling to cell death. *J Physiol*. 2000;529 Pt 1:57-68
287. Echtay KS, Murphy MP, Smith RA, Talbot DA, Brand MD. Superoxide activates mitochondrial uncoupling protein 2 from the matrix side. Studies using targeted antioxidants. *J Biol Chem*. 2002;277:47129-47135
288. Mailloux RJ, Seifert EL, Bouillaud F, Aguer C, Collins S, Harper ME. Glutathionylation acts as a control switch for uncoupling proteins ucp2 and ucp3. *J Biol Chem*. 2011;286:21865-21875
289. Skarka L, Ostadal B. Mitochondrial membrane potential in cardiac myocytes. *Physiol Res*. 2002;51:425-434

290. Hales CA, Kradin RL, Brandstetter RD, Zhu YJ. Impairment of hypoxic pulmonary artery remodeling by heparin in mice. *Am Rev Respir Dis*. 1983;128:747-751
291. Beltran B, Mathur A, Duchen MR, Erusalimsky JD, Moncada S. The effect of nitric oxide on cell respiration: A key to understanding its role in cell survival or death. *Proc Natl Acad Sci U S A*. 2000;97:14602-14607
292. Semenza GL. Regulation of oxygen homeostasis by hypoxia-inducible factor 1. *Physiology (Bethesda)*. 2009;24:97-106
293. Piao L, Fang YH, Cadete VJ, Wietholt C, Urboniene D, Toth PT, Marsboom G, Zhang HJ, Haber I, Rehman J, Lopaschuk GD, Archer SL. The inhibition of pyruvate dehydrogenase kinase improves impaired cardiac function and electrical remodeling in two models of right ventricular hypertrophy: Resuscitating the hibernating right ventricle. *J Mol Med (Berl)*. 2010;88:47-60
294. Xu W, Koeck T, Lara AR, Neumann D, DiFilippo FP, Koo M, Janocha AJ, Masri FA, Arroliga AC, Jennings C, Dweik RA, Tuder RM, Stuehr DJ, Erzurum SC. Alterations of cellular bioenergetics in pulmonary artery endothelial cells. *Proc Natl Acad Sci U S A*. 2007;104:1342-1347
295. Chevrollier A, Loiseau D, Reynier P, Stepien G. Adenine nucleotide translocase 2 is a key mitochondrial protein in cancer metabolism. *Biochim Biophys Acta*. 2011;1807:562-567
296. Grosfeld A, Zilberfarb V, Turban S, Andre J, Guerre-Millo M, Issad T. Hypoxia increases leptin expression in human paz6 adipose cells. *Diabetologia*. 2002;45:527-530
297. Mostyn A, Wilson V, Dandrea J, Yakubu DP, Budge H, Alves-Guerra MC, Pecqueur C, Miroux B, Symonds ME, Stephenson T. Ontogeny and nutritional manipulation of mitochondrial protein abundance in adipose tissue and the lungs of postnatal sheep. *Br J Nutr*. 2003;90:323-328
298. Chen J, Gao Y, Liao W, Huang J, Gao W. Hypoxia affects mitochondrial protein expression in rat skeletal muscle. *OMICS*. 2012;16:98-104
299. Turcotte ML, Parliament M, Franko A, Allalunis-Turner J. Variation in mitochondrial function in hypoxia-sensitive and hypoxia-tolerant human glioma cells. *Br J Cancer*. 2002;86:619-624
300. Heerdt BG, Houston MA, Augenlicht LH. Growth properties of colonic tumor cells are a function of the intrinsic mitochondrial membrane potential. *Cancer Res*. 2006;66:1591-1596
301. Zorov DB, Juhaszova M, Yaniv Y, Nuss HB, Wang S, Sollott SJ. Regulation and pharmacology of the mitochondrial permeability transition pore. *Cardiovasc Res*. 2009;83:213-225
302. Campanella M, Parker N, Tan CH, Hall AM, Duchen MR. If(1): Setting the pace of the f(1)f(o)-atp synthase. *Trends Biochem Sci*. 2009;34:343-350
303. Bell EL, Emerling BM, Ricoult SJ, Guarente L. Sirt3 suppresses hypoxia inducible factor 1alpha and tumor growth by inhibiting mitochondrial ros production. *Oncogene*. 2011;30:2986-2996
304. Frezza C, Zheng L, Tennant DA, Papkovsky DB, Hedley BA, Kalna G, Watson DG, Gottlieb E. Metabolic profiling of hypoxic cells revealed a catabolic signature required for cell survival. *PLoS One*. 2011;6:e24411
305. Burns AT, La Gerche A, Prior DL, Macisaac AI. Left ventricular untwisting is an important determinant of early diastolic function. *JACC Cardiovasc Imaging*. 2009;2:709-716
306. Turner JD, Gaspers LD, Wang G, Thomas AP. Uncoupling protein-2 modulates myocardial excitation-contraction coupling. *Circ Res*. 2010;106:730-738
307. Li N, Wang J, Gao F, Tian Y, Song R, Zhu SJ. The role of uncoupling protein 2 in the apoptosis induced by free fatty acid in rat cardiomyocytes. *J Cardiovasc Pharmacol*. 2010;55:161-167
308. Sastre-Serra J, Valle A, Company MM, Garau I, Oliver J, Roca P. Estrogen down-regulates uncoupling proteins and increases oxidative stress in breast cancer. *Free Radic Biol Med*. 2010;48:506-512
309. Day BJ, Fridovich I, Crapo JD. Manganic porphyrins possess catalase activity and protect endothelial cells against hydrogen peroxide-mediated injury. *Arch Biochem Biophys*. 1997;347:256-262
310. Batinic-Haberle I, Cuzzocrea S, Reboucas JS, Ferrer-Sueta G, Mazzon E, Di Paola R, Radi R, Spasojevic I, Benov L, Salvemini D. Pure mntbap selectively scavenges peroxynitrite over superoxide: Comparison of pure and commercial mntbap samples to mnte-2-pyp in two models of oxidative stress injury, an sod-specific escherichia coli model and carrageenan-induced pleurisy. *Free Radic Biol Med*. 2009;46:192-201
311. Wong CM, Bansal G, Pavlickova L, Marcocci L, Suzuki YJ. Reactive oxygen species and antioxidants in pulmonary hypertension. *Antioxid Redox Signal*. 2012
312. Cracowski JL, Cracowski C, Bessard G, Pepin JL, Bessard J, Schwebel C, Stanke-Labesque F, Pison C. Increased lipid peroxidation in patients with pulmonary hypertension. *Am J Respir Crit Care Med*. 2001;164:1038-1042
313. Bowers R, Cool C, Murphy RC, Tuder RM, Hopken MW, Flores SC, Voelkel NF. Oxidative stress in severe pulmonary hypertension. *Am J Respir Crit Care Med*. 2004;169:764-769
314. Masri FA, Comhair SA, Dostanic-Larson I, Kaneko FT, Dweik RA, Arroliga AC, Erzurum SC. Deficiency of lung antioxidants in idiopathic pulmonary arterial hypertension. *Clin Transl Sci*. 2008;1:99-106
315. Lachmanova V, Hnilickova O, Povysilova V, Hampl V, Herget J. N-acetylcysteine inhibits hypoxic pulmonary hypertension most effectively in the initial phase of chronic hypoxia. *Life Sci*. 2005;77:175-182
316. Jankov RP, Kantores C, Pan J, Belik J. Contribution of xanthine oxidase-derived superoxide to chronic hypoxic pulmonary hypertension in neonatal rats. *Am J Physiol Lung Cell Mol Physiol*. 2008;294:L233-245
317. Uzun O, Balbay O, Comunoglu NU, Yavuz O, Nihat Annakkaya A, Guler S, Silan C, Erbas M, Arbak P. Hypobaric-hypoxia-induced pulmonary damage in rats ameliorated by antioxidant erdosteine. *Acta Histochem*. 2006;108:59-68

318. Redout EM, van der Toorn A, Zuidwijk MJ, van de Kolk CW, van Echteld CJ, Musters RJ, van Hardeveld C, Paulus WJ, Simonides WS. Antioxidant treatment attenuates pulmonary arterial hypertension-induced heart failure. *Am J Physiol Heart Circ Physiol*. 2010;298:H1038-1047
319. Pervaiz S, Clement MV. Superoxide anion: Oncogenic reactive oxygen species? *Int J Biochem Cell Biol*. 2007;39:1297-1304
320. Droge W. Free radicals in the physiological control of cell function. *Physiol Rev*. 2002;82:47-95
321. Hurt EM, Thomas SB, Peng B, Farrar WL. Integrated molecular profiling of sod2 expression in multiple myeloma. *Blood*. 2007;109:3953-3962
322. Oberley LW. Mechanism of the tumor suppressive effect of mnsod overexpression. *Biomed Pharmacother*. 2005;59:143-148
323. Hu Y, Rosen DG, Zhou Y, Feng L, Yang G, Liu J, Huang P. Mitochondrial manganese-superoxide dismutase expression in ovarian cancer: Role in cell proliferation and response to oxidative stress. *J Biol Chem*. 2005;280:39485-39492
324. Li PF, Dietz R, von Harsdorf R. Superoxide induces apoptosis in cardiomyocytes, but proliferation and expression of transforming growth factor-beta1 in cardiac fibroblasts. *FEBS Lett*. 1999;448:206-210
325. Stockl P, Zankl C, Hutter E, Unterluggauer H, Laun P, Heeren G, Bogengruber E, Herndler-Brandstetter D, Breitenbach M, Jansen-Durr P. Partial uncoupling of oxidative phosphorylation induces premature senescence in human fibroblasts and yeast mother cells. *Free Radic Biol Med*. 2007;43:947-958
326. Guimaraes EL, Best J, Dolle L, Najimi M, Sokal E, van Grunsven LA. Mitochondrial uncouplers inhibit hepatic stellate cell activation. *BMC Gastroenterol*. 2012;12:68
327. Carriere A, Fernandez Y, Rigoulet M, Penicaud L, Casteilla L. Inhibition of preadipocyte proliferation by mitochondrial reactive oxygen species. *FEBS Lett*. 2003;550:163-167
328. De Pauw A, Demine S, Tejerina S, Dieu M, Delaive E, Kel A, Renard P, Raes M, Arnould T. Mild mitochondrial uncoupling does not affect mitochondrial biogenesis but downregulates pyruvate carboxylase in adipocytes: Role for triglyceride content reduction. *Am J Physiol Endocrinol Metab*. 2012;302:E1123-1141
329. Alves-Guerra MC, Rousset S, Pecqueur C, Mallat Z, Blanc J, Tedgui A, Bouillaud F, Cassard-Doulcier AM, Ricquier D, Miroux B. Bone marrow transplantation reveals the in vivo expression of the mitochondrial uncoupling protein 2 in immune and nonimmune cells during inflammation. *J Biol Chem*. 2003;278:42307-42312
330. Tian XY, Wong WT, Xu A, Lu Y, Zhang Y, Wang L, Cheang WS, Wang Y, Yao X, Huang Y. Uncoupling protein-2 protects endothelial function in diet-induced obese mice. *Circ Res*. 2012;110:1211-1216
331. Mattiasson G, Shamloo M, Gido G, Mathi K, Tomasevic G, Yi S, Warden CH, Castilho RF, Melcher T, Gonzalez-Zulueta M, Nikolich K, Wieloch T. Uncoupling protein-2 prevents neuronal death and diminishes brain dysfunction after stroke and brain trauma. *Nat Med*. 2003;9:1062-1068
332. Eisner V, Parra V, Lavandero S, Hidalgo C, Jaimovich E. Mitochondria fine-tune the slow ca(2+) transients induced by electrical stimulation of skeletal myotubes. *Cell Calcium*. 2010;48:358-370
333. Fonteriz RI, de la Fuente S, Moreno A, Lobaton CD, Montero M, Alvarez J. Monitoring mitochondrial [ca(2+)] dynamics with rhod-2, ratiometric pericam and aequorin. *Cell Calcium*. 2010;48:61-69
334. Baughman JM, Perocchi F, Girgis HS, Plovanich M, Belcher-Timme CA, Sancak Y, Bao XR, Strittmatter L, Goldberger O, Bogorad RL, Koteliansky V, Mootha VK. Integrative genomics identifies mcu as an essential component of the mitochondrial calcium uniporter. *Nature*. 2011;476:341-345
335. De Stefani D, Raffaello A, Teardo E, Szabo I, Rizzuto R. A forty-kilodalton protein of the inner membrane is the mitochondrial calcium uniporter. *Nature*. 2011;476:336-340
336. Patron M, Raffaello A, Granatiero V, Tosatto A, Merli G, De Stefani D, Wright L, Pallafacchina G, Terrin A, Mammucari C, Rizzuto R. The mitochondrial calcium uniporter (mcu): Molecular identity and physiological roles. *J Biol Chem*. 2013;288:10750-10758
337. Baffy G, Derdak Z, Robson SC. Mitochondrial recoupling: A novel therapeutic strategy for cancer? *Br J Cancer*. 2011;105:469-474
338. Herzig S, Raemy E, Montessuit S, Veuthey JL, Zamboni N, Westermann B, Kunji ER, Martinou JC. Identification and functional expression of the mitochondrial pyruvate carrier. *Science*. 2012;337:93-96
339. Andrews ZB, Liu ZW, Walllingford N, Erion DM, Borok E, Friedman JM, Tschop MH, Shanabrough M, Cline G, Shulman GI, Coppola A, Gao XB, Horvath TL, Diano S. Ucp2 mediates ghrelin's action on npy/agrp neurons by lowering free radicals. *Nature*. 2008;454:846-851

8. Acknowledgements

I would like to reveal my sincere acknowledgment to my supervisor Professor Norbert Weissmann for providing me the opportunity to work in his excellent research group. His friendly personality, patience, guidance and support throughout my doctoral studies helped me to finish my doctoral thesis.

I am extremely grateful to my Postdoc, Dr. Natascha Sommer for all her help, motivation and support whenever I needed. I would never have been able to finish my dissertation without her guidance.

I would like to express deep sense of full respect and gratitude to Prof. Dr. Werner Seeger for this wonderful opportunity to learn science in an international environment of a graduate college.

I would like to thank all GGL and all International Graduate Program MBML team members for their constant adequate pressure that makes my scientific knowledge more complete.

I want to say special thanks to Timm, Adel, Sharon, Phillipe, Bedjan and Azadeh for the wonderful work.

Thanks to all of the Weissmann group members for your friendship, help and for warm atmosphere in the lab every day. I want to specially thank to Karin, Carmen, Liza and Ingrid for a lot of help.
Special thank for my friends in ECCPS building; you make my days in the lab easy and wonderful. So, even on a nice, warm, sunny day I feel better inside of ECCPS, than on the green lawn. Florian, you are the best.

I would like to thank my best friend Djuro for all of his support and love. Хвала пријатељу за све! Thanks to all my friends in Giessen: Diya, Aleksandra, Lukasz, Katarzyna, Sylwia, Daria; Stefan for a lot of fun and the best antidepressant ever created - grill party in Unterhoff.

I would like to say thank to my Kyrgyz friends in Gratz, Austria: Gulsina, Bakyt, Uluk and Djamilya. You are always in my heart. Thanks a lot to Bakyt and Akyl in Giessen, your help mean a lot for me.

Finally, nothing would have been possible without my family. I want to thank my mother Elizaveta, father Aphonasij, my brothers Aleksandr and Sergej for their love, support and existence in my life.